The effects of lubricant starvation on the behaviour of rolling contact bearings

R.A. Hargreaves

THE EFFECTS OF LUBRICANT STARVATION ON THE BEHAVIOUR OF ROLLING CONTACT BEARINGS

by

R. A. HARGREAVES, B. Sc.

A thesis submitted for the degree of Doctor of Philosophy in the Department of Engineering Science, University of Durham.

September 1973

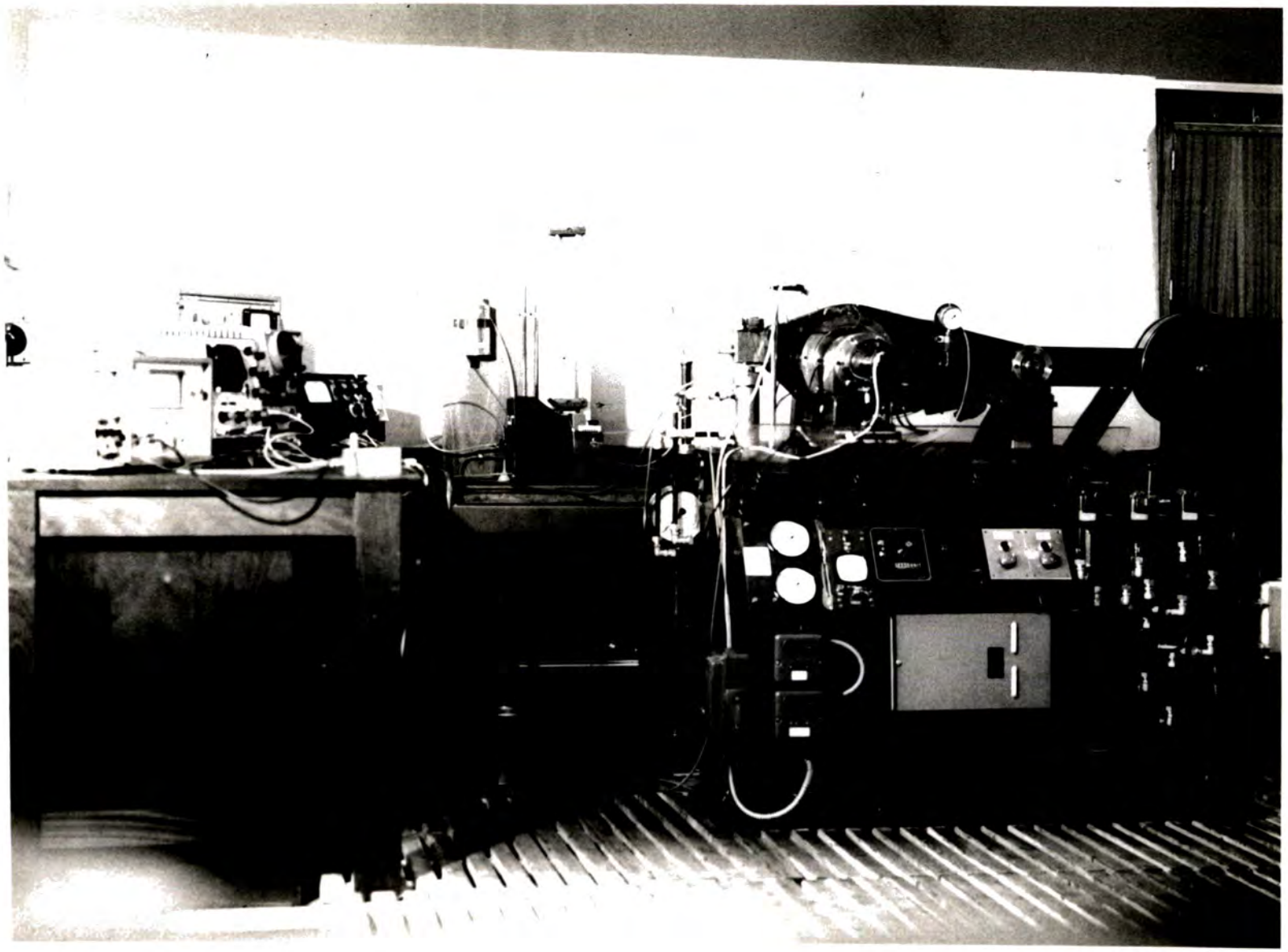

PLATE 1. THE EXPERIMENTAL RIG.

CONTENTS

SECTION 7 General Discussion

SECTION 8 Appendices

ACKNOWLEDGEMENTS

The author is deeply indebted to Professor G. R. Higginson for his valuable guidance and encouragement throughout the work, particularly with the theoretical analyses.

The author wishes to acknowledge the financial support of Rolls-Royce Limited and also the University of Durham. The Department of Mechanical Engineering of Sunderland Polytechnic has been particularly helpful and the author is grateful for their consideration during the writing of this thesis.

Thanks to Shell Research Centre for supplying the lubricants.

SUMMARY

The effects of low lubricant flowrates on both friction torque and temperature distribution in rolling contact bearings is investigated. A theoretical analysis of the effects of lubricant starvation on both film thickness and rolling traction is included.

Experimental results are presented which indicate that both friction torque and component temperatures are reduced with no apparent detrimental effect, except at extremely low values of speed and viscosity.

Comparison between the experimental results and the theoretical analysis shows that, at low loads, the position of the film inlet point is independent of speed but dependent on flowrate. The position of the film inlet point is estimated from this comparison: the film inlet region is shown to be very small.

Notation.

$a = 2.4W$

$2b$ width of the Hertzian contact zone : $b = 4R[W/2\pi]^{1/2}$

E_1, E_2 Elastic Modulii of the solids in contact

$1/E' = \frac{1}{2}\left[\frac{1-\nu_1^2}{E_1} + \frac{1-\nu_2^2}{E_2}\right]$

F Bearing Assembly load

F_1 Bearing Assembly load taken by a roller on the line of action of the load

F_θ Bearing Assembly load taken by a roller at angle θ to the line of action of the load

G Materials parameter : $G = \alpha E'$

h Lubricant film thickness

h_0 Film thickness on line of centres

h_1 Inlet film thickness

$H = h/R$

$H_0 = h_0/R$

H_{0s} the value of H_0 for a starved contact, film inlet $S = s$

$H_{0\infty}$ the value of H_0 for a flooded contact, film inlet $S = \infty$

I Integral value. See Equation 3.1.17.

$I_{S=0}$ Integral value at the edge of the Hertzian zone

$I_{S=s}$ Integral value at a position $S = s$: the film inlet point for a starved contact

$I_{S=\infty}$ Integral value for $S = \infty$

$k = [n-1]^{2/3}$

n a starvation factor defined in Equation 3.4.12

ν a starvation factor defined in Figure S.2, Appendix (S)

p pressure

$P = p/E'$

P_S the value of P at a position S in the inlet film

q reduced pressure defined in Equation 2.2.2.

$Q = q/E'$

Q_S the value of Q at a position S in the inlet film

r roller radius

R equivalent radius of contact

S non - dimensional horizontal coordinate ; See Figure 3.

S_s non - dimensional film inlet point

$\bar{S}$ film inlet parameter defined in Equation 3.1.39.

$\bar{S}_s$ the value of $\bar{S}$ for a film inlet position $S = s$

$\bar{S}_1$ the value of $\bar{S}$ for an assembly roller on the line of action of the load

$\bar{S}_\theta$ the value of $\bar{S}$ for an assembly roller at an angle θ to the line of action of the load

t_S the sliding component of traction

t_R the rolling component of traction

$T_R = t_R/E'R$

$T_{R\infty}$ the value of T_R for a starved contact, film inlet $S=\infty$

$T_{R\infty}$ the value of T_R for a flooded contact, film inlet $S=\infty$

$T_{R\infty TOTAL}$ the total rolling traction for a starved assembly

$u = \frac{1}{2}[u_1 + u_2]$

u_1, u_2 surface velocities of solids in the x direction

$U = \eta_0 u/E'R$

$v = [u_2 - u_1]$

w = load per unit length of cylinder

$W = w/E'R$

x = horizontal coordinate

$X = x/b$

z number of rollers in the bearing assembly

α pressure exponent of viscosity

ϵ total rolling traction ratio : $\epsilon = T_{R\infty TOTAL}/T_{R\infty}$

η viscosity

η_0 viscosity at entry to contact

θ angle measured from load line in a bearing assembly

λ angle to first roller in an assembly from line of action of the load

μ infinite rolling traction ratio : $\mu = T_{R\infty\theta}/T_{R\infty_1}$

ν Poissons ratio

ρ film thickness ratio : $\rho = H_{0\infty}/H_{0\infty}$

τ dummy variable used in the evaluation of Integral I . See Equation 3.1.13

ϕ inlet parameter ratio : $\phi = \bar{S}_\theta/\bar{S}_1$

χ the value of S at which the starved pressure curve starts

ψ rolling traction ratio : $\psi = T_{R\infty}/T_{R\infty}$

SECTION 1

1.1 Introduction and Experimental Background

It is now well established that the mode of lubrication in correctly functioning rolling contact bearings is that of Elasto-hydrodynamic lubrication, and the phenomenon of this type of lubrication has been thoroughly investigated, both theoretically and experimentally, during the past two decades.

The particular problem of contacts operating with minimal lubricant has only lately been considered: in many ways the problem itself can be considered as recent since only lately has the need for separate analysis been appreciated.

The theoretical investigations carried out in the past have in general assumed the case of a contact well supplied with lubricant - an acceptable assumption at the time, since it has been usual in industry for heavily loaded contacts to be copiously lubricated. The results of the theoretical investigations were thought to apply without any severe restrictions to all contact conditions, even those with minimal lubrication, in so far as the condition was thought to exist.

Experimental work carried out by Fogg and Webber (18) during the period 1941 - 1946 noted the fact, since confirmed by many other investigators, that a rolling contact bearing would operate satisfactorily with small amounts of lubricant. However, Fogg and Webber concluded from their results that, for the conditions

investigated (using both ball and roller bearings of 50 mm bore - comparable to the test bearings used in this present investigation), an oil jet feed of 2000 - 3000 gm/minute provided a worthwhile reduction in bearing operating temperature over results obtained for the same bearings lubricated by small quantities of oil supplied as an oil/air mist. It was further concluded that the high lubricant flowrates supplied in jet form did not significantly increase the measured friction torque generated within the bearing.

The results of Fogg and Webber therefore indicated that low flowrate lubrication had little to offer, apart from much reduced lubricant usage, over an oil jet system giving much higher flowrates. Their results, together with the fact that high lubricant flowrates provide a convenient way of satisfying two of the requirements for trouble-free bearing operation (namely, sufficient lubricant and adequate cooling), have helped to establish the practice of copiously lubricating rolling contact bearings. In most applications, of course, such a solution was, and is, perfectly acceptable and much of the later experimental work following that of Fogg and Webber has been concerned with establishing the more important fundamental relationships applicable to the problem of copiously lubricated contacts.

A great deal of this later work has been noted by Garnell and Higginson (21) who initiated a systematic investigation into the lubrication mechanism of

roller bearings. This work has been continued by other investigators, this present work being one of the current investigations in the series. Much of the earlier work in this series, in common with that of other investigators at the time, has been concerned with bearings operating with lubricant flowrates in agreement with or in excess of the recommendations of bearing manufacturers.

The work of Garnell and Higginson contained valuable data on the variation of bearing friction torque with speed, load, lubricant and bearing clearance and was further reported by Garnell (20). In this later work, Garnell reports a preliminary theoretical investigation into the sources of friction in a roller bearing assembly and, in this context, describes their method of obtaining experimental friction torque readings for a bearing with just adequate lubrication with no excess oil. This method was used to obtain the results reported in both the references noted, and consisted of removing the lubricant supply and allowing the bearing to run with no additional lubricant until the oil films in the bearing began to degenerate. In the light of this present investigation, it seems probable that their results are more typical of a bearing operating in a 'starved' condition than in the condition they assumed. However, providing this anomaly is noted, the results presented by Garnell and Higginson provide a sound basis for the later investigations, including

this present work, which have been carried out as a continuation of the series of experiments they instituted.

Lubricant flowrates within the range suggested by Fogg and Webber have, since the date of their work, been common practice in the specialised field of aero engine operation. However, as a result of experiments carried out on aero engine mainshaft bearings, Smith (31) reports that gross slip of rollers and cage is common in copiously lubricated bearings under extreme conditions of speed and load. This result is underlined by Boness (5), who carried out further work in the series initiated by Garnell and Higginson. In the paper noted, Smith also reported that bearing slip of this magnitude could often cause premature bearing failure.

Boness, in addition to fundamental work on the isoviscous lubrication of rigid cylinders (3) (4), performed an experimental investigation into the effects of lubricant flowrate (but at high values - up to 4000 gm/minute) on the dynamics of cage and rollers in a bearing assembly, using both free and fixed cage bearing configurations (5) (6). Although some of this work cannot be directly related to the conditions in a normally operating roller bearing, Boness's results provide an interesting insight into the effects of load, speed and lubricant flowrate on both roller and cage slip. Particularly notable,

within the context of this introductory discussion, are the results which show that a reduction in lubricant supply will reduce the extent of both cage and roller slip. Boness further reports that a reduction in lubricant flow to the minimum required for full hydrodynamic conditions - an elusive target - can reduce cage slip by up to 75%.

It is recognised within the aero engine industry that the problem of slip is inherent to the copious lubrication of bearings. Many attempts have been made to prevent gross slip by means other than a reduction in lubricant supply, with qualified success. One such preventative is the provision of bearing outer race tracks of carefully controlled elliptical form, but such a solution is necessarily costly.

Albeit with lack of other evidence, one presumes that the aero engine industry's present commitment to copious lubrication is based of other factors in addition to the convenience of providing both lubricating and cooling functions simultaneously. Such high lubricant usage requires cooling and filtering equipment to prepare the large volumes of lubricating oil for re-circulation. The severe weight restrictions which are being imposed on present day aero installations have prompted the manufacturers to seek other solutions to the many problems of bearing lubrication. The convenience of copious lubrication is fast becoming an embarrassment.

In terms of the benefits available from a saving in weight, both of lubricant and installation, it appears that an oil/air mist lubricating device used within a 'total-loss' system could offer an acceptable alternative to the present recirculatory method of lubrication. Such a system, in which the small quantities of lubricant used are channelled to waste in the engine exhaust, could, in the light of Boness's results, also provide a means of lubrication in which both roller and cage slip are minimised.

The value of an investigation into the effects of low lubricant flowrates on the behaviour of rolling contact bearings is not of course limited to the particular field of aero engine design: Castle and Dowson (8), for instance, suggest that a study of lubricant 'starvation' is necessary for the full understanding of the behaviour of the small precision bearings used in gyroscopes. In this application, the lubricant quantity in the bearing is extremely limited to ensure precise operation of the instrument.

Many bearings operating in quite mundane situations are lubricated by commercial oil/air mist systems such as those manufactured by Norgren Limited. The quantity of lubricant supplied to these bearings is quite small and so an investigation into the effects of low lubricant flowrates would be applicable to these cases. A further important point, concerned with the operation of bearings outside the field where low flowrates are known to exist, is proposed by

Münnich (26). This author suggests that, even in normal applications, the use of the generally accepted bearing life formulae as a basis for bearing selection results in bearings being operated under conditions where the failure mechanism prevalent in the particular operating regime is akin to the failure mechanism observed for bearings operating with minimal lubricant.

It therefore appears that conditions of lubricant starvation may be a more common occurance than is generally supposed, and that there is a general need for an investigation into the particular effects associated with the operation of bearings with minimal lubricant. It is obviously essential that the lubricant requirements of a particular bearing installation are capable of being accurately assessed so that a small but satisfactory lubricant supply can be provided.

It is the purpose of this thesis to provide a preliminary investigation, both experimentally and theoretically, into the effects of low lubricant flowrate on the behaviour of cylindrical roller bearings.

SECTION 2

2.1 Theoretical Developments

Classical lubrication theory, first introduced by Reynolds, considered the case of solid, underforming materials lubricated by a film of incompressible lubricant. Numerous authors have extended this work to predict film thicknesses and viscous traction in a contact of this nature and the resulting analysis provides an acceptable estimate of these quantities, and also the curve of pressure generation, for a contact operating under conditions of moderate speed and light load.

That analysis is not applicable to more severe conditions since it underestimates, in particular, the lubricant film thickness known to exist at such a contact.

A number of investigations, incorporating either the concept of deformable surfaces or the effect of contact pressures on the properties of the lubricant film have obtained useful extensions to the classical theory, but each of these effects considered separately again predicted lubricant film thicknesses too small to provide total separation of the contacting surfaces.

A full solution to the problem of a lubricated contact incorporating both these effects was given by Dowson and Higginson (14) who, by means of a numerical procedure, obtained an expression for lubricant film thickness in an elastohydrodynamic contact.

The rigorous analysis of Dowson and Higginson was, however, preceded by the analytical analysis of Grubin (22), who, by means of an inspired simplification, was able to provide an expression relating contact parameters and lubricant film thickness in a heavily loaded lubricated contact. The work of Grubin contains the basic assumptions made in the theoretical analysis given in this present work and so Grubin's analysis is described in more detail in the following section.

The work of both Grubin and Dowson and Higginson used the assumption of an inlet boundary to the contact film at a point remote from the conjunction. Such a mathematically convenient assumption was thought to be well justified for the case of a fully lubricated contact, since the extent of the lubricant film though the contact is many times greater than either the film thickness at the contact or the length of the contact region itself. This assumption of an extensive film was also thought to be justifiable when considered in the light of the current industrial practice of amply lubricating heavily loaded contacts.

However, with notable insight, Crook (9) suggested that, as a result of experiments carried out on a two disc machine, "the development of pressure in the oil may not commence at a point remote from the conjunction of the discs on the entry side ---- but may commence at a point comparatively close to the

conjunction. The effect of this would be ---------
to reduce the predicted film thickness".

Crook also showed that the lubricant on the discs remained on the surfaces for many cycles and was only slowly replaced by fresh oil, suggesting that the lubricant supply need only replace the small lubricant losses at the contact.

Lauder (24), who was also concerned with establishing a more physically acceptable inlet boundary condition than that used by Grubin and by Dowson and Higginson (and who in fact suggested an inlet boundary condition based on visual observation of the film shape at entry to a lubricated contact), noted that Kapitsa had shown that the theoretical distribution of pressure in a lubricated contact was greatly influenced by the position of the inlet boundary.

It therefore appears that the assumption of a remote inlet boundary to a contact could overestimate to some degree the quantity of lubricant in use at a contact and that such an assumption could lead, in some cases, to an erroneous estimate of film thickness and other parameters of the contact.

2.2 Grubin Analysis for EHD Contacts

Grubin (22) considered the case of an elastic cylinder in contact with a rigid plane, the contact being lubricated by a fluid having pressure - dependent viscosity.

Under the effect of an applied external force the cylinder will become flattened within the contact region - the shape of the cylindrical surface outside the contact region will also be modified. An exact solution for the deformation of these surfaces was given by Hertz (see, for example, (32)) who also calculated the stress distribution within the materials in contact.

Grubin considered that the presence of a lubricant film would have little effect on the stress distribution and deformed shape of the contacting surfaces except to cause the surfaces to be separated by a parallel film of fluid of thickness h_0 . This model of deformation is shown in figure 2 .

If the separating fluid has a pressure - viscosity relationship of the form

$$\eta = \eta_0 \exp(\alpha p) \qquad 2.2.1$$

it can be shown that the relationship between the pressure p generated in the fluid and the reduced pressure q which would be generated in a fluid with constant viscosity under the same conditions is

$$p = -\frac{1}{\alpha} \ln(1 - \alpha q) \qquad 2.2.2$$

Grubin considered that the fluid pressure at the

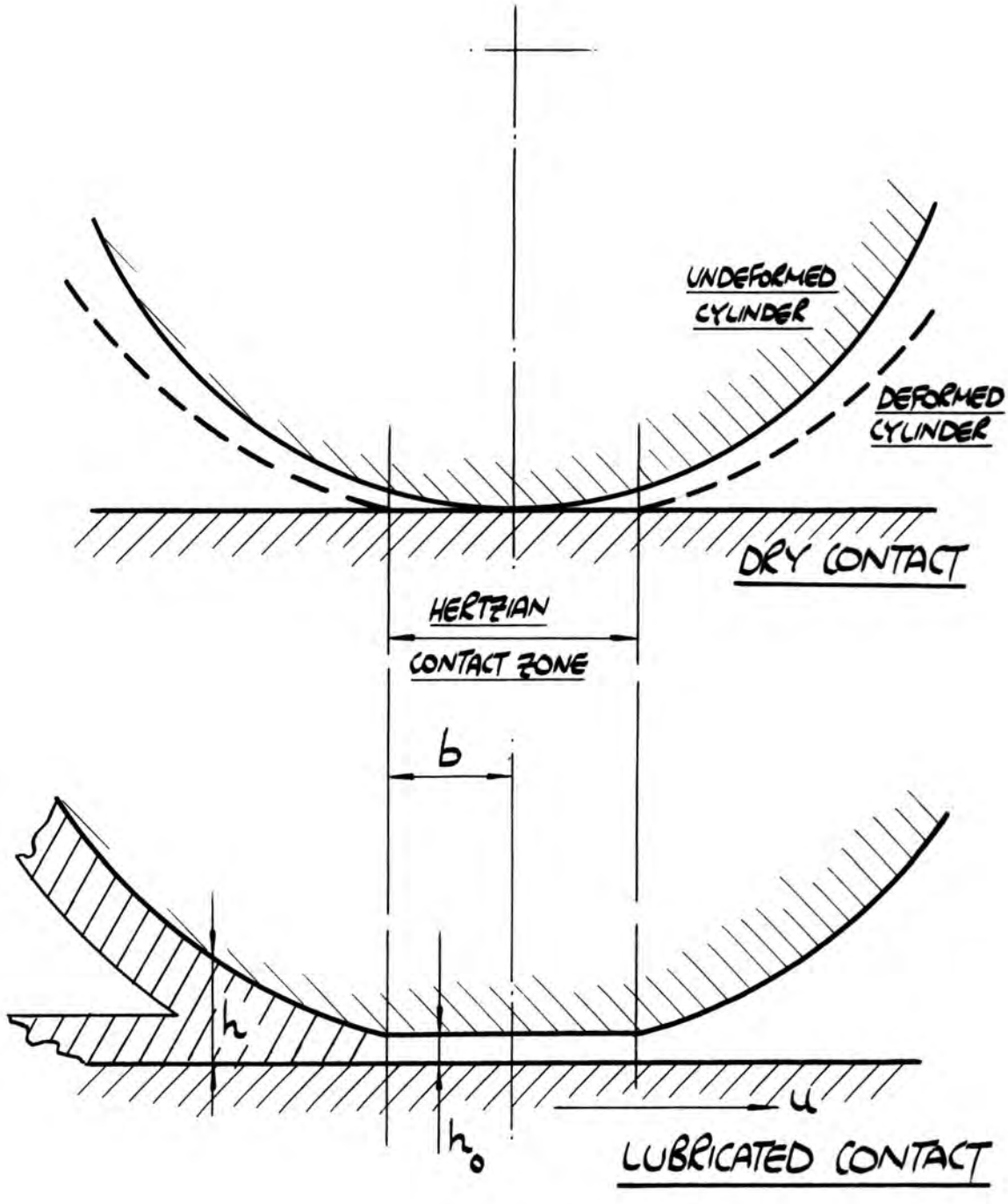

FIGURE 2. GRUBIN MODEL OF AN ELASTO-HYDRODYNAMIC CONTACT. REPRODUCED FROM REFERENCE 14.

inlet to the Hertzian contact region must be very high and took the limiting case of an infinite pressure at this point. The above equation therefore gives that

$$q_r = -\frac{1}{\alpha} \qquad 2.2.3$$

Using this pressure condition and the assumption of contact deformation given by dry contact with a parallel film separation, Grubin produced an expression for film thickness h_0 in close agreement with both subsequent rigorous analysis and with experimental results.

A fuller discussion of Grubins work appears in reference (14).

In common with most other investigators, Grubins analysis assumes that the starting point for the increase in pressure occurs at a large distance from the edge of the Hertzian contact region. It is usual to apply the condition

$$p = q_r = 0 \quad \text{at} \quad x = -\infty \qquad 2.2.4$$

which represents a contact supplied with a copious amount of lubricant: this is referred to as a fully flooded condition.

The present work, in common with that of Wolveridge, Baglin and Archard (36), uses a similar approach to that of Grubin but investigates the effect of taking the starting point of the pressure curve at values of the horizontal co-ordinate x close to the edge of the Hertzian contact region; this inlet condition describing the case of a lubricated contact

with small amounts of lubricant. This condition has come to be known as starved lubrication.

SECTION 3

Theoretical Analysis of Starved Lubrication

3.1 Evaluation of Film Thickness

This particular case of elasto-hydrodynamic lubrication was first investigated analytically by Wolveridge, Baglin and Archard (36), and also in a more general way by Münnich (26).

Wolveridge, Baglin and Archard have developed a systematic analysis of the effects of lubricant starvation on the film thickness for a cylinder in contact with a plane surface. Their analysis uses the assumptions of Grubin: the present analysis follows in principle that of the above authors although the detailed steps in the analysis are different in some respects. This present analysis also extends the work of Wolveridge, Baglin and Archard to estimate the rolling traction associated with a starved lubrication condition. Their work is, in many respects, the basis from which the theoretical analysis contained in this present work commences and explains why it has been considered desirable to take the unusual step of including their publication as an Appendix to this thesis. The reader will note in Appendix (U) that the non-dimensional quantities used by Wolveridge, Baglin and Archard differ from those used in the analysis which follows. It is the authors belief that the use of the more generally accepted non-dimensional variables provides a considerable simplification in the analysis, and it is these

variables that have been used throughout this present work.

Reynolds equation,

$$\frac{dp}{dx} = 12\eta u\left[\frac{h-h_0}{h^3}\right] \qquad 3.1.1$$

can be modified to take account of a lubricant with a pressure-dependent viscosity relationship as given in equation (2.2.1), the equation being expressed in terms of the reduced pressure q_r.

$$\frac{dq_r}{dx} = 12\eta_0 u\left[\frac{h-h_0}{h^3}\right] \qquad 3.1.2$$

In terms of the generally accepted non-dimensional variables,

$$Q = q/E'; \quad U = \frac{\eta_0 u}{E'R}; \quad W = \frac{w}{E'R}; \quad H = \frac{h}{R}; \quad H_0 = \frac{h_0}{R}; \quad X = \frac{x}{b} \qquad 3.1.3$$

the equation becomes

$$\frac{dQ}{dX} = 48\left(\frac{W}{2\pi}\right)^{1/2} U\,\frac{H-H_0}{H^3} \qquad 3.1.4$$

For a contact geometry as assumed by Grubin and shown in figure 2 the gap between the boundary surfaces is given by Hertz as

$$H-H_0 = \frac{h-h_0}{R} = \frac{4W}{2\pi}\left[X\sqrt{X^2-1} - \ln\left[X+\sqrt{X^2-1}\right]\right] \qquad 3.1.5$$

Crook (10) has shown that, in the converging entry region, this can be approximated by

$$H-H_0 = \frac{4W}{\pi}\left(4\frac{\sqrt{2}}{3}\right)\left[|X|-1\right]^{3/2} \qquad 3.1.6$$

The Grubin assumption of a lubricant film shape

given by the deformation of the surfaces in dry contact has been successful in predicting film thicknesses for the condition of fully flooded lubrication. It seems reasonable to suppose that, since the film extent is reduced, the Grubin assumption will be even more applicable for conditions of starved lubrication. Considering also the Crook approximation to the expression for dry Hertzian deformation, Appendix (A) shows that this approximation gives better agreement with the Hertzian expression in the region close to the edge of the Hertzian contact zone. It is again reasonable to assume that the approximation will more nearly represent the true film shape close to the contact region and will therefore be even more applicable to starved conditions than to the fully flooded case.

It is convenient to consider the expression for film thickness in terms of a new horizontal co-ordinate, S, measured from the edge of the Hertzian zone, as shown in figure 3 .

It can be seen that, in the entry region,

$$S = -(X+1) \qquad 3.1.7$$

and

$$\frac{d}{dX} = -\frac{d}{dS} \qquad 3.1.8$$

The Crook approximation therefore becomes

$$H - H_0 = \frac{4W}{\pi}\left(4\frac{\sqrt{2}}{3}\right)S^{3/2} \qquad 3.1.9$$

or

$$H = H_0 + aS^{3/2} \quad ; \quad a = 2.4W \qquad 3.1.10$$

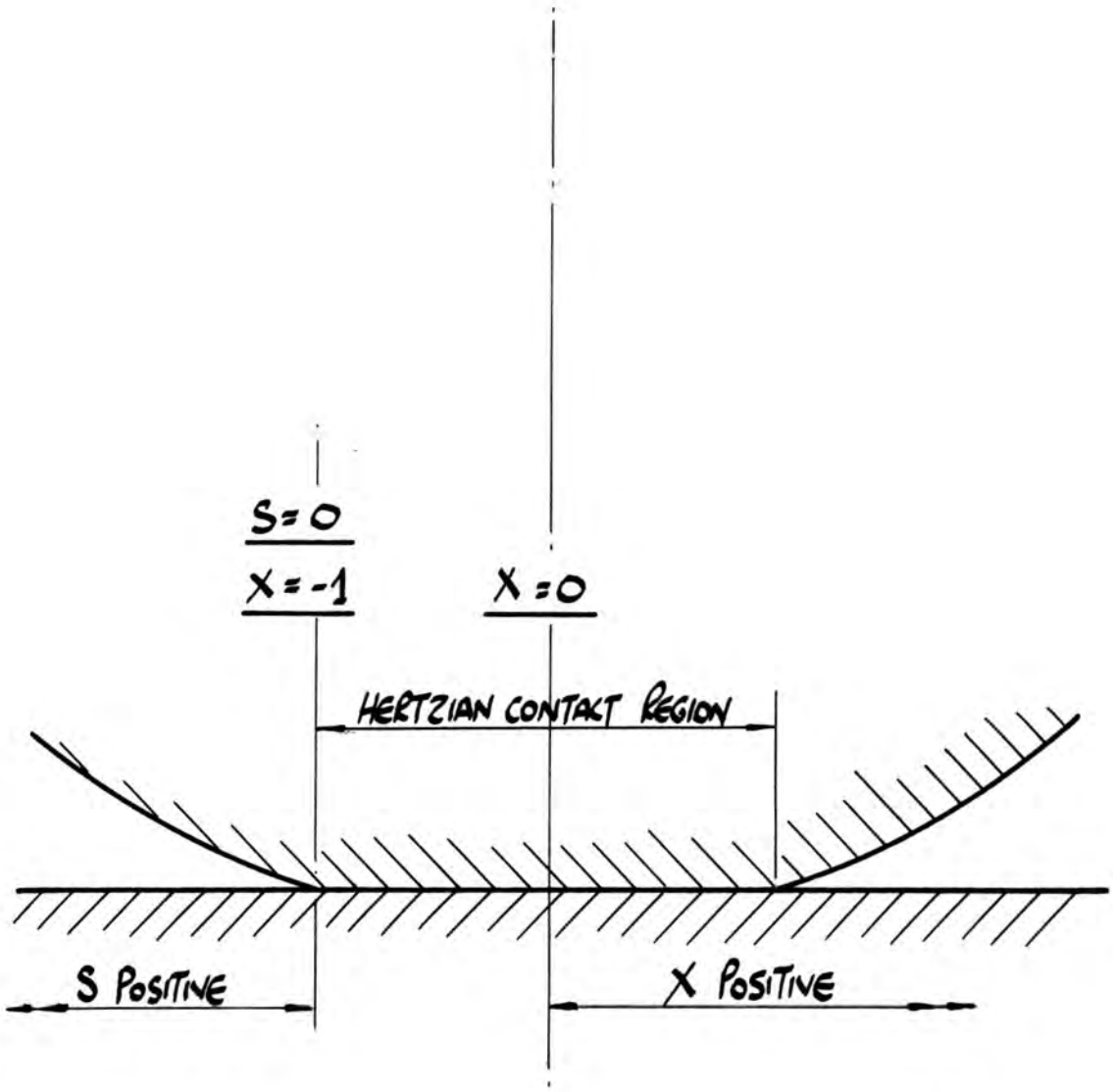

FIGURE 3 . TO SHOW THE RELATIONSHIP BETWEEN THE NON-DIMENSIONAL DISTANCES X AND S.

The non-dimensional form of Reynolds equation

becomes

$$\frac{dQ}{dS} = -48\left(\frac{W}{2\pi}\right)^{1/2} U \frac{H-H_0}{H^3} \qquad 3.1.11$$

From equation (3.1.10)

$$\frac{H-H_0}{H^3} = \frac{1}{H_0^2}\left[\frac{\frac{aS^{3/2}}{H_0}}{\left[1+\frac{aS^{3/2}}{H_0}\right]^3}\right] \qquad 3.1.12$$

and putting

$$\left(\frac{a}{H_0}\right)^{2/3} \cdot S = \zeta \;;\; dS = \left(\frac{H_0}{a}\right)^{2/3} d\zeta \qquad 3.1.13$$

gives

$$\frac{dQ}{d\zeta} = -48\left[\frac{W}{2\pi}\right]^{1/2} \frac{U}{H_0^2}\left[\frac{H_0}{a}\right]^{2/3}\left[\frac{\zeta^{3/2}}{\left[1+\zeta^{3/2}\right]^3}\right] \qquad 3.1.14$$

simplifying,

$$\frac{dQ}{d\zeta} = -10.68 \frac{U}{W^{1/6} H_0^{4/3}}\left[\frac{\zeta^{3/2}}{\left[1+\zeta^{3/2}\right]^3}\right] \qquad 3.1.15$$

Equation (3.1.15) therefore is a "Grubin-type" modified version of Reynolds equation using the Crook approximation to the Hertzian dry contact geometry.

The integration of

$$I = \int \frac{\zeta^{3/2}}{(1+\zeta^{3/2})^3} \cdot d\zeta \qquad 3.1.16$$

has been carried out by Wolveridge, Baglin and Archard, giving

$$I = \frac{(2\zeta^{3/2}-1)\zeta}{9(1+\zeta^{3/2})^2} - \frac{2}{27}\left[\frac{1}{2}\ln\left(\frac{(1+\zeta^{1/2})^2}{(\zeta-\zeta^{1/2}+1)}\right) + \sqrt{3}\tan^{-1}\left(\frac{(2-\zeta^{1/2})}{\sqrt{3}\,\zeta^{1/2}}\right)\right] \qquad 3.1.17$$

The present analysis refers to the value of this

integral for particular values of τ corresponding to S with some finite value $S=\chi$ by the notation $I_{S=\chi}$.

Numerical values of the integral for a full range of the variable τ have been evaluated by Wolveridge, Baglin and Archard and are shown in a modified form in table (4). It is not possible at this stage to evaluate corresponding values of S, the horizontal co-ordinate, since the relationship between τ and S contains an unknown value of H_o but two notable values, corresponding to $S=0$ and $S=\infty$ are:

$$S = \tau = 0 , \quad I_{S=0} = -0.2015 \qquad 3.1.18$$

$$S = \tau = \infty , \quad I_{S=\infty} = +0.0618$$

It will also be seen that

$$I_{S=\infty} - I_{S=0} = 0.26871 \qquad 3.1.19$$

From equation (3.1.19)

$$Q_{S=\chi} - Q_S = -10.68 \frac{U}{W^{1/6} H_0^{4/3}} \left[I \right]_S^i \qquad 3.1.20$$

where the suffix χ refers to the value of S at which the pressure curve starts, and the suffix S identifies the value of Q at any distance S from the edge of the Hertzian contact region.

At the inlet point $S=\chi$ the lubricant pressure will be zero and so the non-dimensional reduced pressure at this point $Q_{S=\chi}$ will be zero, giving

$$Q_S = 10.68 \frac{U}{W^{1/6} H_0^{4/3}} \left[I_{S=\chi} - I_S \right] \qquad 3.1.21$$

TABLE 4.3

Numerical values of the integral

given in equation (3.17)

ζ for $S=\infty$	INTEGRAL VALUE $I_{S=\infty}$	$I_{S=\infty} - I_{S=0}$
0	-0.201533	0
0.15263	-0.198267	0.003266
0.30526	-0.186146	0.015387
0.45789	-0.167240	0.034293
0.61052	-0.145188	0.056345
0.76315	-0.122770	0.078763
0.91578	-0.101598	0.099935
1.06841	-0.082414	0.119119
1.22104	-0.065435	0.136098
1.37367	-0.050599	0.150934
1.52630	-0.037719	0.163814
3.05260	+0.027125	0.228658
4.57890	+0.046976	0.248509
6.10520	0.055157	0.256691
7.63150	0.059247	0.260780
9.15780	0.061567	0.263100
10.68410	0.063004	0.264538
12.21040	0.063955	0.265488
13.73670	0.064615	0.266148
15.26300	0.065092	0.266625
22.89450	0.066238	0.267772
30.52600	0.066646	0.268179
38.15750	0.066837	0.268370
45.78900	0.066941	0.268474
53.42050	0.067003	0.268536
61.05200	0.067044	0.268573
68.68350	0.067072	0.268605
76.31500	0.067092	0.268625
152.63000	0.067156	0.268689
763.15000	0.067176	0.268711
∞	0.067179	0.268711

The second Grubin assumption is that the pressure at the inlet to the Hertzian contact region ($S=0$) will be very high: we take Grubins limiting case of

$q_r = \frac{1}{\alpha}$ at this point.

The relationship between the actual pressure p and the reduced pressure q_r is given by equation (2.22), and using the non-dimensional factors

$$P = p/E' \quad ; \quad Q = q_r/E' \quad ; \quad G = \alpha E' \qquad 3.1.22$$

this becomes

$$GP = -\ln(1-GQ) \qquad 3.1.23$$

for the conditions at inlet to the Hertzian contact region, $P=\infty$ at $S=0$,

$$Q_{S=0} = \frac{1}{G} \qquad 3.1.24$$

Equation (3.1.24) can be re-written for $S=0$ giving

$$Q_{S=0} = \frac{1}{G} = \frac{10.68\ U}{W^{1/6}\ H_0^{4/3}} \left[I_{S=\infty} - I_{S=0} \right] \qquad 3.1.25$$

This expression can be evaluated directly for an inlet point $S=\infty$ allowing a value of H_0 for this inlet condition, corresponding to a fully flooded contact, to be obtained.

This particular value of H_0 for a fully flooded contact will be indicated by $H_{0\infty}$. For this case, equation (3.1.25) becomes

$$\frac{1}{G} = 10.68 \frac{U}{W^{1/6}\ H_{0\infty}^{4/3}} \left[I_{S=\infty} - I_{S=0} \right] \qquad 3.1.26$$

and it has already been noted that

$$\left[I_{S=\infty} - I_{S=0} \right]$$

has a value of 0.26871 giving

$$H_{0\infty} = 2.2049 \frac{(GU)^{3/4}}{W^{1/8}} \qquad 3.1.27$$

Crook (10) gives the value of the film thickness in a fully flooded contact as:

$$H_{0\infty} = 2.4776 (\alpha \eta_0 \bar{u})^{3/4} R^{1/2} b^{-1/4} \qquad 3.1.28$$

where

$$b = 4R\sqrt{\frac{W}{2\pi}} \; ; \; \bar{u} = \tfrac{1}{2}(u_1 + u_2) \qquad 3.1.29$$

Noting that, in the present notation

$$U = \frac{\eta_0 u}{E' R} \; , \; u = \tfrac{1}{2}(u_1 + u_2), \; G = \alpha E' \qquad 3.1.30$$

giving, in particular, $\bar{U} = \dfrac{UE'R}{\eta_0}$

it is easily shown that Crooks formula for a fully flooded contact is equivalent to

$$H_{0\infty} = 2.2 \frac{(GU)^{3/4}}{W^{1/8}} \qquad 3.1.31$$

The present analysis is therefore in close agreement.

For the case of starved lubrication, defined by an inlet condition $S = X$, (where X has some value less than ∞), direct evaluation of equation (3.1.25) is not possible because the variable ζ, as defined in equation (3.1.13), itself contains the film thickness $H_{0_{S=X}}$ (H_{0_X} in short) corresponding to $S = X$, the particular inlet point.

It is possible though to express the film thickness H_{0_X} for this inlet condition as a proportion of the film thickness $H_{0\infty}$ for the fully flooded condition.

For the fully flooded case $S = \infty$, equation (3.1.25)

gives

$$(H_{0\infty})^{4/3} = 10.68 \frac{GU}{W^{1/6}} \left[I_{S=\infty} - I_{S=0} \right] \quad 3.1.32$$

and for the starved case, $S = X$,

$$(H_{0X})^{4/3} = 10.68 \frac{GU}{W^{1/6}} \left[I_{S=X} - I_{S=0} \right] \quad 3.1.33$$

For any starved condition therefore

$$\left[\frac{H_{0X}}{H_{0\infty}} \right]^{4/3} = \frac{\left[I_{S=X} - I_{S=0} \right]}{\left[I_{S=\infty} - I_{S=0} \right]} \quad 3.1.34$$

where $H_{0X}/H_{0\infty} = \rho$, the film thickness ratio.

This equation must itself be evaluated in terms of the variable $\bar{c}$ which contains the starved film thickness H_{0X}. However, if particular values of the non-dimensional factors U, G and W are specified the value of $H_{0\infty}$ can be calculated and, using values of the film thickness ratio ρ obtained from equation (3.1.34), values of H_{0X} can be found.

These values of H_{0X}, together with equation (3.1.13), allow the values of $\bar{c}$ used in the calculation of $I_{S=X}$ in equation (3.1.34) to be related to values of the non-dimensional inlet point $S = X$. This has been done for figure 5, which shows the variation in film thickness ratio ρ with change in inlet point $S = X$ for G = 5000, U = 1 x 10^{-11} and W = 3 x 10^{-5}; these being values typical of a moderately loaded steel-to-steel contact lubricated by a mineral oil.

A curve such as that shown in figure 5 is not generally applicable to any lubricated contact because of this need to specify the non-dimensional factors

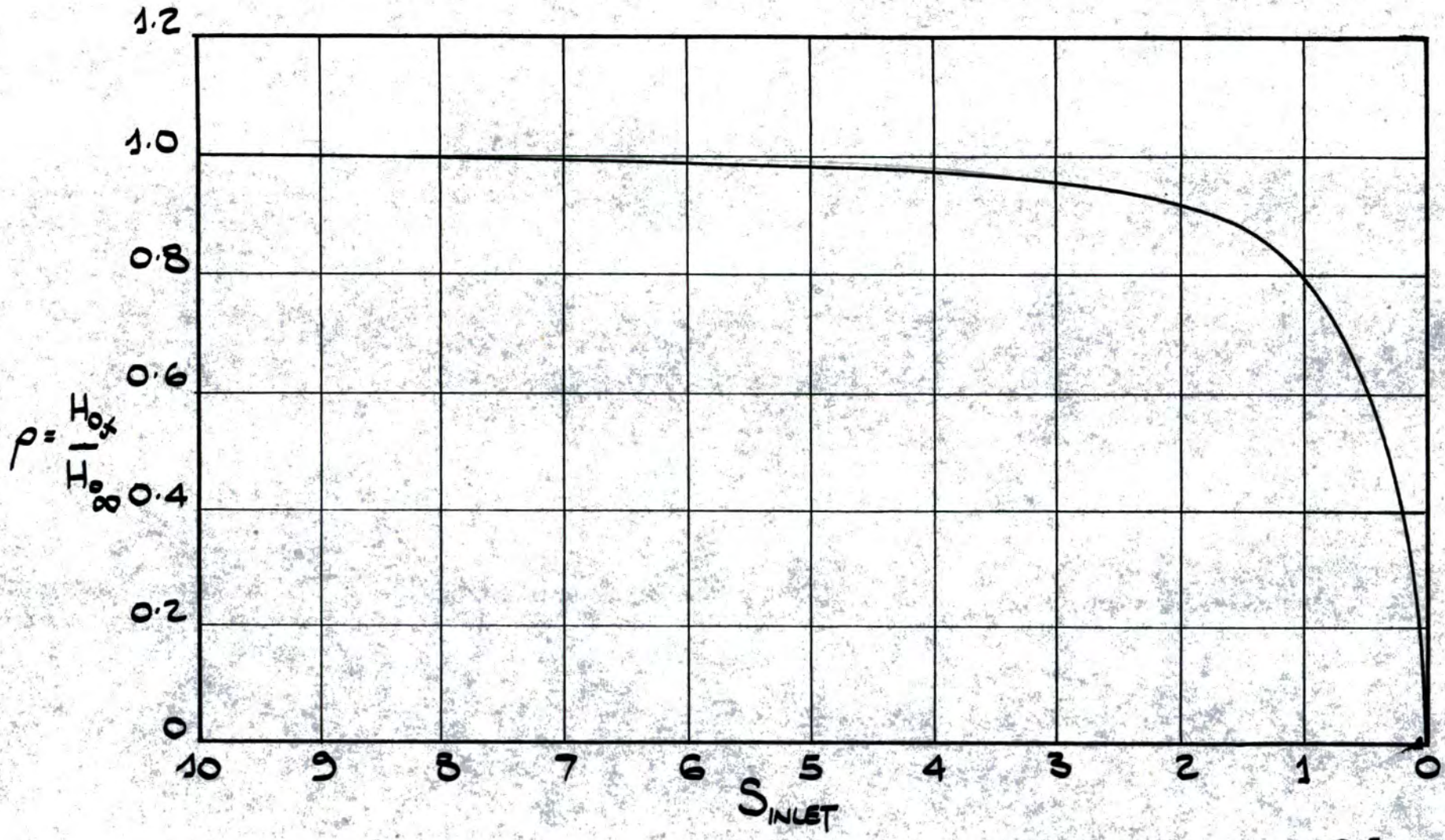

FIGURE 5 . VARIATION IN FILM THICKNESS RATIO WITH FILM INLET POINT

$G = 5000$
$U = 1 \times 10^{-11}$
$W = 3 \times 10^{-5}$

G, U and W before the curve can be plotted.

In order to overcome this difficulty, it is desirable to provide a horizontal co-ordinate based on S but containing the non-dimensional factors G, U and W, such that this new co-ordinate, say $\bar{S}$, is a function of ζ alone.

From equation (3.1.34) it follows that, since the Integral values are all functions of ζ alone,

$$\rho = \frac{H_{0x}}{H_{0\infty}} = f_4(\zeta) \qquad 3.1.35$$

and since

$$H_{0\infty} = \frac{2.2\,(GU)^{3/4}}{W^{1/8}} \; ; \; H_{0x} = 2.2\,\frac{(GU)^{3/4}}{W^{1/8}} \cdot f_4(\zeta) \qquad 3.1.36$$

The relationship given in equation (3.1.3) together with equation (3.1.36) gives

$$\zeta = \left[2.4W \, \frac{W^{1/8}}{2.2\,(GU)^{3/4}} \right]^{2/3} \cdot S \cdot f_4(\zeta) \qquad 3.1.37$$

which reduces to

$$f_4(\zeta) = 1.059 \, \frac{W^{3/4}}{(GU)^{1/2}} \cdot S \qquad 3.1.38$$

If the variable $\bar{S}$ is defined

$$\bar{S} = 1.059 \, \frac{W^{3/4}}{(GU)^{1/2}} \cdot S \qquad 3.1.39$$

it follows that

$$\bar{S} = f_4(\zeta) \qquad 3.1.40$$

Using equations (3.1.27) and (3.1.39) it can easily be shown that

$$\bar{S} = \left(\frac{H_{0x}}{H_{0\infty}} \right)^{2/3} \zeta \qquad 3.1.41$$

and

$$\bar{S} = \left(\frac{2.4W}{H_{o\infty}}\right)^{2/3} S \qquad 3.1.42$$

Figure 6 shows the variation of the film thickness ratio ρ with inlet parameter $\bar{S}$. This curve applies to all cylindrical contacts.

It should be noted that the variable $\bar{S}$ differs by only a numerical factor from the variable Ψ_i defined by Wolveridge, Baglin and Archard. Figure 6 is therefore directly comparable with figure 7 in reference (36) (see Appendix (U)), given that $\bar{S} = 1.44\,\Psi_i$

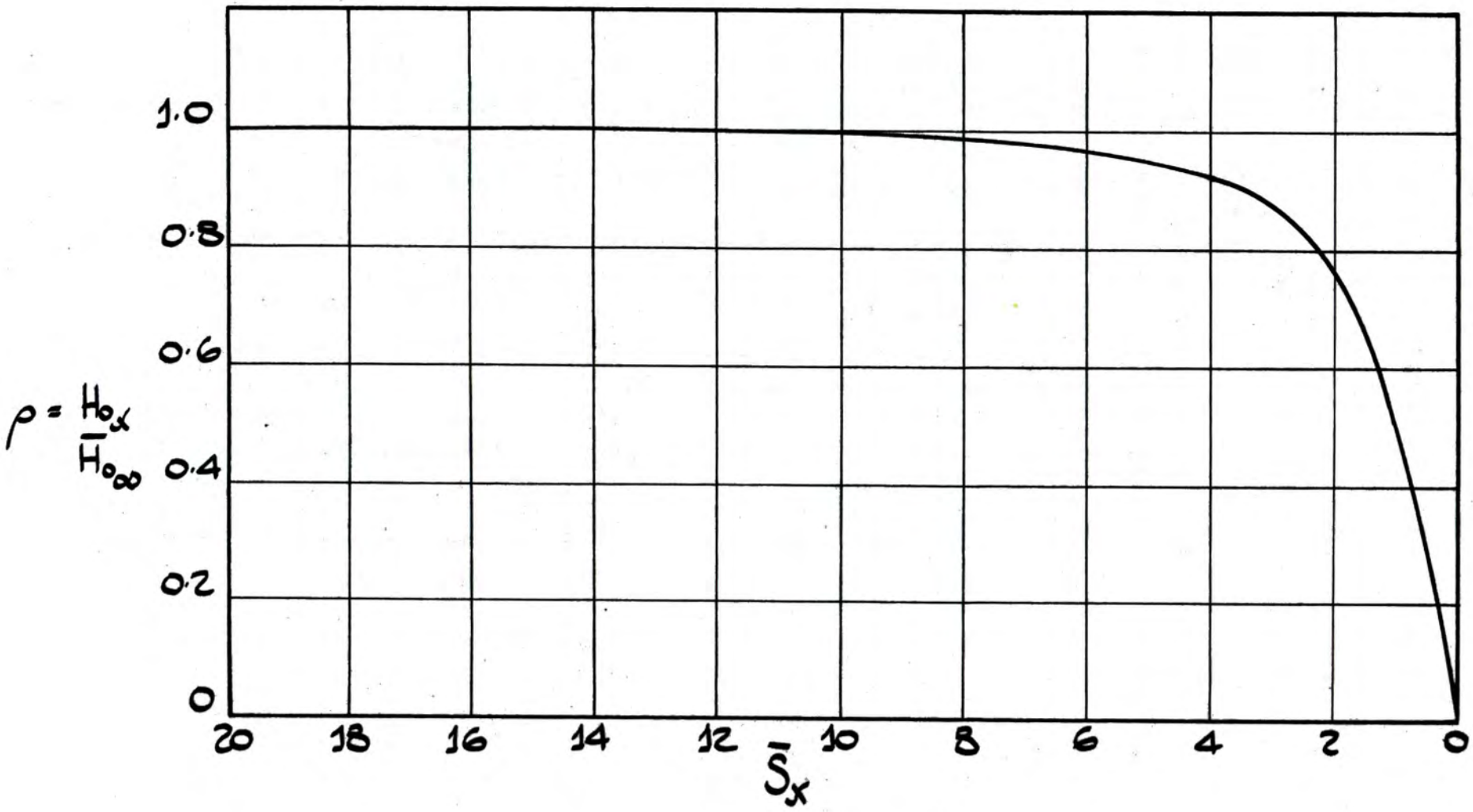

FIGURE 6. VARIATION IN FILM THICKNESS RATIO WITH FILM INLET PARAMETER

3.2 Evaluation of Inlet Pressure Distribution

It has been shown in equation (3.1.23) that the non-dimensional reduced pressure Q_s at any point S in a lubricated contact can be expressed in terms of the value of the integral (defined in equation (3.1.17)) at $S=X$, the inlet point, and the value of the integral at the particular point S.

For a starved contact, where the inlet point is $S=X$, equation (3.1.23) becomes

$$Q_s = 10.68 \frac{U}{H_{0X}^{4/3} W^{1/6}} \left[I_{S=X} - I_S \right] \qquad 3.2.1$$

At the edge of the Hertzian contact region, the Grubin assumption gives the condition $Q_{S=0} \rightarrow \frac{1}{G}$ and so equation (3.2.1) becomes

$$Q_{S=0} = \frac{1}{G} = 10.68 \frac{U}{H_{0X}^{4/3} W^{1/6}} \left[I_{S=X} - I_{S=0} \right] \qquad 3.2.2$$

Combining equations (3.2.1) and (3.2.2),

$$GQ_s = \frac{\left[I_{S=X} - I_S \right]}{\left[I_{S=X} - I_0 \right]} \qquad 3.2.3$$

and from equation (3.1.23),

$$GP_s = -\ln.(1 - GQ_s) \qquad 3.2.4$$

Using the above equations (3.2.3) and (3.2.4) the values of the non-dimensional pressure P_s at any point S in the inlet film of a starved contact can be found and it is possible, therefore, to present a family of curves giving the variation of non-dimensional

pressure P to a base of either S or $\bar{S}$ for a number of film inlet points $S=X$.

Because of the Grubin assumption of an infinite pressure at the edge of the Hertzian contact region, curves such as those proposed above have no physical significance but Castle and Dowson (8), whose results provide solutions in agreement with this present theoretical work, have generated complete pressure curves for a progressively starved practical EHD contact.

These pressure curves are reproduced in figure 7.

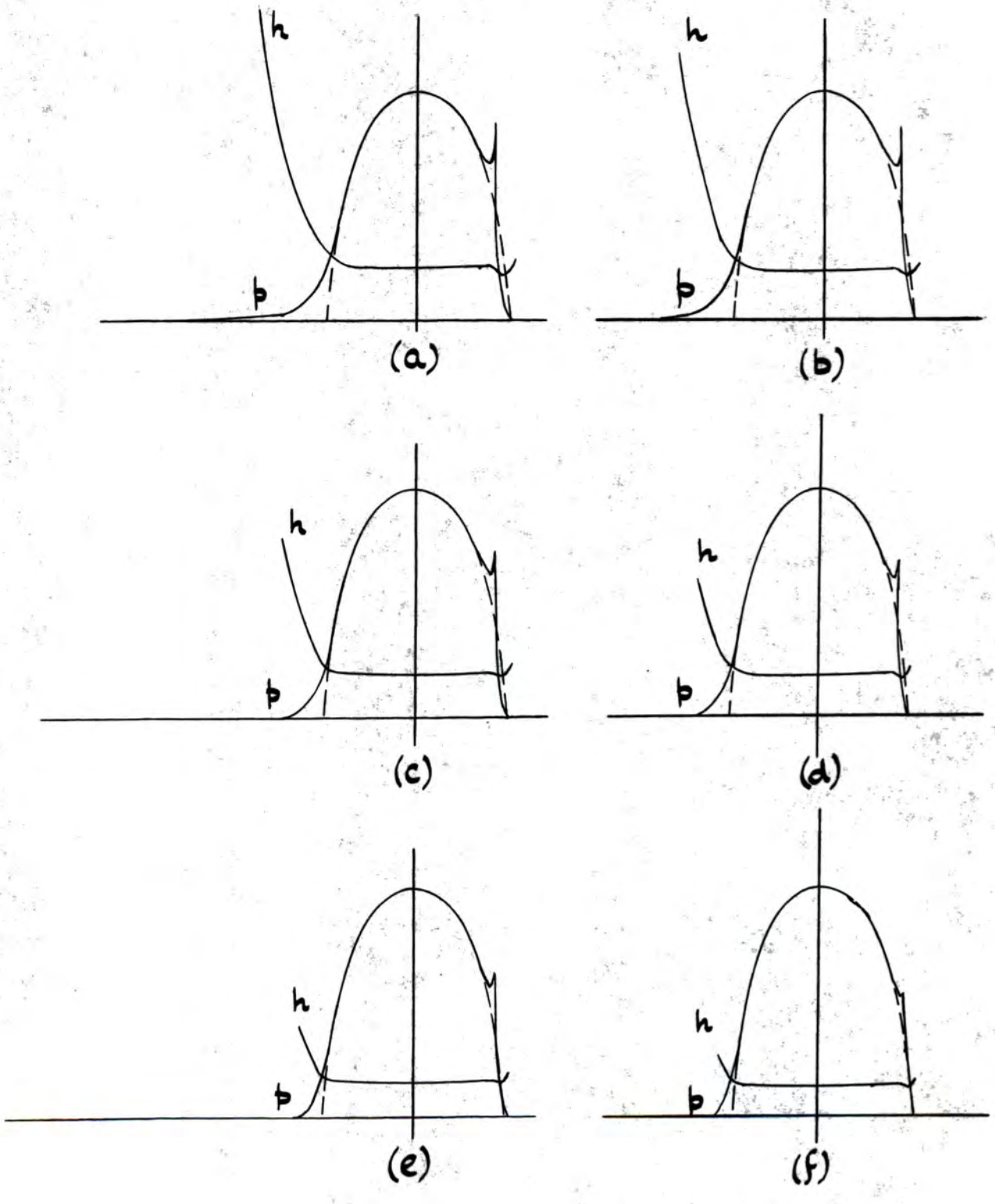

FIGURE 7. TYPICAL PRESSURE AND FILM THICKNESS PROFILES FOR A PROGRESSIVELY STARVED E.H.D CONTACT. MAXIMUM HERTZIAN PRESSURE CONSTANT.

REPRODUCED FROM REFERENCE 8.

3.3 Evaluation of Rolling Traction

The use of the Grubin model for the prediction of rolling traction in a contact is more speculative than the use of this model for the prediction of lubricant film thicknesses because neither the expression for P nor $\frac{dH}{dx}$ used in the analysis accurately represents the conditions known to exist in an actual contact. It cannot therefore be expected that the value of the rolling traction will be very accurate without some supporting evidence.

However, it should be noted that, as shown in Appendix (A), the Crook approximation for $\frac{dH}{dx}$ is in better agreement with the Hertzian value of $\frac{dH}{dx}$ at points close to the Hertzian contact and so would more nearly represent the dry Hertzian contact profile for starved conditions. The present analysis has been used to calculate values of rolling traction for flooded conditions and the results are quite close to the few full computer solutions available as shown in table 8.

Since both the Grubin model and the Crook approximation to film shape (these being the basis of this present analysis) would be expected to give a more accurate representation of the case of a contact operating under starved conditions, there are grounds for hoping that the predictions of the present analysis will be acceptably close to the real situation.

U	10^{-13}	10^{-12}	10^{-11}	10^{-10}	10^{-9}
$t_R/E'R$ FULL ANALYSIS	3.2×10^{-10}	2.1×10^{-9}	1.2×10^{-8}	0.55×10^{-7}	2.1×10^{-7}
$t_R/E'R$ PRESENT ANALYSIS	3.99×10^{-10}	2.24×10^{-9}	1.26×10^{-8}	0.71×10^{-7}	

Figure 8 A comparison between the results for the rolling traction at flooded contacts given by the present analysis and those obtained using a full analysis (reference (21)).

The hydrodynamic force components acting on a typical rolling contact bearing configuration are shown in figure 9.

The frictional traction per unit face width of contact on the surfaces is given by Crook (12) as

$$t_{1,2} = t_R \mp t_S \qquad 3.3.1$$

where

t_R is the contribution due to pure rolling

t_S is the contribution due to pure-sliding

It has also been shown in reference (12) that

$$t_R = -\frac{1}{2} \int_{INLET}^{OUTLET} h \cdot \frac{dp}{dx} \cdot dx \qquad 3.3.2$$

and

$$t_S = u \int_{INLET}^{OUTLET} \frac{\eta}{h} \cdot dx \qquad 3.3.3$$

where

h = the film thickness at a distance x from the centre of the Hertzian contact.

p = the pressure at position x

η = the viscosity at position x

u = the difference in surface velocities through the contact, $u = (u_2 - u_1)$

Considering the roller equilibrium under the action of the rolling and sliding components of the frictional traction, figure 10, it follows that $t_S = +t_R$. The total traction at the outer race is therefore $2t_R$, in the direction of rotation of the inner race. The present analysis considers only the contribution of the rolling traction since the

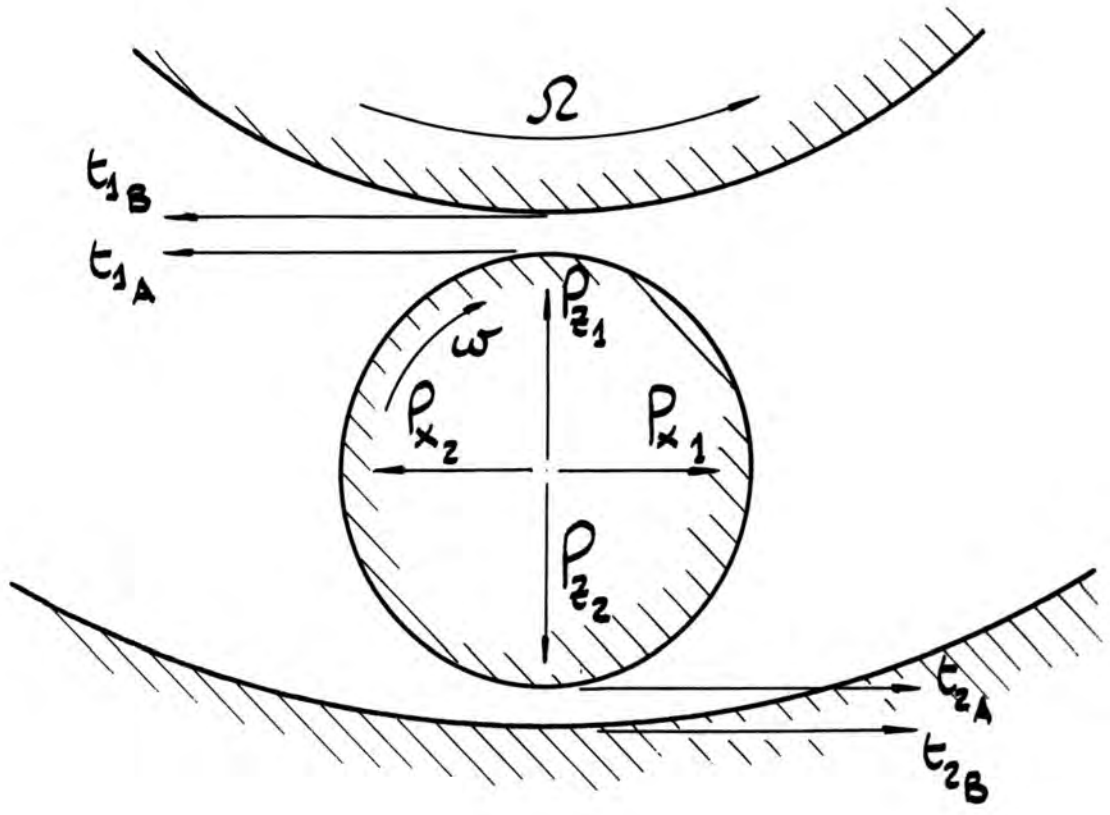

FIGURE 9 . HYDRODYNAMIC FORCE COMPONENTS ON AN E.H.D. CONTACT.

(REPRODUCED FROM REFERENCE 14)

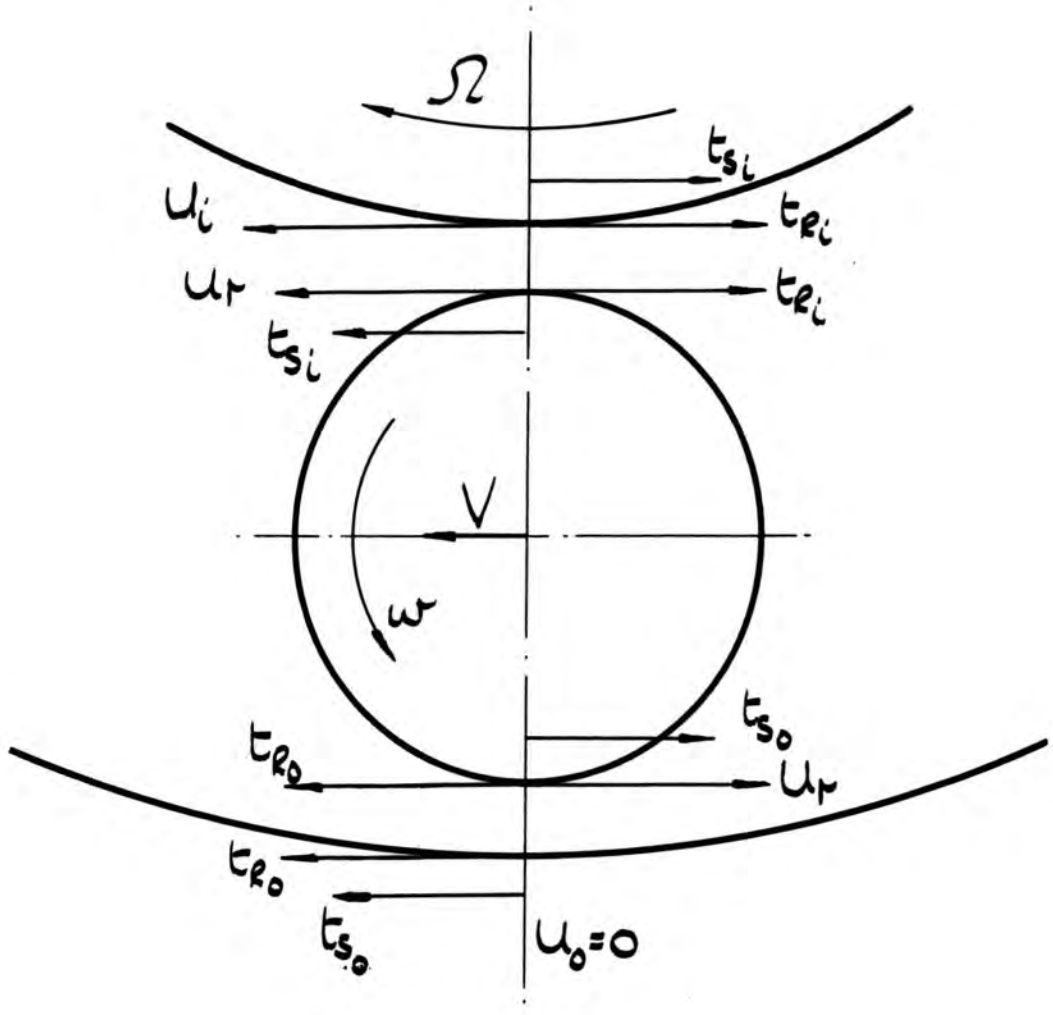

FIGURE 10 . ROLLER EQUILIBRIUM UNDER ROLLING AND SLIDING COMPONENTS OF TRACTION.

contribution of the sliding traction is, in most circumstances, equal to that of the rolling traction.

The contact slip necessary to provide this equilibrium condition can be shown to be very small and experimental evidence suggests that, for roller bearings operating under normal running conditions, the slip is in fact small. For starved lubrication, where lubricant film thicknesses will be somewhat less than those within a comparable contact operating under fully flooded conditions, it would appear that contact slip will be even less than that in the fully flooded case.

Equation (3.3.2) for the rolling traction within the contact can be re-written as

$$T_R = -\frac{1}{2}\int_{INLET}^{OUTLET} H \frac{dP}{dX}.dX \qquad 3.3.4$$

by using the non dimensional factors

$$T_R = \frac{t_R}{E'R} \; ; \; H = \frac{h}{R} \; ; \; P = \frac{p}{E'} \; ; \; X = \frac{x}{b} \; ; \; \frac{b}{R} = 4\sqrt{\frac{W}{2\pi}} \qquad 3.3.5$$

The integral part of equation (3.3.4) can be re-expressed as

$$\int_{INLET}^{OUTLET} H \frac{dP}{dX}.dX = \left[H.P\right]_{INLET}^{OUTLET} - \int_{INLET}^{OUTLET} P \frac{dH}{dX}.dX \qquad 3.3.6$$

and, considering the whole contact, the pressure is zero at both inlet and outlet and so

$$\left[H.P\right]_{INLET}^{OUTLET} = 0 \qquad 3.3.7$$

Equation (3.3.6) therefore reduces to

$$T_R = +\frac{1}{2}\int_{INLET}^{OUTLET} P \frac{dH}{dX}.dX \qquad 3.3.8$$

This equation would normally be evaluated for the whole contact length, but the integral limits can be modified by making certain observations about the nature of the contact. It is helpful to consider the pressure and film thickness profiles for a typical EHD contact and a curve of the variation of pressure p with film thickness h through the contact. These curves are shown in figure 11.

It is obvious from equation (338) that the area contained by the p/h curve is proportional to the rolling traction generated within the contact. It will be noted that:

i) the region of nearly constant h within the Hertzian contact region will make little contribution to the total rolling traction because the area under the p/h curve for this region is small due to the symmetry about the centre-line of the pressure and film shape.

ii) the outlet from the contact is a region where both $\frac{dH}{dx}$ and P will be significant. However, as will be noted from the p/h curve, the area representing the contribution of the outer region is many times less than that representing the contribution of the inlet region. It will also be noted that inclusion of area B in the contribution of the inlet region helps to offset the exclusion of area A, the contribution of the outlet region.

It is therefore in the spirit of this present analysis to consider only the contribution of the inlet

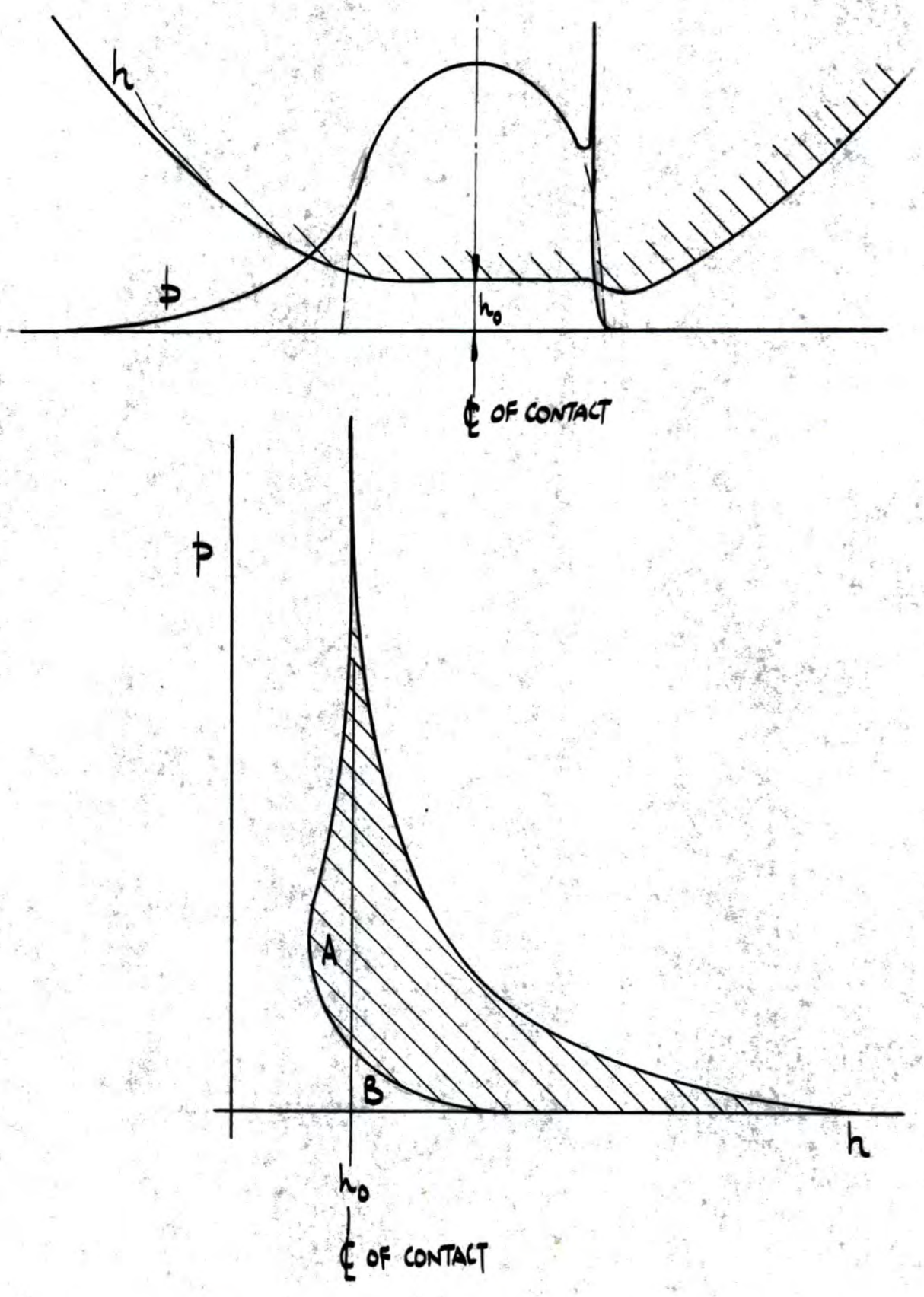

FIGURE 11. SKETCHES SHOWING PRESSURE AND FILM THICKNESS PROFILES FOR A TYPICAL E.H.D CONTACT AND ALSO THE VARIATION IN PRESSURE WITH FILM THICKNESS THROUGH THE CONTACT.

region to the total rolling traction.

Re-writing equation (3.3.8) for the inlet region only, and noting that $dS = -dx$,

$$T_R = -\frac{1}{2} \int_{INLET}^{0} P \frac{dH}{dS} . dS \qquad 3.3.9$$

It has been shown that

$$H - H_0 = 2.4 W S^{3/2}$$

giving

$$\frac{dH}{dS} = 3.6 W S^{1/2} \qquad 3.3.10$$

and, from the previous section

$$GQ_s = \frac{I_{S=x} - I_S}{I_{S=x} - I_0} \; ; \; GP_s = -ln.(1 - GQ_s) \qquad 3.3.11$$

The evaluation of both $\frac{dH}{dS}$ and P_s at incremental points in the inlet film (starting at $S = x$) allows a corresponding value of the rolling traction T_{Rx} to be evaluated. This can be done numerically by a method such as trapezoidal integration and a computer program for the evaluation of T_{Rx} using this method is shown in figure 12.

It is of course possible to show the variation of T_{Rx} with film inlet point $S = x$ by plotting T_{Rx} to a base of S but, as with the film thickness ratio $H_{ox}/H_{o\infty}$ such a curve will only be applicable for particular values of the non-dimensional factors G, U and W. Figure 13 shows this curve for G = 5000, $U = 1 \times 10^{-11}$ and $W = 3 \times 10^{-5}$.

```
      MASTER RAH4
      EVAL.OF ROLLING TRACTION
      REAL T1(30),T9(30),T10(30),T12(30),H2(30),S1(30),S2(30),S3(500),GQ
     1(500),GP(500),P(500),DH(500),PDH(500),S4(30),T15(500)
      READ(6,1) (T1(I),I=1,30)
    1 FORMAT(6G8.1)
      G=5000.
      W=1E-5
      U=1E-10
      N=100.
      H1=2.2049*((G*U)**0.75)/(W**0.125)
      DO 20, I=1,30
      T=T1(I)
      CALL WBA(T,T15)
      T9(I)=T15
      T10(I)=T9(I)*0.2015552627
      T11   =T10(I)/0.2687110169
      T12(I)=T11**0.75
      H2(I) =T12(I)*H1
      S1(I) =T1(I)*((H2(I))/(2.40084*W))**(2/3.0)
      S2(I) =S1(I)*1.06*((W**0.75)/((G*U)**0.5))
      S4(I) =1.0/S2(I)
      WRITE(1,30) G,U,W,T1(I),S1(I),S2(I),H1,T12(I),H2(I),S4(I)
   30 FORMAT(18X,2HG=,F5.0/,18X,2HU=,E13.5/,18X,2HW=,E13.5/,10X,10HTAU I
     1NLET=,F13.5/,12X,8HS INLET=,F13.5/,8X,12HS BAR INLET=,F13.5/,15X,7
     2HHO INF=,E13.5/,6X,14HHO CHI/HO INF=,F13.5/,13X,7HHO CHI=,E13.5/,6
     3X,14H1/S BAR INLET=,F13.5/)
          Y =S1(I)/(N-1)
      S3(1) =S1(I)
      S3(N) =1E-10
      DO 40, J=2,(N-1)
```

FIGURE 12, SHEET 1. PROGRAM FOR THE EVALUATION OF THE NON-DIMENSIONAL STARVED ROLLING TRACTION AT A SINGLE LUBRICATED CONTACT.

```
      S3(J) =S1(I)-((J-1)*Y)
   40 CONTINUE
      DO50,M=1,N,1
          T=S3(M)*(((2.40084*W)/H2(I))**(2/3.0))
      CALL WBA(T,T15)
      T13(M)=T15
       GQ(M)=(T9(I)-T13(M))/(T9(I)+0.20155526271)
       GP(M)=-(ALOG(1-GQ(M)))
        P(M)=((GP(M))/G)
       DH(M)=3.6013*W*(S3(M)**0.5)
      PDH(M)=P(M)*DH(M)
   50 CONTINUE
      TR1   =PDH(1)/2
      TR2   =PDH(N)/2
      TR3   =0.00000000000
      DO60 K=2,(N-1),1
        TR3=TR3+PDH(K)
   60 CONTINUE
        TR =(TR1+TR2+TR3)*(Y/2.0)
      RA1 =TR/0.14942E-07
      RA2 =((S2(I)**3.14159)/(S2(I)**2.0))
      RA3 =((0.212*RA2)/(1.0+(0.212*RA2)))
      RA4 =100.0*((RA1-RA3)/(RA1))
      RA5 =((0.20*RA2)/(1.0+(0.20*RA2)))
      RA6 =100.0*((RA1-RA5)/(RA1))
      WRITE(1,70),TR,RA1,RA3,RA4,RA5,RA6
   70 FORMAT(9X,12HROLL. TRAC.=,E13.5/,9X,17HROLL. TRAC.RATIO=,F13.5/,9X
     1,11HFUNCTION 1=,F13.5/,9X,14HPERCENT ERROR=,F13.5/,9X,11HFUNCTION
     22=,F13.5/,9X,14HPERCENT ERROR=,F13.5///)
   20 CONTINUE
      STOP
      END
```

```
      SUBROUTINE WBA (T,T15)
      T2=T**0.5
      T3=T**1.5
      T4=(T*((2*T3)-1))/(9*((1+T3)**2))
      T5=0.5*ALOG(((1+T2)**2)/(1+T-T2))
      T6=(3**0.5)*ATAN((2-T2)/((3**0.5)*T2))
      T7=T5+T6
      T8=T/*2/27.0
      T15=T4-T8
      RETURN
      END
```

FIGURE 12, SHEET 2.

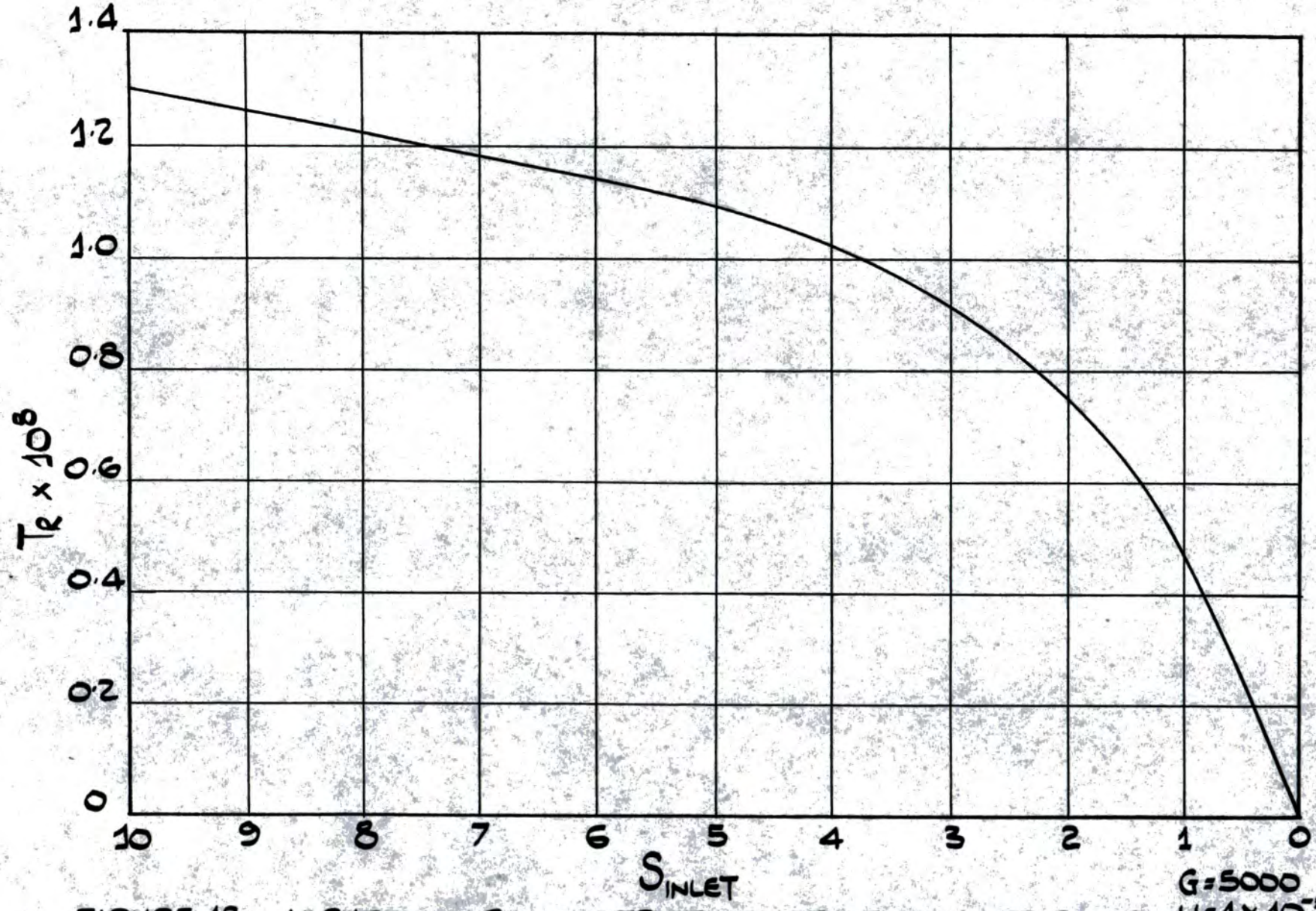

FIGURE 13 . VARIATION IN ROLLING TRACTION WITH FILM INLET POINT

The inlet parameter $\bar{S}$, defined in equation (3.3.9), provides a more useful horizontal co-ordinate, but it will be noted that Re_x itself is not independent of G, U and W.

Considering again the evaluation of Re_x it follows from equations (3.2.3) and (3.2.4) that

$$P_s = \frac{1}{G} f''(\zeta) \qquad 3.3.12$$

Equation (3.3.8) gives

$$dS = \frac{(GU)^{1/2}}{W^{3/4}} . d\zeta \qquad 3.3.13$$

and, from equations (3.3.8) and (3.3.9)

$$\frac{dH}{dS} = W^{5/8} (GU)^{1/4} f''(\zeta) \qquad 3.3.14$$

It can therefore be shown that

$$Re_x = \frac{U^{3/4}}{G^{1/4} W^{1/8}} f''(\zeta)_{S=x} \qquad 3.3.15$$

Similarly for Re_∞,

$$Re_\infty = \frac{U^{3/4}}{G^{1/4} W^{1/8}} f''(\zeta)_{S=\infty} \qquad 3.3.16$$

and of course in this case $f''(\zeta)_{S=\infty}$ will be invariable.

If a rolling traction ratio $\psi = \frac{Re_x}{Re_\infty}$ is defined it will be seen that this ratio is a function of $(\zeta)_{S=x}$ alone i.e.

$$\psi = \frac{Re_x}{Re_\infty} = \frac{f''(\zeta)_{S=x}}{f''(\zeta)_{S=\infty}} = f''(\zeta)_{S=x} \qquad 3.3.17$$

The definition of the variable $\bar{S}$ gives

$$\bar{S}_{S=x} = \frac{S}{=x} \cdot \frac{W^{3/4}}{(GU)^{1/2}} = \frac{(GU)^{1/2}}{W^{3/4}} \cdot f''(\zeta)_{S=x} \cdot \frac{W^{3/4}}{(GU)^{1/2}}$$

so

$$\bar{S}_{S=x} = f''(\zeta)_{S=x} \qquad 3.3.18$$

It therefore follows that

$$\psi = \frac{T_{e_x}}{T_{e_\infty}} = f^4(\bar{S})_{S=x} \qquad 3.3.19$$

where $(\bar{S})_{S=x} = \bar{S}_x$.

The present analysis evaluates T_{e_x} for particular values of G, U and W but equation (3.3.19) shows that, provided the results are expressed in terms of the rolling traction ratio and relative to the inlet parameter $\bar{S}_x$ the results obtained are applicable to any lubricated cylindrical contact.

The value of T_{e_∞} cannot be evaluated directly because of the integral limits necessary in equation (3.3.9) and the value must be estimated by extrapolation from results obtained for large values of $\bar{S}_x$. Figure 14 shows the variation of T_{e_x} with log $1/\bar{S}_x$ for the values of G, U and W used previously. It will be noted that as $1/\bar{S}_x$ approaches zero, T_{e_x} approaches a value of 1.5×10^8. This value has been assigned to T_{e_∞} for this particular set of non-dimensional conditions.

Figure 15 shows the variation of the rolling traction ratio ψ with inlet parameter $\bar{S}_x$. As stated previously, although this curve has been plotted for particular values of G, U and W, equation (3.3.19) shows that this curve is applicable to any single lubricated cylindrical contact.

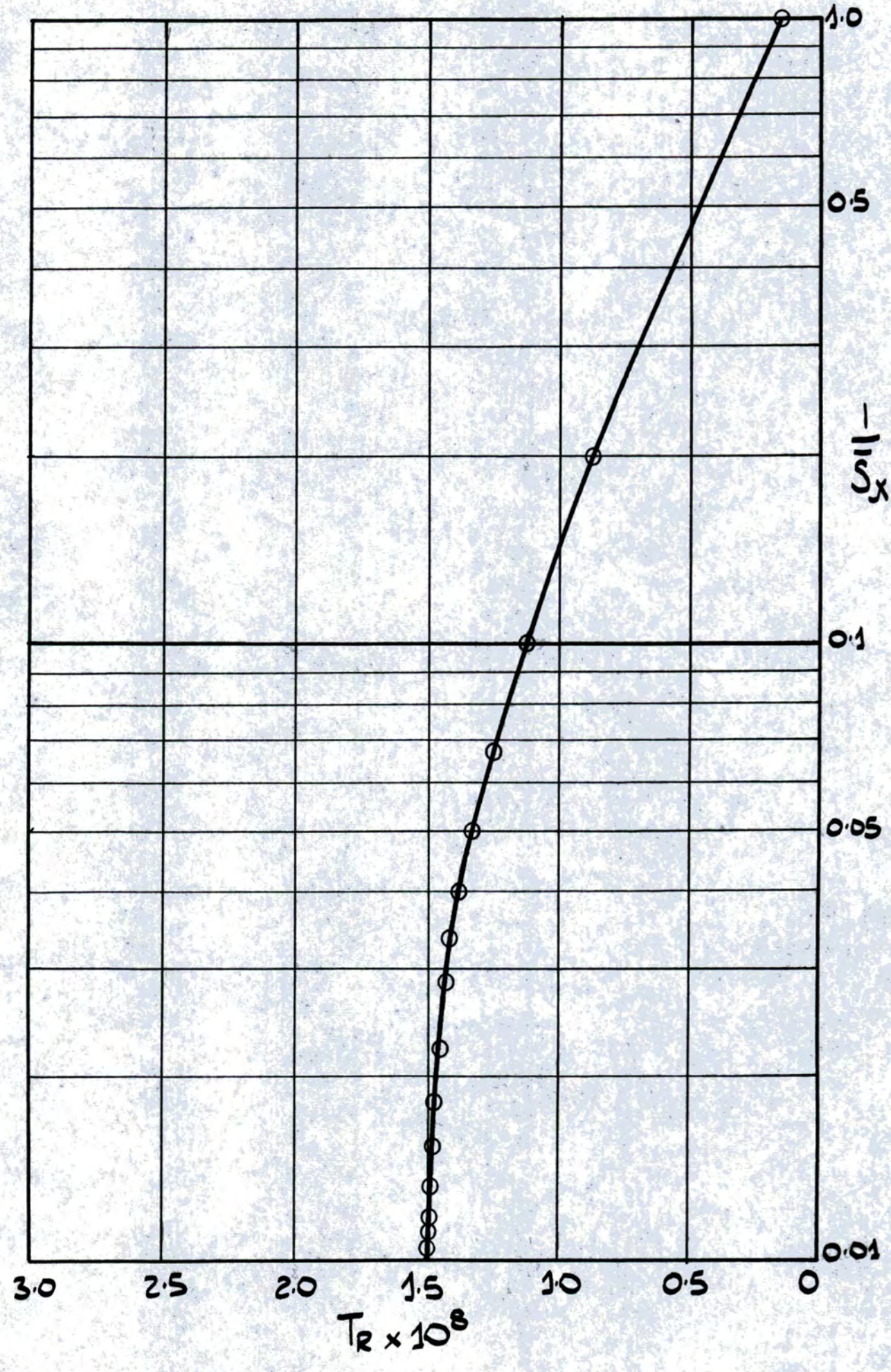

FIGURE 14 . VARIATION IN ROLLING TRACTION WITH $1/\bar{S}_x$

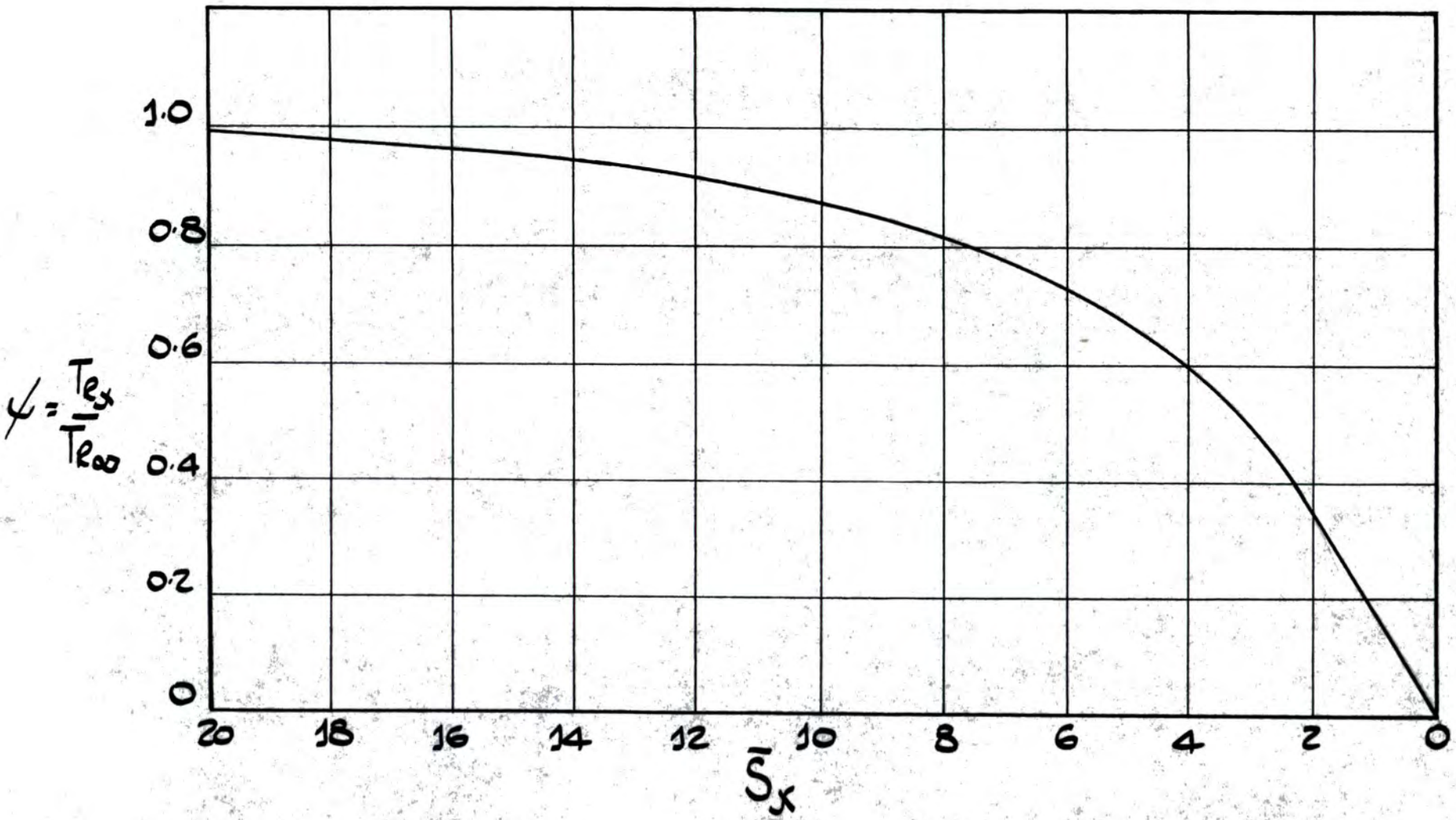

FIGURE 15 . VARIATION IN ROLLING TRACTION RATIO WITH FILM INLET PARAMETER

3.4 The Bearing Assembly

The analysis so far developed has been wholly concerned with the effects of lubricant starvation on a single cylindrical contact.

This theoretical work can be extended to predict the effects of lubricant starvation in a roller bearing assembly providing assumptions of load sharing and lubricant distribution are made. Figure 16 shows a typical bearing assembly and also the theoretical load distribution assuming a rigid bearing housing and perfect bearing geometry.

The present analysis uses the above simplifying assumptions, but it will be appreciated that these assumptions are limited in the extent to which they model an actual bearing assembly. A deviation from either of the above conditions can have a considerable effect on the load sharing between the rollers of an assembly. Dowson and Higginson (14) have analysed the case of non rigid components and bearing clearance; Münnich, Erhard and Niemeyer (28) have investigated the effects of housing stiffness. Each analysis shows that the effect under consideration causes an appreciable change in load distribution within the assembly.

For the idealised case shown in figure 16, Dowson and Higginson have shown that

$$F_{max} \approx \frac{4P}{z} \qquad 3.4.1$$

where P is the total bearing load and z is the number of rollers in the assembly.

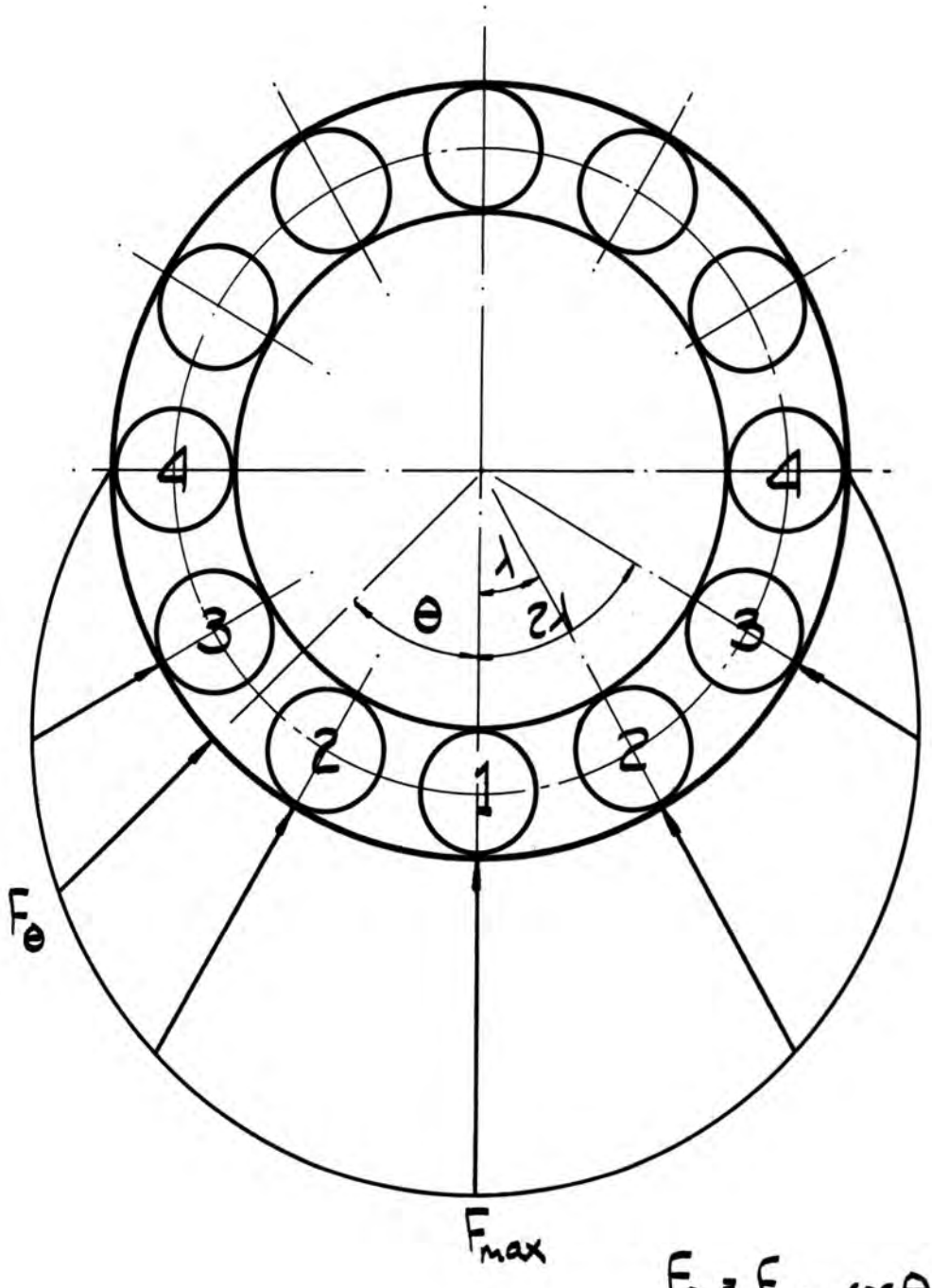

FIGURE 16 . THEORETICAL LOAD DISTRIBUTION IN A BEARING ASSEMBLY.

It follows that

$$F_\theta = \frac{4P}{z}\cos\theta \qquad 3.4.2$$

Considering again equation (3.3.9), it will be seen that the variable $\bar{S}_x$ to which both film thickness ratio ρ and rolling traction ratio ψ have been related, is a function of the contact parameters G, U and W in addition to being a function of the film inlet point $S=x$. For a given inlet condition therefore, $\bar{S}_x$ will vary with G, U and W. Whilst G and U will be constant for given operating conditions and bearing material, W, the non dimensional roller load, will depend on the roller's position in the assembly.

The variation in $\bar{S}_x$ with roller position is of the utmost importance, since it allows the evaluation of contact conditions for all rollers from known, or assumed, contact conditions for the most heavily loaded roller. It is necessary to make certain assumptions regarding the distribution of lubricant in the assembly before this variation in $\bar{S}_x$ can be determined.

Crook (9) has noted that, in experiments conducted on a two disc machine, the lubricant films on the rolling surfaces were tenaciously maintained during tests and that the lubricant was only slowly replaced from the supply.

Lauder (24), discussing experiments carried out on a disc slider machine modelling the conditions of isoviscous, incompressible lubricant and rigid surfaces

(lubricant flowrate being just adequate to maintain full lubrication) noted that at any given load and speed condition the inlet boundary of the lubricant film took up a well defined position. One of Lauder's aims was the visual observation of the film profile at inlet: he noted that this profile was disturbed by an increase in lubricant flowrate and also that the actual position of the inlet boundary appeared to move away from the conjunction, albeit slightly. Readings of film thickness, pressure and friction force were not noticeably changed. As a result of the work reported in reference (24), Lauder proposed the film inlet condition

$$p=0,\ u=\frac{\partial u}{\partial y}=0 \qquad 3.4.3$$

Boness (7) has considered the work of Lauder and, additionally, carried out a theoretical investigation into the effects of lubricant starvation on both lightly loaded and EHD lubricated rolling contacts. Although difficulties in computation prevented Boness from satisfactorily concluding this work, he suggests that the position of the inlet boundary will have a dramatic effect on both the load carrying capacity and friction force at the rolling contact, the effect on the friction force being less marked. He is also of the opinion that the inlet condition proposed by Lauder represents the minimum oil supply required by a lubricated contact, and is not unique to all problems.

Boness states that at the time of his work, no general up-stream boundary condition has been found which

can be applied to all contacts. To the author's knowledge, this is still the case.

As a result of his work, Boness considers that the position of the inlet boundary is primarily determined by the oil flowrate to the contact zone.

The observations of Lauder for the case of sliding contact and the predictions of Boness for the case of rolling contact would appear to indicate different mechanisms for the determination of the inlet position of the lubricant film. Both authors do agree, though, that the position of the inlet boundary is determined by the rate of lubricant flow together with load and speed conditions at the contact. The emphasis placed on each differs with the contact condition, either rolling or sliding, being considered.

Boness's work can be directly related to the rolling contacts within a bearing assembly, suggesting that in this case the lubricant flowrate will be a primary deciding factor in the positioning of the inlet boundary. Once the flowrate has been fixed, less significant variations in inlet point will take place as speed and load conditions at the contact are altered.

Further, the observations of Crook (whilst particular to a single lubricated contact) can possibly be applied to a bearing assembly as well. This suggests that once the quantity of lubricant on a roller has been determined by the rate of lubricant supply, this quantity remains sensibly constant.

irrespective of the roller's position in the assembly.

The following work makes no attempt to provide a solution to the obviously complex problem of defining the film inlet point in terms of all the variables which could affect this parameter but rather considers that, as an initial step, the position of the inlet boundary is known. Crook's results have been taken as giving some justification to the assumption that the lubricant films on the rolling surfaces within the bearing will not vary with position in the assembly.

From figure 17 , showing a single lubricated contact, it is proposed that the film inlet point can simply be described as the point $h_{INLET} = h_1$, this value of h_1 being the same for all rollers in the assembly.

Other criteria describing the inlet points for the rollers in the assembly could be proposed, and Appendix (S) contains an alternative analysis based on another assumption. In this case it is argued that since the inlet contact geometry is only slightly modified by variations in load on the contact (figure Appendix (S)), variations in inlet point with load will be slight. The film inlet point can simply be taken as occuring at a given value of x , measured from the centre line of the contact and (once again assuming that the lubricant films on the rolling surfaces do not vary with the position in the assembly) that this value of x will be the same for all the assembly rollers.

From equation (342),

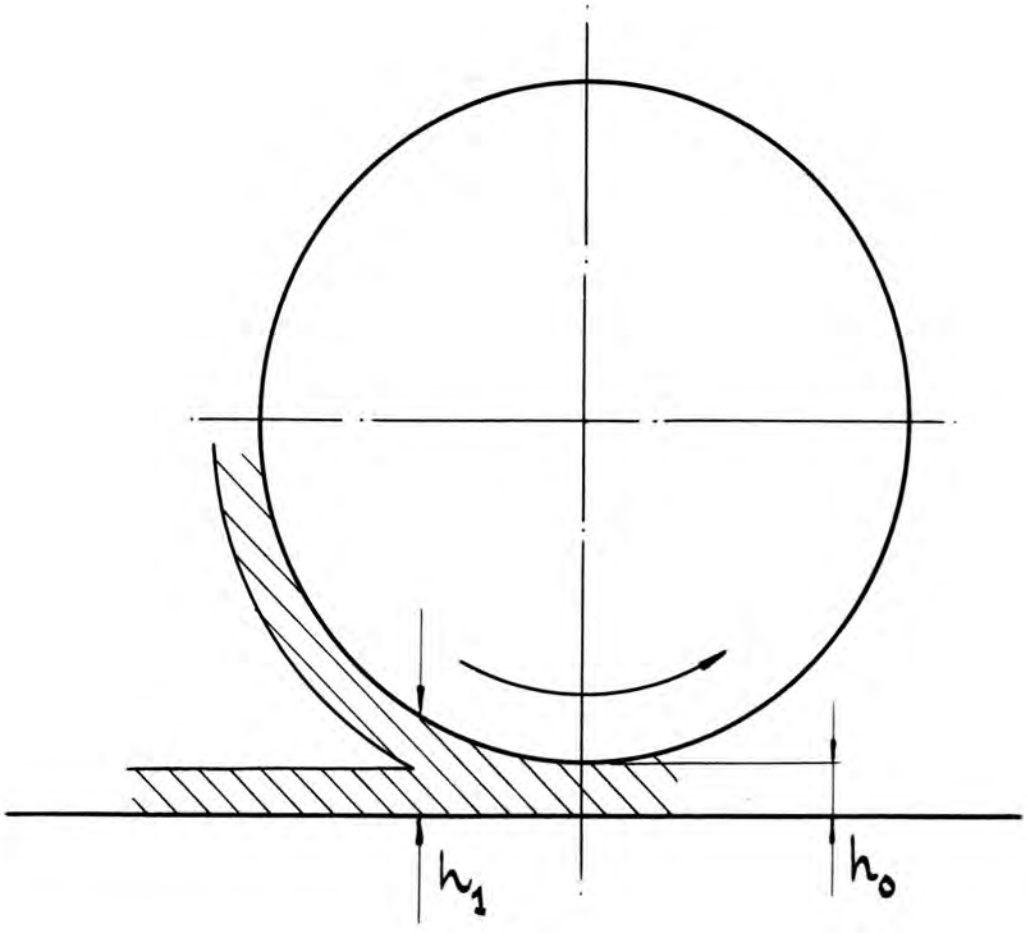

FIGURE 17 . SINGLE LUBRICATED CONTACT SHOWING THE FILM INLET POINT ASSUMPTION $h_{INLET} = h_1 = \text{constant.}$

$$W_\theta = W_1 \cos\theta \qquad 3.4.4$$

where W_θ is the non-dimensional load on a roller at angle θ to the line of action of the load, and W_1 is the load on the most heavily loaded roller.

The assumed film inlet point $h = h_1$ for all rollers in the assembly is, in non-dimensional terms, $H = H_1$ and so from equation (3.1.10),

$$2.4\, W_1\, S_x^{3/2} = H_1 - H_o \qquad 3.4.5$$

for the most heavily loaded roller.

The film thickness ratio ρ has been shown to be a function of $\bar{S}_x$ alone and, from figure 6, it will be seen that $\rho > 0.8$ for $\bar{S}_x > 2$. For contacts other than those severely starved therefore, the ratio ρ can be considered as unity, and so $H_{ox} = H_{o\infty}$. From equation (3.4.5),

$$S_x = \left(\frac{H_1 - H_{o\infty}}{2.4\, W_1} \right)^{2/3} \qquad 3.4.6$$

, $H_{o\infty}$ being given in equation (3.1.27) as

$$H_{o\infty} = \frac{2.2\,(GU)^{3/4}}{W_1^{1/8}} \qquad 3.4.7$$

The term $W_1^{1/8}$ will be small compared with $(1/W_1)^{2/3}$ and so, to a good approximation,

$$S_x \propto \left(\frac{1}{W_1} \right)^{2/3} \qquad 3.4.8$$

G and U being constant. From the definition of $\bar{S}_x$ given in equation (3.1.39),

$$\bar{S}_x \propto W_1^{1/12} \qquad 3.4.9$$

for the most heavily loaded roller.

In general therefore,

$$\frac{\bar{S}_\theta}{\bar{S}_1} = (\cos\theta)^{1/12} \qquad 3.4.10$$

where $\bar{S}_\theta$ is the value of $\bar{S}_x$ for a roller at angle θ, and $\bar{S}_1$ is the value of $\bar{S}_x$ for the most heavily loaded roller. This ratio can be taken as unity for the values of θ for which EHD theory can be considered to apply, and so $\bar{S}_x$ can be taken as constant for the rollers in the assembly.

It will be noted in Appendix (S) that the alternative analysis gives a corresponding equation (S.7)

$$\frac{\bar{S}_\theta}{\bar{S}_1} = (\cos\theta)^{1/4} \qquad 3.4.11$$

which cannot be considered as unity.

This present analysis gives, in an exactly parallel way to that used by Garnell and Higginson (21), that the total rolling traction for a bearing operating under starved conditions can simply be obtained by evaluating the starved rolling traction for the most heavily loaded roller and multiplying by the number of rollers known to be in contact.

It will be noted that the foregoing paragraphs require that the value of H_1 is initially defined and this is most easily done by taking

$$H_1 = m H_{0\infty} \qquad 3.4.12$$

in equation (3.46), the value of m effectively determining the degree of starvation. It can easily be shown that, if

$$k = (m-1)^{2/3} \qquad 3.4.13$$

equation (3.48) simply becomes

$$\bar{S}_x = k \qquad 3.4.14$$

using the definition of $\bar{S}_x$ in equation (3.49).

The preceding work can easily be applied to the test bearings used in the experimental work reported in later sections. Figure 18 shows the program used to evaluate the friction torque on the test bearing outer race due to the rolling traction at all the outer race/roller contacts.

For the test bearings, the non-dimensional parameters used in the program are given by

$$\begin{aligned} U &= 0.985 \times 10^{-13} \times \eta_0 N \\ W &= 1.085 \times 10^{-5} \times Q \\ G &= 5000 \end{aligned} \qquad 3.4.15$$

where

η_0 = lubricant viscosity in poise
N = shaft speed in rev/minute
Q = total bearing load in kN.

Also, the relationship between the non-dimensional starved rolling traction Tr_x and the friction torque on the test bearing outer race, f_{r_0}, is

$$f_{R_0} = 1.46 \times 10^{6} \times T_{R_s} \qquad 3.4.16$$

Figures 19 , 20 , and 21 show the variation in test bearing friction torque due to rolling traction alone with γN for various values of the starvation factor m for bearing loads of 1kN, 10kN and 20kN respectively, using the results obtained from the program shown in figure 18 .

Figures 20 and 21 , both for loading conditions where 5 rollers are in contact, show that at high values of the starvation factor, the Garnell and Higginson curve, reference (21), for flooded rollers is well followed - agreement could possibly be improved if the slight differences in test bearing geometry were taken into account.

Figure 19 , for a loading condition where only three rollers are in contact, indicates that the Garnell and Higginson curve is exceeded at high values of the starvation factor.

This apparent anomoly is due to the slight inverse variation of T_{R_s} with load which has been included in all the theoretical curves shown in figures 19 , 20 and 21 . The Garnell and Higginson analysis for flooded rollers was based on values of T_{R_∞} which are virtually independant of load, as shown in Appendix (T). Their analysis rightly considers T_{R_∞} constant: the present analysis does not consider T_{R_s} constant since its variation with load appears to be more significant.

```
      MASTER RAH10
      EVAL, OF VARIATION IN TOTAL OUTER RACE/ROLLER FRICTION TORQUE WITH
      ETA N FOR TEST BEARINGS NU310 AND N 310 USING INLET CONDITION H=H1
      =CONSTANT,
      REAL Q(5),W(5),EN(8),HOINF(8),SBAR(8),S(8),Y,S3(500),T15(500),GQ(
     1500),GP(500),P(500),DH(500),PDH(500),TRA,TRB,TRC,TR(8),FR(8),A,G,U
     2(8),T,T2,T3,T4,T5,T6,T7,T8,T15,H1(8)
      INTEGER N,B,V,K,J,M,R
      DIMENSION ESBAR(50,5,8),EHOINF(50,3,8),EEN(50,3,8),EH1(50,3,8),ETR
     1(50,5,8),EFR(50,3,8)
      READ(6,1) (Q(V),V=1,5,1)
    1 FORMAT(5G8.1)
      G=5000
      N=100
      DO2,B=2,50,4
      A=((B-1.0)**(2/3.0))
      DO5,V=1,5,1
      W(V)=Q(V)*1.085E-5
      DO 20,K=1,8,1
      EN(K) = 500.0*K
      EEN(B,V,K)=EN(K)
      U(K)=EN(K)*0.985E-13
      HOINF(K)=2.2049*((G*U(K))**0.75)/(W(V)**0.125)
      EHOINF(B,V,K)=HOINF(K)
      H1(K)=B*HOINF(K)
      EH1(B,V,K)=H1(K)
      S(K)=((HOINF(K)/(2.40084*W(V)))**(2/5.0))*A
      SBAR(K) = A
      ESBAR(B,V,K)=SBAR(K)
      Y = S(K)/(N-1)
      S3(1)=S(K)
      S3(N)=1E-10
      DO40 J = 2,(N-1),1
      S3(J)=S(K)-((J-1)*Y)
   40 CONTINUE
      DO 50 M = 1,N,1
      T = S3(M)*(((2.40084*W(V))/HOINF(K))**(2/3.0))
      T2=T**0.5
      T3=T**1.5
      T4=(T*((2*T3)-1))/(9*((1+T3)**2))
      T5=0.5*ALOG(((1+T2)**2)/(1+T-T2))
      T6=(3**0.5)*ATAN((2-T2)/((3**0.5)*T2))
```

FIGURE 18, SHEET 1. PROGRAM FOR THE EVALUATION OF TOTAL TEST BEARING FRICTION TORQUE DUE TO THE ROLLING CONTACTS.

```
      T7=T5+T6
      T8=T7*2/27.0
      T15=T4-T8
      T13(M)=T15
      GQ(M)=(T13(1)-T13(M))/(T13(1)+0.2015532627)
      GP(M)=-(ALOG(1-GQ(M)))
      P(M)=((GP(M))/G)
      DH(M)=3.6013*W(V)*(S3(M)**0.5)
      PDH(M)=P(M)*DH(M)
   50 CONTINUE
      TRA=PDH(1)/2.0
      TRB=PDH(N)/2.0
      TRC=0.0000000000
      DO60 R = 2,(N-1),1
      TRC=TRC+PDH(R)
   60 CONTINUE
      TR(K)=(TRA+TRB+TRC)*(Y*0.5)
      ETR(B,V,K) =TR(K)
      GO TO (62,63,63),V
   62 TR(K)=3*TR(K)
      GOTO 65
   63 TR(K)=5*TR(K)
   65 FR(K)=TR(K)*1.46E6
      EFR(B,V,K)=FR(K)
   20 CONTINUE
    3 CONTINUE
    2 CONTINUE
      DO 80 V = 1,3,1
      DO85,B=2,50,4
      WRITE(1,86)Q(V),G,B
   86 FORMAT(10X,15HBEARING LOAD=,F5.1,3HKN./,21X,2HG=,F7.1/,10X,9HHO IN
     1LET=,I5,9HX HO INF./,4X,86HETA N (POISE*RPM)  SBAR INLET  HO INF
     2HO CHI  N/D ROLL. TRAC.  FRICTION TORQUE (N.M.)///)
      DO 90 K=1,8,1
      WRITE(1,91) EEN(B,V,K),ESBAR(B,V,K),EHOINF(B,V,K),EH1(B,V,K),ETR(B
     1,V,K),EFR(B,V,K)
   91 FORMAT(/X,F7.1,8X,F8.3,8X,E13.5,8X,E13.5,8X,E13.5,8X,E13.5//)
   90 CONTINUE
   85 CONTINUE
   80 CONTINUE
      STOP
      END
```

FIGURE 18, SHEET 2.

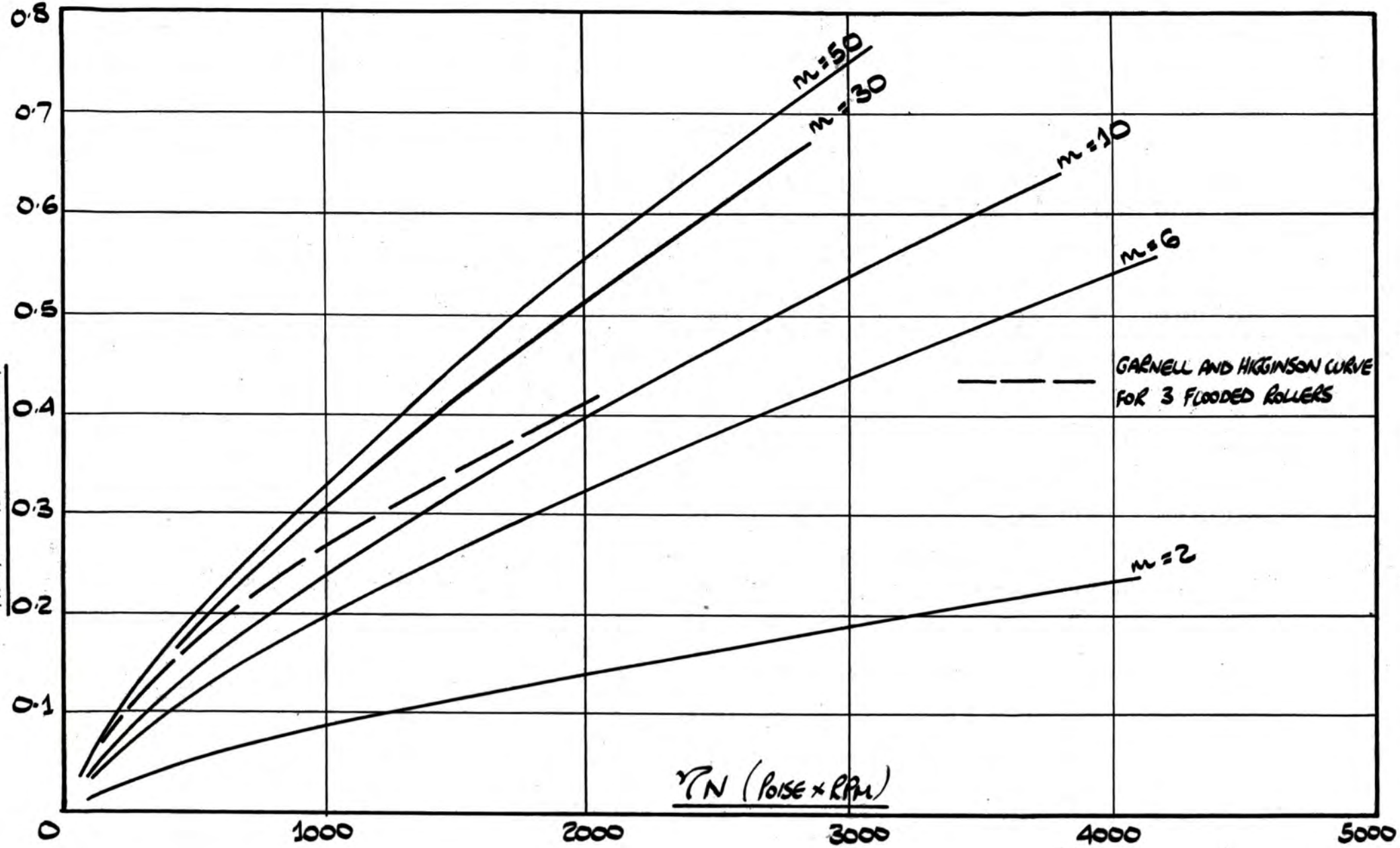

FIGURE 19 . THEORETICAL TOTAL ROLLING FRICTION CURVES FOR THE TEST BEARINGS, SHOWING THE EFFECT OF LUBRICANT STARVATION. BEARING LOAD 1kN, 3 ROLLERS IN CONTACT

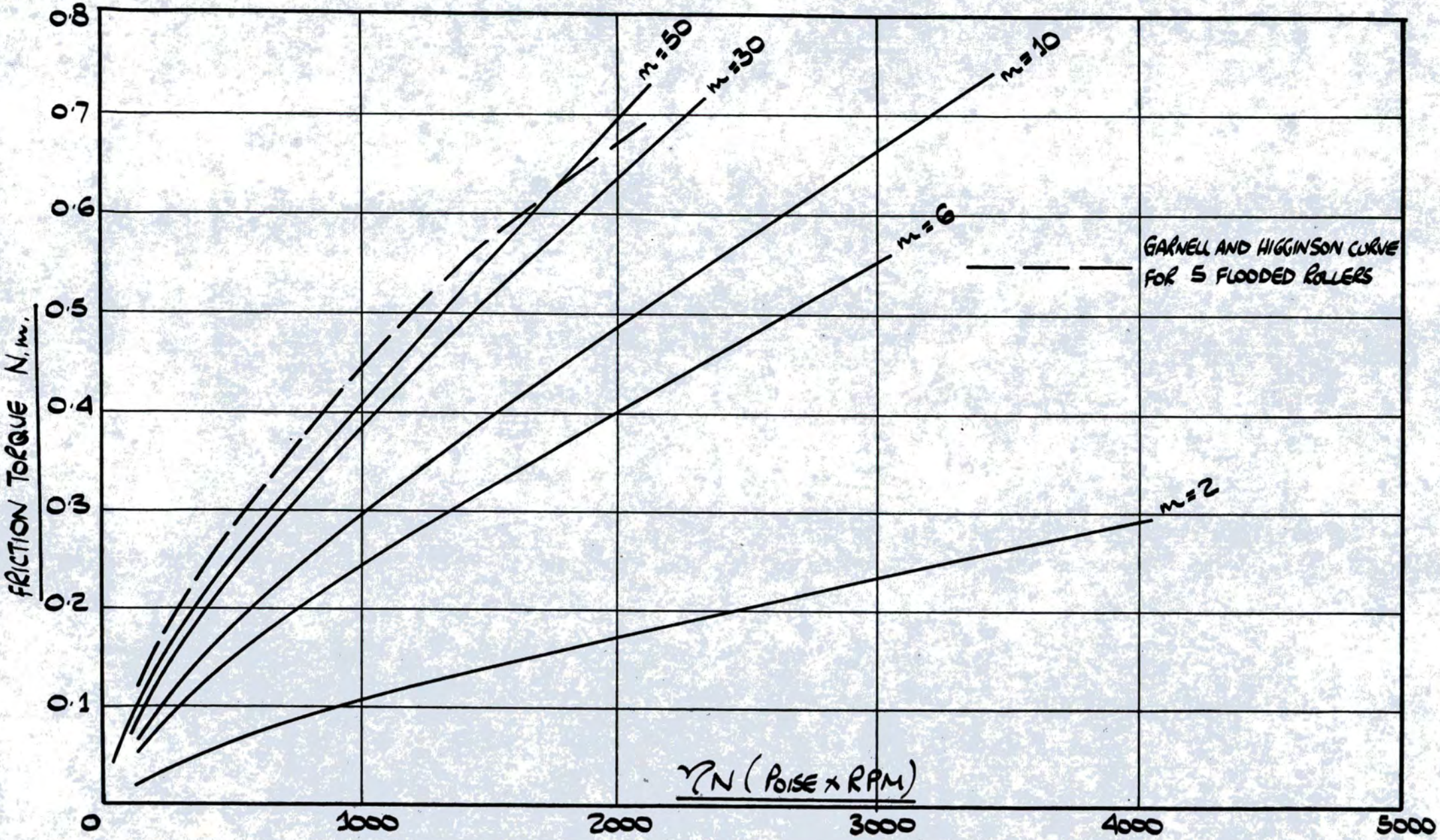

FIGURE 20. THEORETICAL TOTAL ROLLING FRICTION CURVES FOR THE TEST BEARINGS, SHOWING THE EFFECT OF LUBRICANT STARVATION. BEARING LOAD 10 kN, 5 ROLLERS IN CONTACT

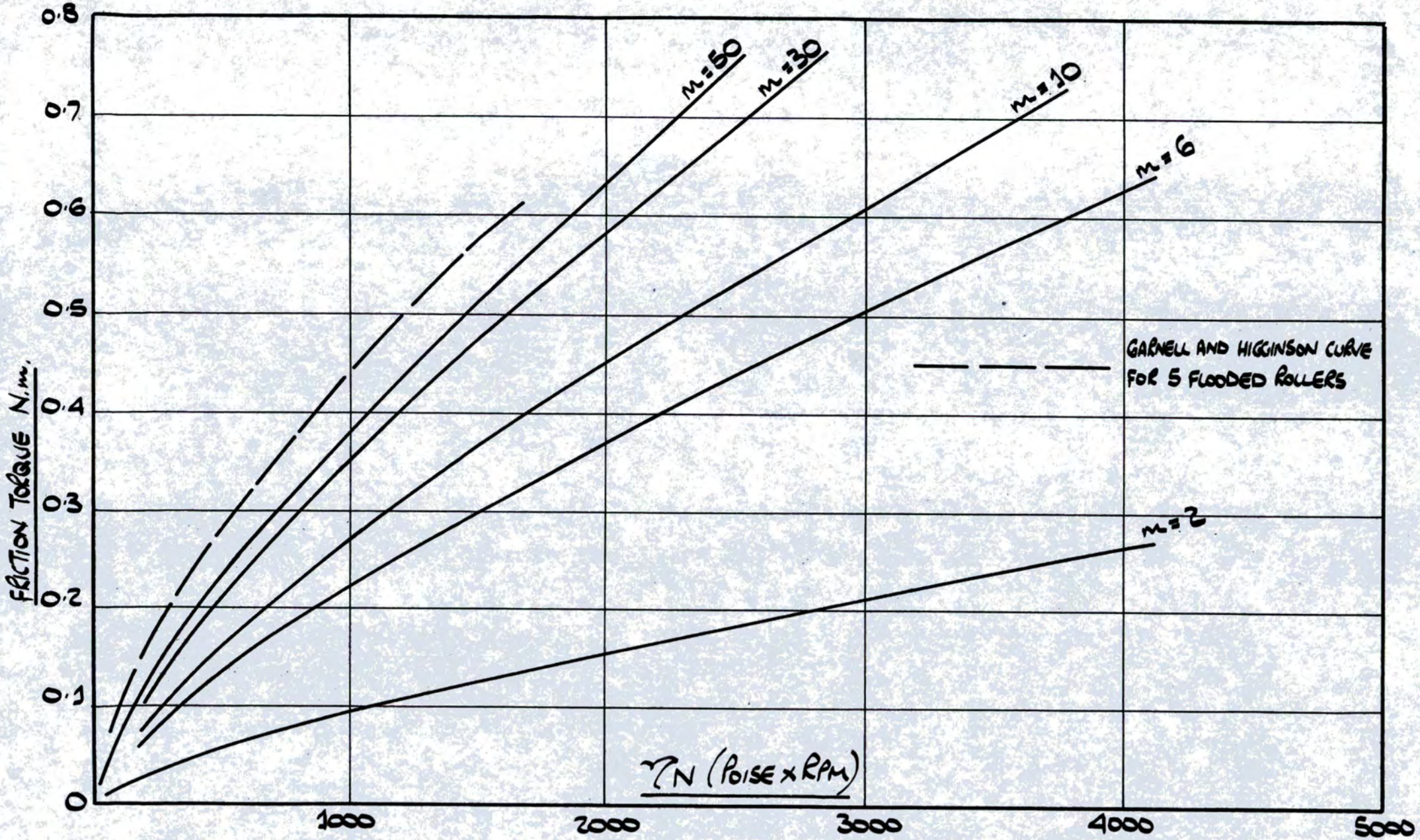

FIGURE 21. THEORETICAL TOTAL ROLLING FRICTION CURVES FOR THE TEST BEARINGS, SHOWING THE EFFECT OF LUBRICANT STARVATION. BEARING LOAD 20 kN, 5 ROLLERS IN CONTACT.

The remarks contained in the preceeding paragraph apply equally to figures S.8 , S.9 and S.10 in Appendix (S).

Additionally, since all six figures show only the contribution of the rolling traction to the total friction torque - to allow a direct comparison with the published results of Garnell and Higginson - the inclusion of the sliding friction's contribution to the total friction torque will in fact double all torque values, including those of the Garnell and Higginson curve. The comparison of course will be unaffected.

The general discussion which follows uses figures 19 , 20 and 21 , to estimate the degrees of starvation present at the experimental test conditions reported in Section (6.2).

SECTION 4

4.1 The Experimental Programme

The theoretical analysis contained in the previous section has predicted that a reduction in the quantity of lubricant at the rolling contacts within an assembly will reduce the bearing friction due to the rolling contacts without a proportional reduction in the lubricant film thicknesses at those contacts.

A theoretical estimation of the relative magnitudes of the sources of heat generation within a bearing assembly has been made by Astridge and Smith (1) on the basis of a list of sources suggested by Garnell and Higginson (21).

The table giving the relative magnitudes of the various sources obtained by Astridge and Smith can, by inference, be equally applied to the sources of friction torque in an assembly and in this context is reproduced by a modified form below. It should be noted that the analysis conducted by Astridge and Smith assumed that the bearing under consideration was closely contained in a housing - a common practice, it appears, in aero engine design - and since this would not normally be the case, the contribution assigned to the torque developed between the bearing cage and the chamber walls has been neglected and the percentages shown in the table re-adjusted.

The major sources of torque generation in an assembly are given by Astridge and Smith as:-

1.	Viscous friction between rollers and tracks	68.80%
2.	Viscous friction between roller ends and guide lips	0.15%
3.	Elastic Hysterisis in rollers and tracks	1.33%
4.	Viscous friction in lubricant films separating cylindrical end faces of rollers and cage	9.06%
5.	Viscous friction in films separating cage and tracks	10.25%
6.	Viscous friction in films separating cage side faces and chamber wall	0%
7.	Displacement of oil by rollers	1.92%
8.	Flinging of oil from rotating surfaces	7.90%
9.	Oil feed jet kinetic energy loss	0.59%
10.	Abrasive wear and asperity removal	0%
		100.00%

Since both the mechanisms described in items 7 and 8 can be assigned to a general classification of oil churning, the list can be simplified to show the following major sources of bearing friction torque.

(a)	Viscous friction at roller/ track contacts	70%
(b)	Viscous friction at cage/track contacts	10%

(c) Oil churning 10%

(d) Viscous friction at roller/cage contacts 9%

(e) Other sources 1%

It can therefore be seen that a reduction in the viscous friction at roller/track contacts and a reduction in the amount of oil churning in the assembly - both factors directly influenced by the rate at which lubricant is supplied to the assembly - could theoretically, affect 80% of the total friction torque developed.

However, an analysis such as that used by Astridge and Smith to predict the total friction torque in a lubricated assembly has, in many cases, been found to lead to an overestimation of the total friction torque developed. The analysis is based on a careful consideration of, amongst other things, the lubricant temperatures at each of the rolling and sliding contacts within the assembly and of course an underestimation of these temperatures could account for the reported discrepancy in the theoretical prediction when compared with experimental results.

To allow better estimates of the lubricant film temperatures to be made a fuller knowledge of the temperatures of the various elements of the bearing is necessary. Whilst the measurement of outer and inner race temperatures is straight forward, the roller and cage temperatures are more elusive.

The experimental programme contained in this preliminary investigation into the effects of lubricant starvation provides for the measurement of total friction torque and bearing temperatures (including roller and cage temperatures) on two bearings, both cylindrical roller, but of differing geometries. Three lubricants of widely differing viscosities have been used. Roller and cage speeds were also monitored in a number of tests.

Figure 22 shows the test programme in diagrammatic form. Brief details of the test bearings and the lubricants appear in this figure: full details appear in Appendices (B) and (C) respectively.

It may be said at this time that the original experimental programme, in many respects the basis of this thesis, was severely curtailed due to difficulties with the experimental rig, and the programme shown in figure 22 represents only those results which were obtained with an acceptable degree of confidence. The problems encountered with the experimental rig are noted in the following section.

The General discussion contained in Section 7 considers the experimental results obtained, both in relation to the theoretical work contained in Section 3 and also in the context of published work by other authors.

TEST PROGRAMME

BEARING	BEARING DESCRIPTION	LUBRICANTS	TEMPERATURE MEASUREMENT	SPEED MEASUREMENT	BEARING LOAD	LUBRICANT FLOWRATES	COOLING AIR FLOWRATE
S.K.F. N.U310 50 mm. Nominal Bore	Flanged Outer Race Plain Inner Race 12 Crowned Rollers Bronze Cage, Outer Race Guided	HVI 160 S. only	Race, Roller and Cage Temperatures	Inner Race, Cage and Roller Speeds	1 kN, 10 kN	1.6 gm/min. 0.2 gm/min. 0.06 gm/min. 0.004gm/min.	0.14 kg/minute
S.K.F. N.310 50 mm. Nominal Bore	Plain Outer Race Flanged Inner Race 12 Crowned Rollers Bronze Cage, Inner Race Guided	HVI 160 S	Race, Roller and Cage Temperatures	Inner Race, Cage and Roller Speeds	1 kN, 10 kN	1.6 gm/min. 0.2 gm/min. 0.06 gm/min. 0.004gm/min.	
		HVI 55	Race Temperatures only	Inner Race Speed only	10 kN only	0.92 gm/min. 0.13 gm/min. 0.022gm/min. 0.009gm/min.	
		Paraffin	Race Temperatures only	Inner Race Speed only	10 kN only	1.4 gm/min. 0.26 gm/min. 0.1 gm/min. 0.033gm/min.	

OIL FILM RESISTANCE MONITOR WAS USED IN ALL TESTS.

FIGURE 22. THE TEST PROGRAMME.

SECTION 5

The Experimental Rig

A general view of the experimental rig is shown in plate 1.

5.1 The Testing Machine

A general arrangement of the machine is shown in figure 23 and a more detailed drawing of the test shaft assembly in figure 24.

The machine was not specifically designed to carry out the test programme shown in figure 22 but was designed in the Department of Mechanical Engineering of the University of Leeds to a specification which would allow a number of different types of experiment to be carried out on a range of rolling contact bearings, all of 50mm nominal bore; the test bearings were to be easily interchangeable. In particular, the specification called for a machine which would allow investigations into the effects of inner race misalignment on the behaviour of the test bearing.

This wide design specification is responsible for the complex arrangement of the machine. It has been necessary to modify the original design in a number of ways, the most important of these being the redesign of the hydrostatic support bearing. The work done on this component is described in Appendix (E).

Referring to figure 24 , the test shaft assembly,

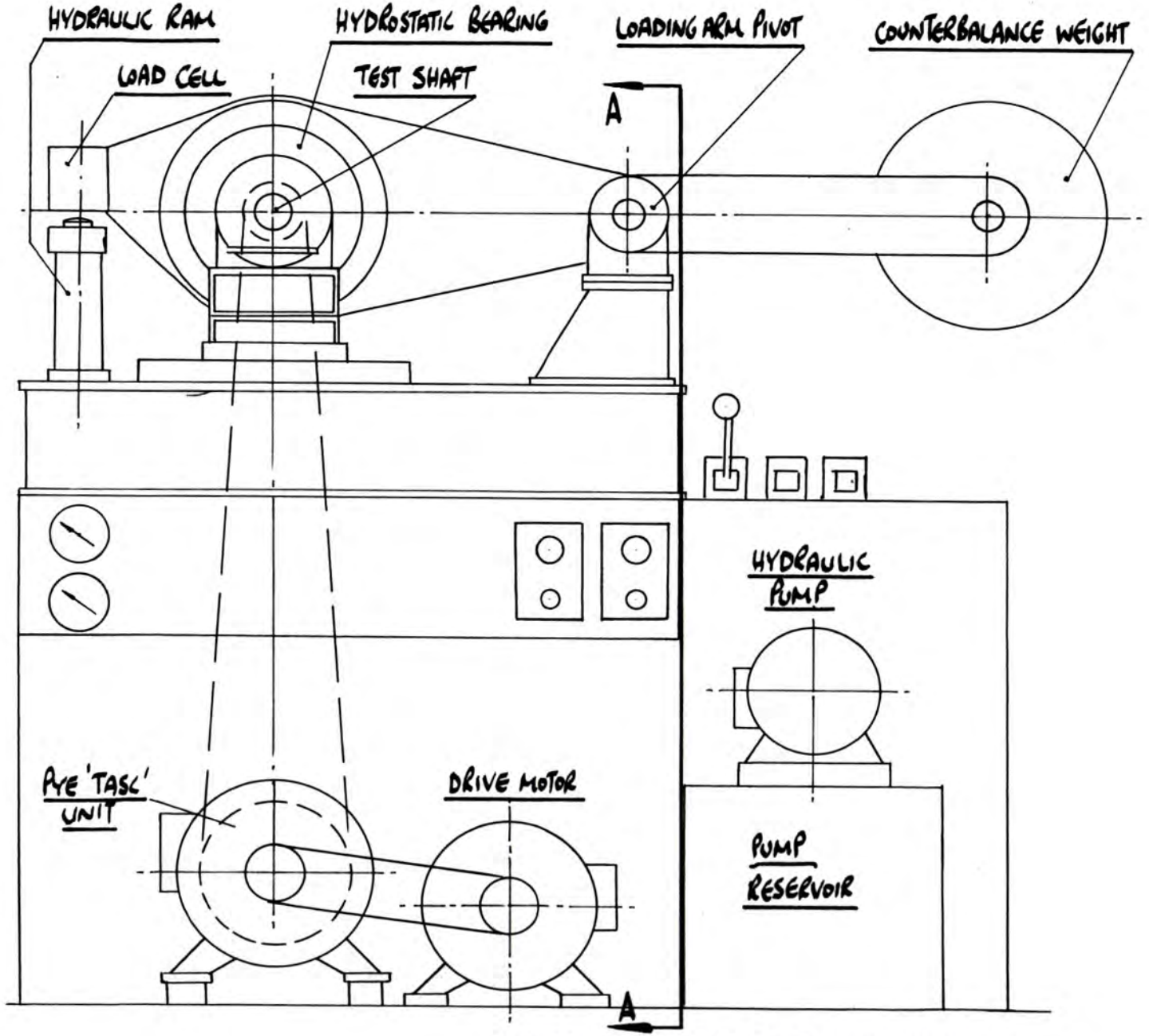

FIGURE 23 . THE TESTING MACHINE.

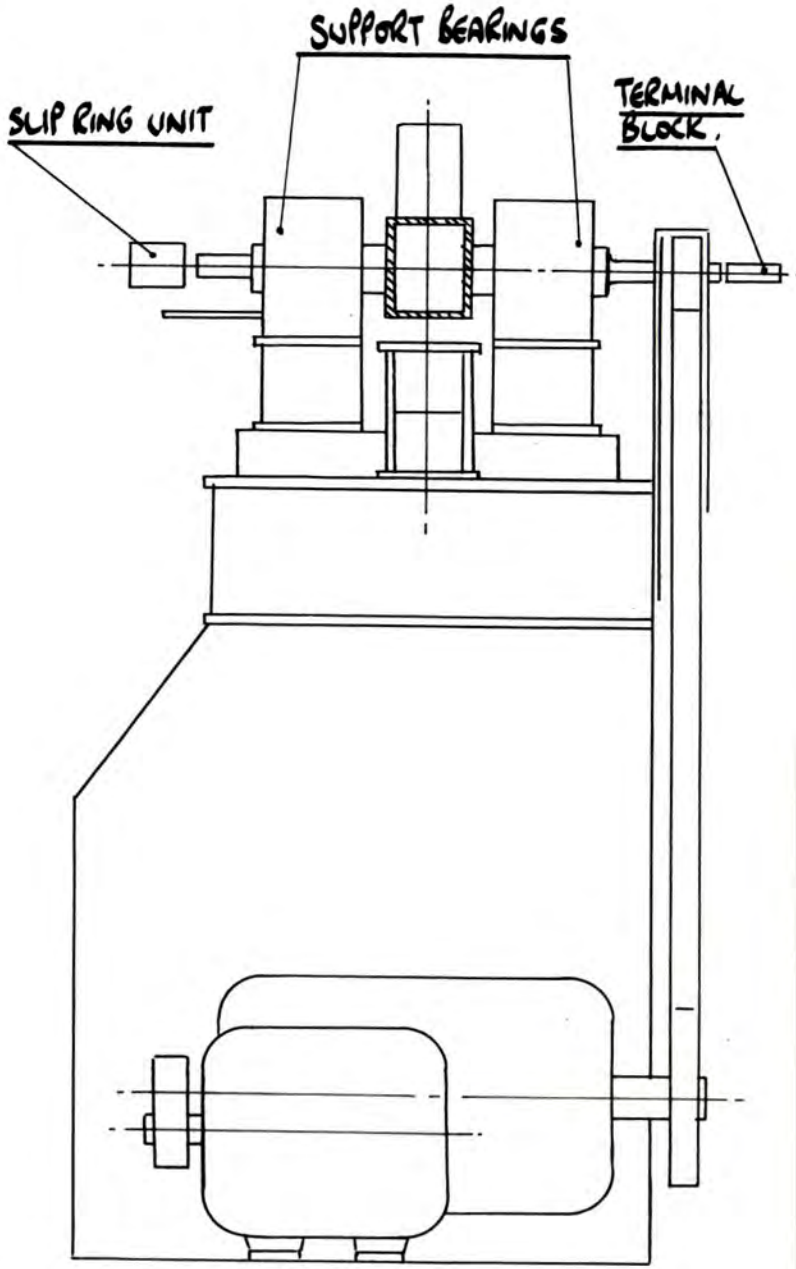

SECTION A-A

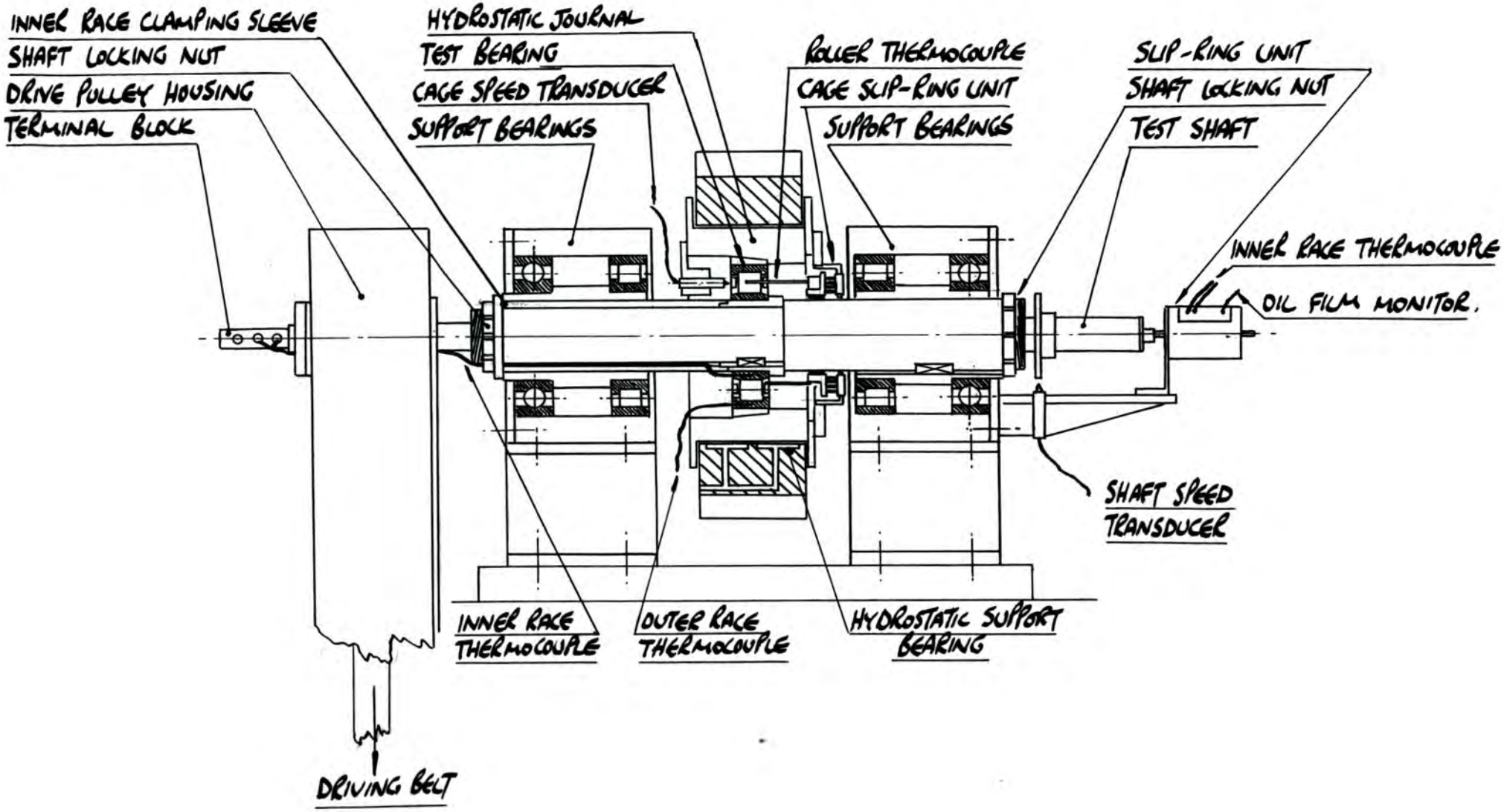

FIGURE 24 . THE TEST SHAFT ASSEMBLY

it will be noted that, because of the requirement that test bearings be easily interchangeable, both inner and outer races of the test bearing are held in position by clamping pressure alone. Whilst this has proved quite satisfactory for the outer race, the lack of positive location of the inner race has been a major source of trouble. The presence of sliding parts rotating under load has been the cause of a great deal of fretting corrosion. Even quite modest running has caused this type of surface distress and this has made the machine extremely difficult to maintain. During the experimental programme described in this work four test shafts have been destroyed, - one shaft was broken into two parts as a result of fatigue cracking, compounded by fretting corrosion. However, material changes for components in direct contact with the test shaft, and judicious use of anti-scuffing compounds have helped to minimise the destructive effects of this corrosion.

In its present form, the testing machine will accept most test bearings of 50mm nominal bore although, as shown in the test programme in figure 22 , only two types of parallel roller bearing have been used in the present work. Bearing details are shown in Appendix (B).

The test shaft on which the inner race of the test bearing is mounted is supported by ball and roller bearings, these bearings being fitted in the support bearing housings shown in figure 24 The

support bearings are lubricated by a 'Norgren' oil/ air mist system. The test shaft is driven through a multi-vee belt drive and a specially designed pulley system. The maximum shaft speed and bearing load that can be provided by the machine are 5000 RPM and 20kN respectively. The shaft drive is provided by a 5 H.P., 3 phase motor driving through a PYE TASC unit. The latter allows shaft speeds to be continously varied from about 50 RPM up to the maximum.

The load is applied to the test bearing by a hydraulic ram acting under the free end of the machine arm, the ram being activated by a hand operated pump (Dowty type HP5A). Because of the geometry of the machine arm, the bearing load is 1.55 times greater than the applied ram load.

A low friction interface between the machine arm and the outer race of the test bearing is provided by a 4 pocket, 120^{o} hydrostatic bearing - this allows test bearing friction torque to be measured for the various test conditions. The high pressure oil necessary for the operation of the hydrostatic bearing is provided by a motor driven positive displacement pump.

The hydrostatic support bearing has been considerably modified from the original design and notes on this work appear in Appendix (E). The modifications to this component have occupied a large proportion of the author's period of registration for the degree, but its correct functioning was vital

since the measurement of friction torque was a central part of the experimental programme.

Unfortunately, even after considerable attention, it was not possible to completely eliminate the faults in this bearing. Appendix (E) gives details of the compensations necessary before values of test bearing friction torque could be determined.

5.2 Instrumentation used on the Testing Machine

The measurements taken during the experimental work are similar to those recorded by Garnell (20) and by Boness (7). In addition, measurement of roller and cage temperatures were made, together with a thorough investigation of the outer race temperatures.

It has not been possible for all possible experimental readings to be taken for all tests, but the complete range of readings that could have been made is:

Bearing load

Bearing friction torque

Shaft, cage and roller speed

Outer race, inner race, cage and roller temperatures - 12 readings in all.

Lubricant and cooling air flowrates

Lubricant film electrical resistance

The following paragraphs give brief descriptions of the techniques used to measure each of these quantities but the reader is referred to the relevant Appendices for fuller details of the experimental apparatus used.

Bearing load was measured by a Vibrometer load cell of 20 kN capacity and readings taken by means of a Vibrometer carrier frequency amplifier and calibrated galvanometer.

See Appendix (D).

Bearing torque was measured by the use of a strain

gauged berrylium copper proof ring and readings taken on a calibrated strain bridge instrument. A number of instruments have been used and in each case calibration curves were obtained by applying known loads to the proof ring.

See Appendix (E).

Shaft speed was measured by means of a toothed impulse wheel fitted to the shaft, the wheel running close to a magnetic pick up. Readings were taken by the use of a digital counter.

See Appendix (G).

Cage speed was measured by the use of a magnetic pick - up placed adjacent to steel bolts in the bearing cage. Readings were taken by using the digital counter.

See Appendix (H).

Roller speed. Measured by the use of embedded magnets in one of the bearing rollers. As the roller rotated, the magnets induced a small sinusoidal e.m.f. in a stationary pick up coil. The frequency of the signal (and thus the speed of the roller) was measured by the digital counter and monitored by oscilloscope trace.

See Appendix (I).

Outer race temperature was measured by copper constantan thermocouples embedded at 7 points around the circumference of the test bearing outer race. Readings of thermocouple e.m.f. were taken by the use of a digital voltmeter.

See Appendix (J).

Inner Race Temperature. A single copper constantan thermocouple was embedded in the inner race and readings of thermocouple e.m.f. taken by the use of the digital voltmeter via slip rings fitted to the end of the test shaft.

See Appendix (K).

Roller and Cage temperatures. A slip ring unit, specially designed for this investigation, was fitted onto the cage of the test bearing and copper constantan thermocouples fitted into one roller and into the test bearing cage. Readings of thermocouple e.m.f. were taken by use of the digital voltmeter.

See Appendix (L).

A model of the cage slip ring assembly is shown in plates (25) and (26).

Test Lubricant Flowrate. Lubricant flow was provided by a peristaltic pump and flowrate determined by measuring the rate of flow of lubricant from a calibrated burette.

See Appendix (O).

Cooling air flowrate. Mass flow of cooling air was determined from readings taken from a previously calibrated 'Rotameter' instrument.

See Appendix (P).

Lubricant film resistance was measured by a circuit similar to that devised by Furey and used by, amongst others, Leaver (26).

The instrumentation was used purely as a monitoring device.

See Appendix (Q).

Full details of the test bearings used appear in Appendix (B) and details of lubricant parameters in Appendix (C).

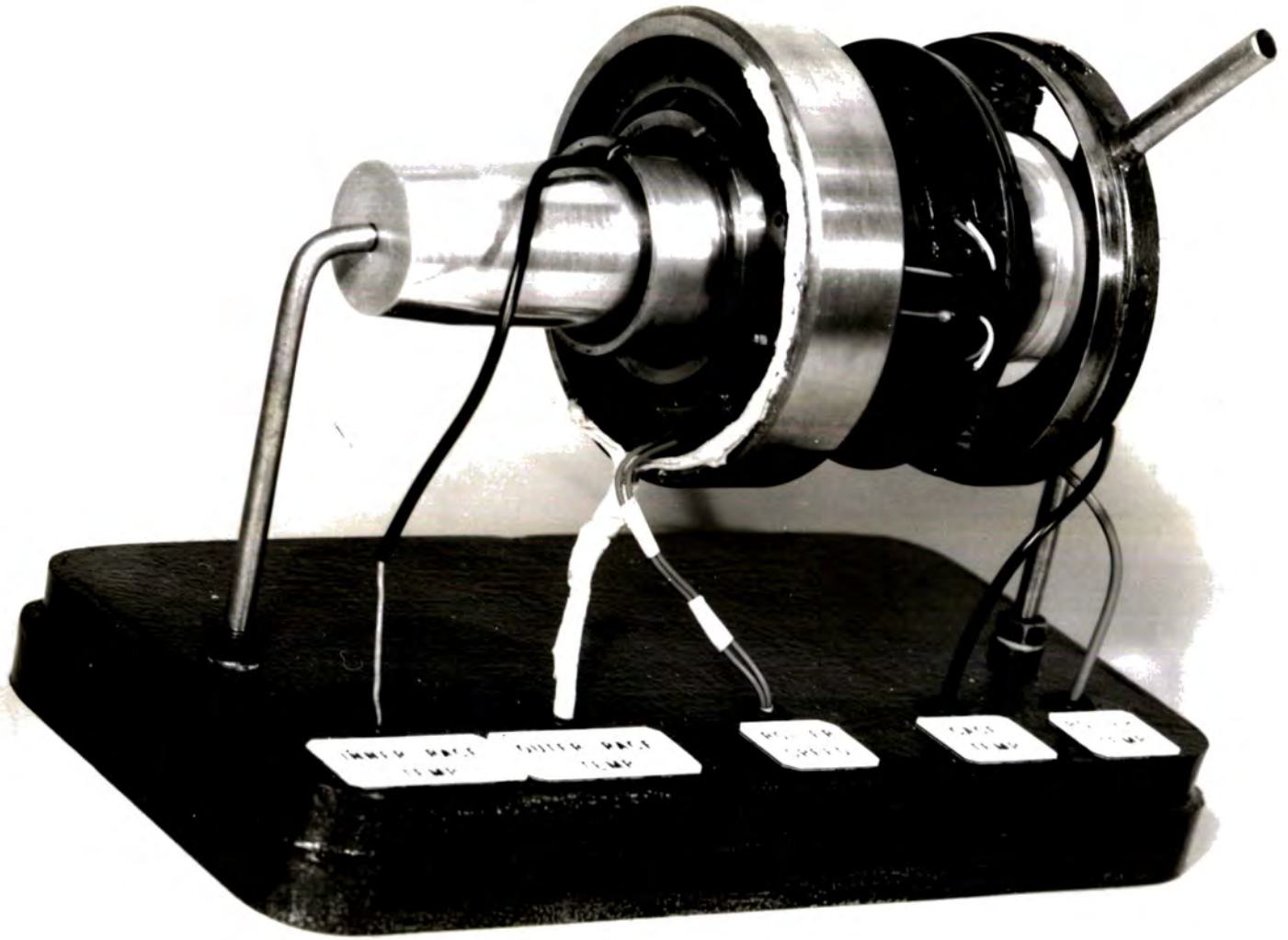

PLATE 25. MODEL OF THE CAGE SLIP-RING ASSEMBLY.

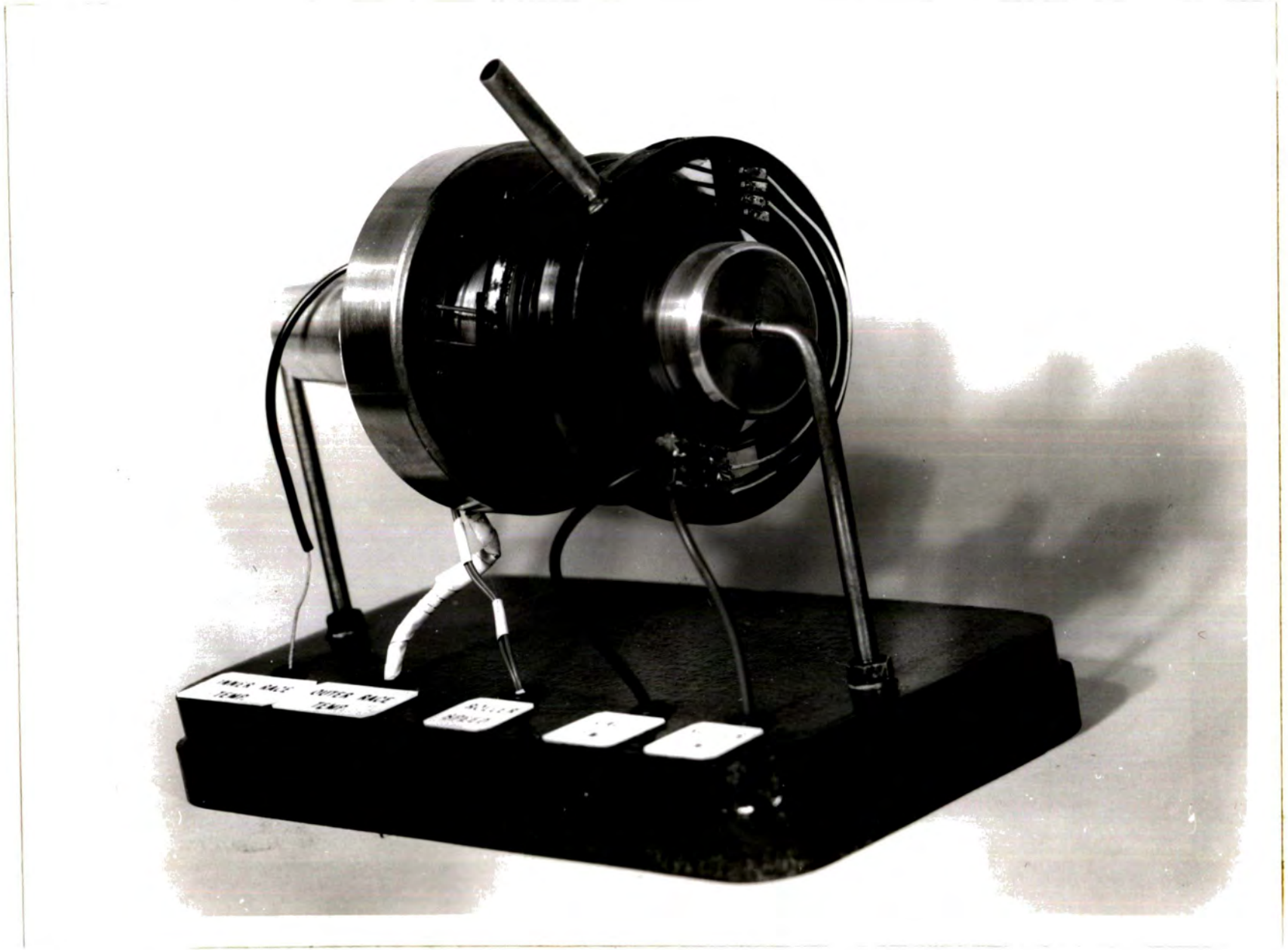

PLATE 26. MODEL OF THE CAGE SLIP-RING ASSEMBLY.

SECTION 6

Experimental Results

The experimental results obtained can be divided into two main categories:

i) those concerned with the effects of lubricant flowrate on the total friction torque in a bearing assembly.

ii) those concerned with the effects of lubricant flowrate on the temperatures of the components within the assembly.

Observations of the effects of the low flowrate used on the speeds of rollers and cage have shown little variation from epicyclic speed. This result will be considered in the discussion which follows.

6.1 Preliminary tests

Before the main test programme was decided, a series of preliminary tests were carried out. The results of these tests are on interest because they indicate in general terms the effects of a change in lubricant flowrate on a bearing. The results are shown in figures 27 , 28 , 29 and 30 . It will be noted that, for all speeds, an increase in lubricant flowrate was accompanied by increases in both bearing friction torque and component temperatures.

When the lubricant supply was cut off, the reduction in these quantities was in all cases significant and in some cases dramatic. The sharp initial fall in these quantities was followed by further

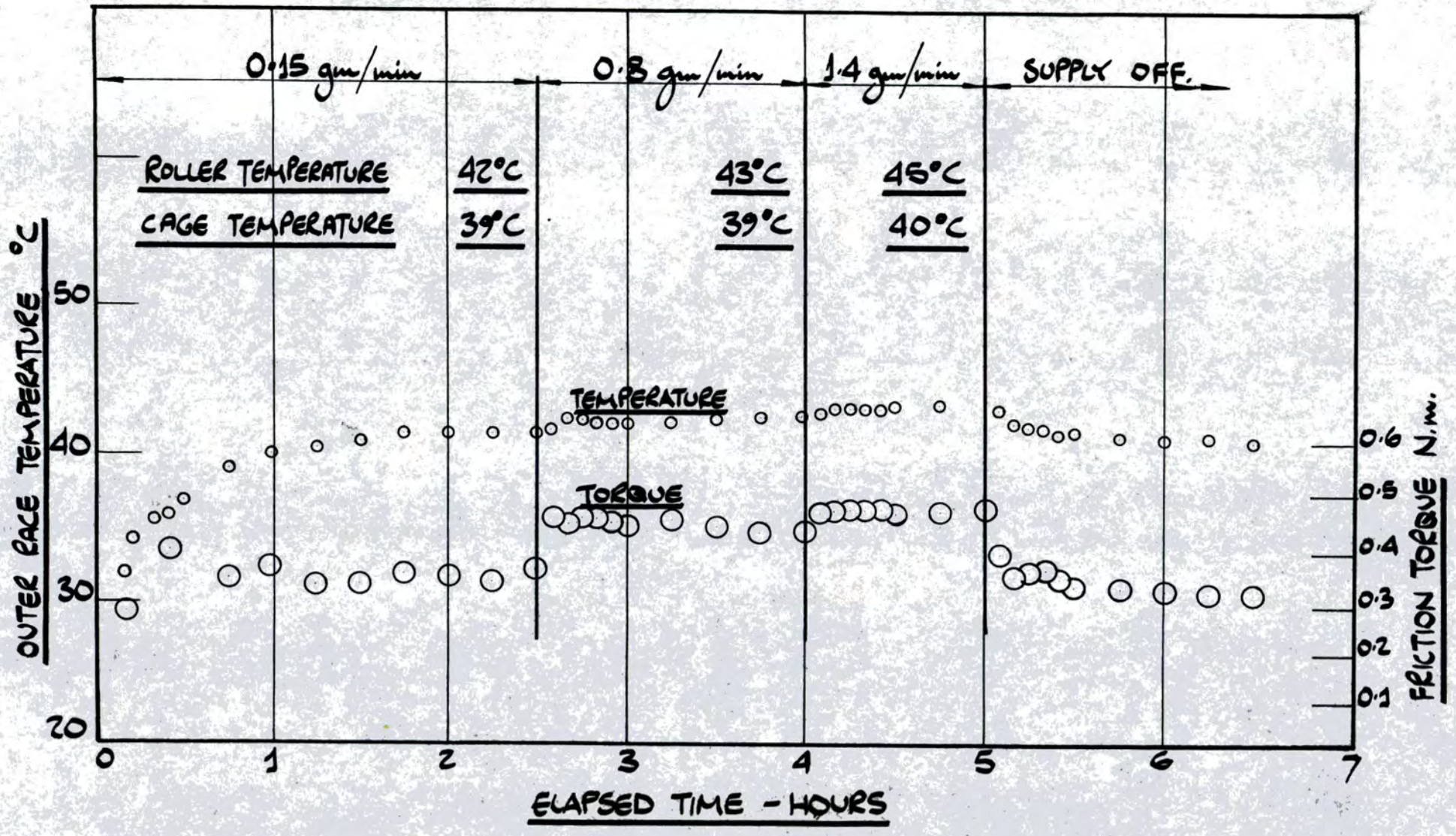

FIGURE 27 . RESULTS OF PRELIMINARY TEST AT 10kN LOAD, 1250 RPM

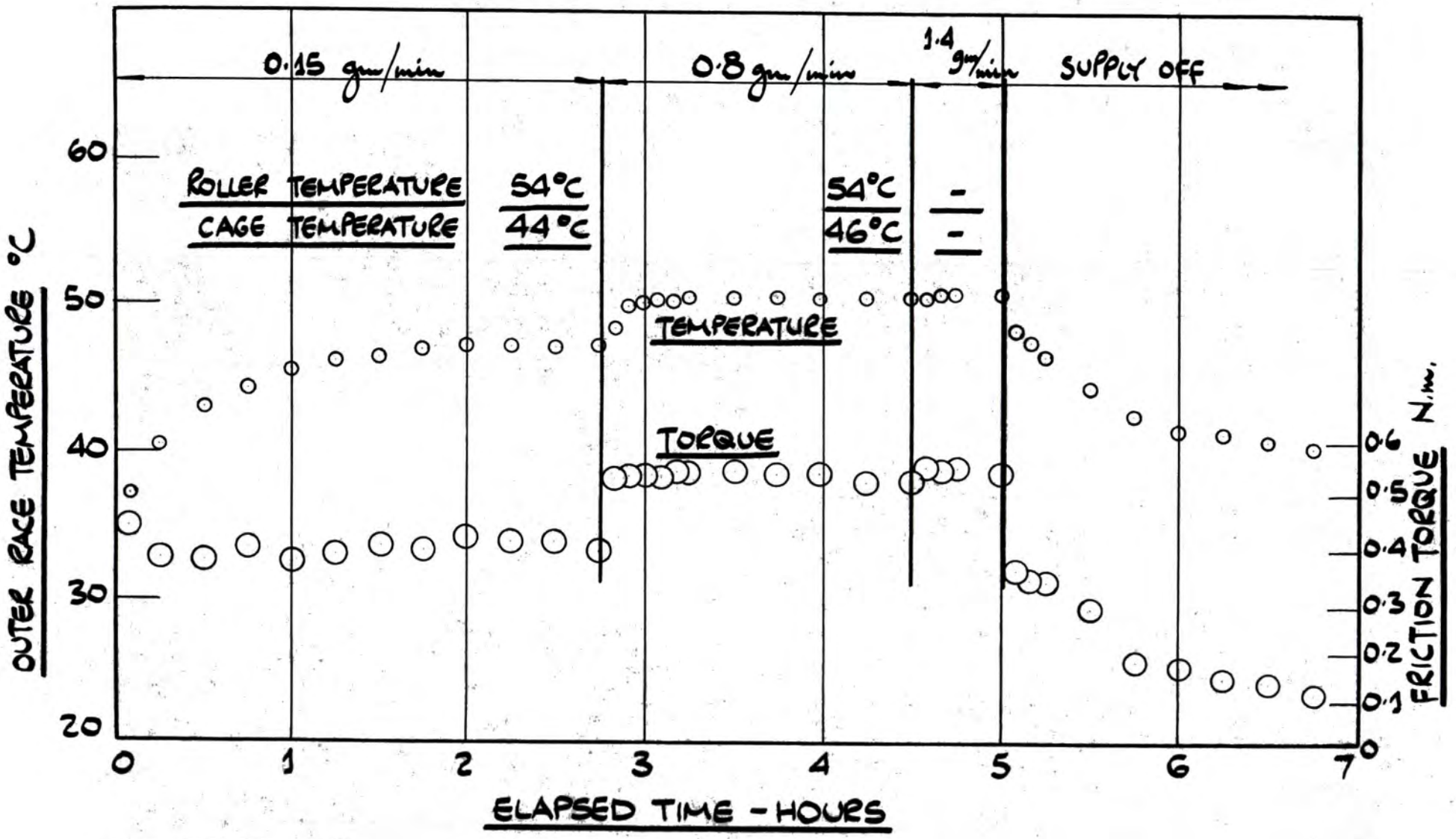

FIGURE 28. RESULTS OF PRELIMINARY TEST AT 10KN LOAD, 2500 RPM

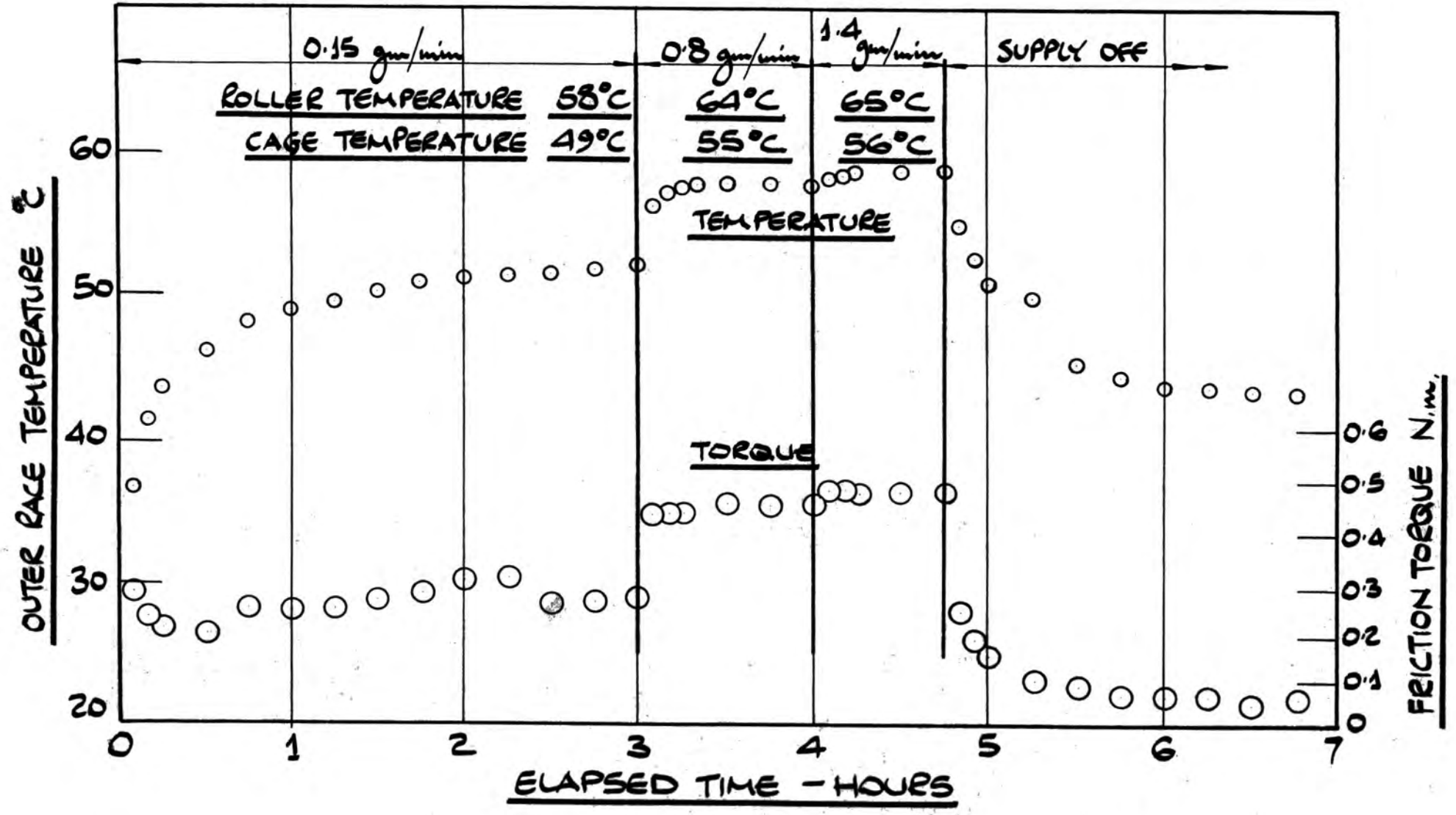

FIGURE 29. RESULTS OF PRELIMINARY TEST AT 10 KN LOAD, 3750 RPM

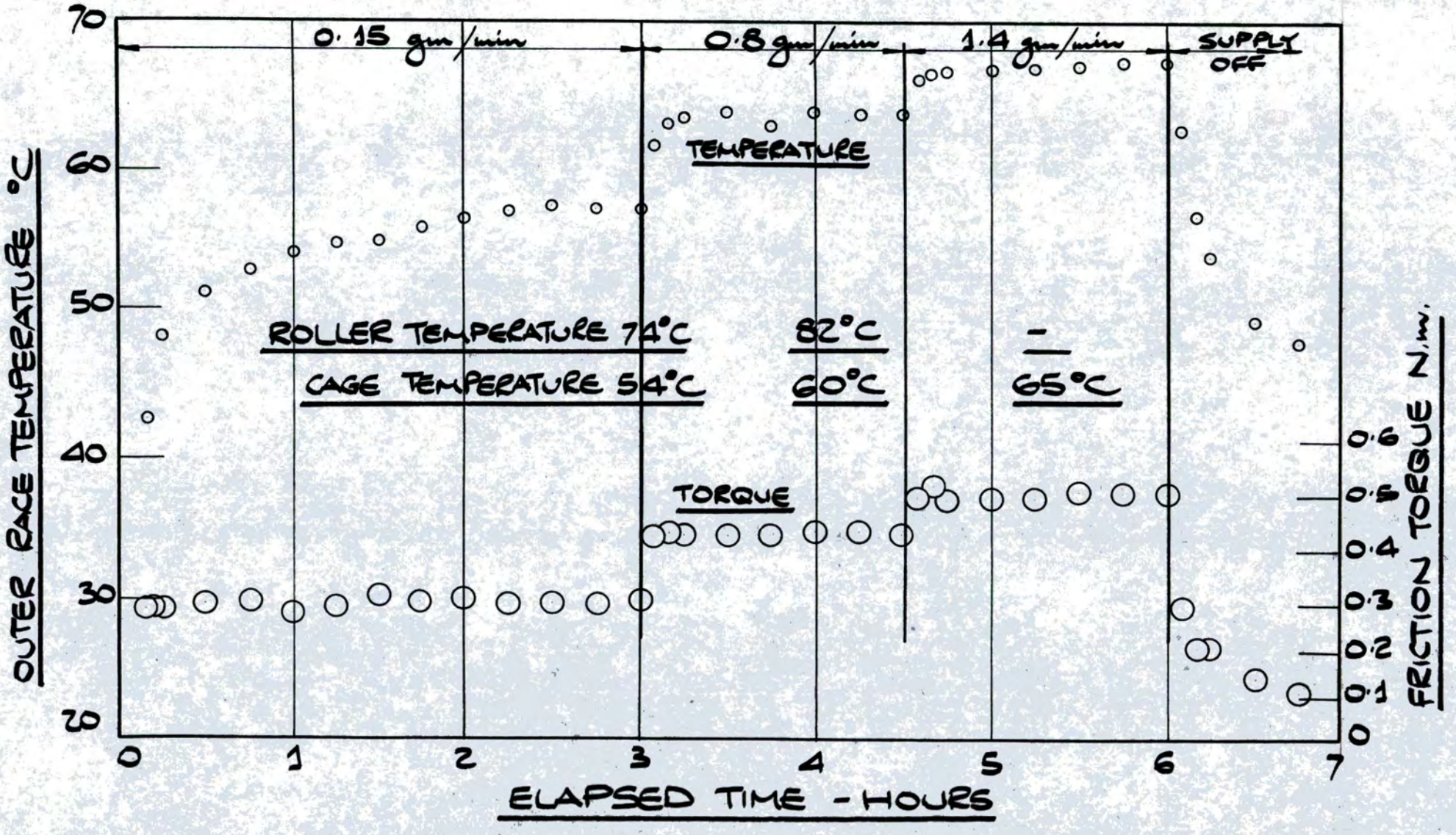

FIGURE 30. RESULTS OF PRELIMINARY TEST AT 10 kN LOAD, 5000 RPM

reductions, albeit at a slower rate.

It was of interest to determine just how long a bearing would continue to run with no lubricant supply whatsoever and so a further test was carried out at the conditions indicated in figure 30 . After stopping the lubricant supply, the bearing was allowed to continue running for an extended period. During this test it was hoped to observe the failure of the bearing due to lack of lubricant but even after running for 15 hours without further lubrication, the bearing was still operating satisfactorily. Subsequent examination of the bearing components showed them to be in reasonable condition.

These few preliminary tests were sufficient to indicate the need for the fuller experimental programme later carried out (see figure 22) and also confirmed in some small way Crook's belief that oil films adhere tenaciously to the surfaces they lubricate.

6.2 Experimental results to show the effect of lubricant flowrate on total friction torque in an assembly

The friction torque tests carried out were of two types, namely those done with the cage slip ring unit fitted to the test bearing, and those without the slip ring unit.

The results from the two types of test were in good agreement and all results obtained are shown on the experimental curves which follow. All torque readings have been compensated for the effect of the parasitic torque present in the hydrostatic support bearing, details of this compensation appearing in Appendix (E). The torque values obtained from the tests carried out with the cage slip ring unit fitted to the test bearing were subject to a further compensation to take account of the slip ring unit. Details of the compensation applied appears in Appendix (F).

Figures 31 and 32 show the effect of lubricant supply rate on the total friction torque of test bearing NU310, the bearing with flanged outer race and outer race guided cage. Both sets of curves are drawn to a base of (inner race speed x lubricant viscosity) in units (RPM x poise), figure 31 showing the variation at 1kN bearing load and figure 32 the variation at 10kN load.

For these and all subsequent graphs, the lubricant viscosity used is that calculated from the outer race temperature directly below the load.

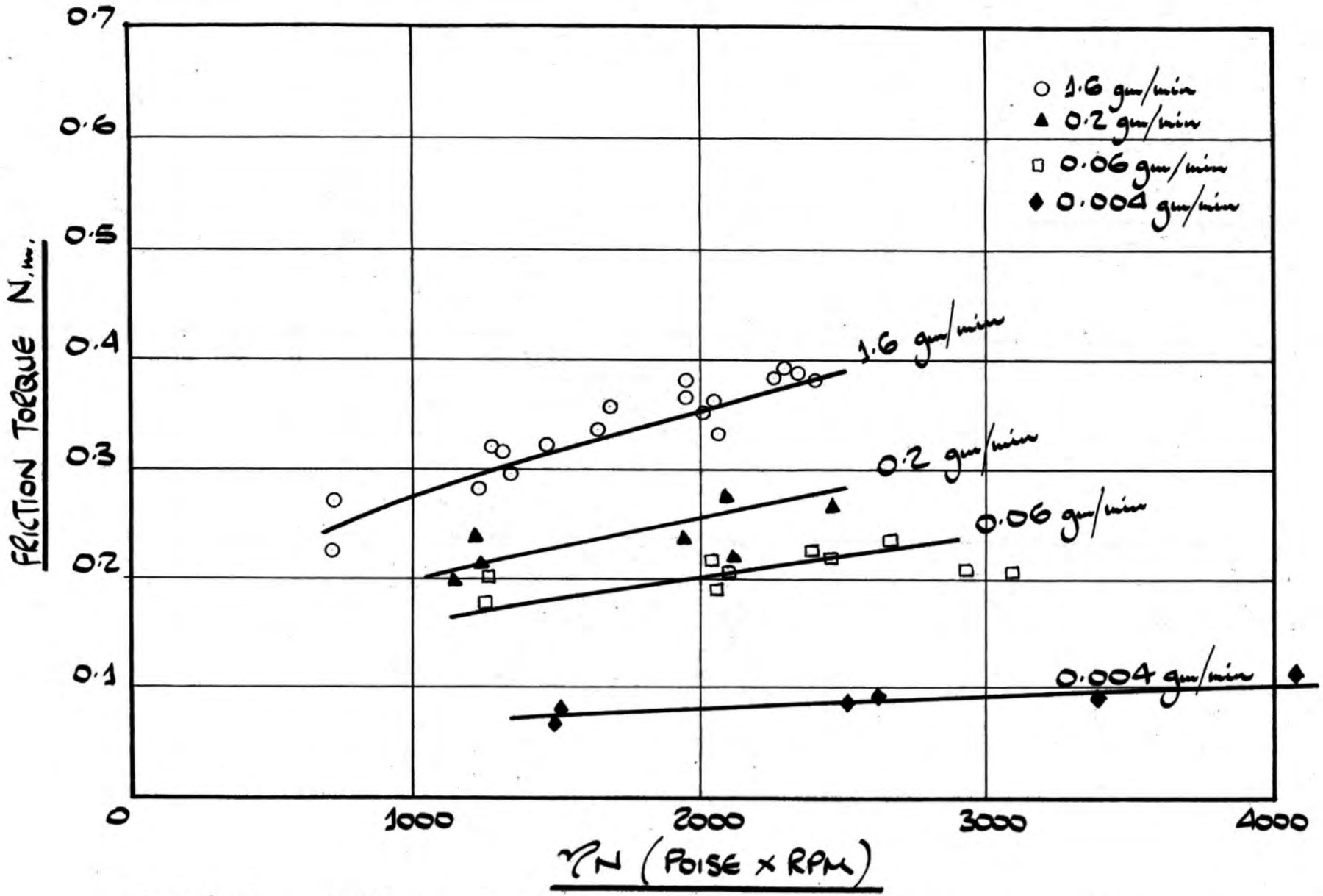

FIGURE 31. EFFECT OF LUBRICANT SUPPLY RATE ON TOTAL FRICTION TORQUE. BEARING TYPE NU310, 1 kN LOAD, HVI 160 LUBRICANT.

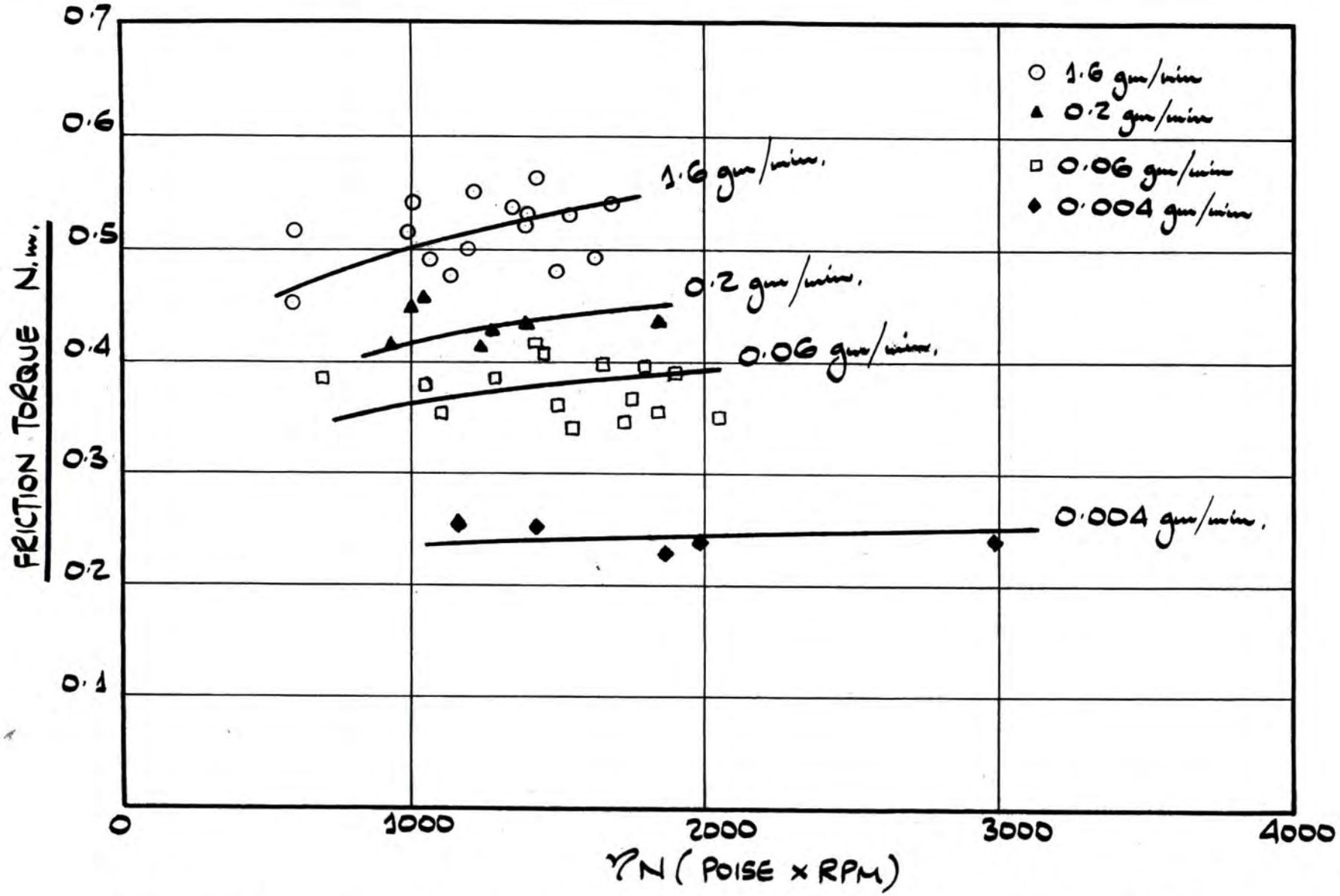

FIGURE 32 . EFFECT OF LUBRICANT SUPPLY RATE ON TOTAL FRICTION TORQUE. BEARING NU310, 10 kN LOAD, HVI 160 LUBRICANT.

Figures 33 and 34 show the effect of lubricant supply rate on the total friction torque of test bearing N310, the bearing with flanged inner race and inner ring guided cage. Figure 33 shows the variation at 1kN load and figure 34 the variation at 10kN load.

The results shown in figures 31 , 32 , 33 and 34 have been obtained from tests carried out using the HV1 160S lubricant and it will be seen that the range of (speed x viscosity) within which these results lie is limited. A further set of experimental results using lower viscosity lubricants have been obtained for bearing N310 running at 10kN load as part of a final Honours year undergraduate project (16) and these results are shown in figures 35 and 36 .

Unfortunately, these results, whilst being compatible within themselves, are not directly comparable with the results shown in figure 34 . In most cases the results given in figures 35 and 36 are lower than would be expected by extrapolation of the curves of figure 34 , a typical deviation being of the order of 0.1Nm. This deviation can be explained in qualitative terms as resulting from a change in the operating conditions under which the tests were made. This matter is referred to in the following sub-section.

The results for bearing NU310 using lubricant HV1 160S (shown in figures 31 and 32) have been re-plotted to a base of (ln. lubricant flowrate) in

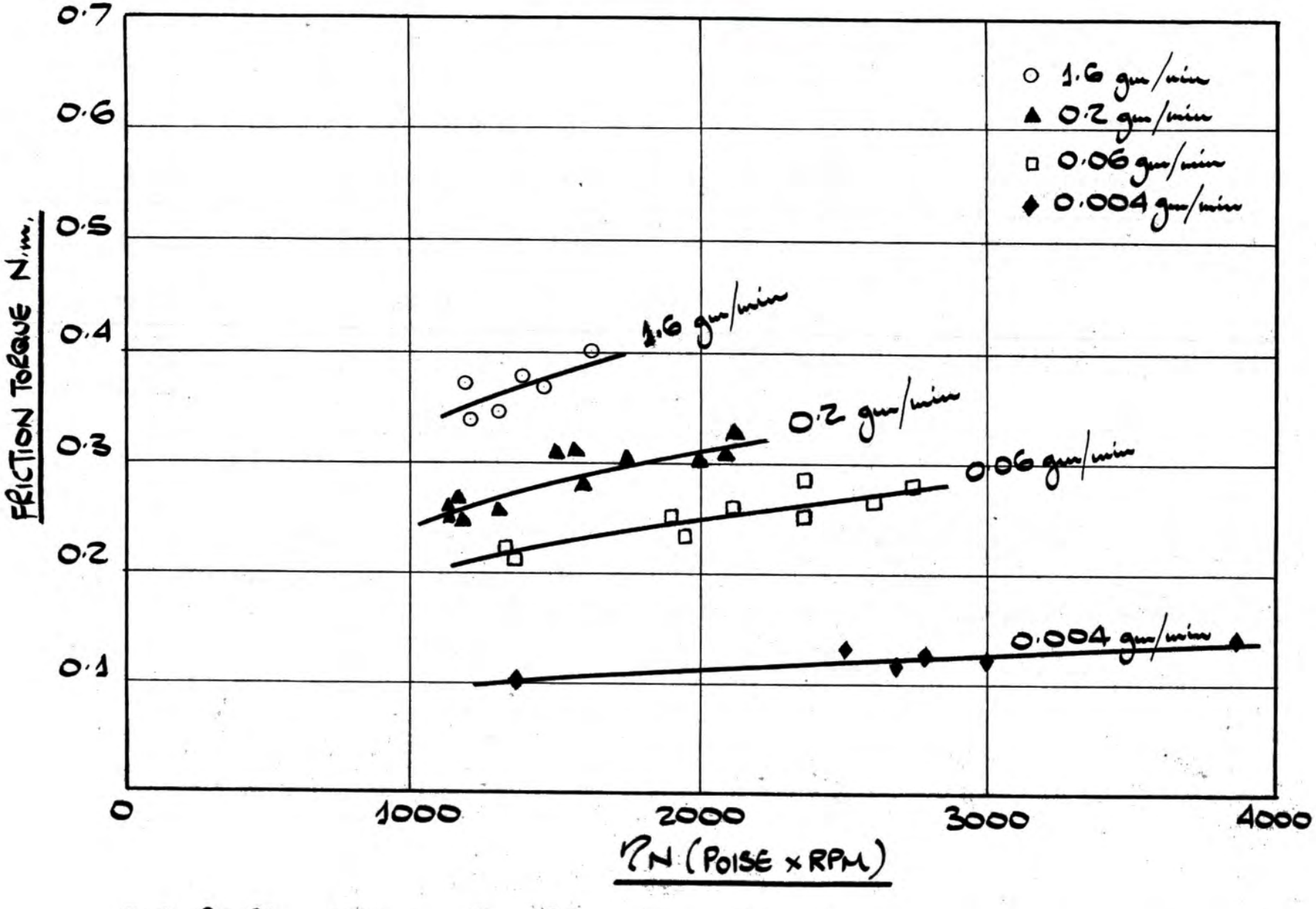

FIGURE 33. EFFECT OF LUBRICANT SUPPLY RATE ON TOTAL FRICTION TORQUE. BEARING TYPE N310, 1kN LOAD., HVI 160 LUBRICANT.

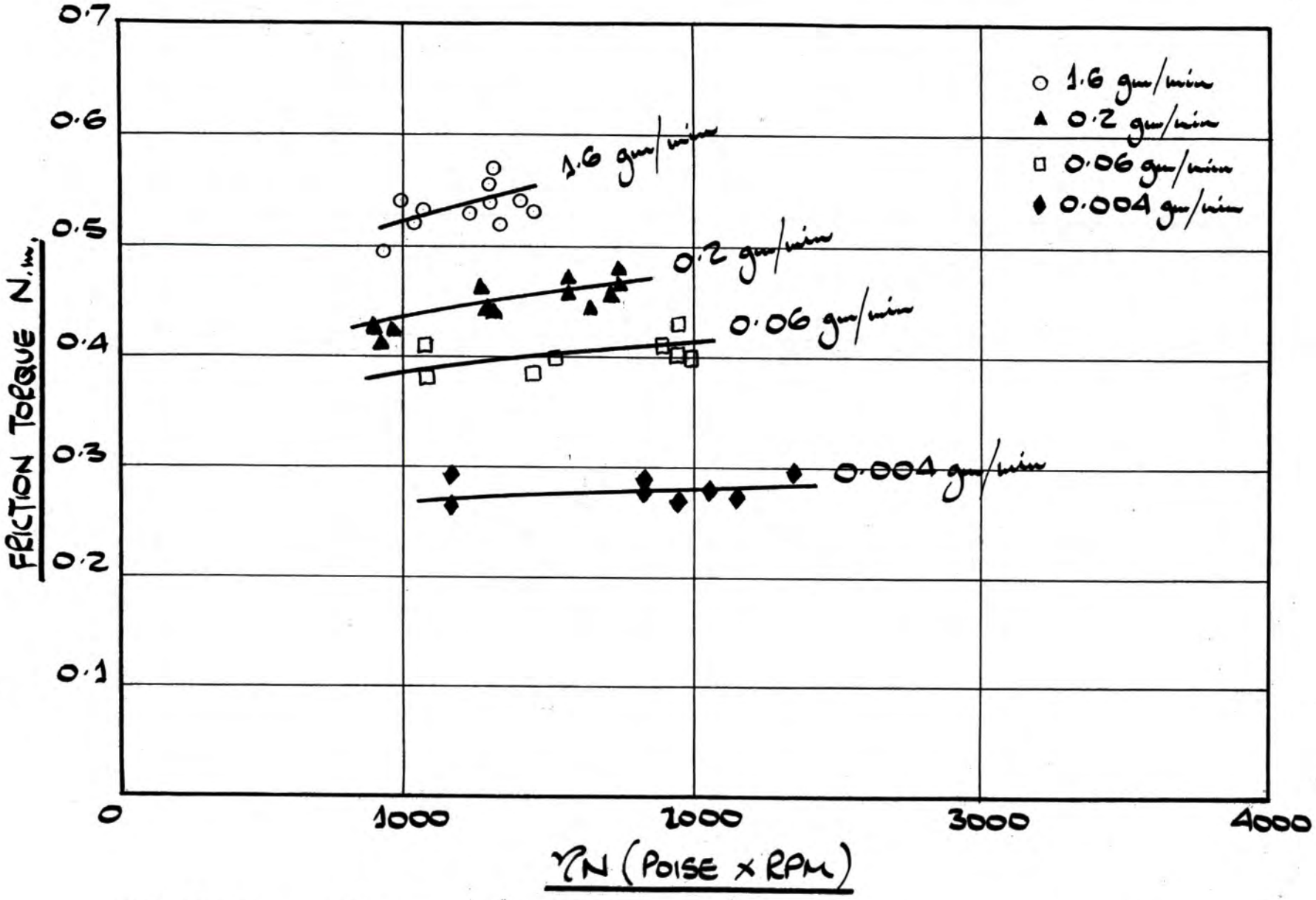

FIGURE 34. EFFECT OF LUBRICANT SUPPLY RATE ON TOTAL FRICTION TORQUE BEARING TYPE N310, 10 kN LOAD, HVI 160 LUBRICANT.

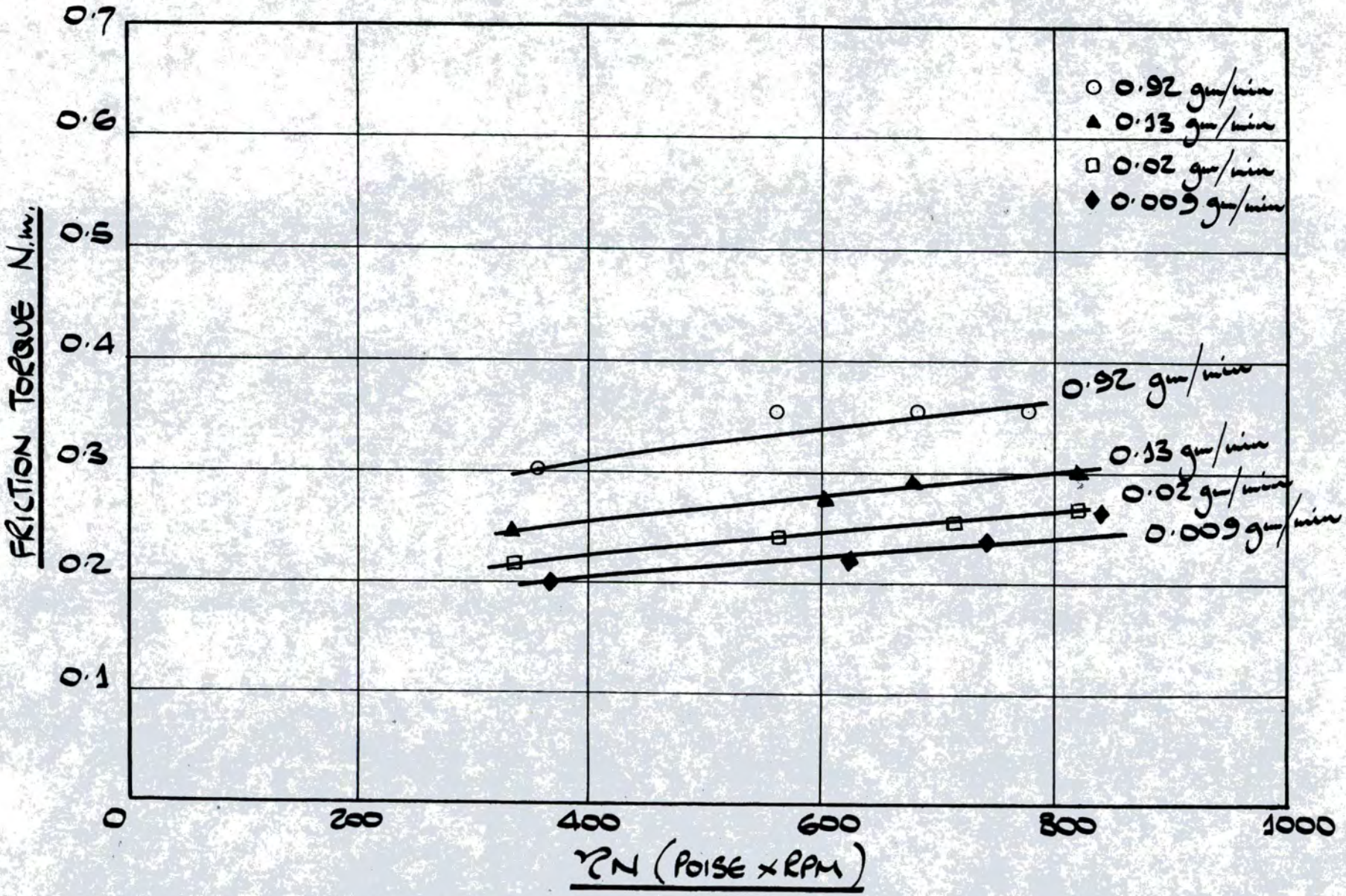

FIGURE 35. EFFECT OF LUBRICANT SUPPLY RATE ON TOTAL FRICTION TORQUE BEARING TYPE N310, 10 kN LOAD, HVI 55 LUBRICANT.

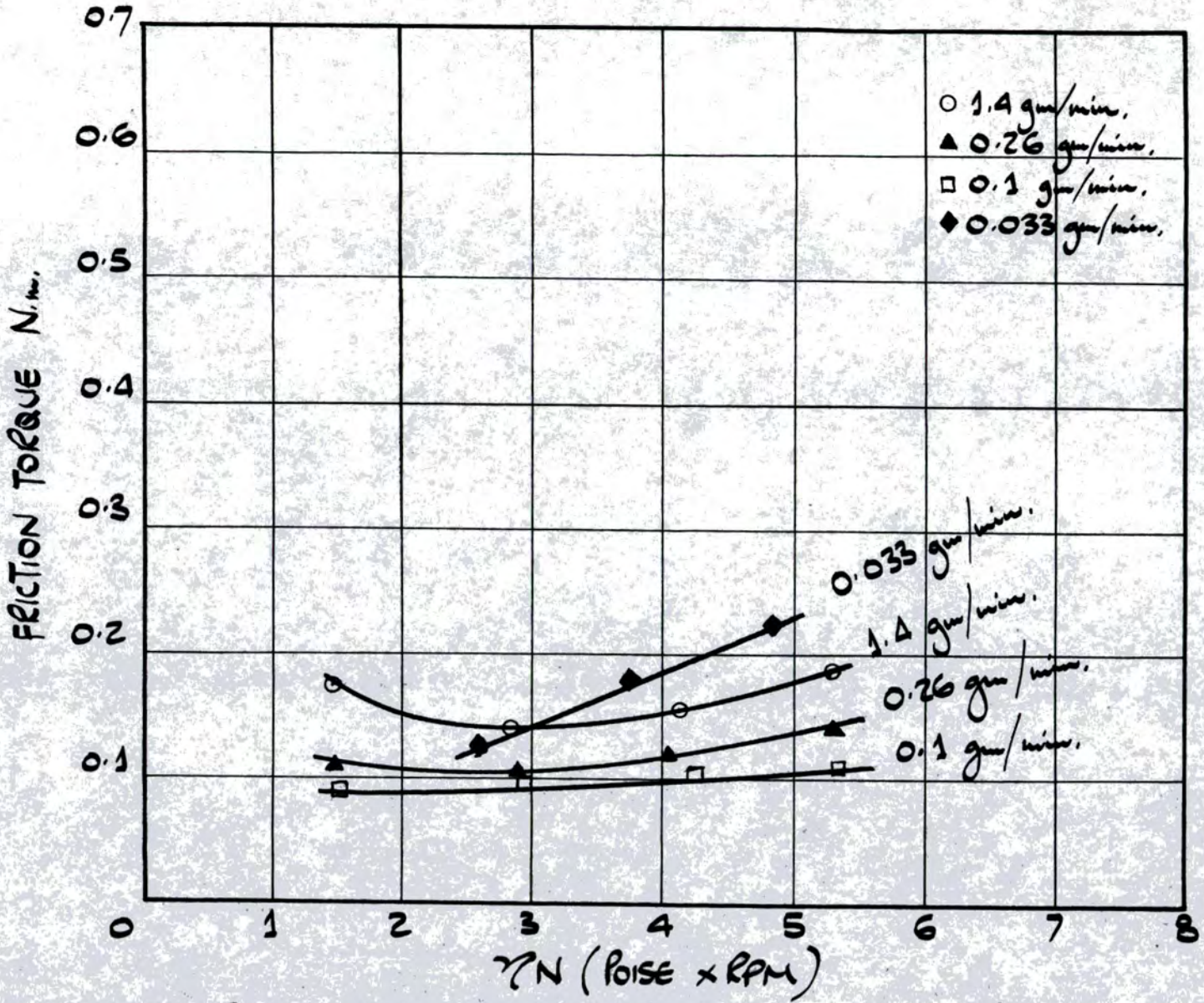

FIGURE 36. EFFECT OF LUBRICANT SUPPLY RATE ON TOTAL FRICTION TORQUE, BEARING TYPE N310, 10kN LOAD, LUBRICATED BY PARAFFIN.

figure 37 and the results for bearing N310 with lubricant HV1 160S (shown in figures 33 and 34), re-plotted in figure 38 .

The results for bearing N310 using lubricant HV1 55 (shown in figure 35) are re-plotted in figure 39 and the results for bearing N310 using paraffin (shown in figure 36) are re-plotted in figure 40 .

It will be noted that figures 39 and 40 contain results for 10kN bearing load only.

The interpretation of these curves appears in the discussion which follows but it is interesting to note at this stage that the results for bearing N310 lubricated with paraffin (shown in figure 40) are of the form unlike the other three figures in the series: the dramatic increase in friction torque at lower flowrates suggest that the bearing was running under conditions where the normally tenacious lubricant film had broken down. However it was reported that during these tests the film resistance monitoring circuit still indicated readings suggesting a full lubricant film. It would therefore appear that the film breakdown causing the increased friction torque had not occured at roller/race contacts but at some other contact, possibly the cage/roller or cage/race contacts.

Other, more tentative, tests (at much higher lubricant flowrates - up to 45 gm/minute, the highest value obtainable with the experimental equipment in

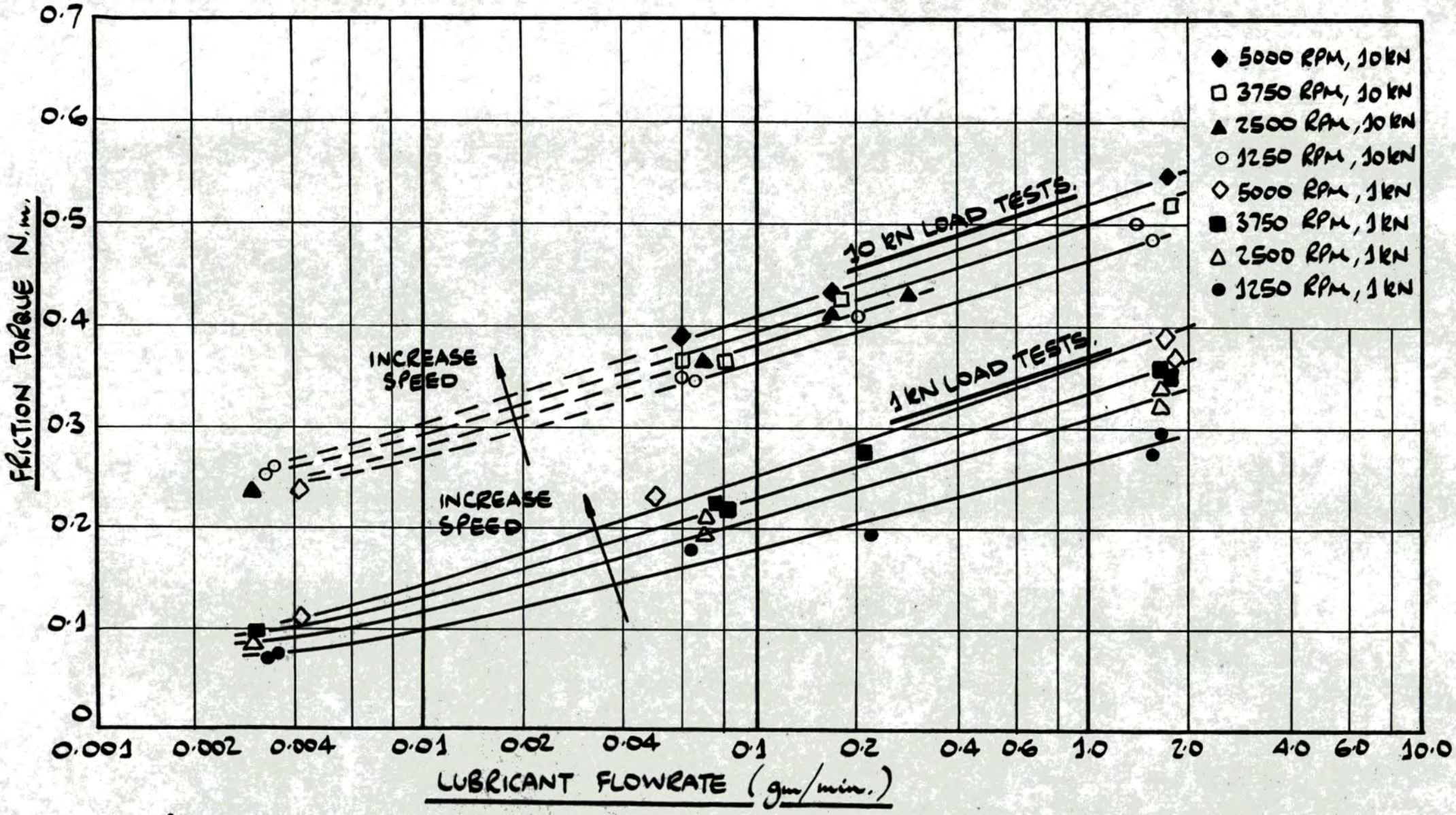

FIGURE 37. TOTAL FRICTION TORQUE FOR TEST BEARING NU 310, USING HVI 160 LUBRICANT

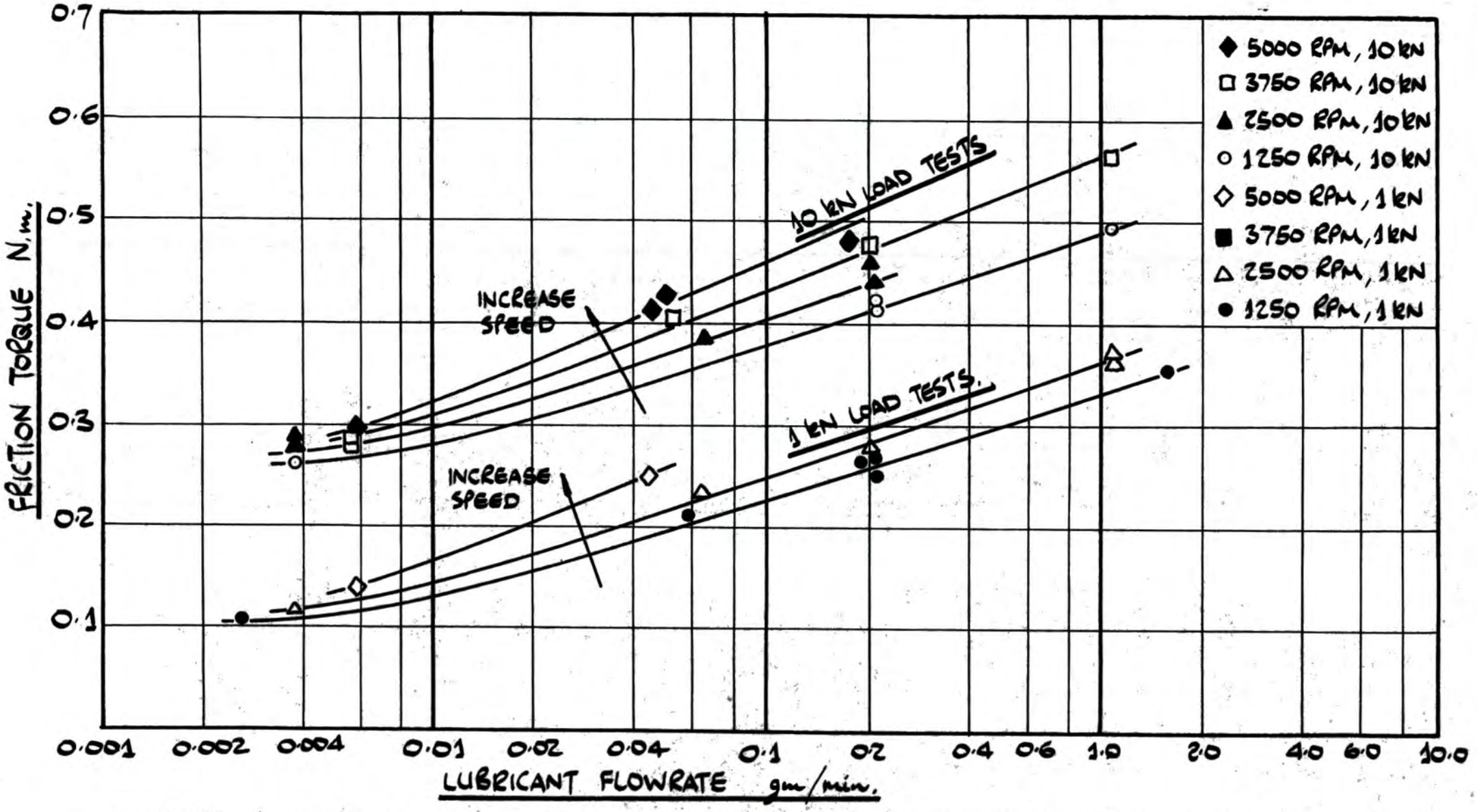

FIGURE 38 . TOTAL FRICTION TORQUE FOR TEST BEARING N310, USING HVI 160 LUBRICANT.

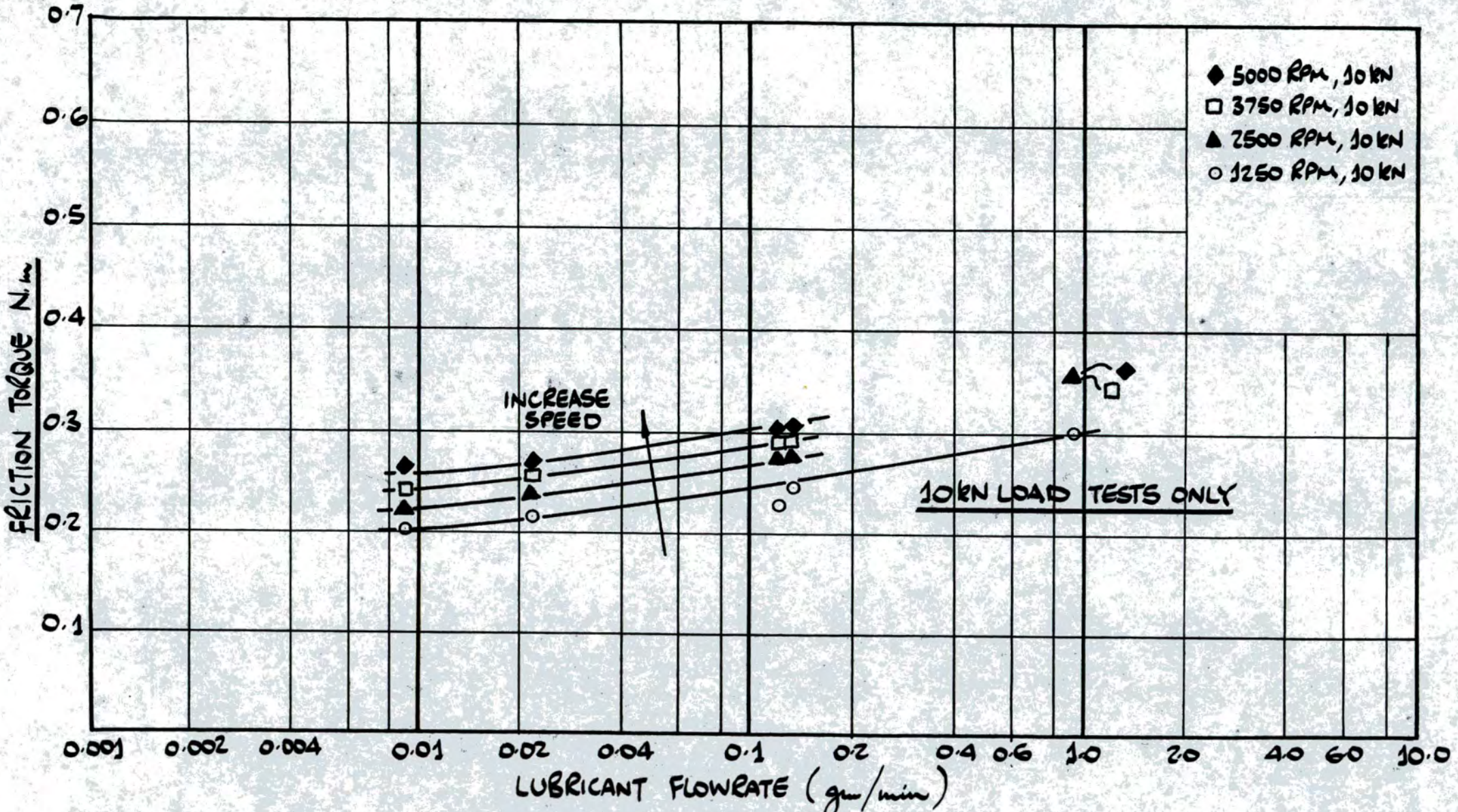

FIGURE 39. TOTAL FRICTION TORQUE FOR TEST BEARING N310, USING HVI 55 LUBRICANT.

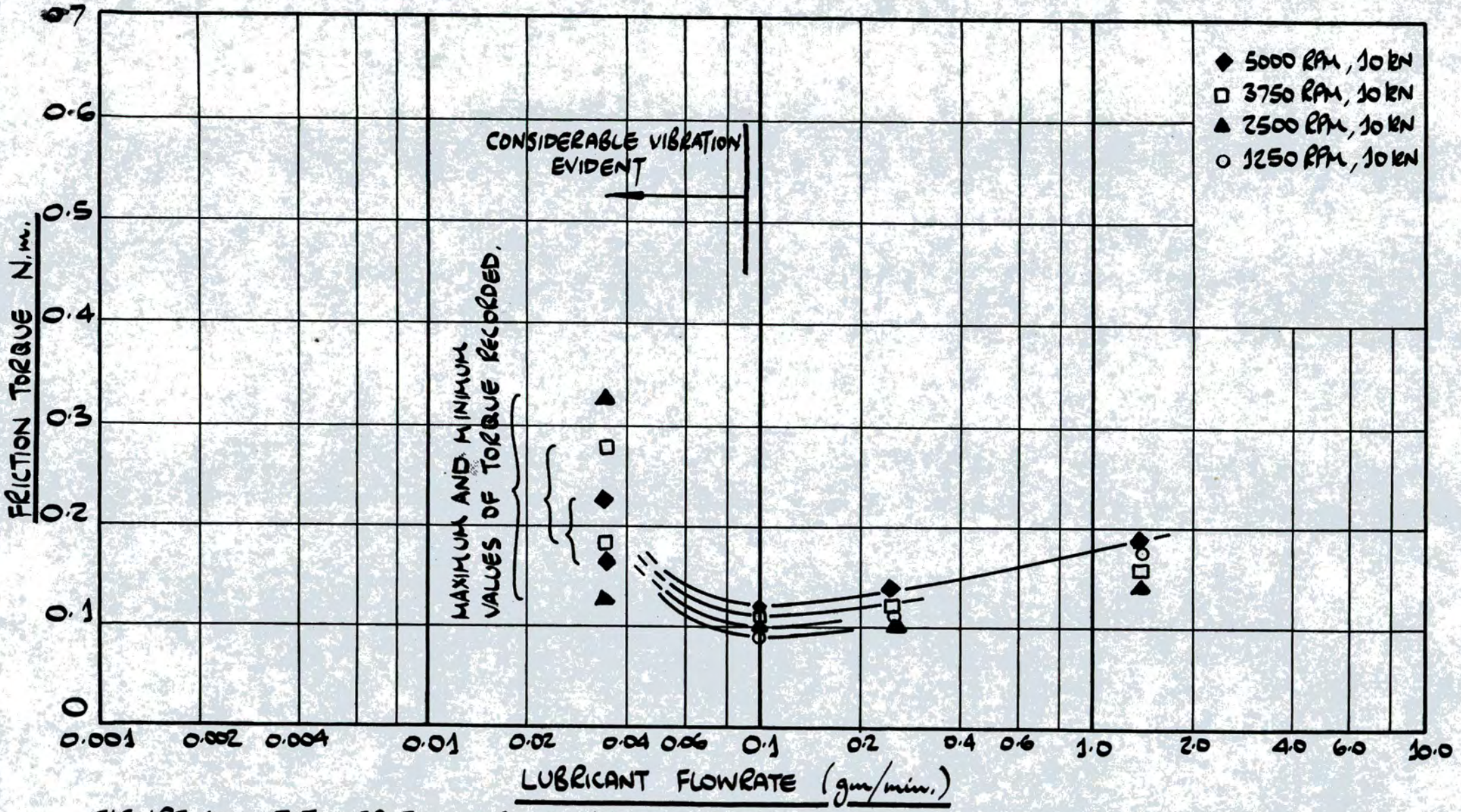

FIGURE 40 . TOTAL FRICTION TORQUE FOR TEST BEARING N310 , USING PARAFFIN AS LUBRICANT

use) were carried out to provide a better comparison with the results obtained by Boness, whose lowest lubricant flowrate was in excess of 500 gm/minute. The results of this further work, together with those from other tests carried out at much lower cooling air flowrates, have not been reported here because it was felt that they should be the subject of further investigation.

6.3 Experimental results showing the effect of lubricant flowrate on the temperatures of bearing components

It has not been possible to obtain results showing roller and cage temperatures for all the experiments using test bearing type N310, although most experimental results for bearing type NU310 do contain these temperatures.

When fitted in the testing machine, the test bearing is closely contained within the machine component forming the journal of the hydrostatic support bearing.

When in operation, the high pressure oil used in the support bearing causes heating of the test bearing components and this heating will of course affect the temperature distribution within the test bearing.

This effect cannot be completely taken into account when interpreting results - all bearings are influenced in some respect by their particular housings and the environment in which they are operating - but any variation in the quantity of heat dissipated with variation in one or more of the actual test variables would obviously be relevant and would have to be taken into account. The only test variable likely to influence the operation of the hydrostatic support bearing is test bearing load and the effect of this variable was investigated before the main experimental programme was started.

During this preliminary test, the hydrostatic support bearing was operated under a number of values of static load and the variation in test bearing outer race temperature (measured at a point directly under the applied load) with time was noted.

Figure 41 shows the results of the tests for three typical bearing loads and it will be noted that, although the rate of temperature rise is not constant with applied load, the bearing temperature settles to a constant figure independent of load after about three hours duration. It is evident that providing the testing machine is allowed to reach this equilibrium condition, no compensation for this effect is necessary.

Before the experiments forming part of the undergraduate project were carried out, an oil cooler was fitted into the hydraulic circuit of the hydrostatic support bearing. After fitting the cooler, a similar set of static load tests to those described above were carried out and the results of these tests also appear in figure 41 .

The test bearing temperature again settled to a constant figure independent of applied load after a period of time, but this figure was 6.5 degrees C. below the corresponding figure for the tests conducted without the oil cooler.

This variation in 'datum' temperature is thought to be responsible for the anomalies evident between experimental results taken before and after

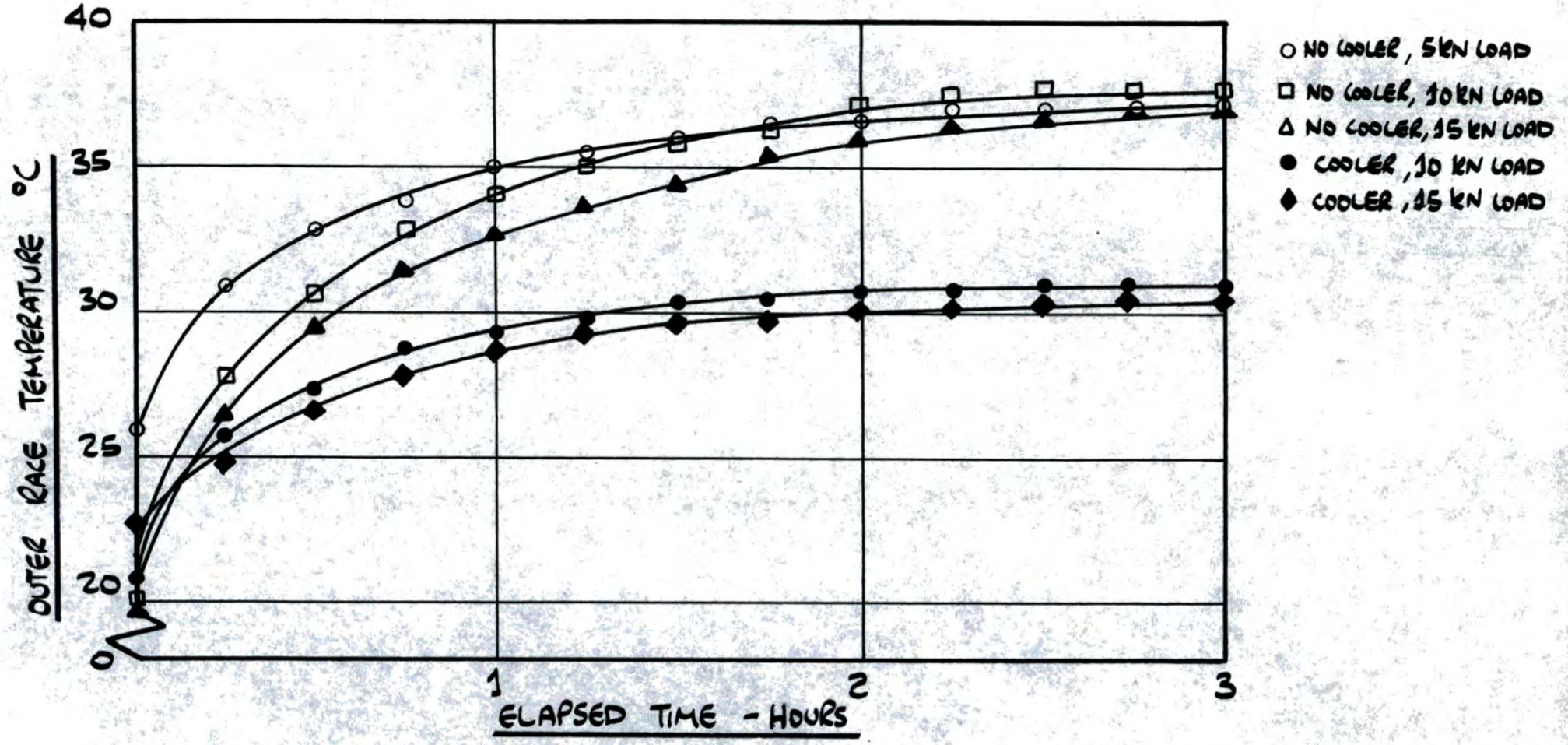

FIGURE 41. THE EFFECT OF STATIC LOAD ON THE TEMPERATURE OF THE OUTER RACE OF THE TEST BEARING, AND CHANGES DUE TO FITTING AN OIL COOLER TO THE HYDROSTATIC BEARING SUPPLY.

the fitting of the oil cooler. For temperature readings, the results of the static load tests suggest that a compensation of 6.5 degrees C should be added to the results taken after the fitting of the oil cooler for them to be directly comparable with the results taken before the fitting of the oil cooler. The relevant test results have been modified in this way before presentation.

Figures 42 , 43 , 44 and 45 show the variation in outer race, inner race, cage and roller temperatures with inner race speed, load and flowrate for bearing NU310 using HV1 160S lubricant.

Figures 46 , 47 , 48 and 49 show the corresponding curves for bearing N310, again using HV1 160S lubricant.

Figures 50 and 51 show the variation in outer race temperature with inner race speed and flowrate for bearing N310, figure 50 showing the variation using HV1 55 lubricant, and figure 51 the variation with paraffin as a lubricant. Each figure contains curves for 10kN bearing load only.

Figure 42 has been re-plotted to a base of flowrate in figure 52 and figure 46 in figure 53.

The circumfrential temperature variation around the outer race of the test bearing would be expected to have a maximum value at the point of application of the load and then fall gradually around the circumference, having a minimum value diametrically

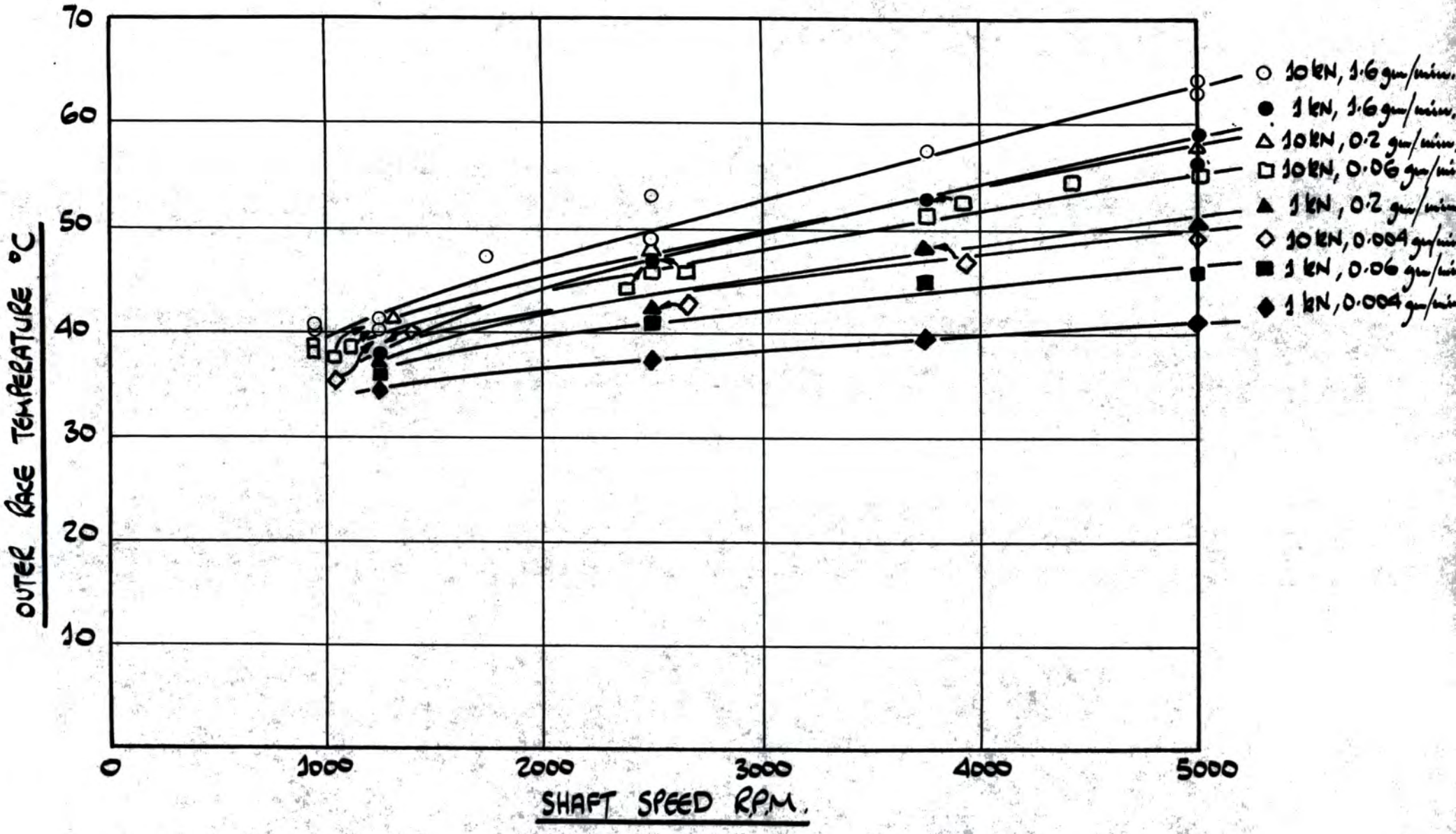

FIGURE 42. VARIATION IN OUTER RACE TEMPERATURE WITH SPEED AND FLOWRATE TEST BEARING NU310, USING HVI 160 LUBRICANT.

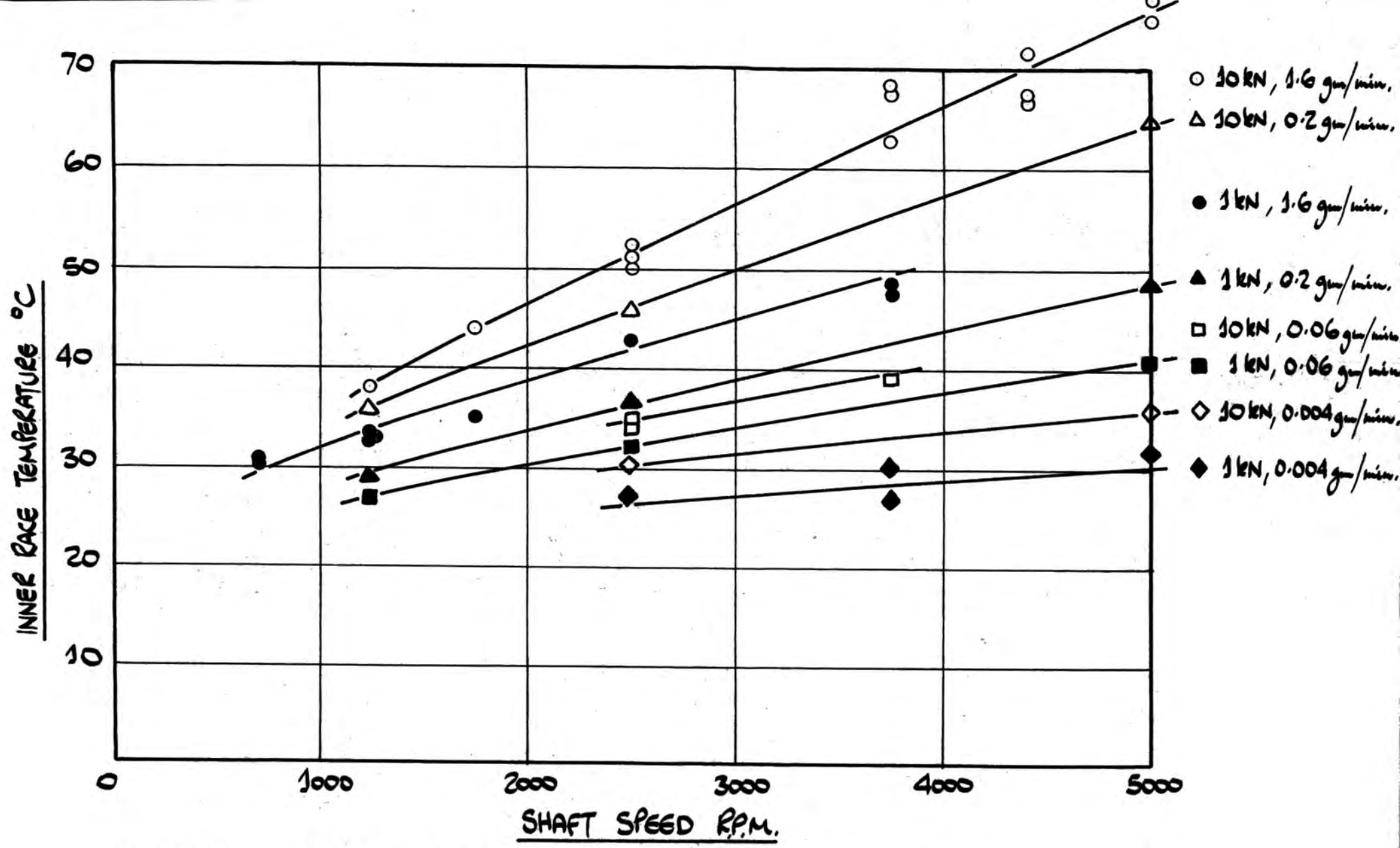

FIGURE 43 . VARIATION IN INNER RACE TEMPERATURE WITH SPEED AND FLOWRATE. TEST BEARING NU310, USING HVI 160 LUBRICANT.

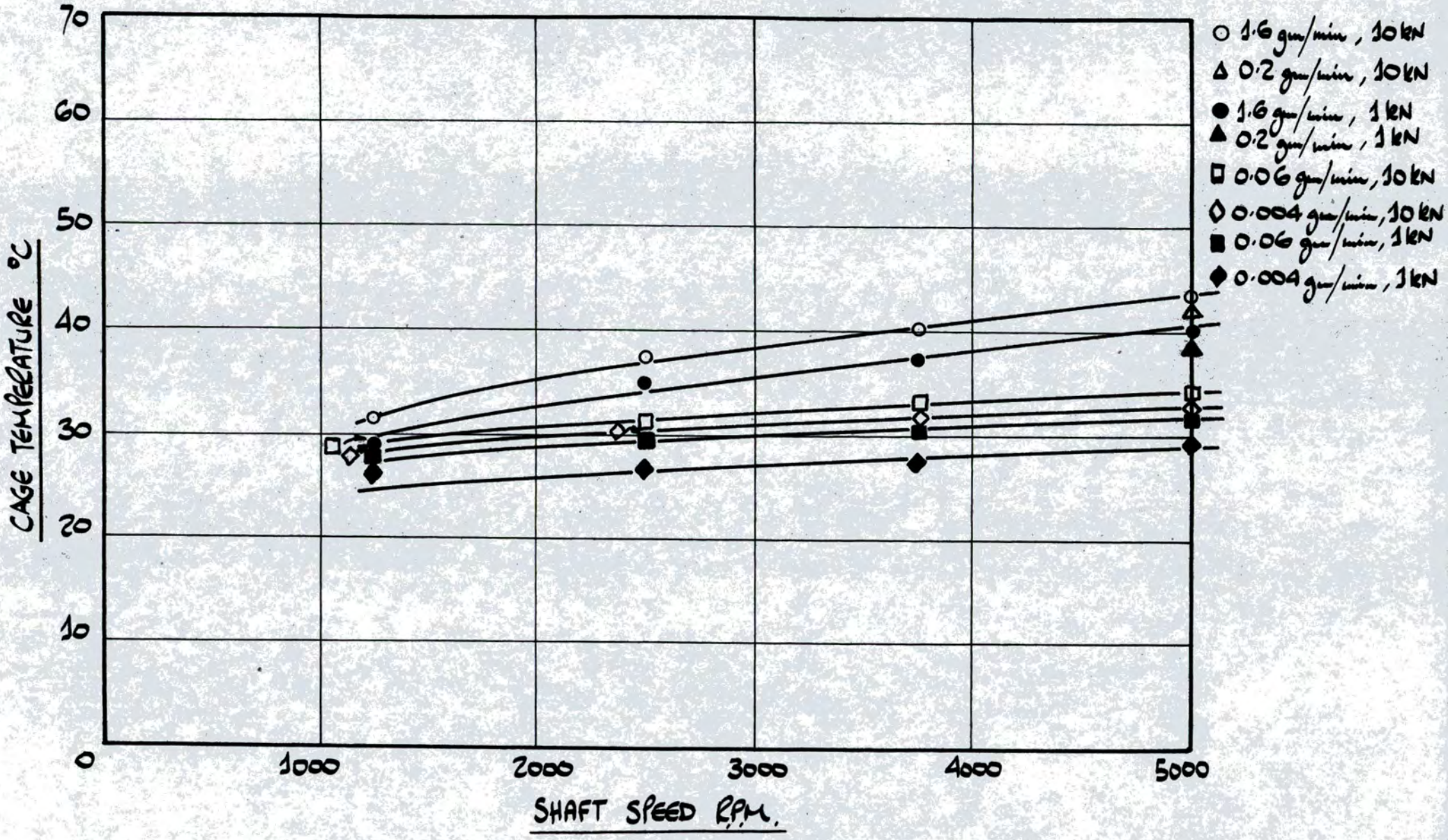

FIGURE 44. VARIATION IN CAGE TEMPERATURE WITH SPEED AND FLOWRATE. TEST BEARING NU310, USING HVI 160 LUBRICANT.

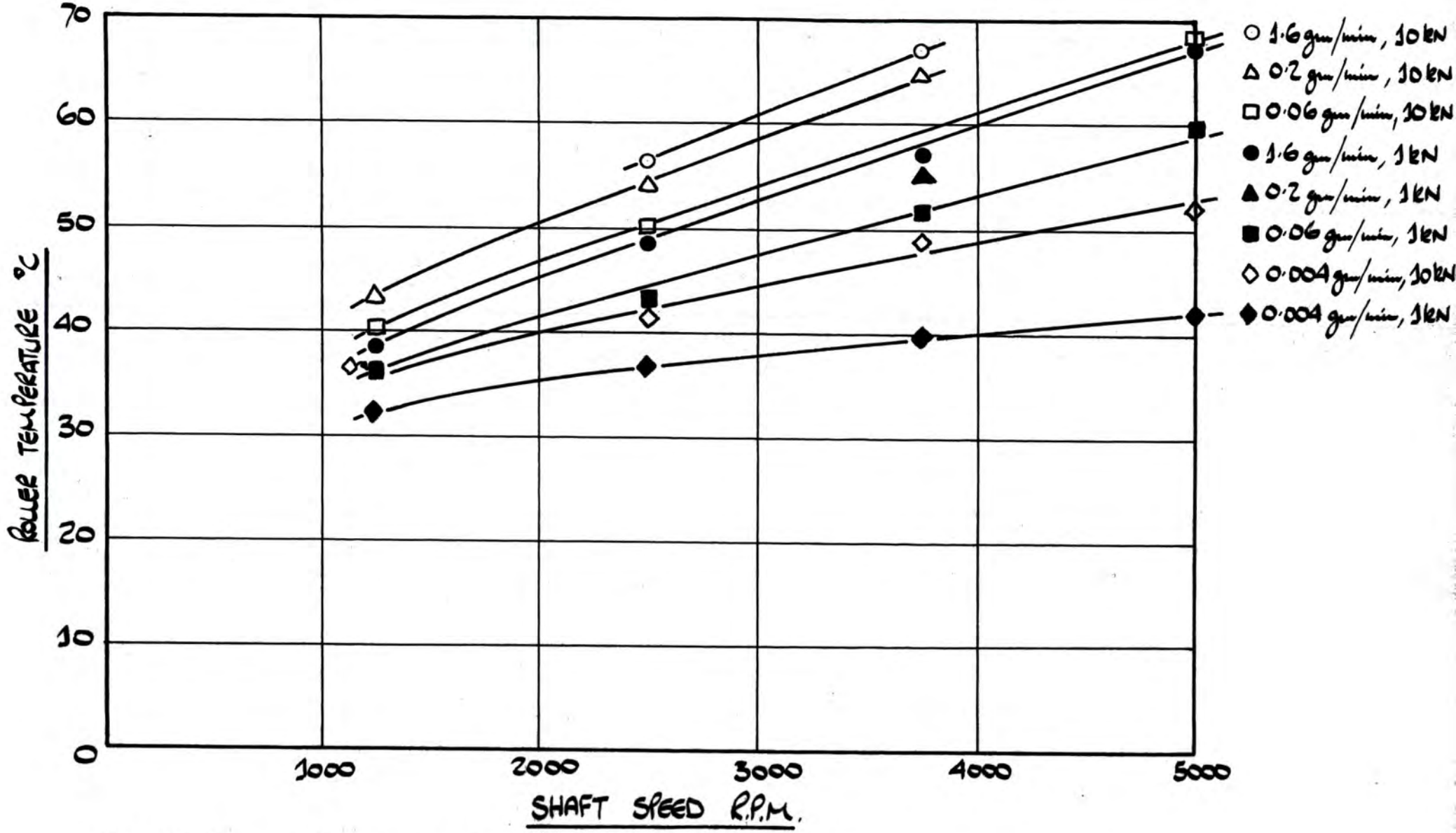

FIGURE 45 . VARIATION IN ROLLER TEMPERATURE WITH SPEED AND FLOWRATE. TEST BEARING NU310 , USING HVI 160 LUBRICANT.

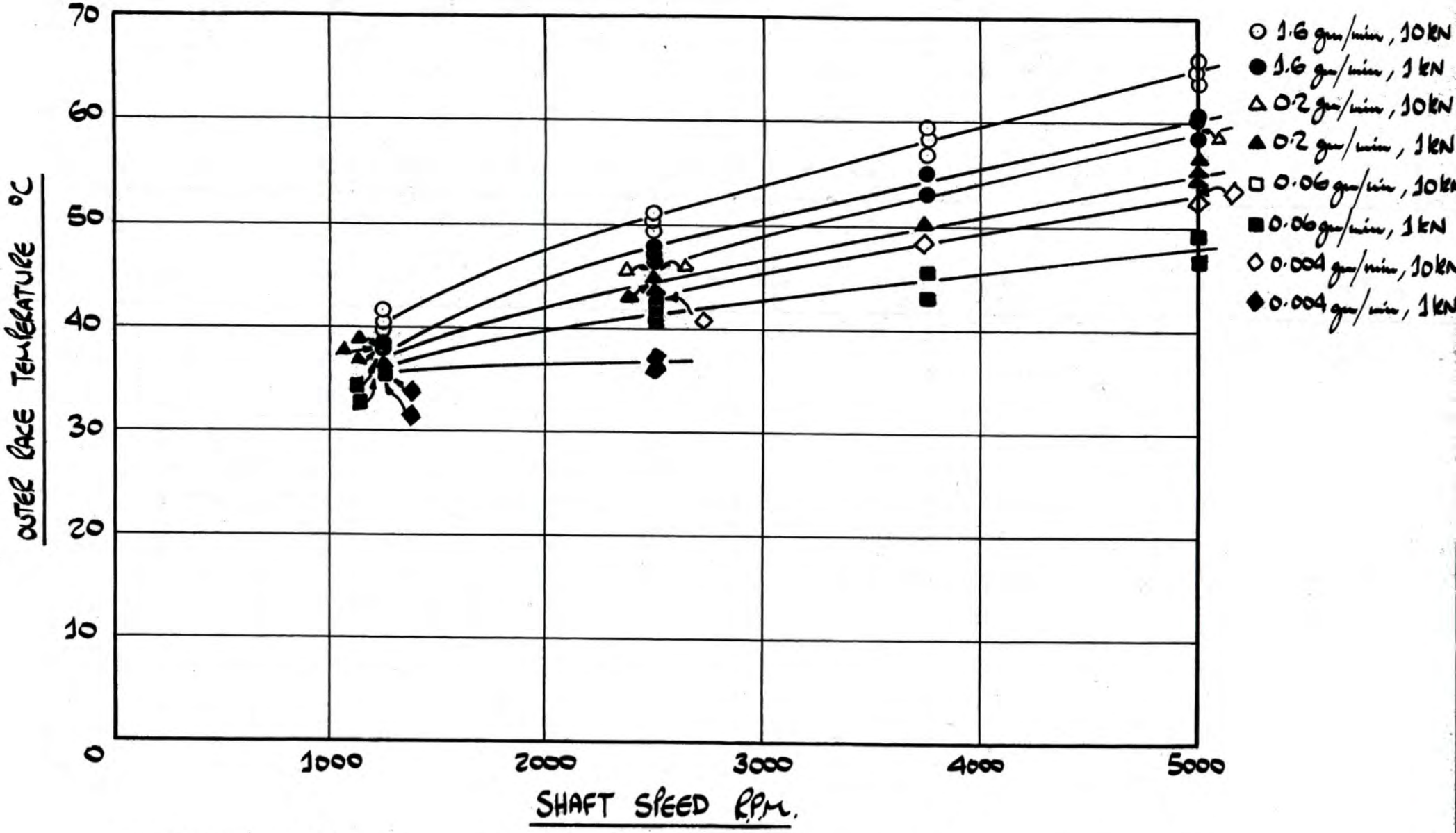

FIGURE 46. VARIATION IN OUTER RACE TEMPERATURE WITH SPEED AND FLOWRATE. TEST BEARING N310, USING HVI 160 LUBRICANT.

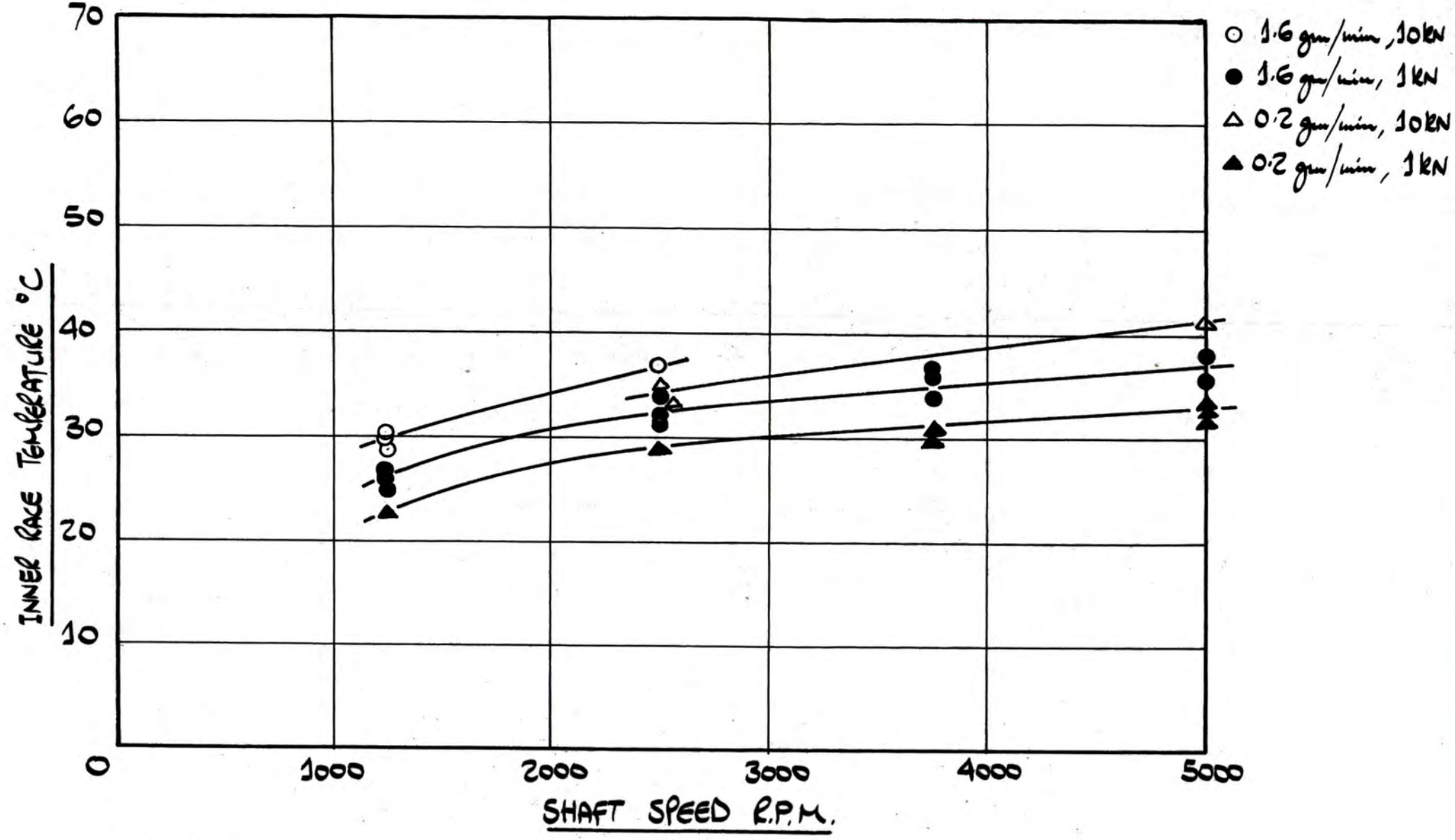

FIGURE 47 . VARIATION IN INNER RACE TEMPERATURE WITH SPEED AND FLOWRATE. TEST BEARING N310, USING HVI 160 LUBRICANT.

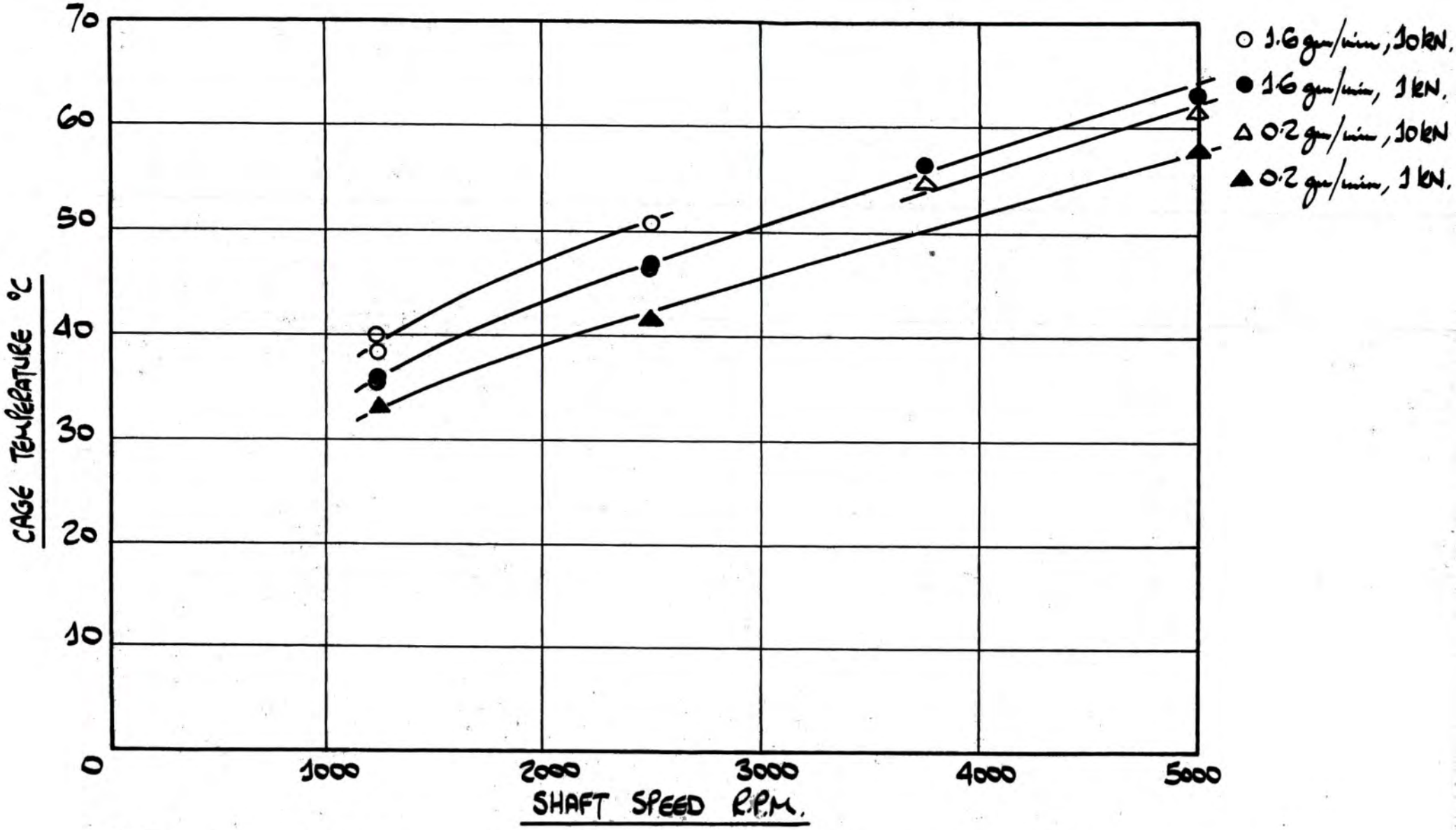

FIGURE 48 . VARIATION IN CAGE TEMPERATURE WITH SPEED AND FLOWRATE. TEST BEARING N310, USING HVI 160 LUBRICANT.

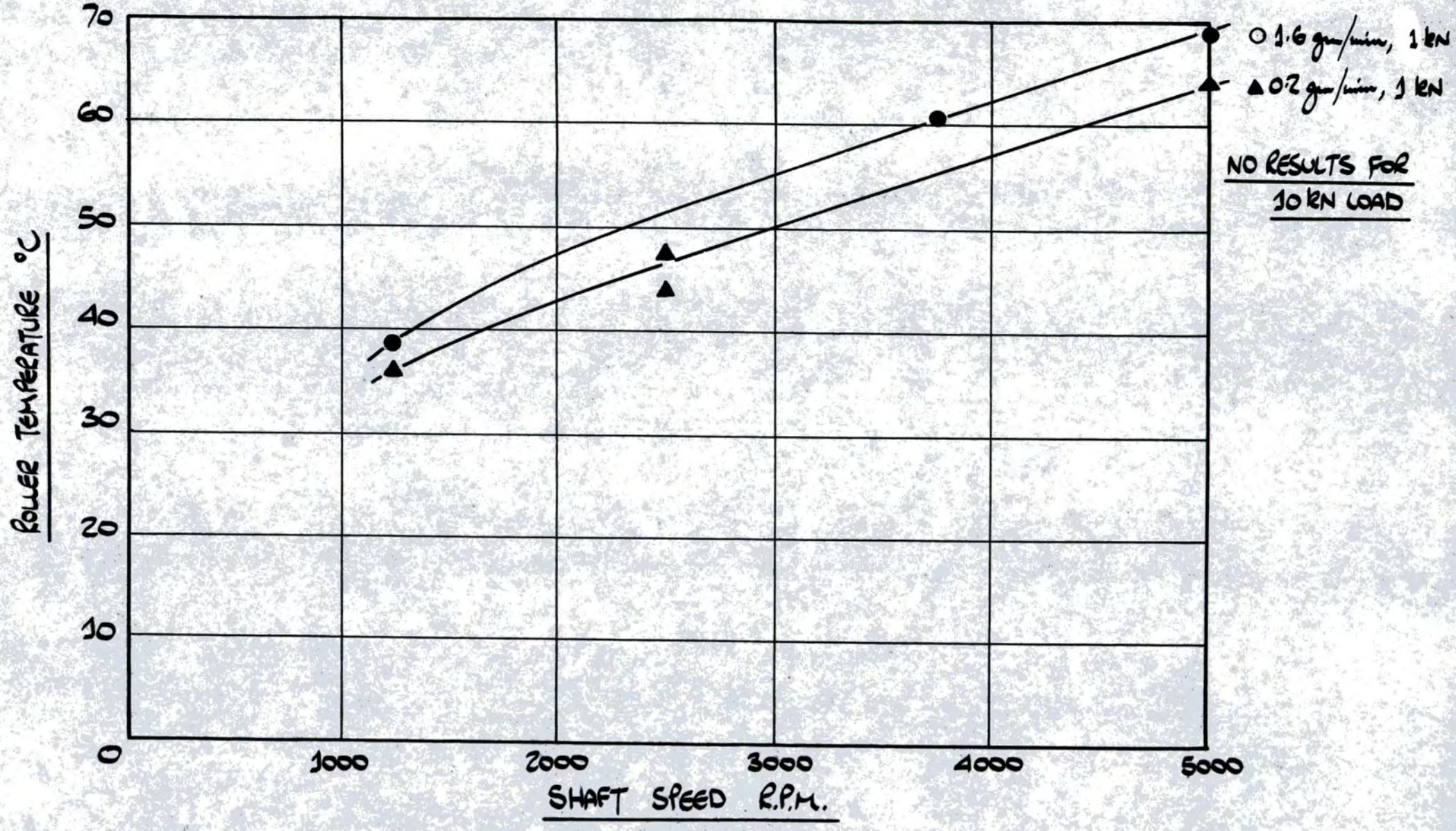

FIGURE 49. VARIATION IN ROLLER TEMPERATURE WITH SPEED AND FLOWRATE. TEST BEARING N310, USING HVI 160 LUBRICANT.

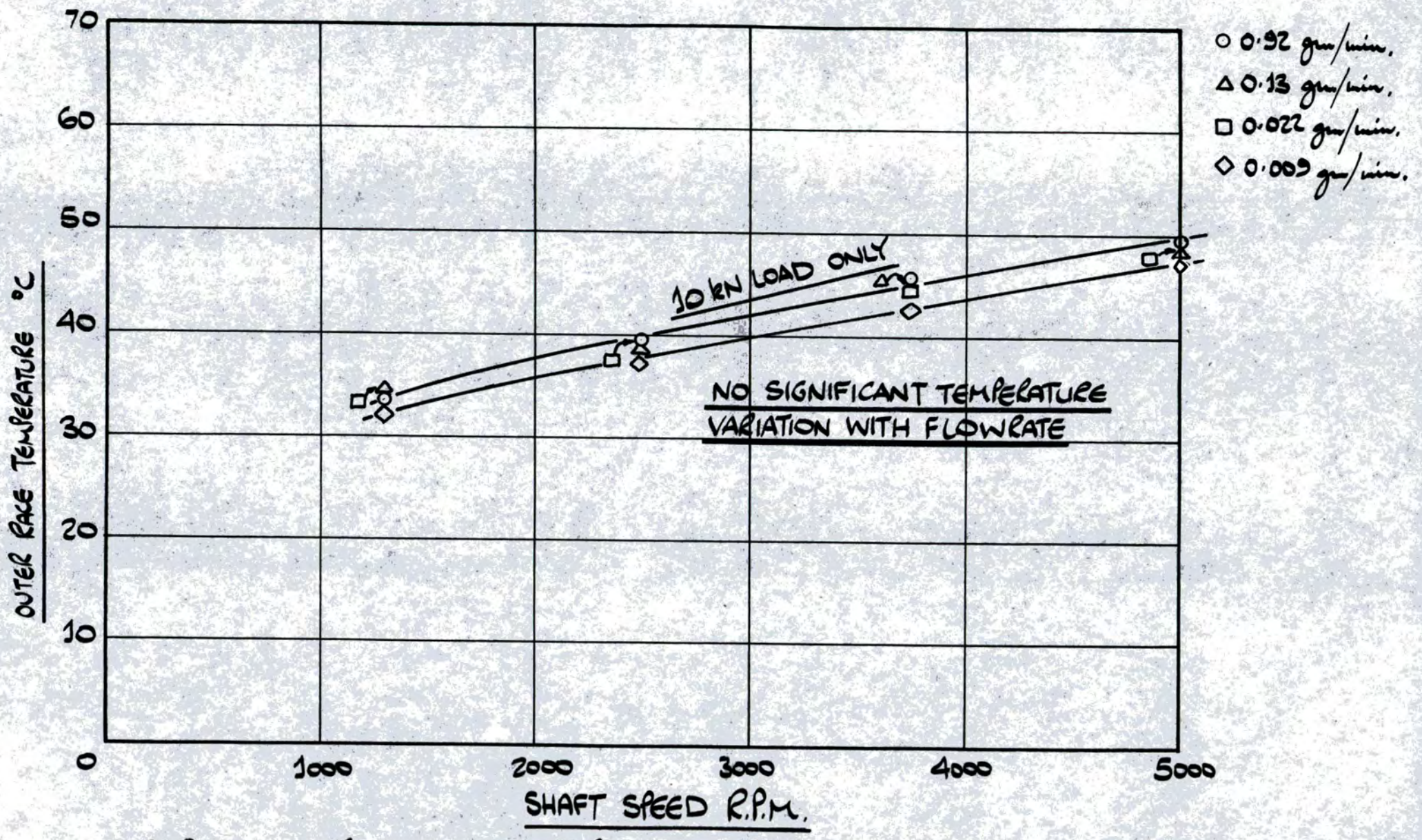

FIGURE 50 . VARIATION IN OUTER RACE TEMPERATURE WITH SPEED AND FLOWRATE. TEST BEARING N310, USING HVI 55 LUBRICANT

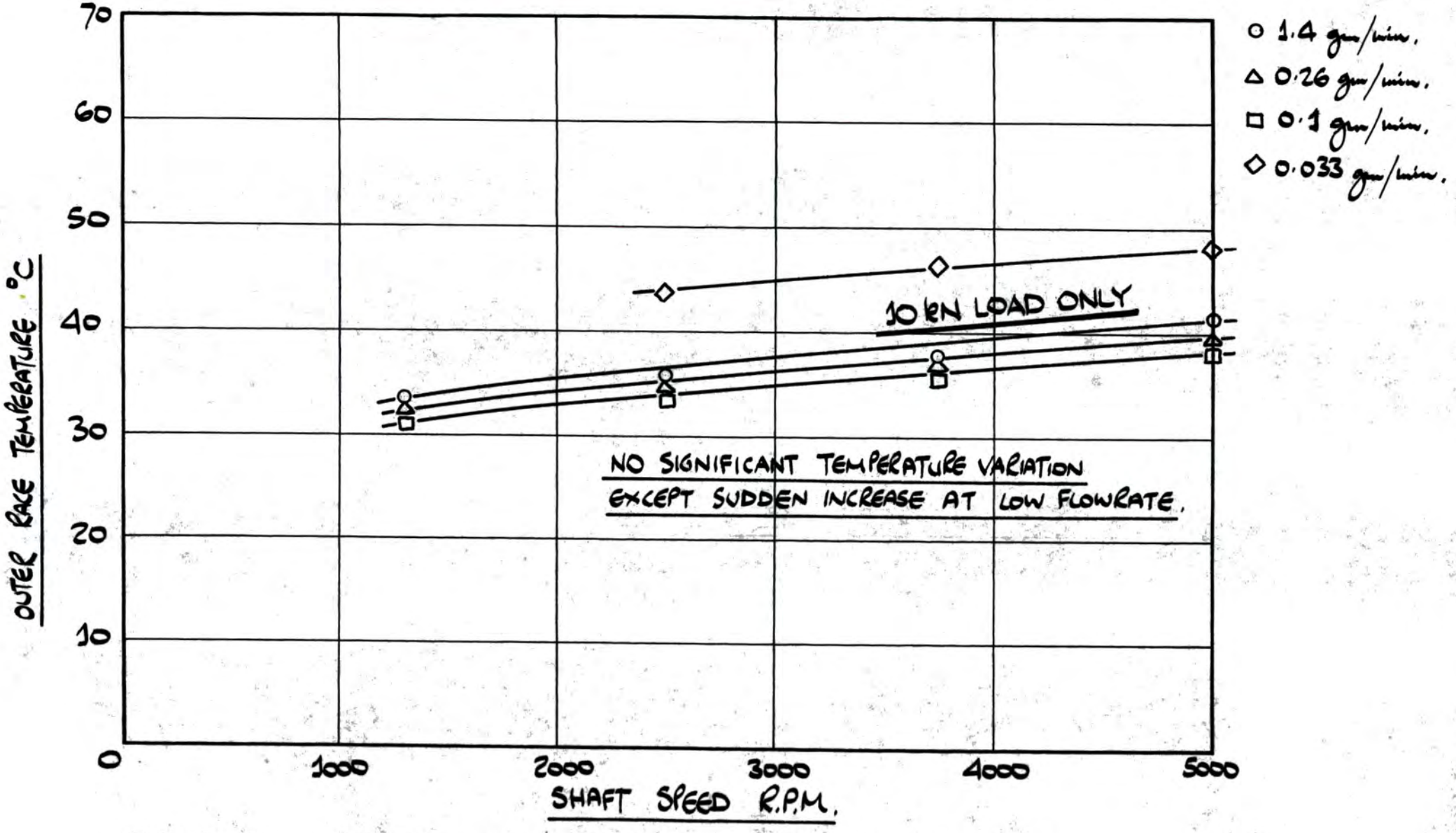

FIGURE 51 . VARIATION IN OUTER RACE TEMPERATURE WITH SPEED AND FLOWRATE.
TEST BEARING N310, USING PARAFFIN AS A LUBRICANT.

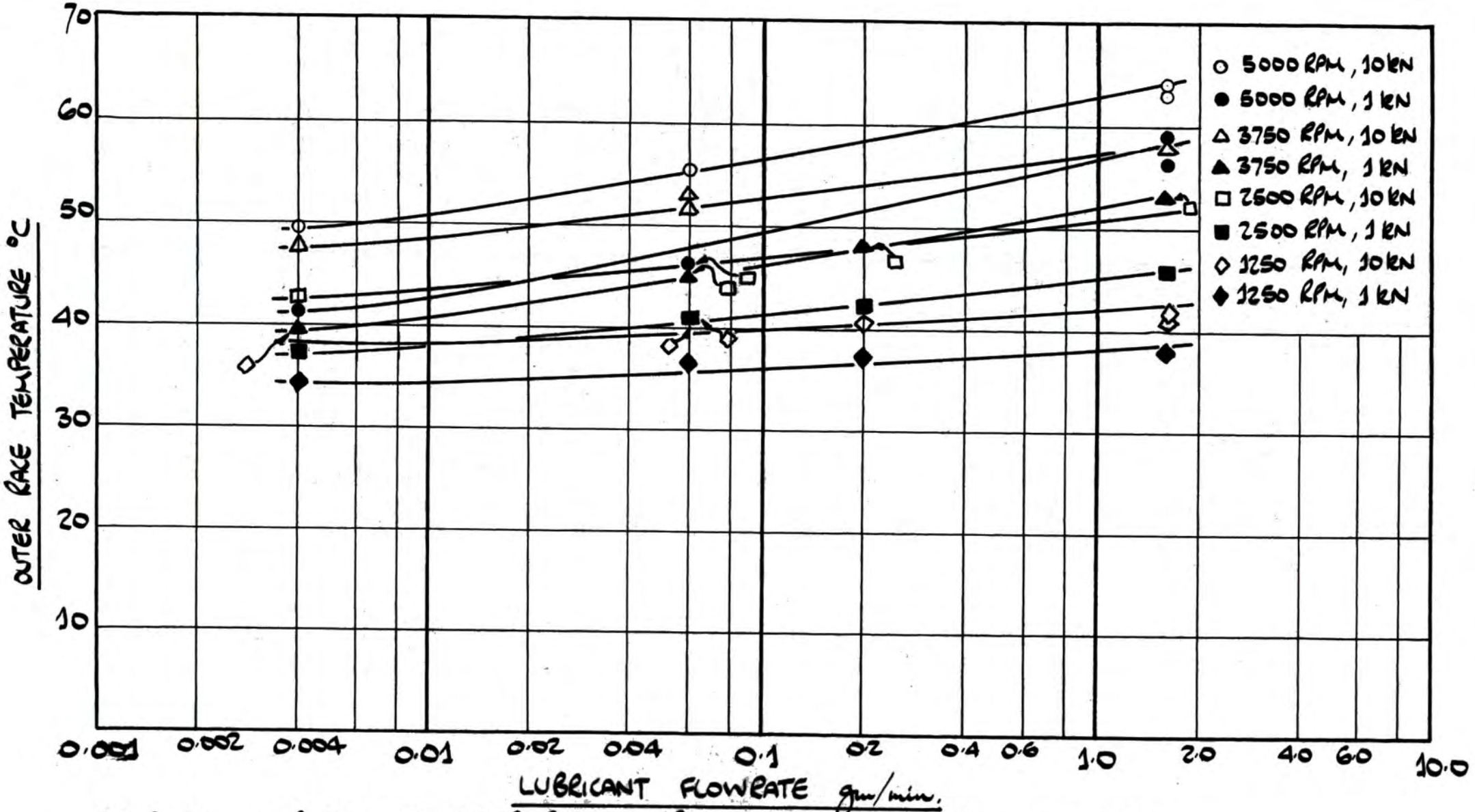

FIGURE 52. VARIATION IN OUTER RACE TEMPERATURE WITH FLOWRATE AND SPEED TEST BEARING NU310, USING HVI 160 LUBRICANT.

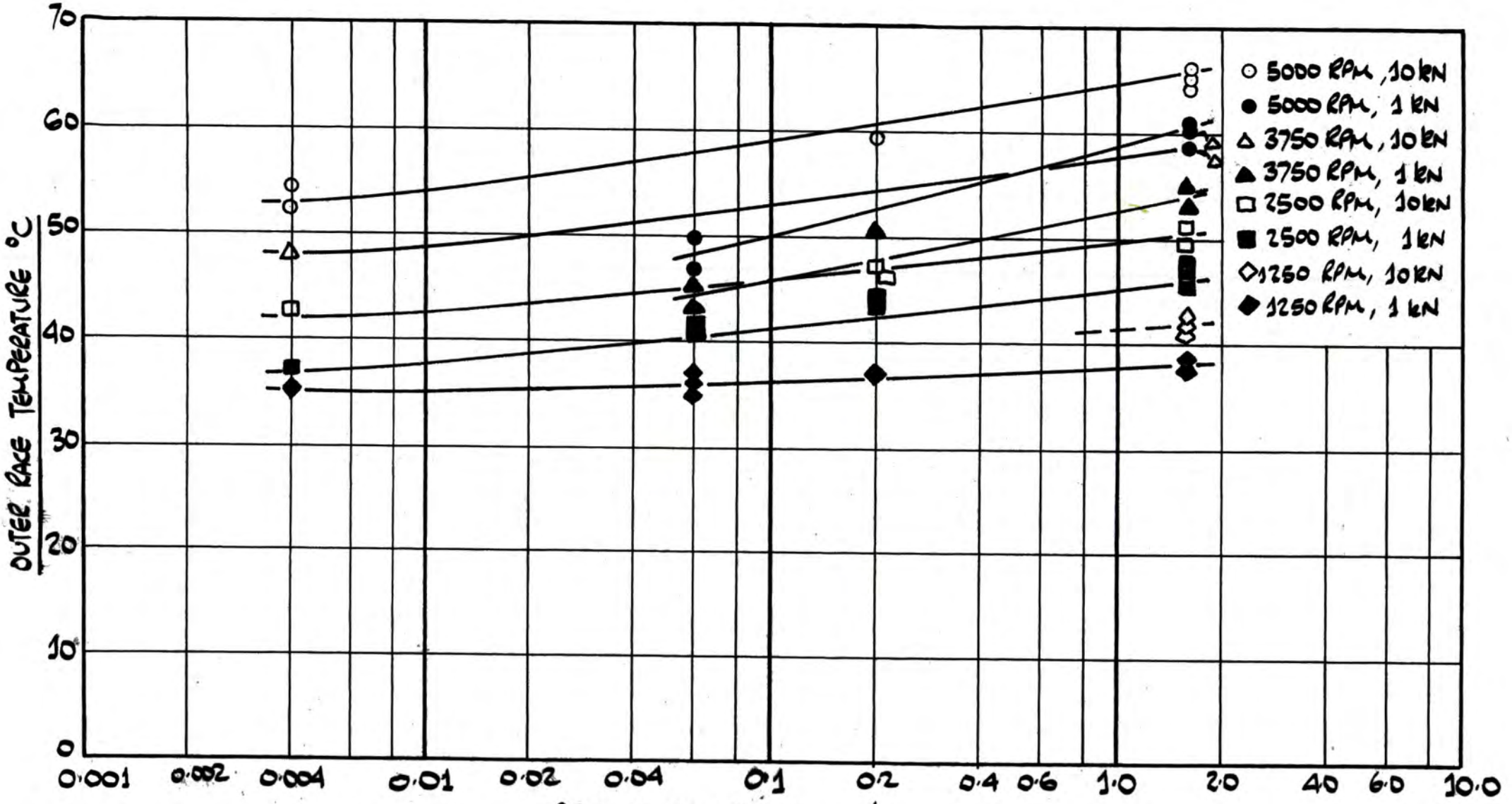

FIGURE 53. VARIATION IN OUTER RACE TEMPERATURE WITH FLOWRATE AND SPEED. TEST BEARING N310, USING HVI 160 LUBRICANT.

opposite the loading point. All the experimental results that have been obtained do exhibit this tendancy to some degree, but a number of minor variations from this smooth pattern were observed.

It is of interest to compare typical circumfrential temperature distributions with 'Talyrond' traces showing the out-of-roundness of the outer races of the test bearings. These comparisons are shown in figures 54 and 55 .

It will be noted that the temperature variation follows the 'Talyrond' traces remarkably closely. This suggests that even minor deviations from true roundness in bearing races can have a noticeable effect on the temperature variation within the component.

TEST BEARING NU310, 10 kN LOAD, 2500 RPM.
LUBRICANT FLOWRATE 1.6 gm/min.

INNER RACE TEMPERATURE 42°C
CAGE TEMPERATURE 54°C
ROLLER TEMPERATURE 56°C

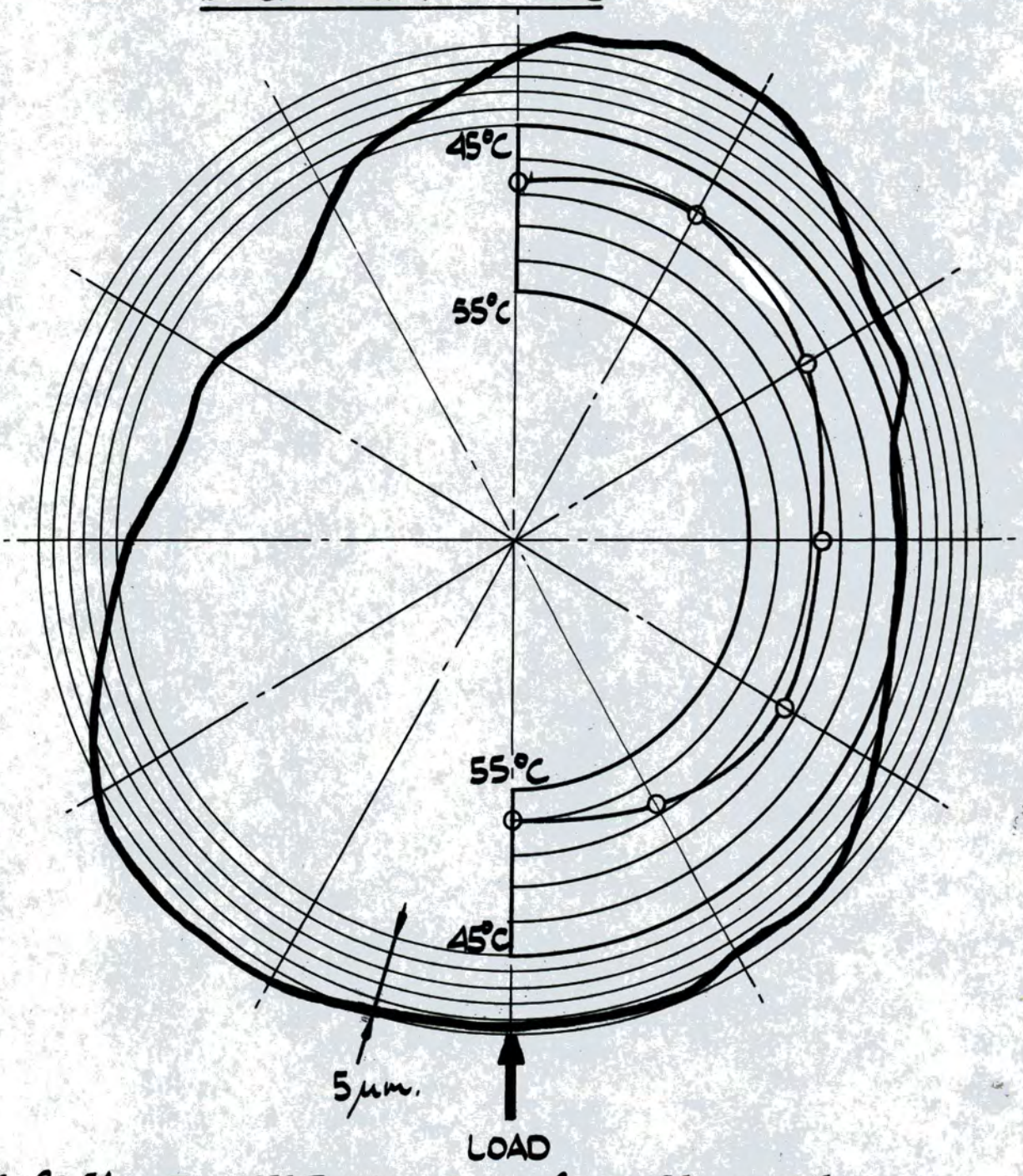

FIGURE 54. THE EFFECT OF OUT-OF-ROUNDNESS ON THE CIRCUMFRENTIAL TEMPERATURE DISTRIBUTION OF THE TEST BEARING OUTER RACE. NU310 BEARING

TEST BEARING N310, 1kN LOAD, 3750 RPM.
LUBRICANT FLOWRATE 1.6 gm/min.
INNER RACE TEMPERATURE 36°C
CAGE TEMPERATURE 56°C
ROLLER TEMPERATURE 60°C

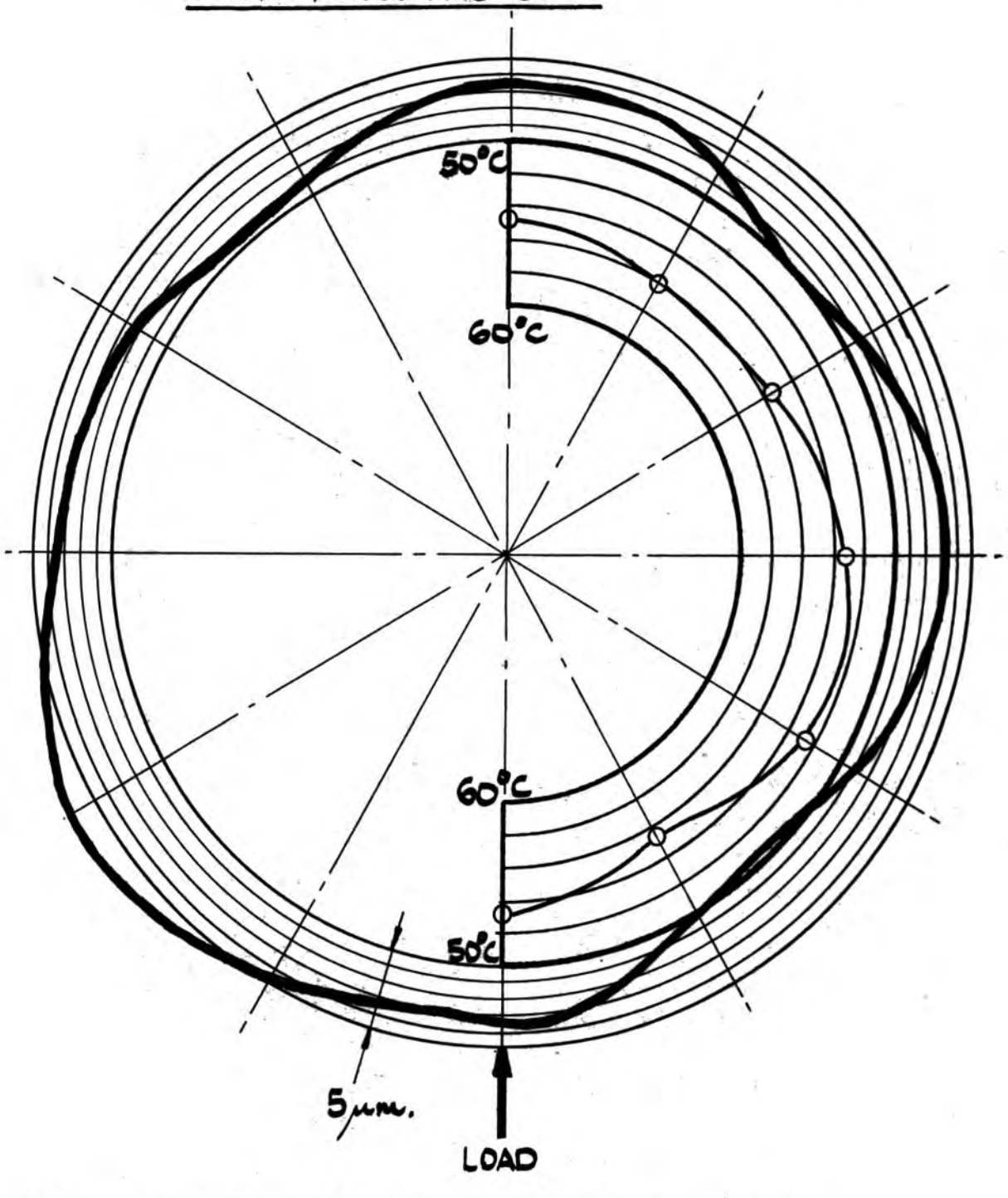

FIGURE 55. THE EFFECT OF OUT-OF-ROUNDNESS ON THE CIRCUMFRENTIAL TEMPERATURE DISTRIBUTION OF THE TEST BEARING OUTER RACE. N310 BEARING

SECTION 7

General Discussion

7.1 Theoretical considerations

The concept of lubricant starvation has received a great deal of attention within very recent times and is also the subject of a considerable amount of current investigation. This present work has attempted to re-express, and extend, the theoretical work of other authors particularly with respect to rolling contact bearings. Experimental results have been presented which show the effects of extremely low lubricant flowrates on component temperatures and friction torque in a bearing assembly.

The need for an investigation into the case of a contact where the commencement of pressure build-up occurs only a small distance from the conjunction was first recognised by Crook (9) although some opinion would prefer to attribute the recognition of this problem to Floberg (17). More recent work, as noted, by Wolveridge, Baglin and Archard (36) and by Wedeven, Evans and Cameron (35) is of fundamental importance: the former for line contacts, the latter for point contacts.

Considering again figure 6 , showing the variation of the film thickness ratio with inlet point parameter (identical to published work by Wolveridge, Baglin and Archard), it may be said that this curve has been amply justified by a number of authors as applying equally well to both line and point

contacts. Both Wolveridge et.al. and Wedeven et.al. take this curve as being so applicable: Castle and Dowson (8), using a numerical procedure, have obtained the same result and Baglin and Archard (2) have shown that this curve applies to low Modulus materials as well. Further, Wedeven, Evans and Cameron have shown in the reference noted that this curve was closely followed during experiments on starved point contact.

Figure 15 , showing the variation in rolling traction with inlet point parameter was first developed during the course of this present work and has been similarly well received, both Wolveridge et.al. (36) and Castle and Dowson (8) providing confirmation.

Castle and Dowson's work (8) has shown that lubricant starvation also affects other variables within the contact but that as starvation is increased conditions approach those of dry Hertzian contact, as shown in figure 7 . It appears from their work that the load capacity of the contact is only slightly affected (if the maximum Hertzian pressure is held constant) which, coupled with the reduction in rolling traction, indicates that the friction coefficient is continuously reduced as the degree of starvation is increased.

There is reason to believe that the concept of lubricant starvation must be taken into account when considering all problems of lubricated contact. There is some opinion (23), which suggests that even in

copiously lubricated contacts, pressure build-up commences relatively close to the conjunction: this implies that the assumption of a remote inlet point will in some respects mis-represent the contact conditions. Also, lubricant starvation as considered in this present work does not necessarily indicate lack of lubricant but rather a low value of the inlet point parameter $\bar{S}$: apparently adequate lubrication could disguise a starvation condition if other variables reduce the value of the inlet point parameter for the contact.

Wedeven, Evans and Cameron (35) have proposed definitions for two cases of lubrication, namely flooded and starved. Their definition of flooded lubrication is that the inlet region is adequately filled with lubricant and the resulting film thickness at the conjunction is insensitive to lubricant supply: a starved condition is defined as a case where the inlet region is inadequately filled and the inlet pressure build-up is delayed, the resulting film thickness being dependent on the available lubricant supply. Whilst these definitions present an acceptable view of the case where contact conditions are invariable and so any variation in the degree of starvation (as defined by $\bar{S}$) is due solely to the change in position of the physical inlet point of the lubricant film, they do understate the problem to some extent. The author believes that starvation can simply be taken to mean that the value of the inlet point parameter is

low, no matter how this reduction is caused. In many respects therefore, the use of a description such as 'reduced EHD' rather than 'starved EHD' (which suggests lack of lubricant) is to be preferred.

It has been seen that the film extent is important in this particular lubrication regime but from some view-points the dependence of the degree of starvation on physical film inlet point is unfortunate since this dimension is not generally known in practice. There is little evidence to suggest that the position of the film inlet point can be theoretically predicted at present. As noted, Lauder (24) and Boness (7) both suggest that load, speed, viscosity and lubricant flowrate have an effect, although Boness considers that any attempt to use gross lubricant flowrate to a contact to predict film inlet point must be at the best speculative: the distribution of lubricant depends to a large degree on operating conditions. Further, one would expect that the prediction of film inlet point in a rolling contact bearing to be even more complex because of the influence of preceding rolling elements on the lubricant distribution. However, it is obviously necessary for the film inlet point to be capable of prediction, or the theoretical work referred to a more convenient parameter. In this context, it is interesting to note that Floberg, in the reference noted, refers contact parameters to the exit point of the lubricant film.

7.2 The experimental torque curves

In order to establish that the experimental test conditions do occur within the starvation regime, the work of Boness (7) has been considered: a direct comparison between the results presented in this thesis and those of Boness is however difficult. Boness's results have been obtained at somewhat different test conditions and also occur at flowrates 5 orders of magnitude higher than the highest flowrate used in this present work.

In general, though, Boness's results indicate friction torques only nominally higher than those obtained for the highest flowrate presented here and also show little variation with flowrate within the range (500 - 4000 gm/min.) investigated. The results of Boness must be for a fully flooded bearing because of the high flowrates involved: the similarity of the higher flowrate results of this present investigation to those of Boness show that the former results approach conditions of full EHD lubrication.

The additional friction torque curves shown in figure 40 for low values of γN turn up at the lower limits of the curves. It has been reported that this upturning, and the accompanying instability, appeared to be due to film breakdown at some contact within the test bearing assembly although, from the oil film resistance measuring circuit, the films at the roller/race contacts appeared to be intact. Whilst it cannot be presumed that complete starvation of the

rolling contacts was even approached, it is obvious that the limit of effective lubrication of the assembly had been reached.

The experimental results presented are therefore confined to the region of lubricant starvation and cover conditions from the limit of effective lubrication of the assembly as a lower bound to conditions approaching full EHD lubrication as an upper bound.

The experimental friction torque curves shown in figures 31 , 32 , 33 and 34 indicate that in general the torque developed in bearing N310, the bearing with flangeless outer race and flanged inner race, is slightly higher than that developed in bearing NU310. This variation is most probably due to differences in bearing metrology (as shown in Appendix (B)) and not to flange location; it is for all practical purposes insignificant.

The figures do show that bearing friction torque is lessened as the oil flowrate is reduced. This reduction in friction torque is accompanied by a similar reduction in bearing component temperatures, as shown in figures 42 to 49 . It has been established that the operating regime is that of starvation: the reduction in friction torque arises directly from lubricant starvation and is certainly not due to a reduction in lubricant viscosity. On the contrary, the reduction in friction torque takes place as lubricant viscosity is increased, suggesting

that the friction torque reduction due to lubricant starvation is much more significant than would at first appear.

Figures 37 and 38 show the variation in test bearing friction torque with load to a base of flowrate.

Variation in this within the range investigated has been found to be quite linear with (ln. flowrate) and also dependent on shaft speed. Figures 56 and 57 have been plotted from the curves shown in figures 37 and 38 , providing a better illustration of these relationships. The variation of test bearing outer race temperatures exhibit a similar dependence, but to a lesser degree. This is referred to in Section (7.4) which follows.

Boness's results show that this dependence of friction torque on lubricant flowrate cannot be extended to predict test bearing conditions at flowrates outside the range investigated. If Wedeven, Evans and Cameron's (35) definitions of flooded and starved lubrication can be taken as valid for this comparison of geometrically similar bearings operating within the same γN range, it follows that the results presented here represent contacts within their 'starved' region, where conditions are to some degree dependent on lubricant flowrate: Boness's results fall into their category of 'flooded' where flowrate is relatively unimportant.

In concluding this discussion on bearing friction

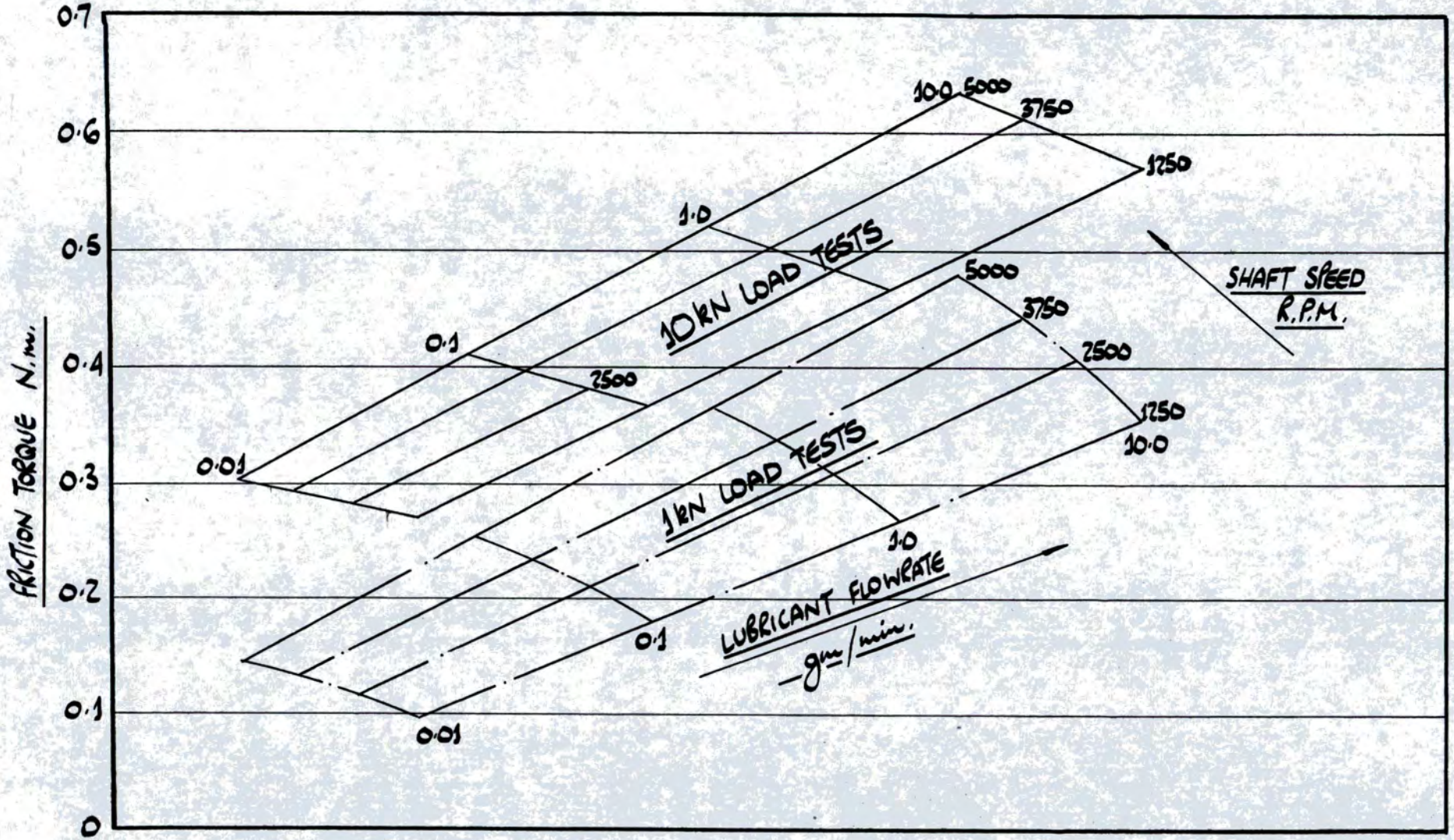

FIGURE 56. VARIATION IN TEST BEARING FRICTION TORQUE WITH SHAFT SPEED AND LUBRICANT FLOWRATE.
TEST BEARING NU310 ; LUBRICANT HVI 160S.

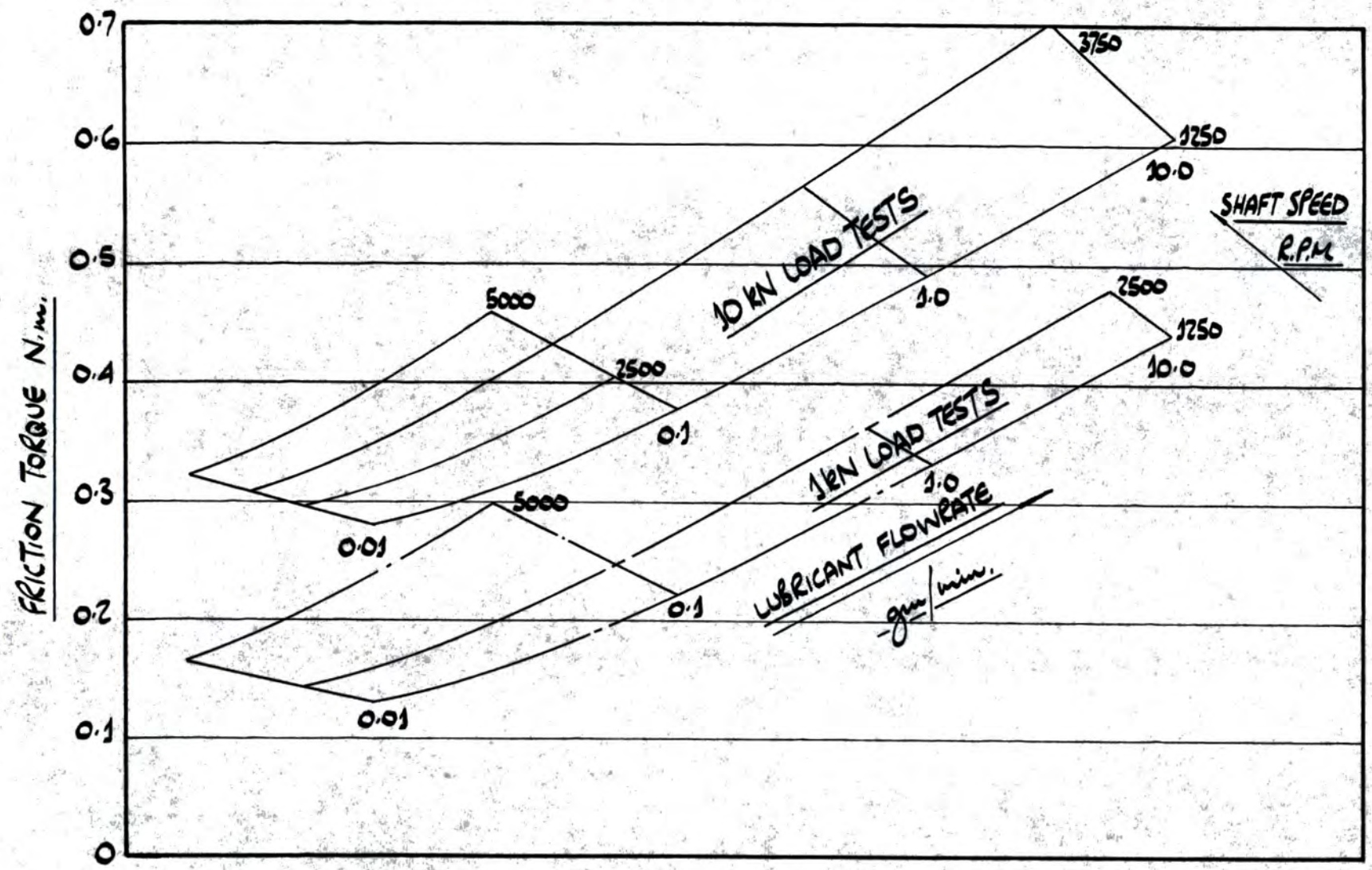

FIGURE 57. VARIATION IN TEST BEARING FRICTION TORQUE WITH SHAFT SPEED AND LUBRICANT FLOWRATE. TEST BEARING N310 ; LUBRICANT HVI 160S.

torque it is interesting to consider the work of an author first noted in the introductory paragraph to Section 3. Münnich's (26) approach to the problem of lubricant starvation differs from both the theoretical treatment contained in the body of this thesis and also that of the other authors so far noted.

Whilst this latter work is concerned with purely theoretical investigations into the starvation problem, Münnichs work is primarily based on the interpretation of experimental results from tests on parallel roller thrust bearings. His experiments were all of extremely short duration and do not therefore reflect equilibrium conditions. Because of the speed of the tests there is no change in bearing temperature and therefore no change in lubricant viscosity. A typical set of experimental results are reproduced in figure 58 , from reference (26).

Münnich claims that the results of such tests provide more information than those in which static equilibrium conditions have been attained, and proceeds to consider the various contributions to the total friction torque as measured. A particular conclusion of Münnichs is that the surfaces at the rolling contacts are not fully separated by lubricant at the rolling speed for which the friction torque is a minimum. The value of the speed-viscosity parameter at which the friction torque is minimum was further shown to be depdendent on composite surface roughness.

Figure 59 , also reproduced from Münnichs work,(27)

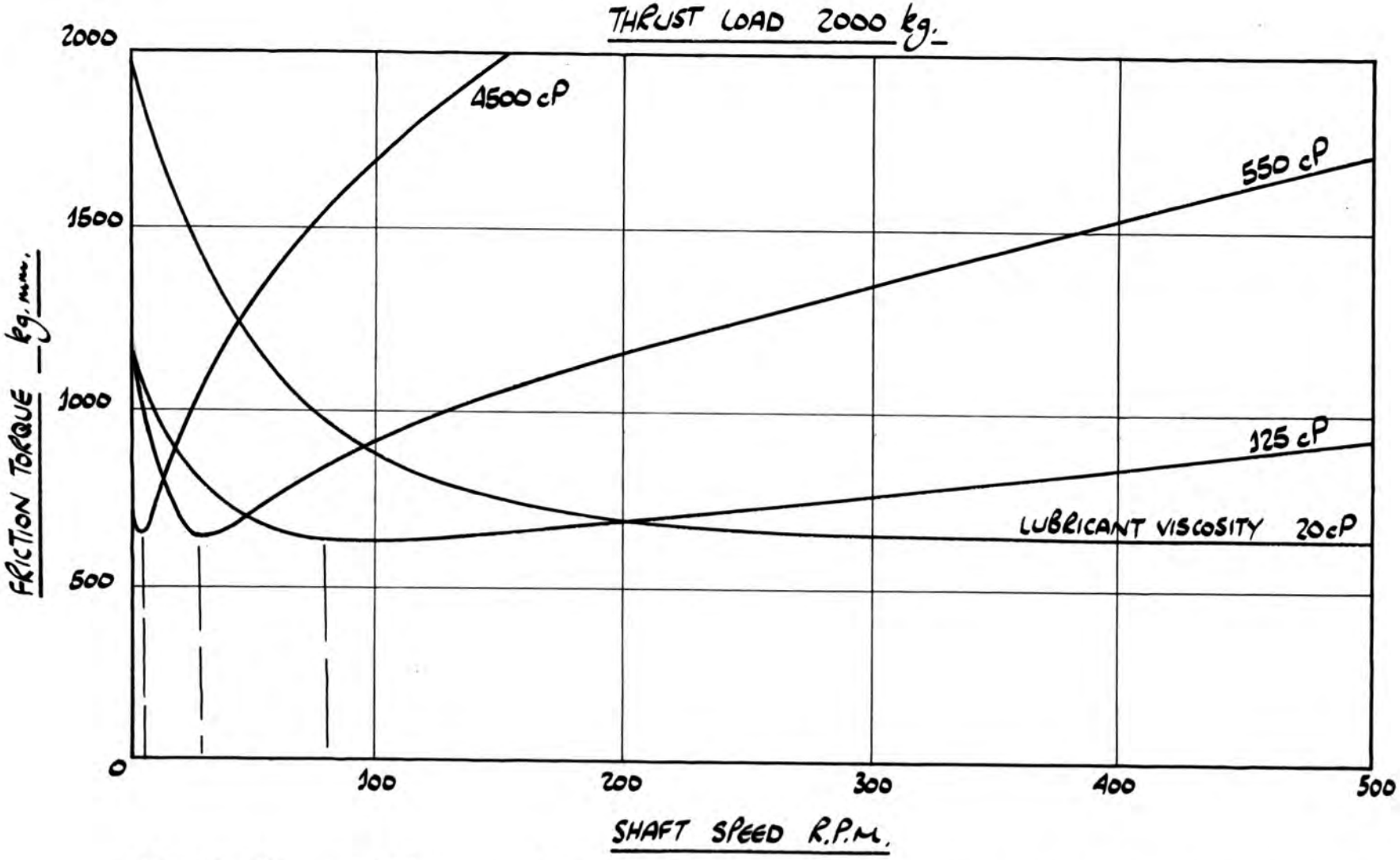

FIGURE 58. VARIATION IN FRICTION TORQUE IN A CYLINDRICAL ROLLER THRUST BEARING LUBRICATED WITH MINERAL OIL OF VARYING VISCOSITY. RE-PRODUCED FROM REF. (26)

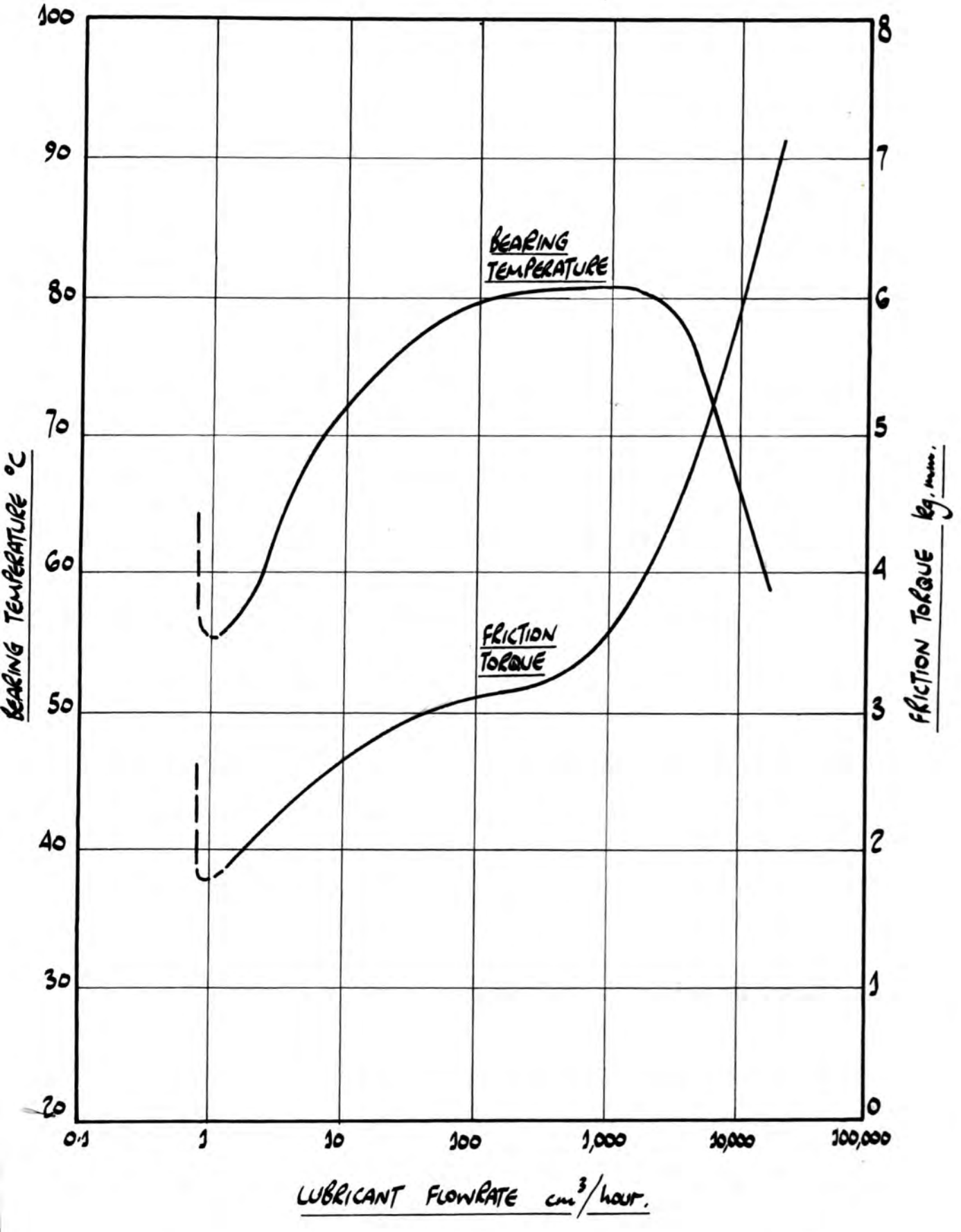

FIGURE 59. VARIATION OF FRICTION TORQUE AND BEARING TEMPERATURE WITH LUBRICANT FLOWRATE FOR A CYLINDRICAL ROLLER THRUST BEARING. RE-PRODUCED FROM REFERENCE (27)

indicates the variation in bearing friction torque and temperature with lubricant flowrate. This figure is particularly interesting in that it illustrates the form of both friction torque and bearing temperature results obtainable over a very wide range of flowrates. The experimental curves contained in this present work correspond to conditions to the left of this figure, whilst those of Boness probably represent conditions within the plateau region at the centre of the figure.

Münnich explains figure 59 as follows: especially low friction torque and low running temperatures are achieved with small quantities of lubricant. If the quantity of lubricant is reduced to a point where substantial asperity contact is taking place, a rise in both friction torque and temperature occurs. This is indicated at the left of the figure. However, if the quantity of lubricant is increased from the previously considered low value, both friction torque and bearing temperature increase, not only because of losses in the EHD film but also "because of the work involved in passing the excess lubricant through the conjunction". Large quantities of lubricant, whilst further increasing friction torque have the effect of cooling the bearing, as indicated to the right of the figure.

The statement quoted from Münnich (27) above is incorrect: the quantity of lubricant passing through the conjunction is fixed by the film thickness and the

entraining velocity and is independent of flowrate. The increase in friction torque is due to a build-up of lubricant in the inlet region as flowrate is increased. However, providing this error is noted, the work of Münnich serves the valuable function of placing the experimental data obtained here into the broader context of the complete range of practicable flowrates.

7.3 Comparison of the theoretical work and the experimental values of friction torque

The general theoretical aspects of lubricant starvation contained in Section 3 and discussed in Section 7.1 above are extended in the body of the work to the particular case of cylindrical roller bearings. The assumption of lubricant distribution that has been made - that the lubricant films will be identical at each contact irrespective of position in the assembly - is tentative but does at least provide a simple basis for the extension of the theory. However, Wedeven, Evans and Cameron (35) have shown experimentally that the film inlet position is relatively insensitive to contact load, this being the one parameter which does vary significantly with position in the assembly, and so there are grounds for hoping that the simple model of lubricant distribution used in this work will, like Grubin's, provide an acceptable approximation to the physical conditions within the assembly.

Figures 19 , 20 and 21 show the theoretical effects of lubricant starvation on the friction torque generated within the roller bearings used in the experimental work. Remembering that the three figures noted show only the contribution of rolling traction to total bearing friction - all torque values require multiplying by a factor of 2 to include the effects of

sliding traction (see page 29) - it will be seen that, by comparison with the experimental torque curves shown in figures 31 , 32 , 33 and 34 , the conditions under which the experimental results have been obtained constitute modest to severe lubricant starvation, confirming the deductions of the previous sub-section.

Using the theoretical curves shown in figures 19 and 20 , the value of the starvation factor m for each of the experimental curves can be estimated and these are summarised in figure 60 .

It will be seen that the value of m is not constant for each flowrate condition. Rather, m decreases as γN is increased indicating that the degree of starvation becomes more severe as, in particular, speed is increased. It should be noted, though, that the theoretical curves on which this comparison is based have been plotted for the condition $H_1 = m H_{oo}$ and of course H_{oo} will increase with speed. The theoretical curves therefore represent the condition where the inlet film thickness increases in direct proportion to H_{oo} as speed is increased.

For the conditions where either H_1 varies less than directly with H_{oo}, is constant, or varies inversely with speed, it follows that an increase in speed will cause the starvation factor to be reduced, as observed in the experimental results. To find which of these alternatives the experimental torque curves correspond to, the variation in inlet film

BEARING TYPE	BEARING LOAD (kN.)	Speed x Viscosity (Poise x R.P.M.)	1000		1500		2000		2500		3000		3500		4000	
		Lubricant Flowrate (gm/min)	m	$H_1 \times 10^3$	m	$H_1 \times 10^3$	m	$H_1 \times 10^3$	m	$H_1 \times 10^3$	m	$H_1 \times 10^3$	m	$H_1 \times 10^3$	m	$H_1 \times 10^3$
NU310	1	1.6	3.4	0.582	2.8	0.65	2.6	0.75	2.4	0.816	2.3	0.898				
		0.2	2.4	0.41	2.1	0.487	1.90	0.547	1.78	0.605	1.7	0.664				
		0.06	1.9	0.325	1.7	0.394	1.63	0.47	1.54	0.524	1.49	0.581	1.44	0.631		
		0.004	1.4	0.239	1.3	0.302	1.24	0.357	1.2	0.408	1.18	0.461	1.16	0.509	1.14	0.551
	10	1.6	6.6	0.845	4.2	0.731	3.3	0.71	2.8	0.715						
		0.2	4.7	0.602	3.2	0.557	2.6	0.56	2.3	0.586						
		0.06	3.8	0.486	2.7	0.47	2.2	0.473	2.0	0.51	1.7	0.496				
		0.004	2.3	0.295	1.68	0.292	1.47	0.316	1.37	0.35	1.3	0.379	1.25	0.41		
N310	1	1.6	4.5	0.770	3.5	0.812	3.0	0.864	2.8	0.952						
		0.2	2.95	0.505	2.6	0.604	2.3	0.662	2.1	0.714	1.9	0.741				
		0.06	2.3	0.393	2.0	0.476	1.8	0.518	1.68	0.572	1.6	0.624				
		0.004	1.5	0.256	1.4	0.325	1.32	0.38	1.27	0.432	1.24	0.484	1.21	0.53	1.19	0.575
	10	1.6	7.5	0.96	4.5	0.783										
		0.2	5.0	0.64	3.4	0.592	2.7	0.582	2.3	0.587						
		0.06	4.0	0.512	2.8	0.487	2.4	0.516	2.1	0.535						
		0.004	2.6	0.333	2.0	0.348	1.6	0.344	1.44	0.368						

Figure 60. Values of starvation factor m and inlet film thickness H_1 for experimental test conditions

thickness H_1 with load, γN and flowrate has been determined from knowledge of $H_{o\infty}$ for the test conditions and the estimated values of the starvation factor m.

The results are also tabulated in figure 60 and, for bearing NU310, shown graphically in figures 61 and 62. Similar curves have been obtained for bearing N310. Whilst figure 61 for 1kN load provides a reasonable illustration of the variation of H_1 with lubricant flowrate and γN, figure 62 for 10kN load is less explanatory. Figures 63 and 64 have been produced to show the variation in H_1, for both 1kN and 10kN load, for both test bearings. Also included on the two figures is the variation in $H_{o\infty}$ with γN for each load condition.

The curves presented for 1kN load show that, at this load, the variation in H_1 with γN at the various flowrates is almost identical to the variation in $H_{o\infty}$ with γN. The curves are displaced from the curve of $H_{o\infty}$ by an amount dependent on lubricant flowrate. It follows from the curves, and from equation (3.4.5), that at this constant load condition the physical film inlet point S is constant for each value of flowrate, the variation in H_1 being due entirely to the variation in H_o, taken to be $H_{o\infty}$ in this analysis. For this load therefore, the position of the film inlet point is dependent only on lubricant flowrate and independent of speed, although H_1, varying with $H_{o\infty}$, is dependent on speed.

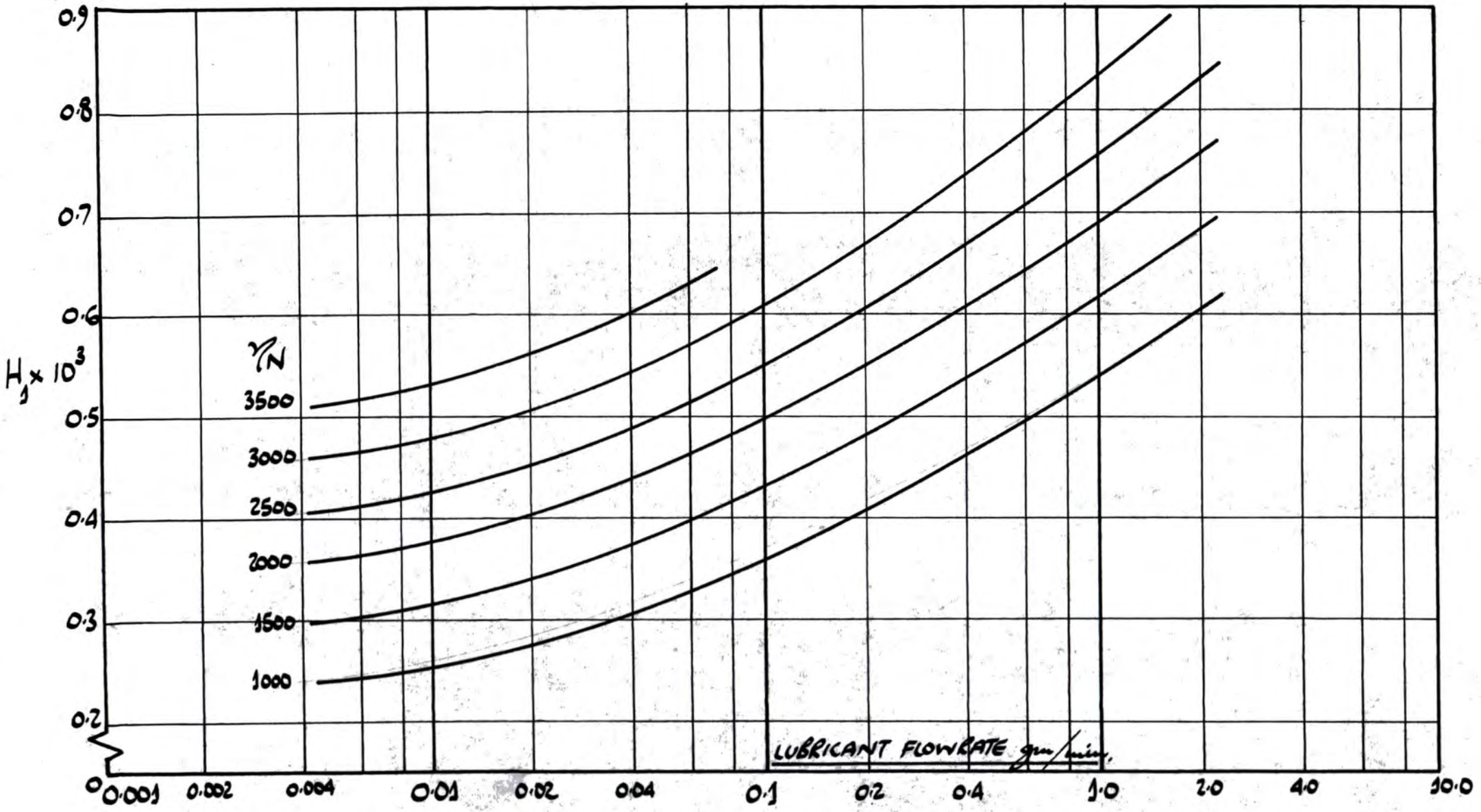

FIGURE G1. VARIATION IN INLET FILM THICKNESS WITH LUBRICANT FLOWRATE AND (SPEED × VISCOSITY). TEST BEARING NU310, LOAD 1kN.

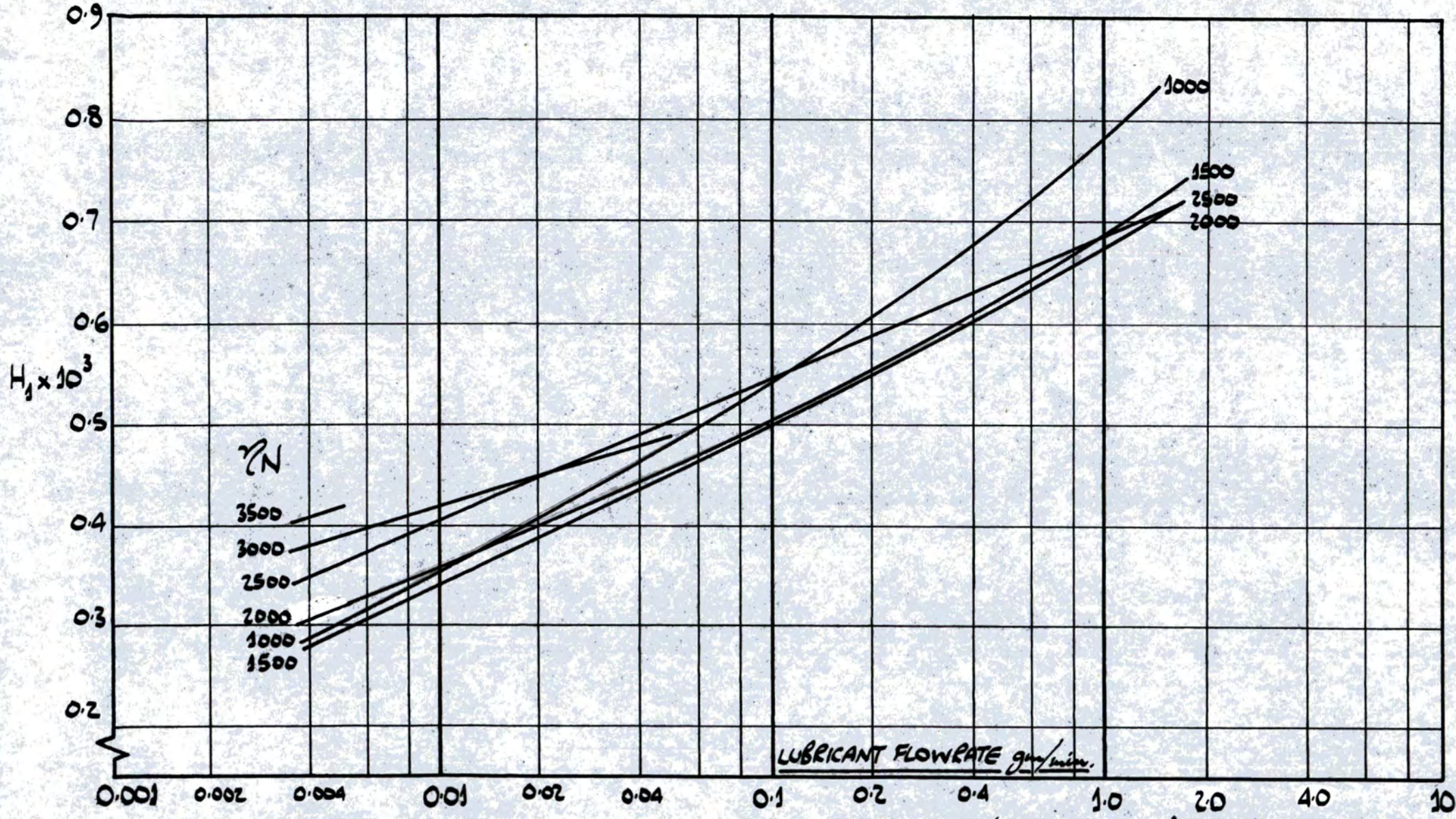

FIGURE 62. VARIATION IN INLET FILM THICKNESS WITH LUBRICANT FLOWRATE AND (SPEED × VISCOSITY): TEST BEARING NU310, LOAD 10 kN.

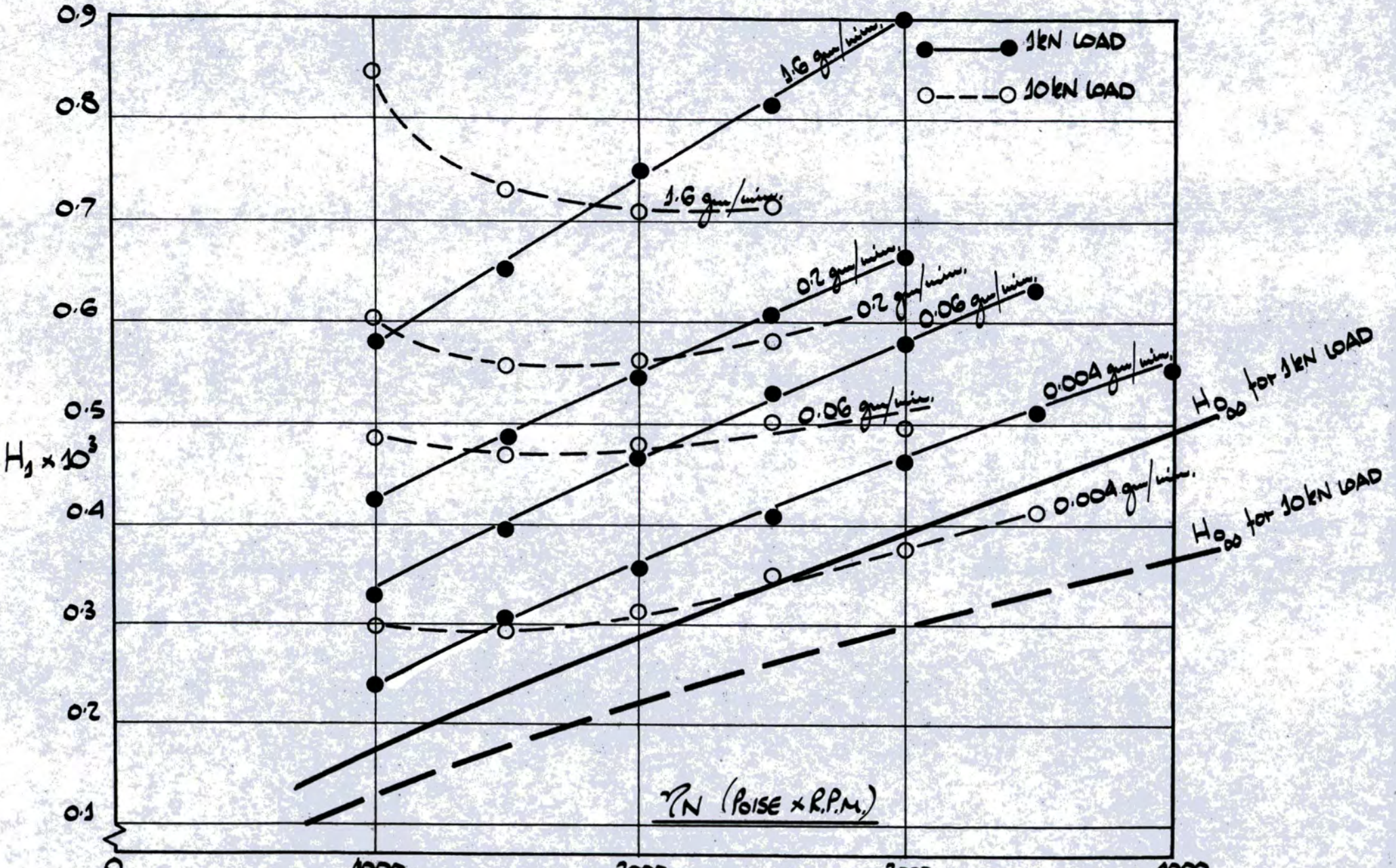

FIGURE 63. VARIATION IN INLET FILM THICKNESS WITH (SPEED × VISCOSITY) AND LUBRICANT FLOWRATE. TEST BEARING NU 310, 1kN AND 10kN LOADS.

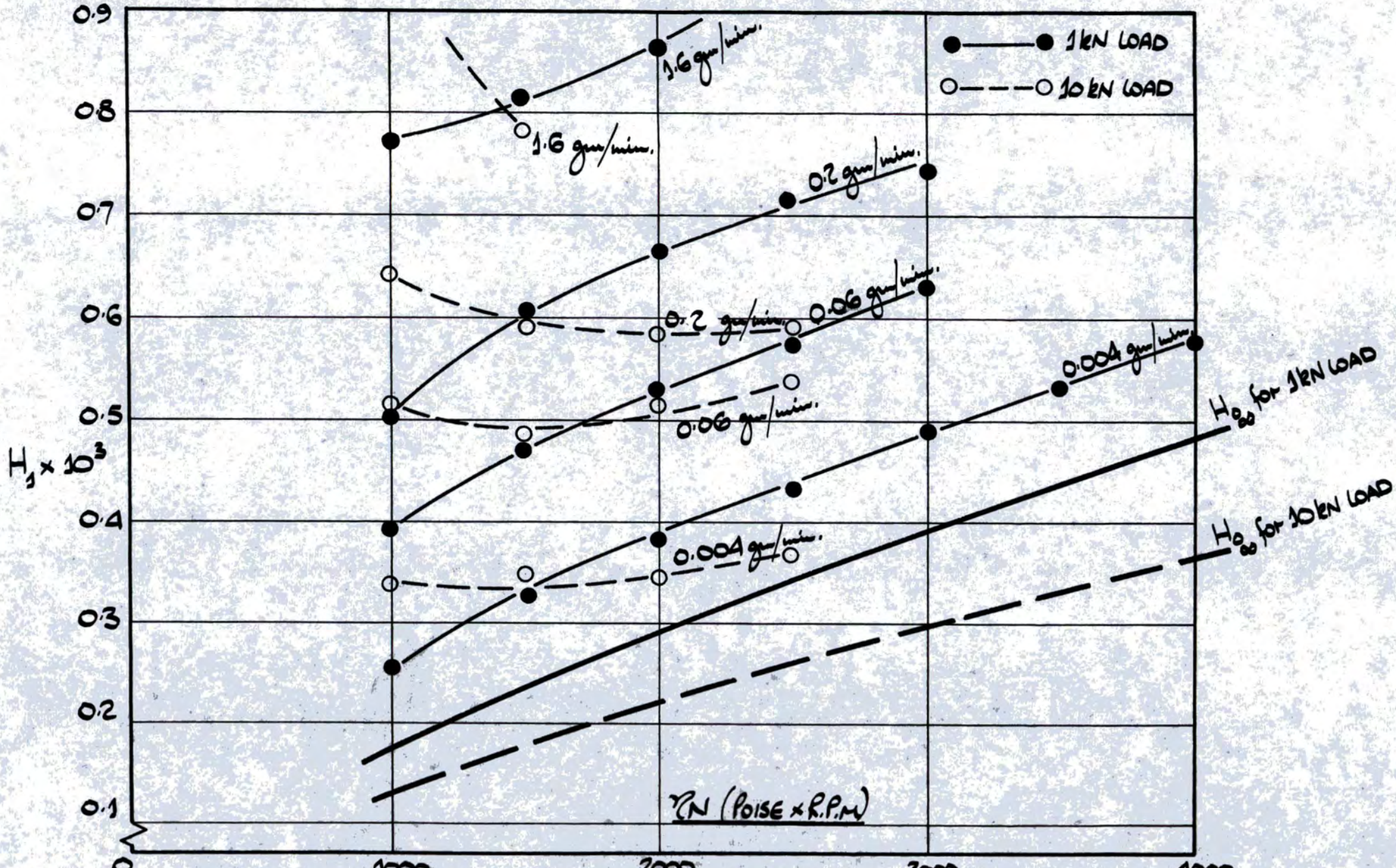

FIGURE 64. VARIATION IN INLET FILM THICKNESS WITH (SPEED × VISCOSITY) AND LUBRICANT FLOWRATE. TEST BEARING N310, 1 kN AND 10 kN LOADS.

It also follows that the variation in inlet point parameter $\bar{S}$ is due solely to changes in the non-dimensional variables G and U: since $\bar{S}$ is proportional to an inverse power of G x U, the noted reduction in starvation factor m as γ_N is increased is in agreement.

It will be remembered that the alternative analysis given in Appendix (S) was based on an assumption of constant film inlet point $x = x_1$ for all contacts within the assembly. The resulting theoretical torque curves as presented in figure S.8, S.9 and S.10 therefore provide curves for the condition of constant film inlet point with variation in γ_N as well as encompassing the assumption of constant film inlet point for all assembly rolling contacts.

The experimental torque curves for bearing NU310, figures 31 and 32 have been reproduced in figures 65 and 66. The over-lays to these figures have been produced from data obtained from the program used to produce the theoretical torque curves, figures S.8 and S.9 in Appendix (S): they are effectively the same curves as the latter, but have been modified to include the effects of sliding traction.

For 1kN load at least, the comparison is remarkable, indicating that the experimental friction torque curves within the range investigated can be well represented by the analysis contained in Appendix (S).

Neglecting the 20% of total friction due to sources other than roller/track contacts, it can be seen

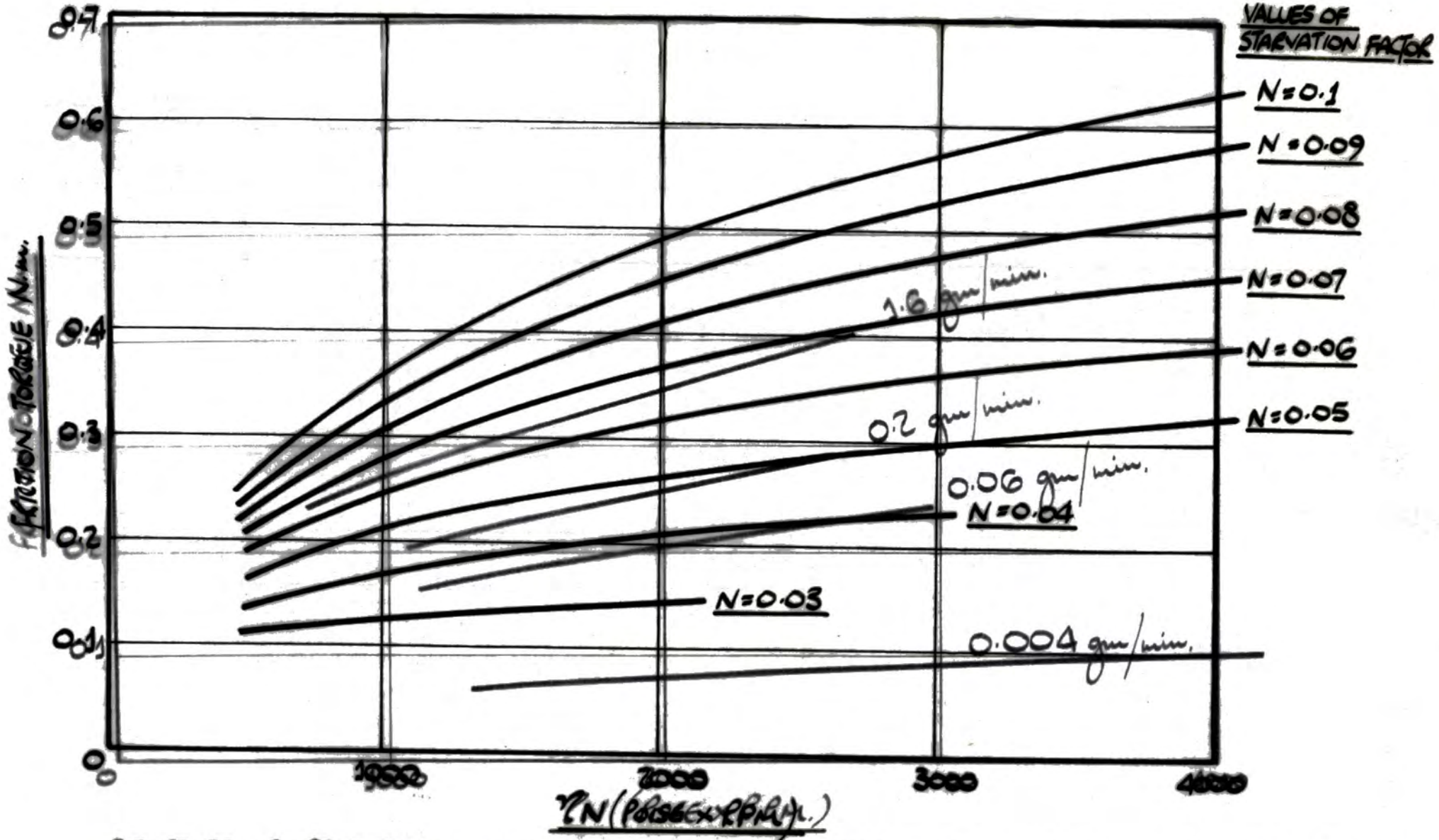

FIGURE 65 - RE-PRESENTATION OF FIGURE 3.8 (THEORETICAL FRICTION TORQUE CURVES FOR 1 KN LOAD

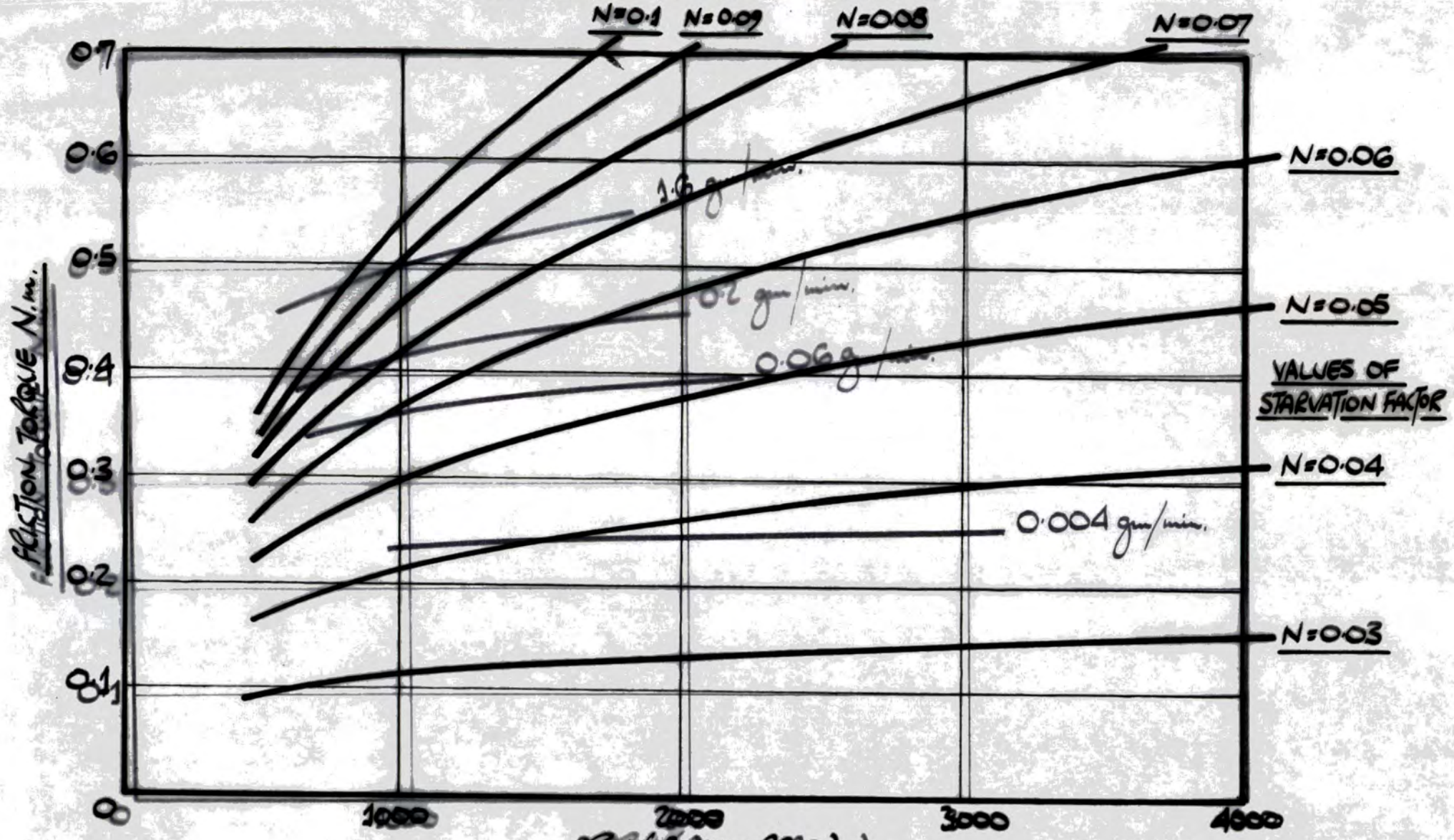

FIGURE 66. RE-PRESENTATION OF FIGURE 5. SHOWING THEORETICAL FRICTION TORQUE CURVES FOR NO AND HEAVY LOAD.

that the experimental test results correspond to film inlet positions of:

For flowrate 1.6 gm/min., $= 0.07 \times \frac{\text{roller}}{\text{radius}} = 0.525\text{m.m.}$

For flowrate 0.2 gm/min., $= 0.05 \times \frac{\text{roller}}{\text{radius}} = 0.375\text{m.m.}$

For flowrate 0.06 gm/min., $= 0.04 \times \frac{\text{roller}}{\text{radius}} = 0.3\text{m.}$

For flowrate 0.004 gm/min., $= 0.02 \times \frac{\text{roller}}{\text{radius}} = 0.15\text{m.m.}$

The physical distances from the centre-line of the roller to the inlet edge of the lubricant films are minute compared to other dimensions of the bearing. Similar results have been obtained for test bearing N310.

The curves for 10kN load in figures 63 and 64 do not follow this simple pattern. These curves indicate that the inlet film thicknesses at low values of γ_N are high and that as γ_N is increased, the film thicknesses fall to a minimum and then tend towards a condition similar to the curves for 1kN load, i.e. following lines parallel to the curve of H_{o_∞} for this load condition. The curves therefore tend towards a condition of fixed film inlet position for a given lubricant flowrate. In most instances though, the curves for 10kN do not reach this condition within the range of γ_N investigated.

Explanations of this observation might include the following.

The centre-line film thickness of the contact, H_o, is reduced with increase in load. At low loads,

when the contact film thickness is comparatively large, the volume of lubricant supplied can pass through the conjunction. There is no build-up of lubricant within the inlet region of the contact and the position of the physical film inlet point depends solely on oil flowrate, and is independent of γN. For the higher load however, the contact film thickness is reduced and at low speeds the quantity of lubricant being supplied is too great to pass through the conjunction. A build-up of lubricant occurs in the entry to the contact, causing the physical film inlet point and therefore the inlet film thickness, to be increased. As speed is increased, this condition is rectified as more oil is transported through the conjunction. The film inlet point tends towards a position dependent only on oil flowrate to the contact. From the curves for 10kN load, it will be seen that this effect is more noticeable at higher flowrates, as would be expected.

For many of the test conditions at lower values of γN, the inlet film thickness is greater at 10kN load than at 1kN load. This condition, the reverse of that for the variation of H_{oo} with load, can therefore be explained in terms of the filling of the entry region, as proposed above.

Accepting the above explanation, the mechanism for the positioning of the physical film inlet point of the lubricant film can be summarised as follows.

The lubrication condition towards which the position of the film inlet point tends is that of constant

film inlet position for a given load and flowrate. This condition is maintained irrespective of ηN : as ηN is increased, re-cycling of lubricant to maintain this condition can be imagined. However, if ηN is too low to transport the amount of lubricant supplied through the conjunction a build-up of lubricant in the inlet region takes place. This build-up can be reduced by increasing ηN , or reducing load, both of these causing the contact film thickness to increase.

The reduction in lubricant flowrate does have some effect on the build-up of lubricant but not as much as might at first be supposed. Such a reduction will of course reduce the inlet film thickness and also the film extent, causing the reduction in friction torque as observed, but because flowrate is reduced, the test condition will now lie on a lower 10kN curve in the figures, tending towards a different line parallel to the $H_{o\infty}$ curve. The lubricant flowrate may still be too great for this new condition of constant film inlet point to be achieved. The inlet film thickness may therefore still reflect a condition of excess lubricant, but now for the new constant film inlet condition, not the original one.

7.4 Bearing component temperatures

As noted previously, the test bearing outer race temperatures have shown a dependence on (ln. flowrate), and also speed and load, within the range investigated. Figures 52 and 53 have been re-presented in figures 67 and 68 to illustrate this more effectively. It will be seen that the dependence of temperature on speed is greater at higher flowrate, although the dependence on load is reduced.

The outer race temperatures obtained for bearing N310 are in all cases higher than those for bearing NU310, although the variation is not significant. As with the observed variation in friction torque, this slight variation is most probably attributable to differences in bearing metrology and not to flange location.

Figures 54 and 55 in Section 6 show typical circumfrential temperature distributions in the test bearing outer races, superimposed on 'Talyrond' traces of the outer races. The comparison is interesting since it shows in both figures that, although bearing temperatures do not vary greatly around the circumference, noticeable deviations from a smooth distribution can be attributed to quite small variations from true roundness in the bearing races.

Radial temperature distribution was measured at one point in each of the test bearing outer races, but temperature variation was insignificant, being of the

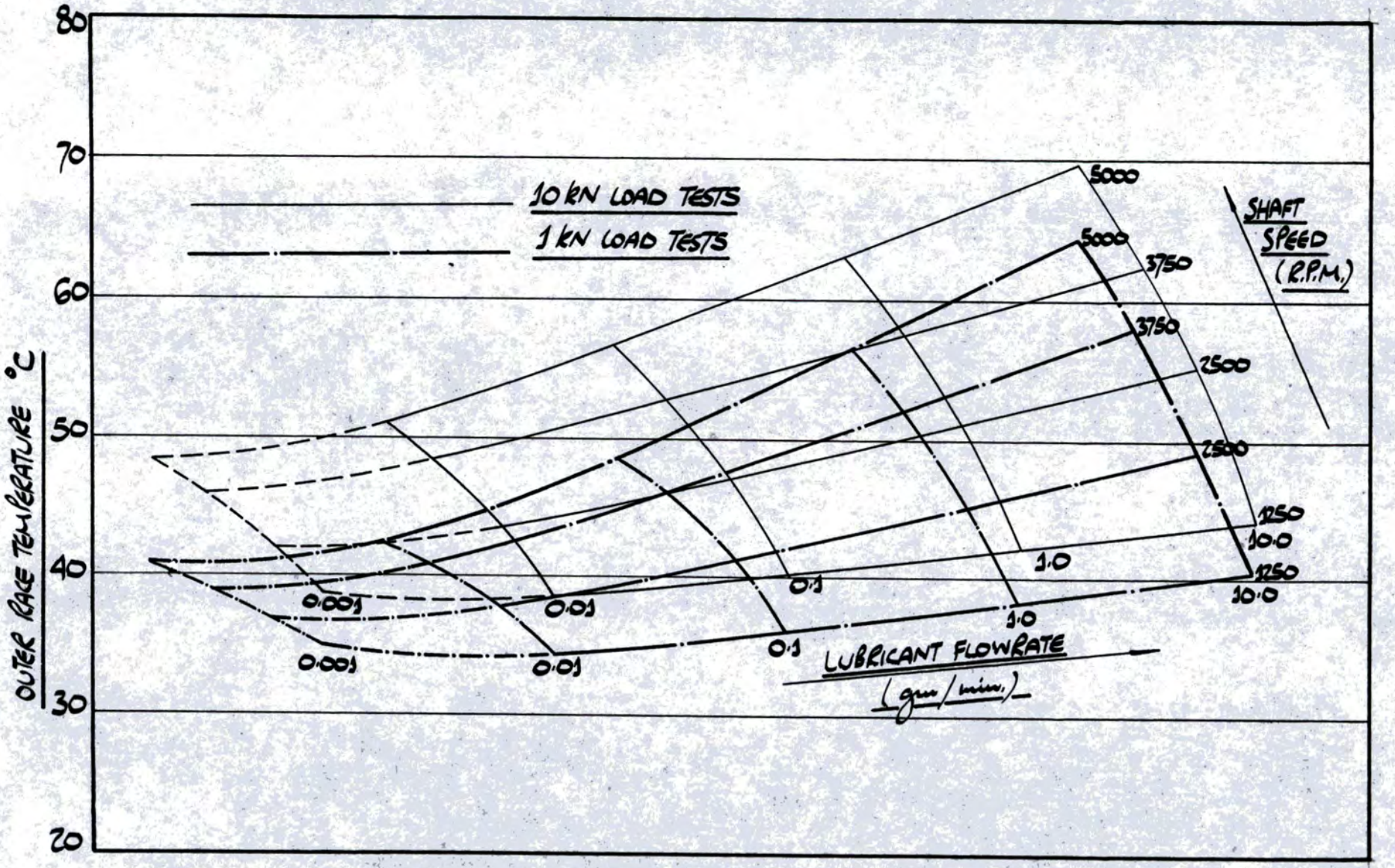

FIGURE 67. VARIATION IN TEST BEARING OUTER RACE TEMPERATURE WITH SHAFT SPEED AND LUBRICANT FLOWRATE. TEST BEARING NU 310, LUBRICANT HVI 160S.

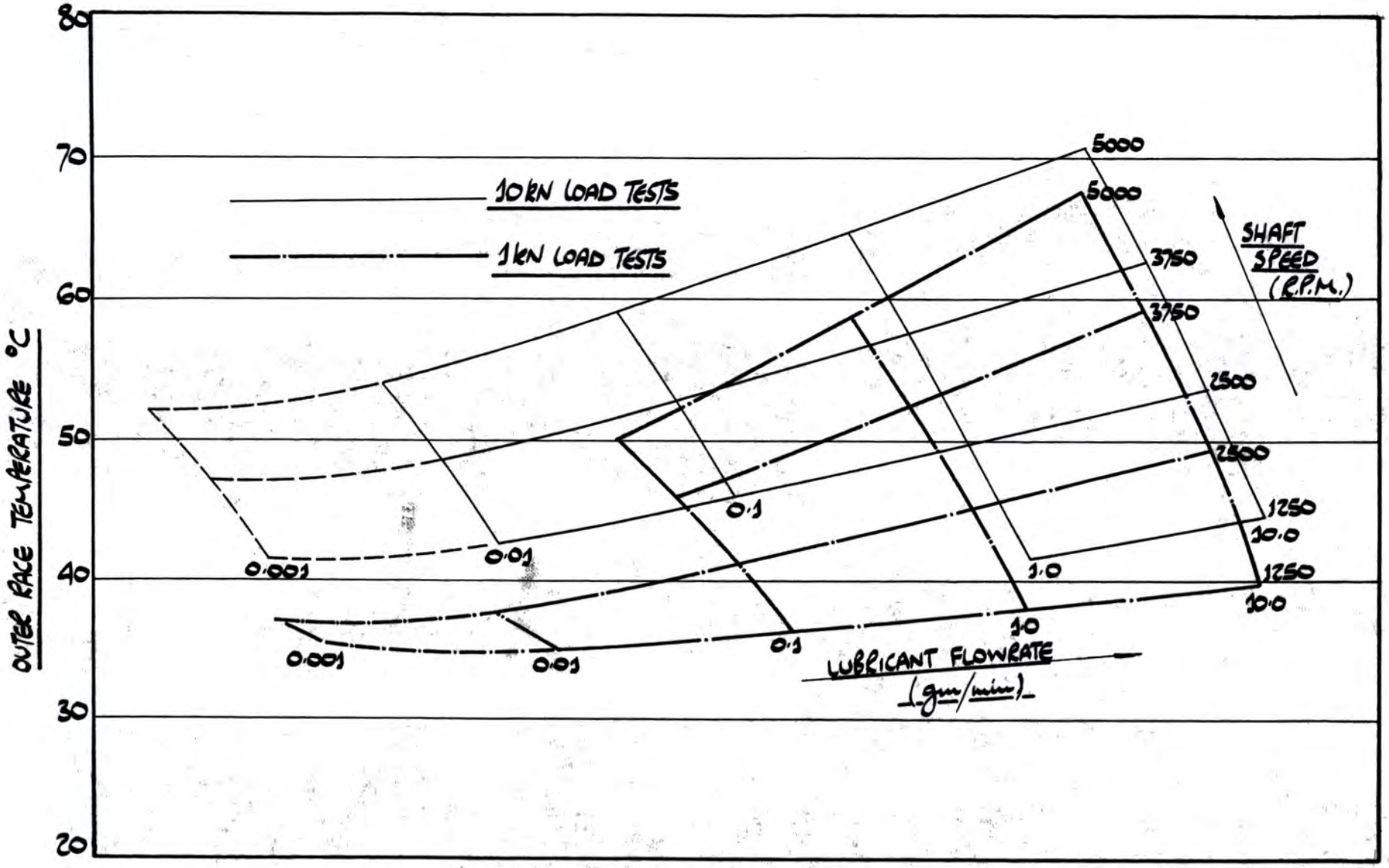

FIGURE 68. VARIATION IN TEST BEARING OUTER RACE TEMPERATURE WITH SHAFT SPEED AND LUBRICANT FLOWRATE. TEST BEARING N310, LUBRICANT HVI 160S.

order of 0.2 degrees C.

Figures 42 , 43 , 44 and 45 show outer race, inner race, cage and roller temperature variation with load, speed and flowrate for bearing NU310 and figures 46 , 47 , 48 and 49 similar curves for bearing N310.

Considering first bearing NU310 and taking the outer race temperatures, Figure 42 , as the basis for discussion.

It will be seen that inner race temperatures, figure 43 , are consistently lower than outer race temperatures at low speeds, but as speed is increased the increase in temperature is dependent on flowrate. For high flowrates, the inner race temperature rises above that of the outer race, whilst at low flowrates it remains below. The effect of bearing load also differs: for the outer race the effect of load is less at higher flowrates whilst the converse is true for the inner race.

Cage temperatures, figure 44 , are in all cases significantly less than outer race temperatures, differing typically by about 10 - 15 degrees C. The effect of flowrate is less marked on the temperature of this component although temperatures at higher speed appear to be slightly more dependent on flowrate. An increase in bearing load merely causes a small parallel shift of the experimental curve, irrespective of speed.

The results obtained for roller temperature, figure 45 , are most interesting. In general, they

are remarkably close to those obtained for outer race temperature although, like inner race temperature, the curves for roller temperature diverge more with increase in speed than those for outer race temperature. At low flowrates, roller and outer race temperatures are indistinguishable, irrespective of speed: at higher flowrates, temperatures are equal at lower speed but roller temperature exceeds race temperature by about 10 - 15 degrees C. at higher speeds.

In Section 4, Experimental Programme, it was noted that the use of bulk outer race temperatures for the evaluation of theoretical friction torque has led to an overestimation of this quantity - it was supposed that a fuller knowledge of component temperatures would allow a more accurate assessment to be made. The results discussed above would indicate that at higher speeds and flowrates the temperature difference is significant - at lower speeds and flowrates outer race temperatures only are a suitable basis for calculation, although overestimating the inner race and cage temperature to some small degree.

It appears that at higher speeds and flowrates, where flooded EHD theory can be taken to apply, component temperature differences must be taken into account. At lower flowrates, component temperature differences are not significant but starved EHD theory will be applicable and so starvation at the rolling contacts must be taken into account. So in any event, calculations of theoretical friction torque must

include one effect or the other.

Both effects do of course reduce the theoretical friction torque and would therefore tend to bring the predicted torques into line with observed experimental values.

The similarity of outer race temperatures may suggest that comparable effects would be observed in the temperature curves obtained for test bearing N310, the bearing with flangeless outer race and flanged inner race. Even though results for this bearing are not complete, it is evident that this is not the case.

In this bearing, inner race temperature, figure 47 , is in all cases less than outer race temperature and much less than the corresponding inner race temperature for bearing NU310. The variation in inner race temperature with speed is less, although increase in temperature with load is similar to that produced in the outer race.

Cage temperatures, figure 48 , are much higher than those obtained for bearing NU310 and in some instances exceed the outer race temperatures.

Roller temperatures, figure 49 , are about 10 degrees C. higher than outer race temperatures at higher speeds, but equal at lower speeds: they do in fact follow quite well the curves for roller temperature in test bearing NU310.

The different trends for inner race and cage temperatures for this bearing as compared to bearing NU310 cannot be satisfactorily explained except as

as being a result of the different bearing geometries. Perhaps when more experimental results containing full component temperatures are available, this particular temperature variation will be seen to be inherent to this type of bearing.

A recent work by Norlander and Stackling (29) gives brief details of temperature distribution in a deep groove ball bearing running at 25,500 rev/min. using oil mist lubrication. Temperatures were measured using a "Thermovision" technique, this allowing thermal radiation of the bearing components to be observed and recorded.

For the bearing in question, outer race temperature was found to be 37°C, inner race temperature 40°C and ball temperature 47°C. These are in general agreement with the results presented here. Further details of Norlander and Stacklings work has been requested, but is not available at present.

Summarising this section, it has been shown that in certain circumstances the component temperatures, particularly the roller temperature, should be taken into account when carrying out theoretical investigations into the sources of friction in an assembly: in those cases where component temperatures are sensibly equal, lubricant starvation should be considered.

Circumfrential temperature distribution in the bearing outer races appears to be more dependent on metrology than might at first be expected: radial temperature variation is insignificant.

7.5 Roller and Cage Slip

As noted in the introductory discussion, Smith (31) has reported that the copious lubrication of rolling contact bearings is often accompanied by gross roller and cage slip, in many cases causing premature bearing failure.

The present experimental work has included the measurement of cage and roller speeds for a proportion of the tests carried out: no significant variation from epicyclic speed has been observed, and so detailed results have not been presented.

The absence of slip in the test bearings was not unexpected: any reduction in film thickness at the rolling contacts will increase the sliding component of friction, as given in Equation (3.3.3) and so reduce the tendency for roller slip. Possibly more relevant, the out-of-roundness of the test bearing outer races would tend to inhibit roller slip, this in turn preventing cage slip. This latter point does suggest that the single observation made - that no slip took place - cannot be validly applied to other bearings operating under starved conditions without further evidence being presented.

However, Garnell (20), whose results have been briefly referred to in the introductory discussion and which are almost certainly for conditions of lubricant starvation, reports that no significant cage or roller slip was observed during these tests: in most cases, positive slip was extremely small and

some cases of small negative slip were observed. It is known that Garnell's test bearings were more accurately circular than the bearings used in this present investigation.

It therefore appears that conditions of lubricant starvation tend to suppress the development of roller slip, this in turn preventing cage slip.

Boness (6) has reported significant slip at the high flowrates used during his experimental work and observes that slip is reduced if speed is reduced, load increased or lubricant viscosity reduced. It will be remembered that Boness's results were taken at extremely high lubricant flowrates: it is likely that his slip observations are the result of the inertia effects of much excess lubricant. When considered with the fact that many of the results were obtained using a fixed cage configuration, Boness's results appear inapplicable to a bearing operating under conventional conditions.

7.6 Bearing Life

This present work has not included any consideration of the effects of lubricant flowrate on the life expectancy of rolling contact bearings. This short discussion is therefore confined to consideration of the work of other authors.

Münnich (27) has presented a curve (see figure 69) showing the relationship between expected life and the ratio of film thickness to surface roughness at the rolling contacts within an assembly. He states that the experimental results on which present-day life calculations are based are for lubrication with a conventional lubricant in the region of the most frequently occurring values of speed factor dm.n (dm being the roller pitch diameter and n the rotational speed). For these conditions, Münnich suggests that the operating regime in which these experiments were carried out occurs at values of the horizontal co-ordinate in figure 69 within the region in which bearing life is reduced. Further experiments using higher viscosity lubricants and higher speeds, bringing the operating regime further to the right of the figure show that increased bearing life is obtained. Work on this investigation is being continued.

Münnich therefore concludes that the use of the bearing life and lubricant selection data at present contained in manufacturers catalogues leads to, in particular, the selection of a lubricant of too low a viscosity to give complete separation of the rolling

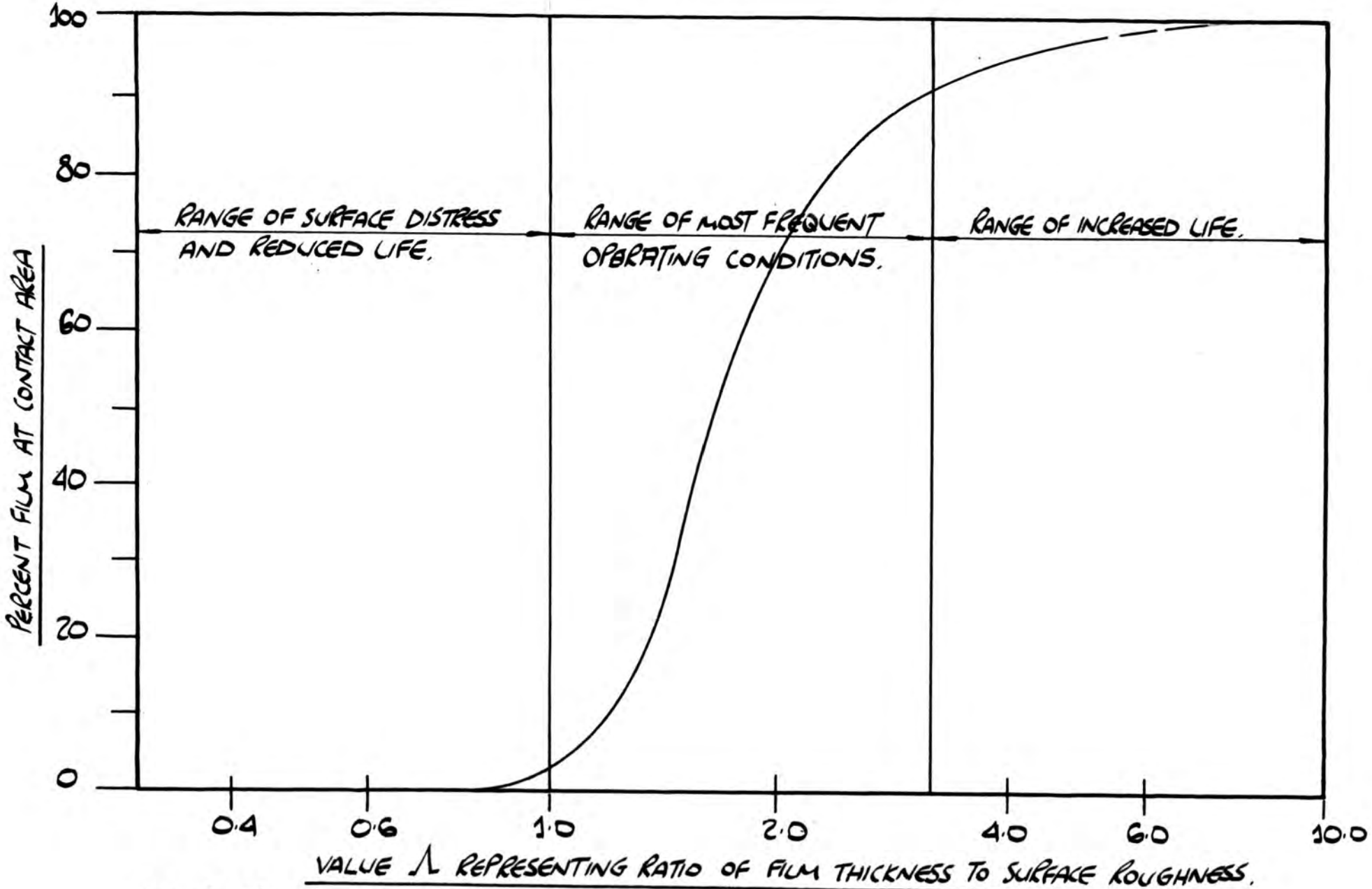

FIGURE 69. THE EFFECT OF LUBRICATION ON BEARING LIFE.

surfaces within the most frequently occuring speed range.

Similar curves to figure 69 have been presented by other authors, including Skurka (30) and Townsend et.al.(33) the latter attributing the curve to Zaretsky and Anderson. Skurka's version of the curve uses L_{10} life as vertical ordinate ; in this form, Kannel (33) suggests that the curve should not become flattened at values of the horizontal co-ordinate above 3 ; Danner (33) proposes that the type of surface finish is as important as the C.L.A. value.

Vaessen and DeGee (34) present a curve which indicates that steel quality has an effect on expected bearing life, vacuum remelted steel being significantly superior to electro-slag remelted steel.

The theoretical analysis contained in this present work has shown that lubricant starvation has little effect on the film thickness at the contacts unless severe starvation takes place. It would not be expected, for the roller/race contacts at least, that lubricant starvation would have any significant effect on bearing life, but the experimental results have indicated that film breakdown first occurs at other contacts within the assembly. If these other contacts are not being amply lubricated whilst the rolling contacts enjoy lubricant starvation, then assembly life might well be curtailed.

It should be mentioned though that examination of the test bearing components after prolonged running under starvation conditions give no indication that the test bearings were even approaching failure.

7.7 Conclusions and suggestions for further work

The conclusions reached during this work can be briefly summarised as follows:

It is the authors opinion that the concept of lubricant starvation must be considered in all problems of lubricated contact.

Within this range of lubricant starvation, friction torque is much reduced from fully flooded values and shows a dependence on (ln. lubricant flowrate). Load and speed are also variables to be taken into account. The experimental torque curves for low load lead to the conclusion that the position of the film inlet point of the lubricant film is independant of γN, but dependent on load and flowrate. Estimates of the positions of film inlet points shows that the inlet region to the contact is very small.

The effect of lubricant starvation is to reduce the temperature of the bearing components. Roller temperature is significantly different from race temperature at high flowrates, but indistinguishable at low flowrates.

Radial temperature variation in the outer race is insignificant.

Circumfrential temperature variation is susceptible to race geometry.

No significant cage and roller slip were recorded under starvation conditions. The out-of-roundness of the races has already been referred to, and this would probably tend to supress slip. It should be recalled, also, that Garnell's experiments at low lubricant supply rates showed no roller or cage slip at all.

Further work which might be considered includes the investigation into the distribution of lubricant in a bearing assembly and also full consideration of the complex problem of the positioning of the film inlet point for a lubricated roller. The variation of film inlet thickness at the higher load condition investigated poses a problem - a more satisfactory explanation of this effect would be welcome.

APPENDIX (A)

A comparison between the exact expression for Hertzian deformation of a contact and the approximation proposed by Crook (ref. 10)

The solution of Reynolds equation for the Grubin model of an elasto-hydrodynamic contact requires an expression relating the film thickness h at any point, to a horizontal co-ordinate x. The exact solution, derived by Hertz and used by Grubin is given in equation (3.1.5) and is reproduced below (equation (A.1)), this expression being in terms of the generally accepted non-dimensional variables given in equation (3.1.3)

$$H_H = H - H_0 = \frac{4W}{\pi}\left[X(X^2-1)^{1/2} - \ln\left(X + [X^2-1]^{1/2}\right)\right] \qquad A.1$$

It follows that

$$\frac{dH_H}{dX} = \frac{8W}{\pi}(X^2-1)^{1/2} \qquad A.2$$

Crook's approximation to the exact solution given in equation (A.1) is

$$H_c = \frac{8W}{\pi}(X-1)^{3/2} \qquad A.3$$

giving

$$\frac{dH_c}{dX} = \frac{12W}{\pi}(X-1)^{1/2} \qquad A.4$$

Figure A.1 shows the variation of H_H and H_c with horizontal co-ordinate X for $W = 3 \times 10^{-5}$, a value typical of a moderately loaded steel contact.

Figure A.2 shows the variation of $\frac{dH_H}{dX}$ and $\frac{dH_c}{dX}$ with horizontal co-ordinate X, again for $W = 3 \times 10^{-5}$.

It will be noted that both H_c and $\frac{dH_c}{dX}$ are in better

agreement with H_H and $\frac{dH_H}{dX}$ at values of X close to the Hertzian contact region.

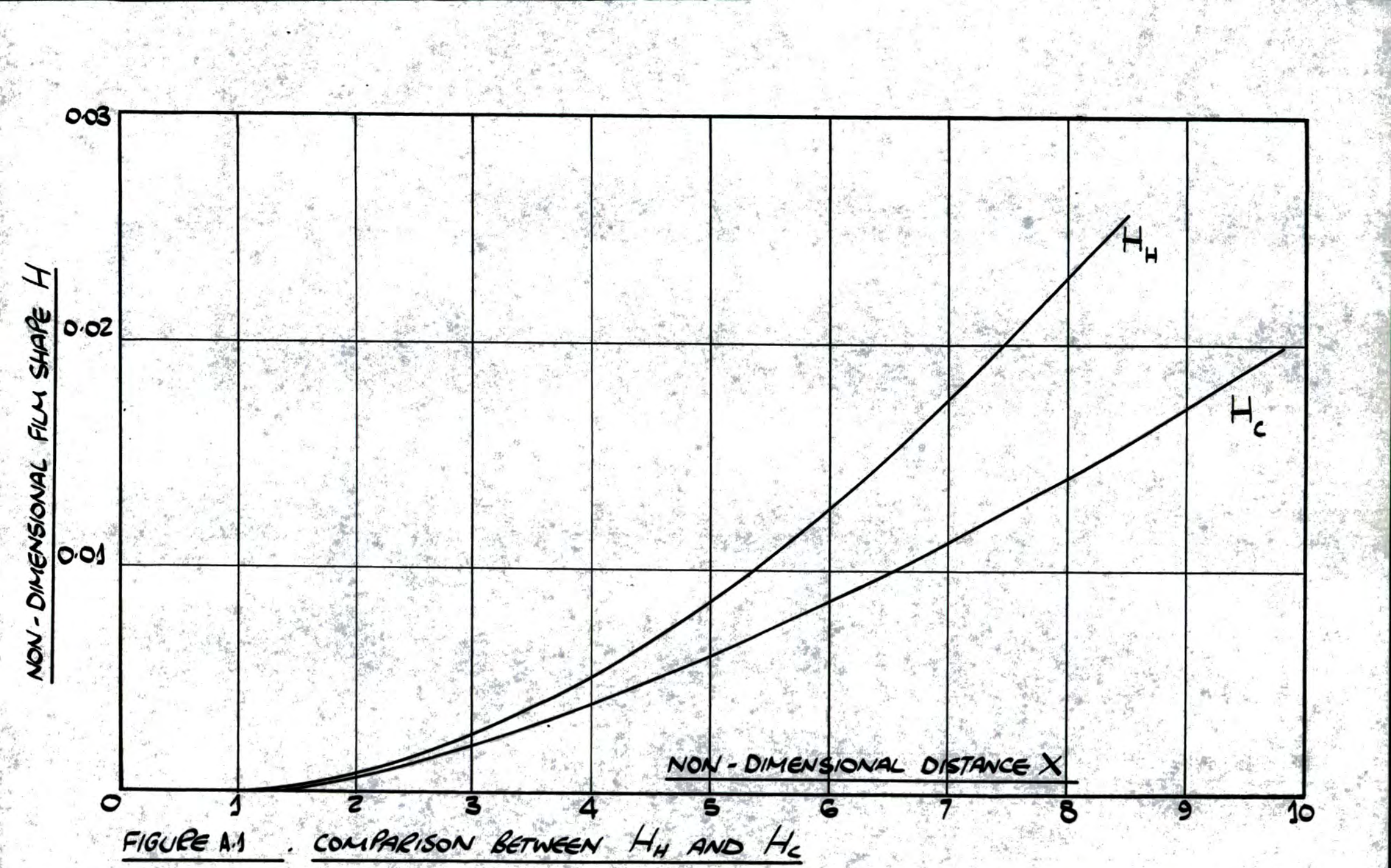

FIGURE A.1 . COMPARISON BETWEEN H_H AND H_c

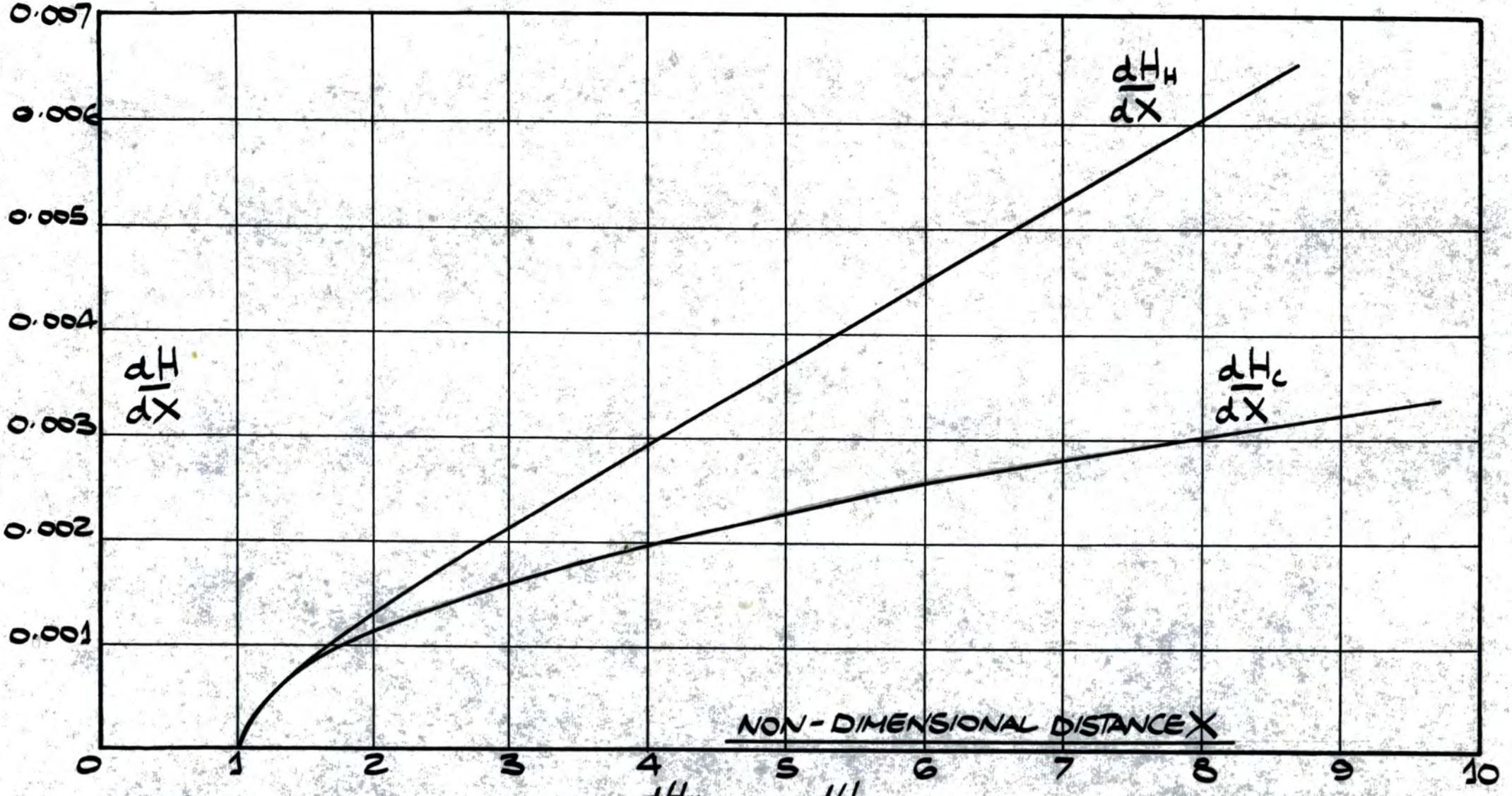

FIGURE A.2. COMPARISON BETWEEN $\frac{dH_H}{dX}$ AND $\frac{dH_c}{dX}$.

APPENDIX (B)

Details of test bearings used during the experimental programme

Two types of cylindrical roller bearings have been investigated in this present work and these are shown in figure B.1 .

Both bearings are 50mm nominal bore.

Bearing type NU310 has a flanged outer race and plain inner race. The 12 taper - ended rollers are contained by a brass cage which is guided by the flanges on the outer race.

Bearing type N310 has a flanged inner race and plain outer race. The 12 taper - ended rollers are contained by a brass cage which is guided by the flanges on the inner race.

The experimental work has been carried out on a single bearing specimen of each type. Details of the metrology of these bearings appears in figure B.2 .

Measurements of linear bearing dimensions were made using a Hilger and Watts Horizontal Microptic measuring machine. Surface finish values were obtained by the use of a 'Talysurf' 4 and measurement of the out-of-roundness of the bearing races made using a 'Talyrond' Model 51 instrument.

Figure B.3 shows 'Talyrond' traces for bearing NU310 and figure B.4 'Talyrond' traces for bearing N310.

ALL DIMENSIONS IN MILLIMETRES.

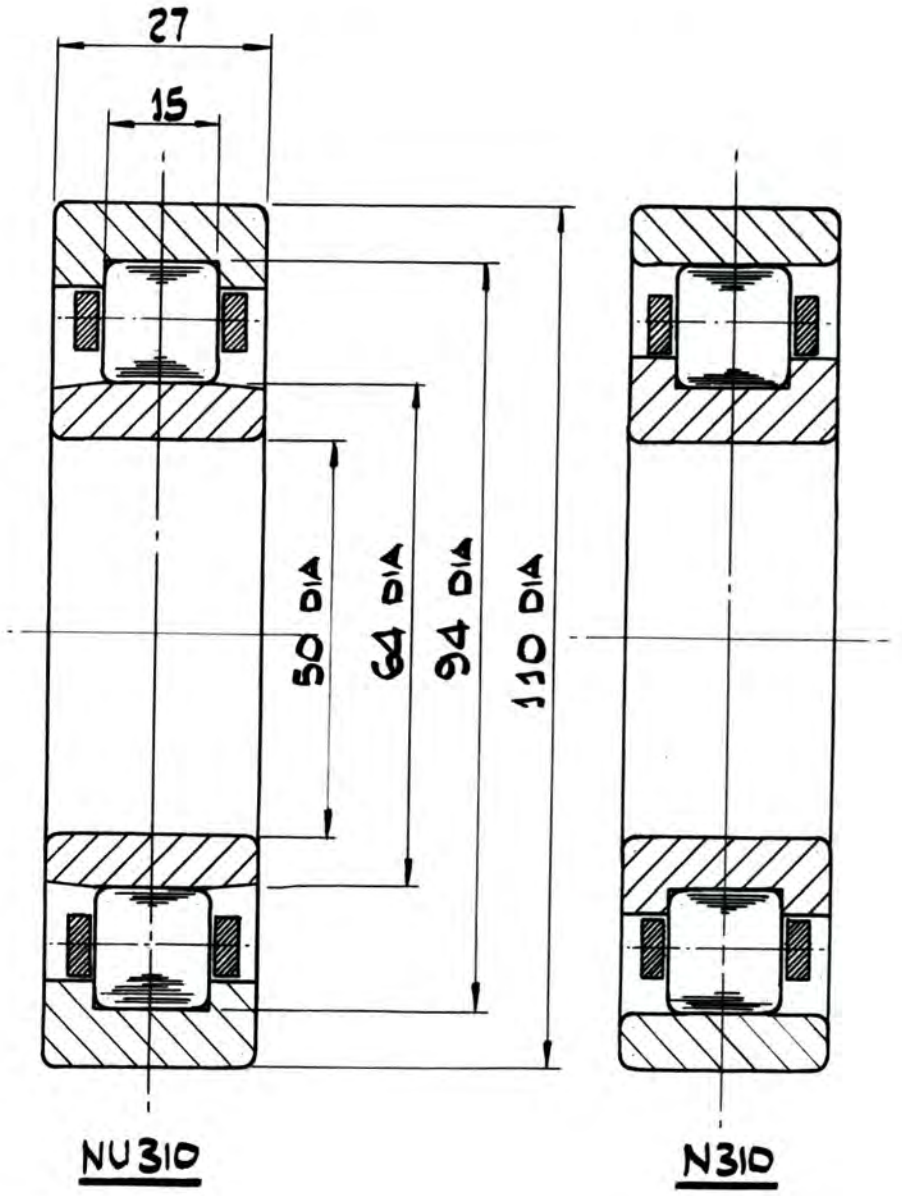

FIGURE 6.1. TEST BEARING DETAILS.

Measurement	NU310	N310
Inner race track diameter	64.9717mm ± .0012mm	64.9950mm ± .0050mm
Surface finish of inner race track	0.09 µm CLA	0.37 µm CLA
Roller diameter	15.0022mm ± .0007mm	15.0016mm ± .0006mm
Roller length	15.0018mm ± .0015mm	15.0014mm ± .0013mm
Surface finish of roller	0.05 µm CLA	0.05 µm CLA
Outer race track diameter	95.0073mm ± .004mm	95.0204mm ± .0045mm
Surface finish of outer race track	0.36 µm CLA	0.36 µm CLA

Talysurf and Talyrond traces

FIGURE B.2. TEST BEARING METROLOGY

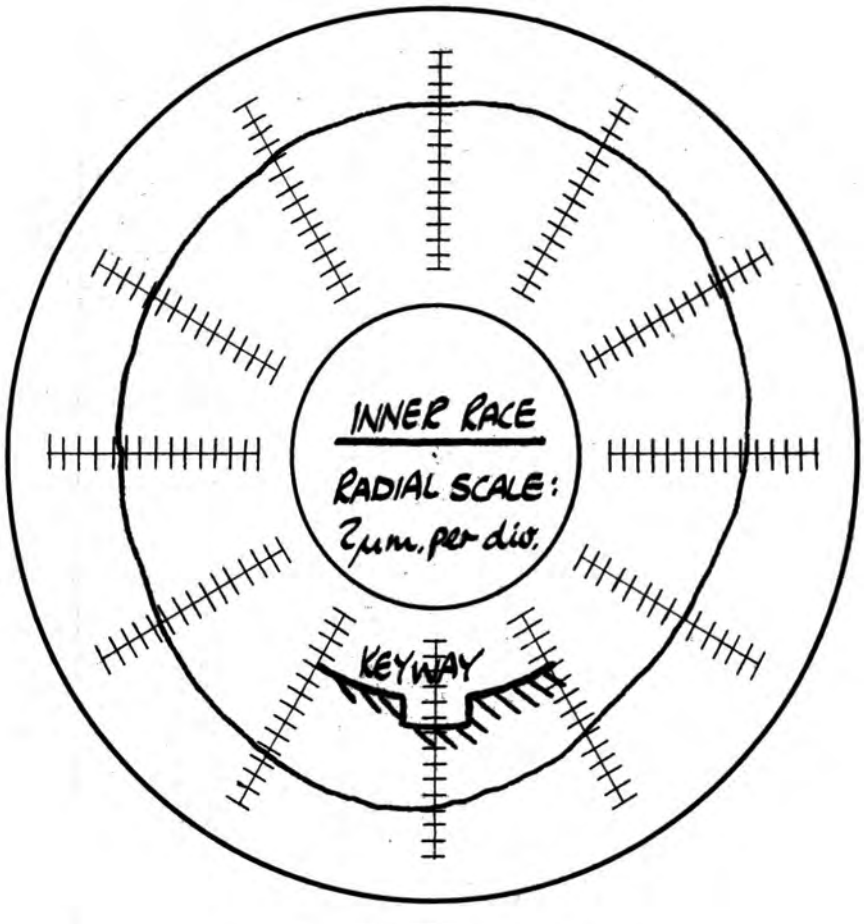

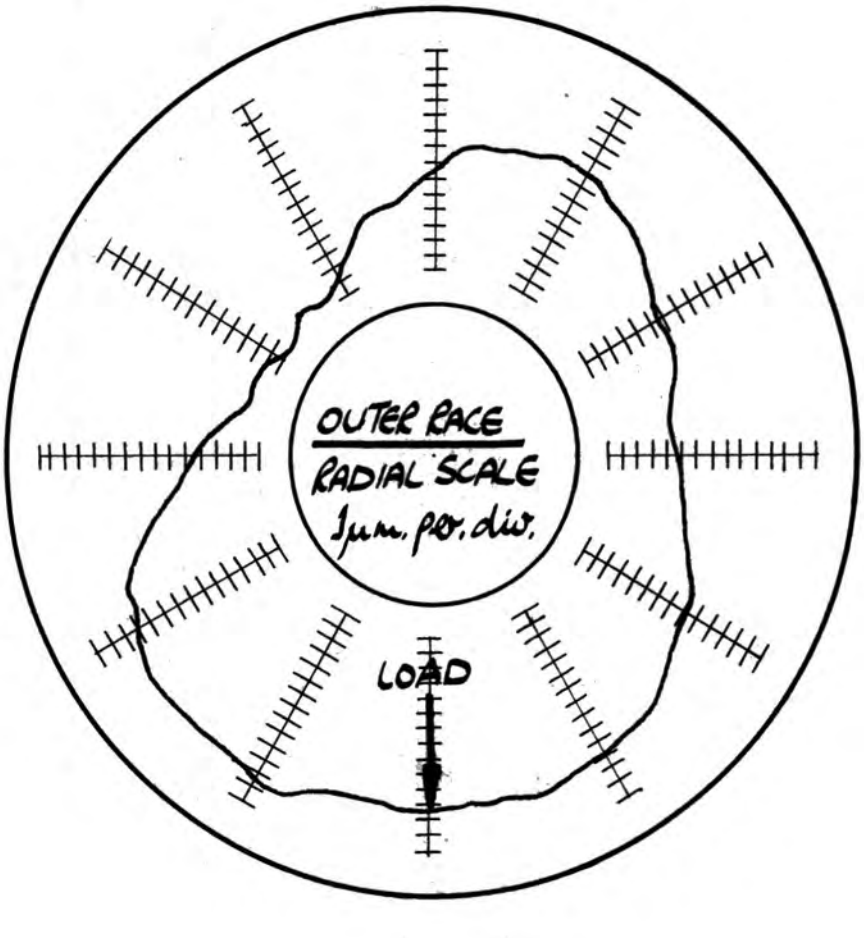

FIGURE B.3 'TALYROND' TRACES - BEARING NU310

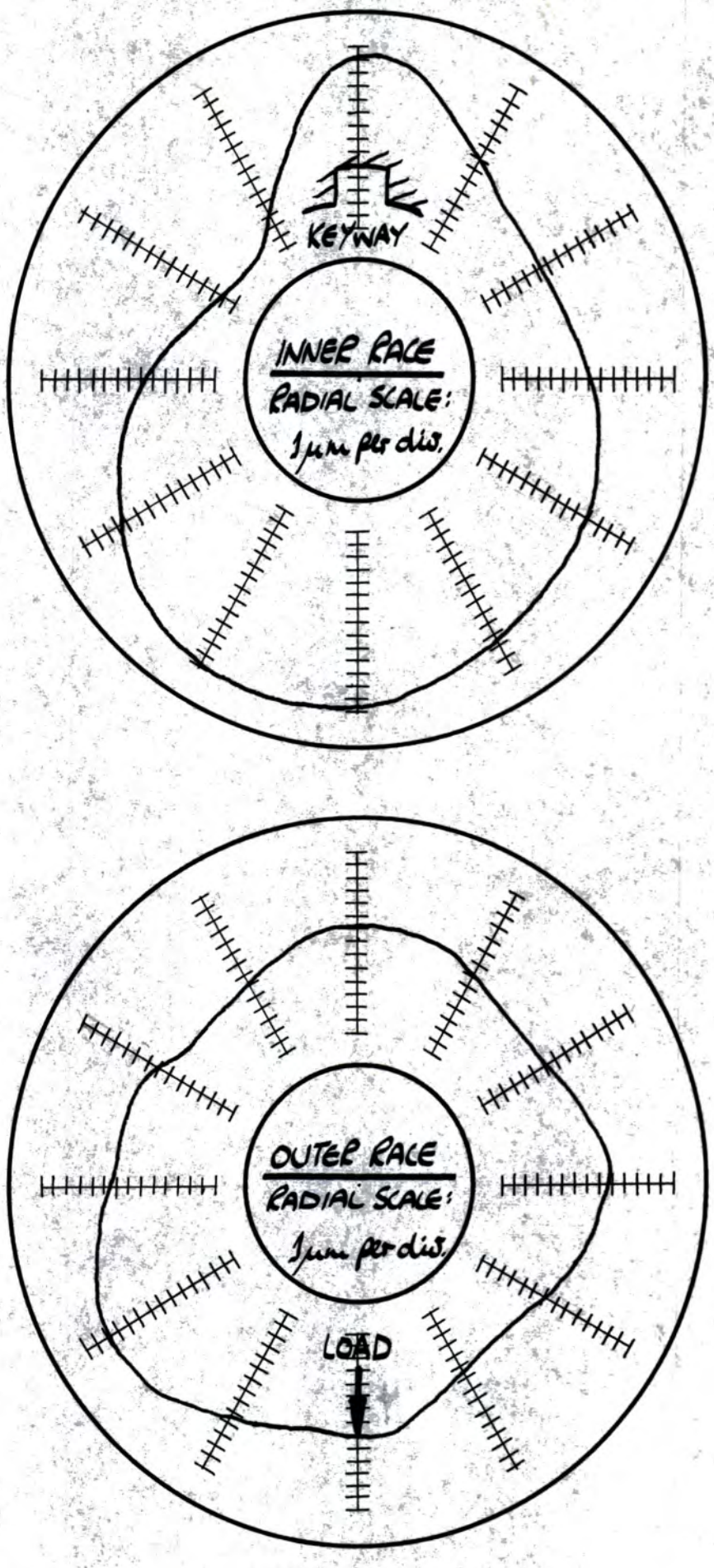

FIGURE B·4 'TALYROND' TRACES - BEARING N310

APPENDIX (C)

Details of test lubricants used during the experimental programme

Three test lubricants have been used during this present work. These are designated as

HVI 160 S

HVI 55

Paraffin

HVI 160 S and HVI 55 are both base mineral oils with no additives. These lubricants are particularly well documented by Shell Limited and have midpoint viscosities at 100°F (37.8°C) of 110 cSt and 21 cSt respectively.

The paraffin used was a commercial grade fluid with a midpoint viscosity at 100°F of 3.15 cSt.

Figure C.1 shows the temperature-viscosity characteristics for each of these lubricants.

For each lubricant, the temperature-viscosity characteristic obtained from the manufacturer was checked in the laboratory in accordance with the recommendations of the British Standard 188 - 1957 using 'U' tube viscometers and a Townson and Mercer type E270 thermostat Bath filled with Shell Risella 17 oil. Oil Bath temperature was measured by two I.P calibrated thermometers and in addition, was accurately set at 3 reference temperatures using I.P calibrated kinematic viscosity thermometers. The variation in lubricant density with temperature was obtained by

suspending an S.G. bottle containing the lubricant in the bath during the viscometry tests: at each test temperature the mass of fluid contained in the S.G. bottle was measured and the fluid density calculated.

In all cases the data obtained from the laboratory tests was in good agreement with the data supplied by the lubricant manufacturers.

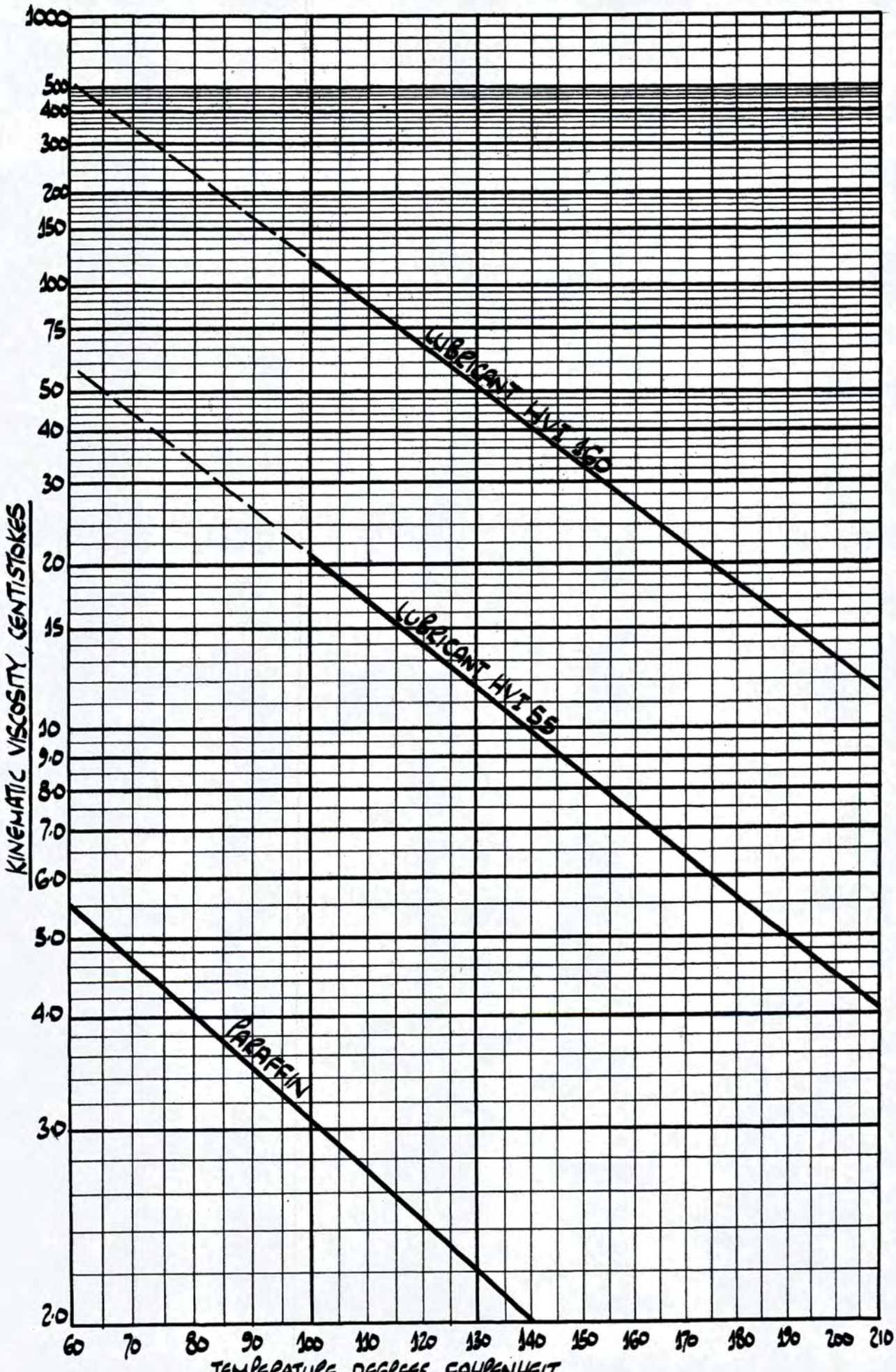

FIGURE C-1 TEMPERATURE / KINEMATIC VISCOSITY CHARACTERISTICS - ASTM CHART.

APPENDIX (D)

Measurement of test bearing load

The load was applied to the end of the machine arm by a 'Dowty' type HP5A hand operated hydraulic ram and was measured by a 'Vibrometer' type LC/2t load cell of 20 kN. capacity. From the geometry of the arm, the bearing load was 1.55 times the ram load. The output e.m.f. from the load cell was initially measured by a Vibrometer type 8-CFA-1/B carrier frequency amplifier which was provided with a galvanometer to measure bridge circuit unbalance. Toward the end of the test programme, the Vibrometer instrument developed a fault and was replaced by a B.P.A. Transducer meter type C52, this instrument also being provided with a measuring galvanometer.

The load cell and measuring circuit were calibrated up to 20 kN. applied load using a Denison Type T42B4 Testing machine.

APPENDIX (E)

Measurement of test bearing friction torque

The original machine design was provided with a torque measuring device using 'Vibrometer' TW5-2/A contactless displacement transducers. This measuring system proved to be unsatisfactory because the transducers were very sensitive to ambient temperature variations. Modifications carried out to reduce this temperature effect were unsuccessful.

The present torque measuring device is shown in figure E.1 and consists of a strain-gauged berrylium copper proof ring. This ring provides a restraint against rotation for the hydrostatic support bearing in which the test bearing is fitted, the torque being transmitted by a 13 cm. torque arm. The strain gauges on the proof ring are connected in the form of a 4 - arm Wheatstone bridge and the bridge circuit unbalance under load measured by a transducer meter. Initially the Vibrometer type 8-CFA-1/B carrier frequency amplifier was used for this purpose but this was later replaced by a B.P.A. type 52C transducer meter.

Calibration of the measuring circuit was by dead weights applied to the proof ring.

The hydrostatic support bearing which allows friction torque readings to be obtained has been the source of a great deal of difficulty and it has been necessary to make some compensation for this bearing before experimental values of test bearing friction

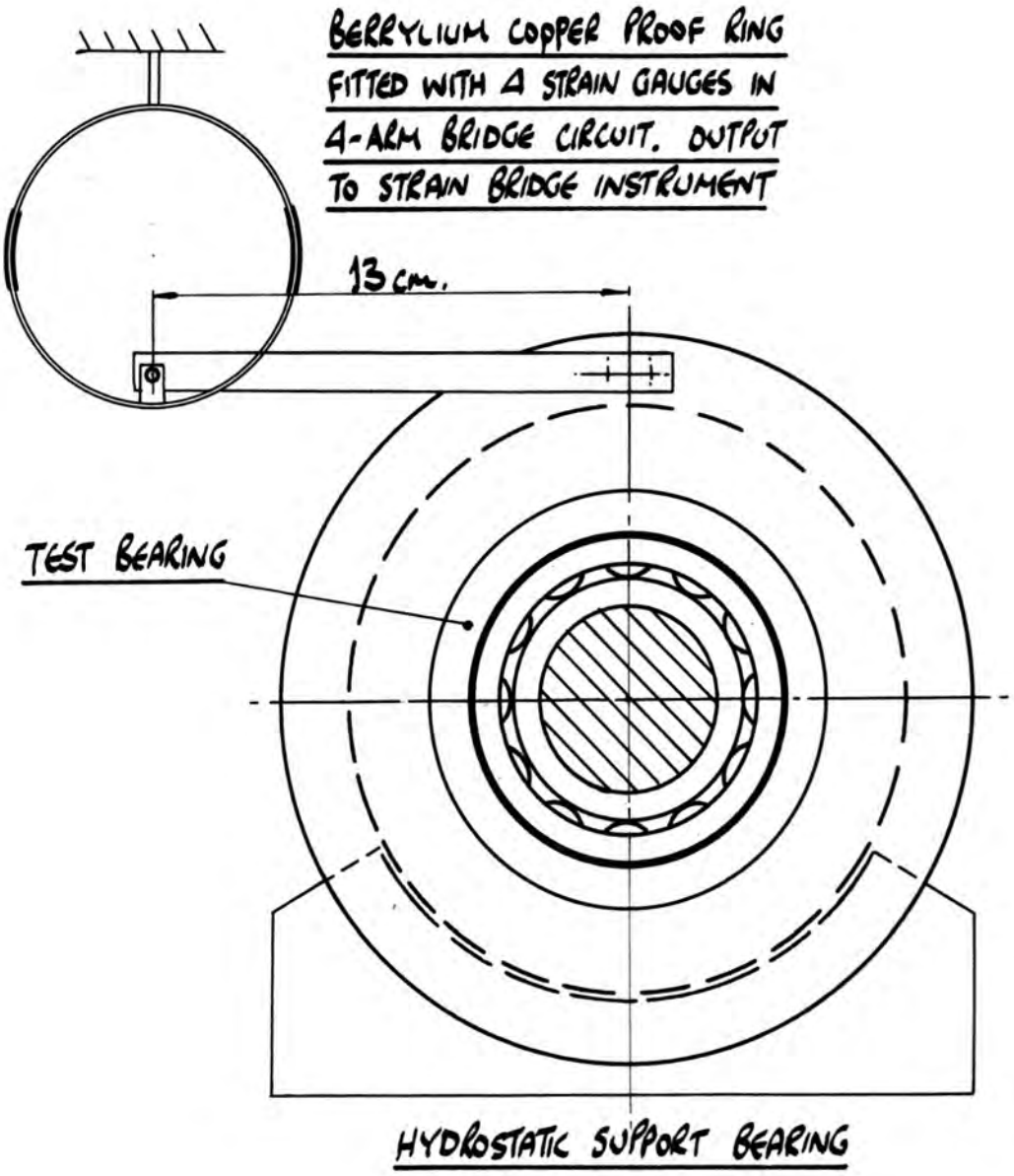

FIGURE E·1 . TORQUE MEASUREMENT.

torque could be evaluated.

As originally designed, this bearing was a 360°, 8 pocket hydrostatic bearing with axial location. Compensation was by capillary tubes. For ease of machining, the pressure pockets were formed in a separate steel ring which was pierced to provide the pockets. This design was unsuccessful because the pocket ring deformed under pressure and locked the bearing. The steel block forming the outer surface of the hydrostatic bearing was redesigned to make this ring unnecessary but the bearing again failed under load because the hydraulic pump was not able to provide the necessary oil flowrate. The bearing was modified to include orifice compensation instead of the original capillary compensation and the oil changed to one of a higher viscosity. (An orifice compensated bearing is inherently stiffer than a capillary compensated bearing for the same oil flowrate).

Because of the small size of the orifices necessary, a 5 micron pressure filter and a magnetic filter were included in the hydraulic circuit.

The bearing worked fairly satisfactorily for a time but had a tendency to lock at higher loads, this fault becoming progressively worse.

'Talyrond' traces of the bearing journal and of the outer steel ring forming the bore of the hydrostatic bearing were taken. The latter was found to be badly distorted and so the bearing was converted to a 120°, 4 pocket bearing: the surfaces were lapped

together to give conformity. In addition, as it was difficult to match flowrates from the orifice compensators, it was decided to return to capillary compensation.

In this form, the bearing would revolve freely under full load without sticking, but it was noted that a parasitic torque was present in the bearing. (A parasitic torque is a torque developed within the hydrostatic bearing and proportional to applied load).

The presence of this parasitic torque was making the measurement of test bearing friction torques difficult and so the cause of this torque was investigated. The torque was found to be due to a small misalignment between the test shaft assembly and the support bracket of the machine arm: this error was imposing an eccentricity onto the hydrostatic bearing which was in turn causing the bearing to develop a torque. This misalignment was carefully measured and corrected and the characteristics of the hydrostatic bearing thoroughly checked. The hydrostatic bearing worked well for a period but was obviously disturbed again during maintenance of the machine.

No further attempts were made to correct this error, and all experimental readings of bearing friction torque have had to be compensated for the effect of parasitic torque in the hydrostatic bearing.

Work on the hydrostatic bearing has occupied a significant proportion of the authors period of registration for the degree.

The compensation factors necessary to take account of the parasitic torque in the hydrostatic support bearing have been estimated from the results of tests conducted for both directions of rotation of the test bearing.

Figure E.2 and E.3 show these results for bearing NU310 at two test lubricant flowrates, figure E.2 showing the variation in test bearing friction torque at a flowrate of 1.6 gm/minute and figure E.3 the variation at 0.06 gm/minute. It will be seen that, on the reasonable assumption of equal friction torques in each direction of rotation, a quite well defined 'zero' line for each test condition can be obtained. The shift in the zero line with load is due to the parasitic torque (proportional to load) developed within the support bearing, and it is this error that the compensation factor is intended to eliminate. Obviously, the use of the relevant parasitic torque base-line for each load provides the necessary compensation.

For the results shown in figure E.2 , the parasitic torque base-line for 1kN. load occurs at a torque scale reading of 0.2010 N.m., this figure being an average value for all the tests conducted at this load. The corresponding value for the results shown in figure E.3 is 0.2126 N.m. A single value of 0.2050 N.m. has been assumed for both sets of results. The standard deviation of the parasitic torque values from this figure is $\pm$ 0.0189 N.m.

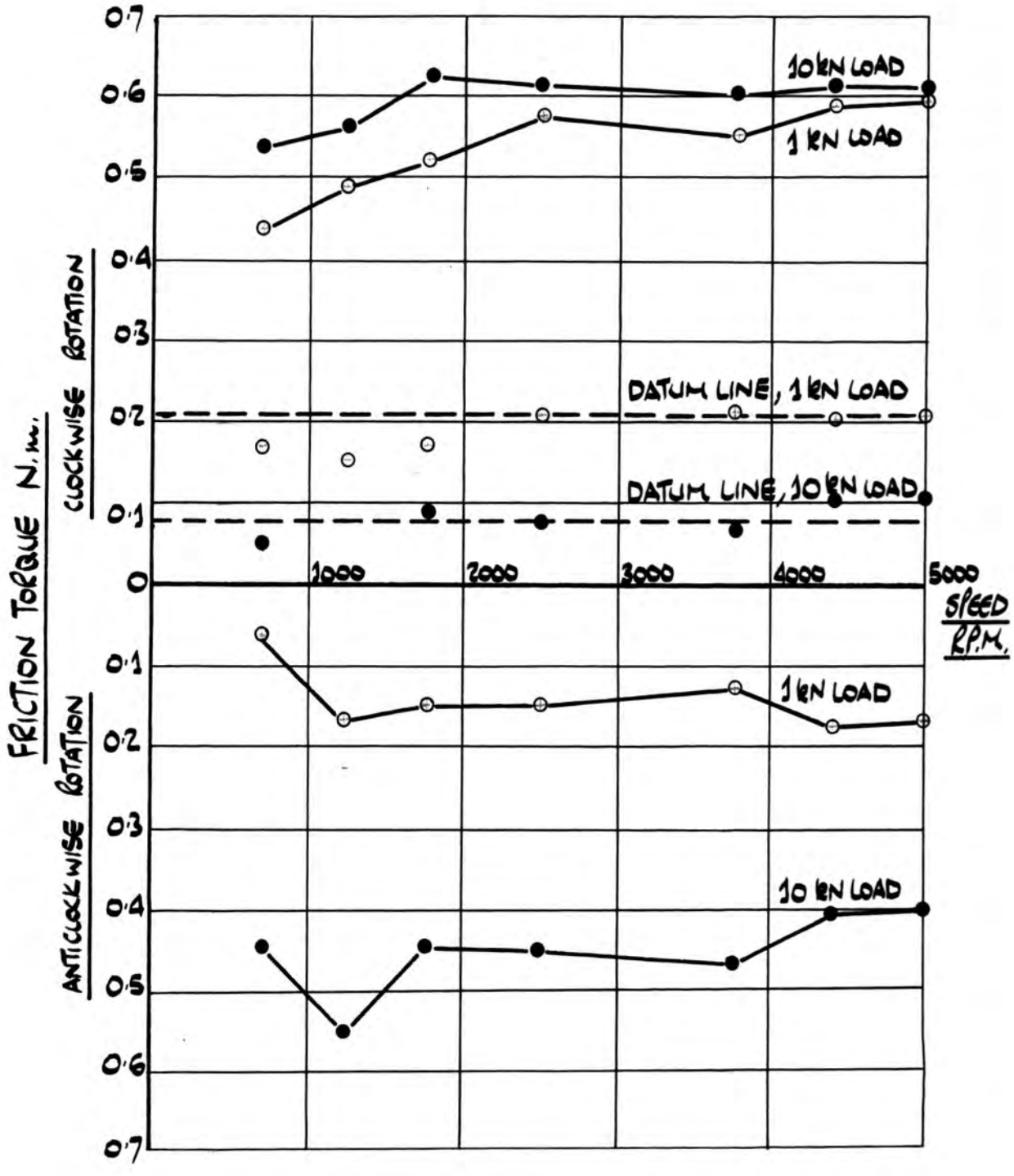

FIGURE E·2. VARIATION IN BEARING FRICTION TORQUE WITH SPEED FOR TEST BEARING NU310. RESULTS TO ALLOW THE EVALUATION OF PARASITIC TORQUE. LUBRICANT FLOWRATE 1·6 gm/min.

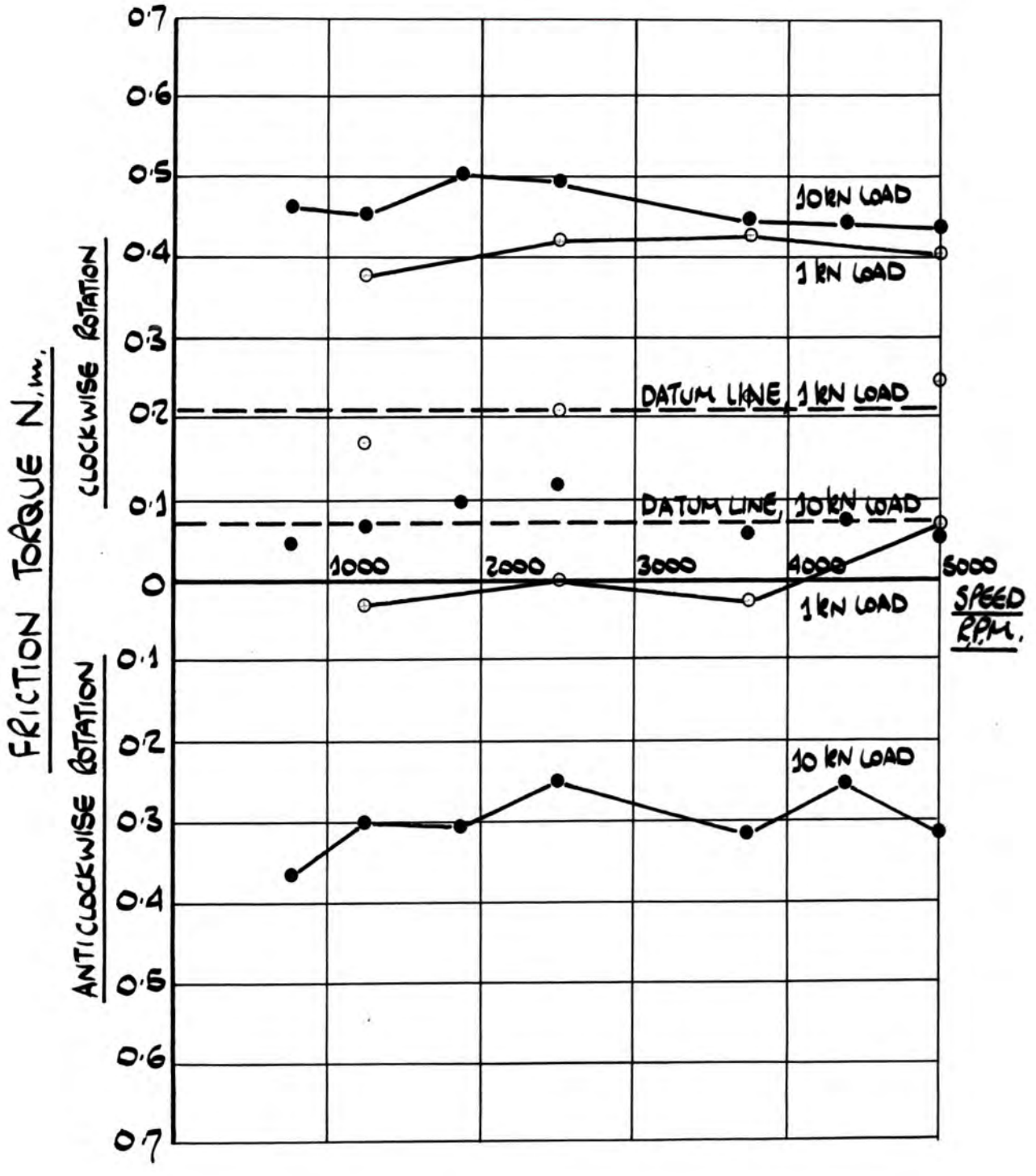

FIGURE E·3. VARIATION IN BEARING FRICTION TORQUE WITH SPEED FOR TEST BEARING NU310. RESULTS TO ALLOW THE EVALUATION OF PARASITIC TORQUE. LUBRICANT FLOWRATE 0·06 gm/min.

Similarly for the tests at 10 kN bearing load, figure E.2 gives a value of 0.0821 N.m., figure E.3 giving 0.0969 N.m. A single value of 0.0811 N.m. for tests at 10 kN bearing load has been assumed.

The standard deviation of the parasitic torque values from this figure is $\pm$ 0.0227 N.m.

Although the standard deviations quoted are large compared to the parasitic torque values obtained, it will be appreciated that, since the zero value of torque shown on the vertical axes of figures E.2 and E.3 is, in this context, arbitary, the standard deviation figures should more properly be referred to the true torque readings. The standard deviation figures therefore constitute an estimation of the zero error in the torque readings after compensation: for the case of 1 kN bearing load and an average bearing friction torque of 0.395 N.m., a zero error of $\pm$ 0.0189 N.m. represents an error of about 5% in true friction torque values.

This compensation procedure has also been carried out on results from test bearing N310 and similar compensation values obtained. The figures quoted above have therefore been used in the compensation of test results from both bearings.

A number of tests from which values of test bearing friction torque have been obtained were carried out with the cage slip-ring unit (described in Appendix (L)) fitted to the bearing and for those tests contrarotational running was not possible because

of the slip-ring brushes. For these tests, the experimental values of test bearing friction torque have first been compensated for parasitic torque by the appropriate factor obtained from the tests described above. The additional compensation necessary to take account of the presence of the slip-ring unit is described in Appendix (F).

APPENDIX (F)

Torque compensation for cage slip-ring unit

A number of the experimental tests which have been carried out have included the measurement of roller and cage temperatures. For this to be done, the test bearing was fitted with the cage slip-ring unit described in Appendix (L). The presence of this unit did, of course, influence the readings of test bearing friction torque obtained during these tests.

The torque readings were, however, consistent with the results obtained from experimental tests carried out on the test bearings alone and so a means of providing some compensation for the presence of the cage slip-ring unit was sought.

Figures F.1 and F.2 show a comparison between friction torque values for test bearings with and without the cage slip-ring unit for a range of values of (speed x viscosity) and for two test bearing loads.

Figure F.1 shows the comparison for a lubricant flowrate of 1.6 gm/minute and figure F.2 for a flow-rate of 0.06 gm/minute.

In all cases it will be seen that a compensation of -0.08 N.m. applied to the results obtained with the cage slip-ring unit fitted to the test bearing will bring these reults into line with those obtained for the test bearing alone. This compensation has been applied to torque values to which it is relevant

before these have been included in the experimental results.

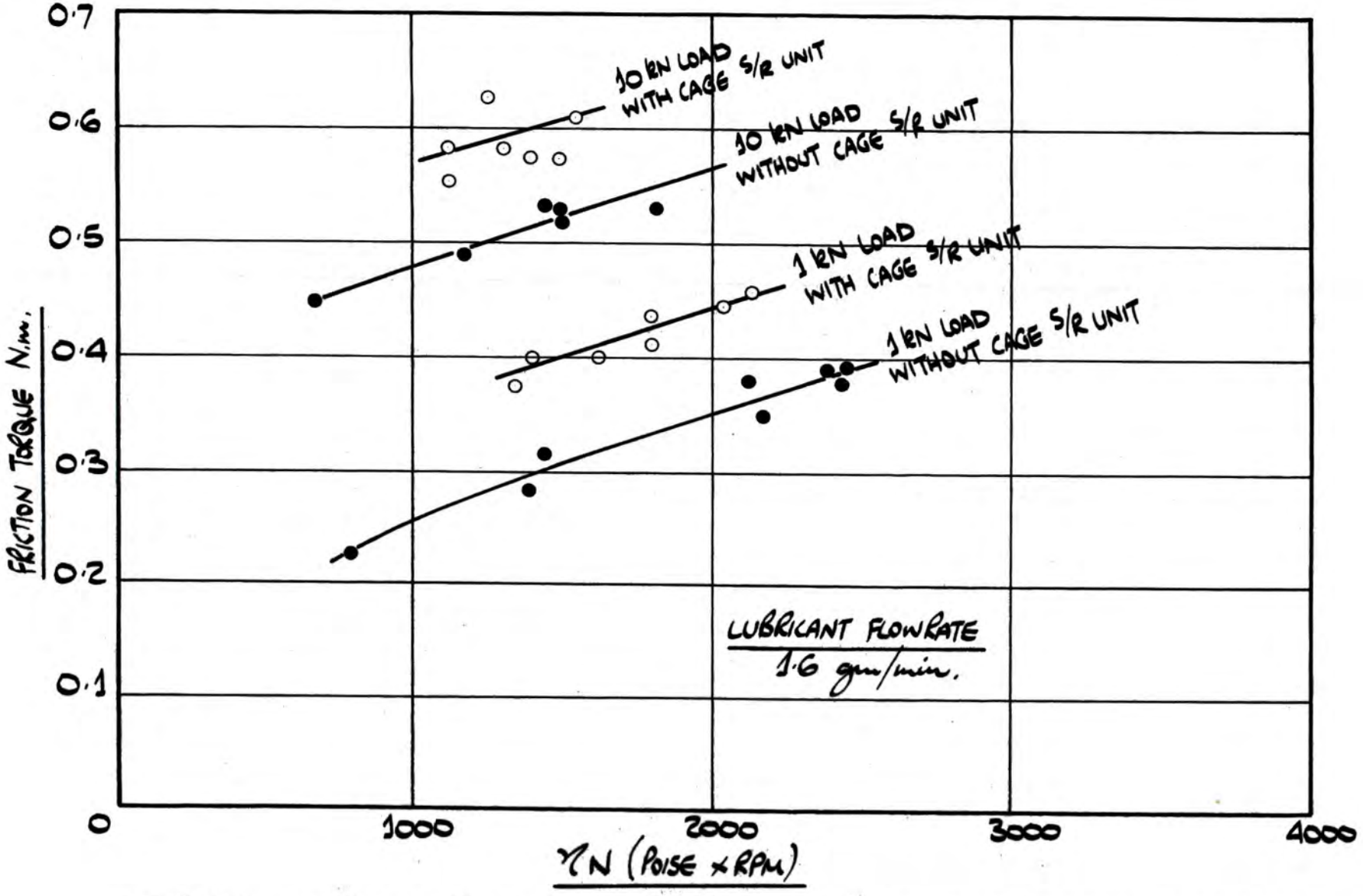

FIGURE F·1 . TORQUE CURVES FOR TEST BEARING NU310, SHOWING EFFECT OF CAGE SLIP-RING UNIT

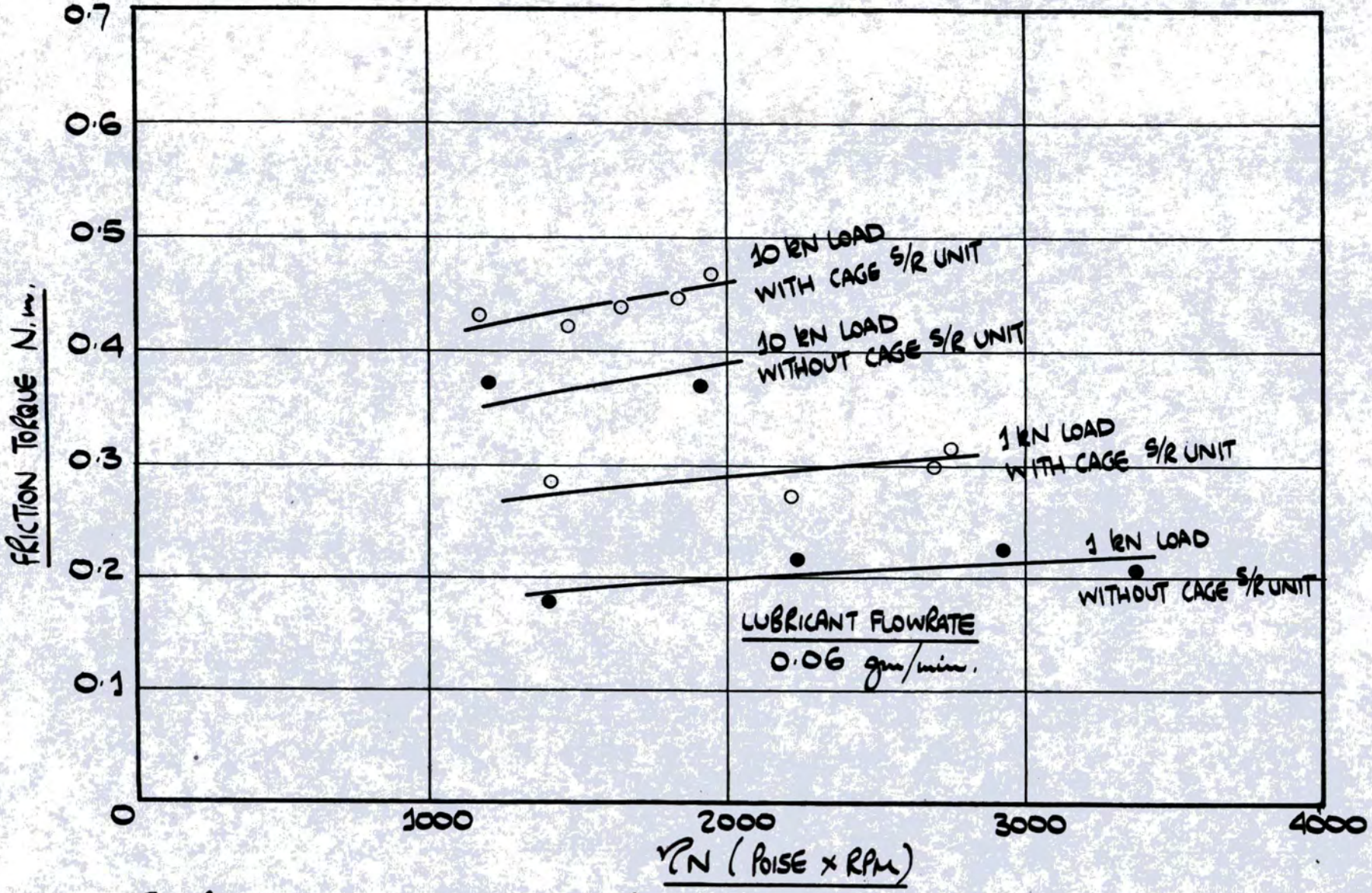

FIGURE F·2. TORQUE CURVES FOR TEST BEARING NU310, SHOWING EFFECT OF CAGE SLIP-RING UNIT

APPENDIX (C)

Measurement of shaft speed

A block diagram of the circuit used for shaft, cage and roller speed measurement is shown in figure 6.1.

The shaft of the machine was fitted with a 7cm. diameter steel disc which had been cut away at 6 points in its circumference.

A magnetic pick-up was placed in close proximity to the disc and, as the shaft rotated, the cut-outs caused a peaked signal e.m.f. to be generated in the coils of the magnetic pick-up. This peaked signal was fed into a Levell type TA605 fixed-gain amplifier, the output being displayed on an oscilloscope. The output was also passed through a switching unit to an Advanced Electronics type TC6 timer/counter, set to read signal frequency in Hertz.

Shaft speed was also measured by a hand held tachometer, but readings from this instrument were found to be unreliable.

The fixed-gain amplifier provided a peak-to-peak signal voltage more than sufficient to ensure accurate counting of pulses by the digital counter and it is confidently expected that the error in shaft speed will be negligible, since great care was taken to ensure that the speed was accurately maintained at the value required.

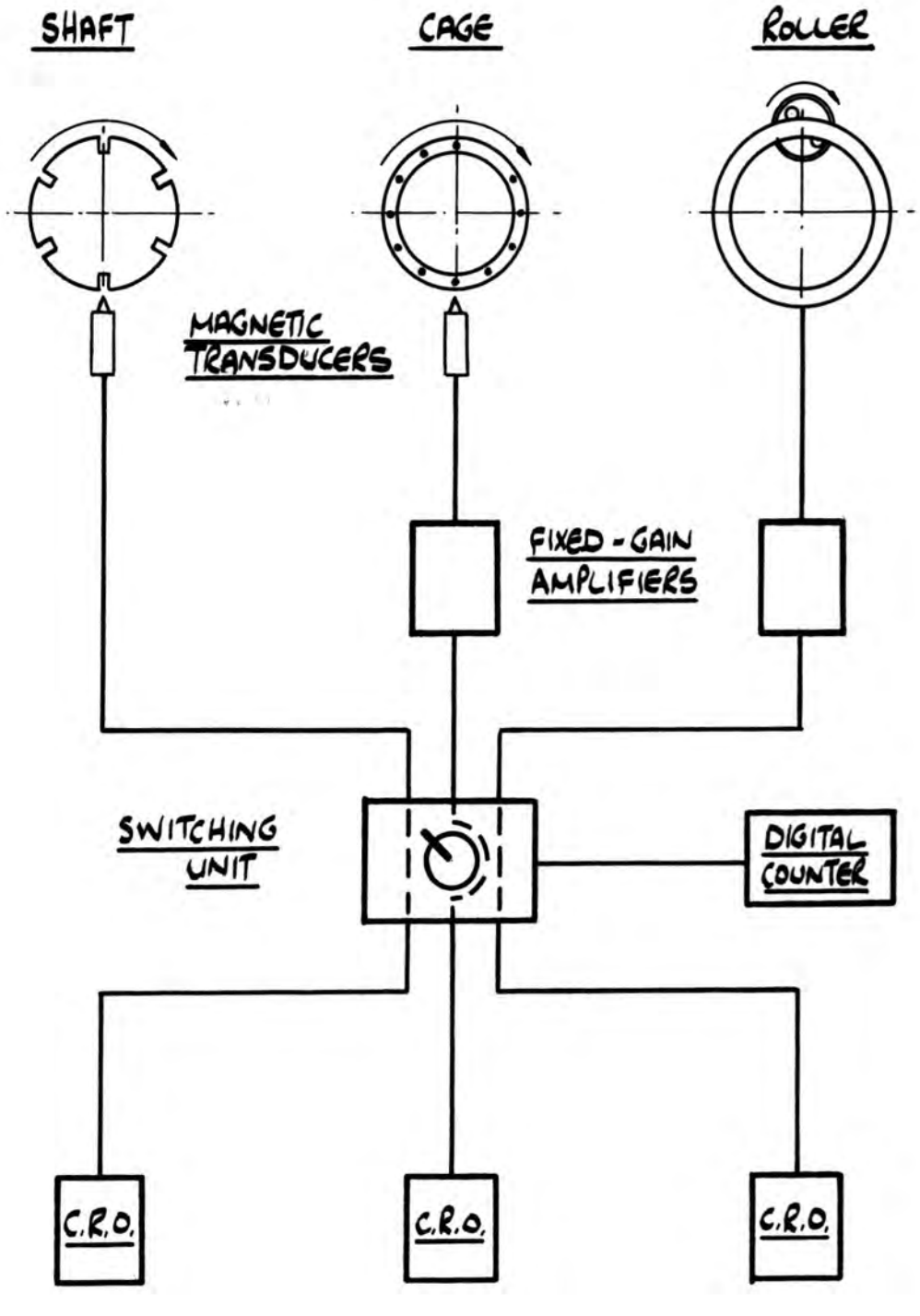

FIGURE G.1 . CIRCUIT BLOCK DIAGRAM FOR THE MEASUREMENT OF SHAFT, CAGE AND ROLLER SPEED.

APPENDIX (H)

Measurement of cage speed

A block diagram of the circuit used for shaft, cage and roller speed is shown in figure G.1 .

The cage of the test bearing was fitted with 12 bolts of which 11 were steel, 1 brass. A magnetic pick-up close to the cage bolts gave a peaked signal when the cage rotated and this signal was fed through a Levell type TA605 fixed-gain amplifier to an oscilloscope and also through the switching unit to the Advance Electronics TC6 timer/counter.

The instrumented roller in the test bearing (described in Appendix (I)) was fitted next to the brass bolt in the cage. The absence of a pulse as the brass bolt passed the magnetic pick-up gave the position of the instrumented roller in the test bearing whilst the bearing was running. It was hoped that, by comparing the cage and roller traces on the oscilloscope, any variation in roller speed could be related to the position of the test roller relative to the loaded region of the test bearing. However, this did not prove possible because the oscilloscope traces obtained were not sufficiently precise.

Both roller and cage speed traces obtained from the digital counter were checked by 'Polaroid' photographs of the oscilloscope traces taken by use of a Shackman Polaroid Land camera type PL1 .

Detailed experimental values of cage speed have

not been included in the experimental results since at no time was significant cage slip observed.

APPENDIX (I)

Measurement of roller speed

A block diagram of the circuit used for shaft, cage and roller speed measurement is shown in figure G.1.

The system used for the measurement of roller speed was similar to that described by Smith (31). A diagram of the system is shown in figure I.1.

A single roller of the test bearing - referred to as the instrumented roller since it also contained the thermocouple used for the measurement of roller temperature (see Appendix (L)). - was fitted with two small magnets embedded in one end and the end counter-bored and filled with Araldite which acted as an insulator. The magnets were 3 mm diameter, 4 mm long and were made from Alcomax III. When fitted with magnets in this manner the roller formed a weak horseshoe magnet. The cage of the test bearing was machined to allow a stationary pick-up coil - 40 turns of 0.1 mm diameter laquered copper wire on a 'tufnol' former - to be fitted round the outer race of the test bearing. The coil was therefore positioned in close proximity to the rollers in the bearing. As the instrumented roller rotated epicyclically in the bearing a small sinusoidal e.m.f. was generated in the pick-up coil. This signal was fed through a Levell type TA605 fixed-gain amplifier to an oscilloscope and, via a switching unit, to the Advance Electronics type TC6 digital timer/

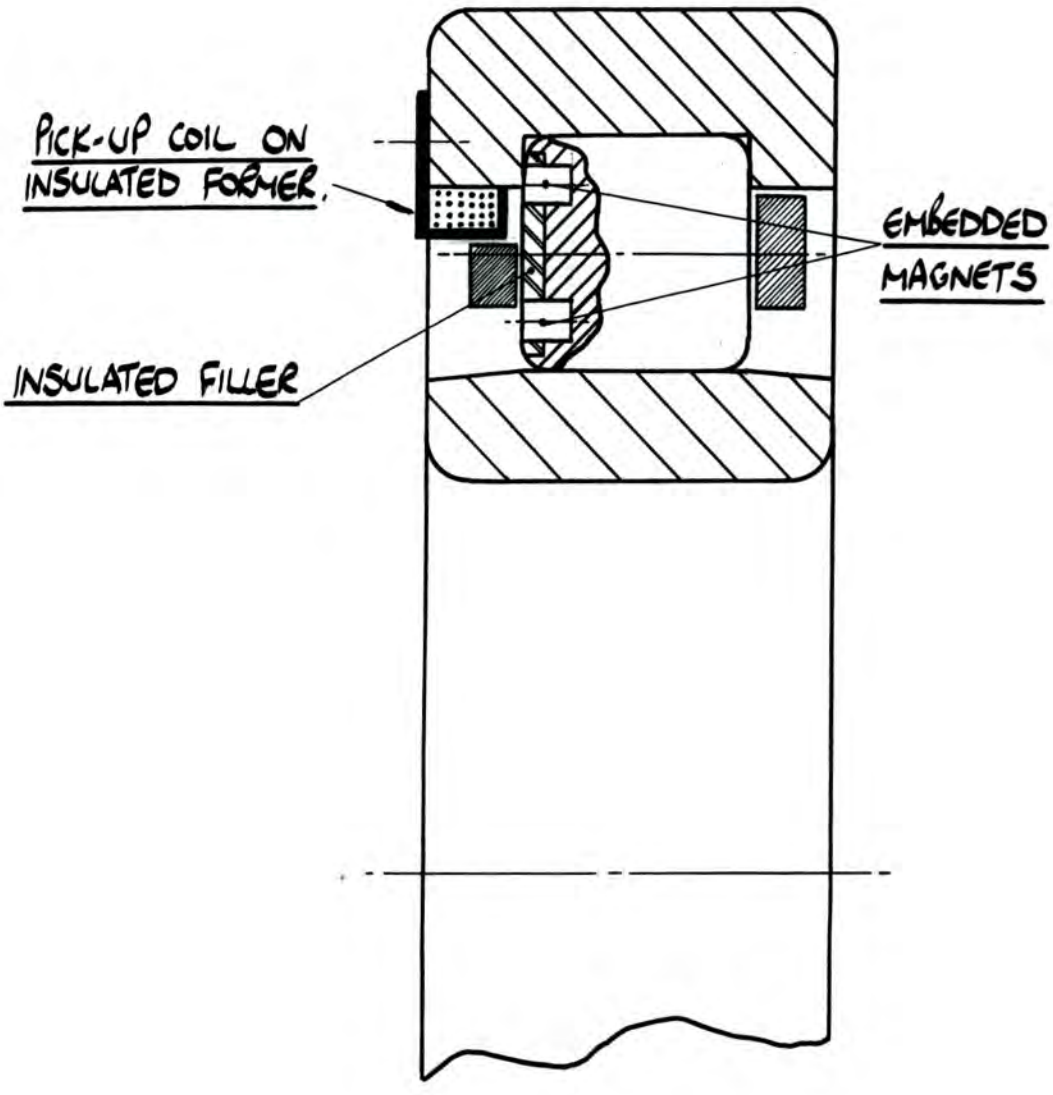

FIGURE I.1 . ARRANGEMENT FOR ROLLER SPEED MEASUREMENT.

counter. The signal was, however, prone to high frequency "noise" and a low pass filter was needed to process the signal before it could be counted satisfactorily.

As mentioned in Appendix (H), 'Polaroid' photographs of the oscilloscope traces were used to check the accuracy of the readings taken from the digital counter. In most cases the counter readings and 'Polaroid' photographs agreed quite well.

Not all tests carried out contained roller speed measurements and the reader is referred to figure 22 showing the test conditions for which roller speed readings have been taken.

APPENDIX (J)

Measurement of outer race temperatures

The temperature of the outer race of the test bearing was measured at 7 stations around the circumference, as shown in figure J.1 . The stations were at the point of maximum load and at intervals of 30° around one side of the bearing to a point diametrically opposite the point of maximum load. The thermocouples were at a depth of 1.27mm below the running surface of the race. In addition to the circumfrentially disposed thermocouples, three thermocouples were fitted at the point of maximum load. These thermocouples were placed at depths of 1.27mm, 2.54mm and 3.8mm below the running surface of the race to allow the radial temperature variation to be measured at this point.

Each thermocouple was fitted into a 0.5mm diameter, 12.7mm deep hole which was spark-eroded into the bearing. At this depth, the thermocouple junctions were on the centre line of the roller track.

The original thermocouples fitted to the machine were 0.5mm diameter chromel/alumel thermocouples manufactured by Pyrotenax Limited. These were changed at a later date, due to calibration problems, and a set of copper/constantan thermocouples permanently fixed into the eroded holes by 'Durofix' cement. These thermocouples proved very satisfactory.

The thermocouple e.m.f's were fed through a 'Cropico' 24 channel thermocouple switch to a Southern Instruments Digital voltmeter type SM211.

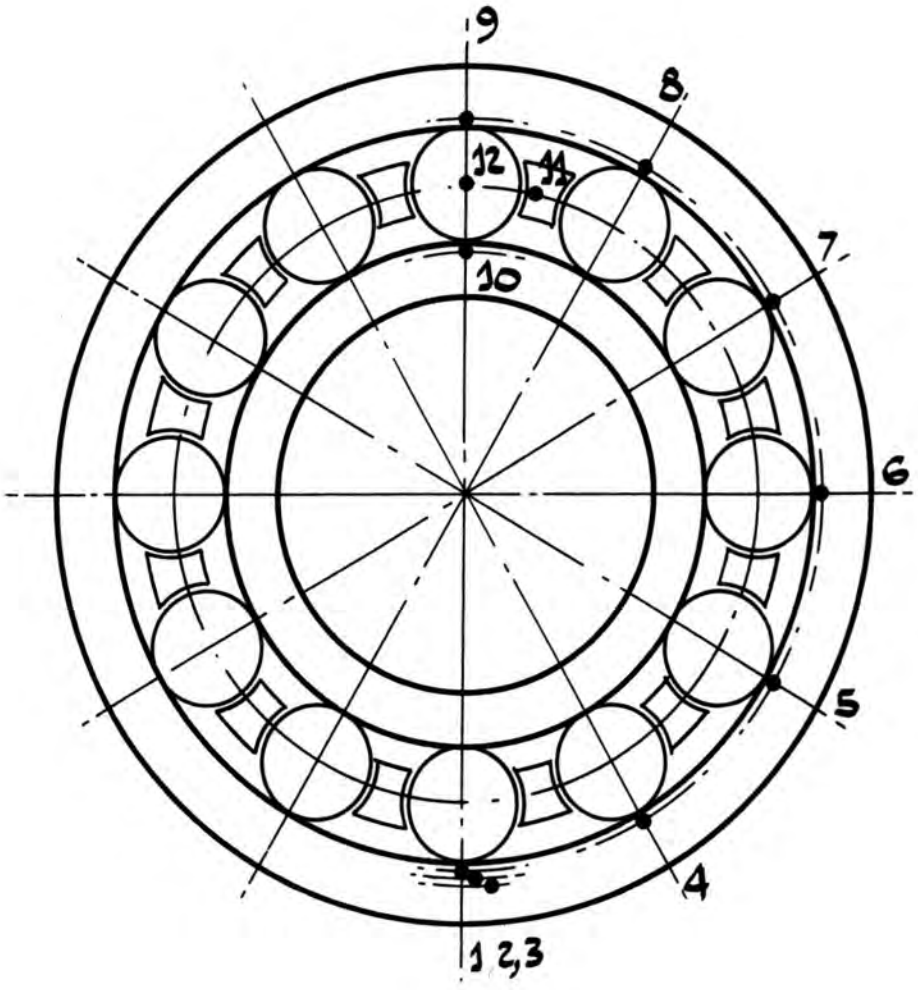

FIGURE J.1 . THERMOCOUPLE POSITIONS IN THE TEST BEARINGS

Cold junction reference was provided by an ice/water mixture.

The thermocouples were calibrated by the method described in Appendix (M).

The thermocouple holes in the inner and outer races of the test bearing were spark - eroded by the technique described in Appendix (N).

APPENDIX (K)

Measurement of inner race temperature

The single copper/constantan thermocouple fitted in the inner race of the test bearing was held in a spark - eroded hole 1.27mm below the running surface of the race by 'Durofix' cement.

It was necessary to fix the inner race thermocouple into the inner race after the test bearing had been assembled in the machine.

After leaving the inner race, the thermocouple wires were passed through a small hole in the inner race clamping sleeve (see figure 24), along the inside of the clamping sleeve and then along the outside of the test shaft. The wires then passed along a keyway through the bore of the drive pulley to a specially designed terminal block fitted to the end of the shaft. From the terminal block the wires passed down a 5mm diameter hole drilled the full length of the shaft to an I.D.M. type PL, 8 track slip-ring unit fitted to the other end of the shaft. The slip-ring unit was provided with silver tracks, each track having two silver impregnated graphite brushes. Each wire of the thermocouple was connected to three tracks (in parallel) of the unit to minimise the effects of the slip-ring contacts. The thermocouple e.m.f. was fed from the slip-ring unit to the 'Cropico' thermocouple switch and then to the Southern Instruments digital voltmeter.

The inner race thermocouple was calibrated by the method described in Appendix (M).

The technique used for the erosion of thermocouple holes is described in Appendix (N).

APPENDIX (L)

Measurement of roller and cage temperatures

The slip-ring unit and thermocouples specially designed for the measurement of roller and cage temperatures is shown in Figure L.1 .

The roller of the test bearing fitted with magnets for roller speed measurement (see Appendix (I)) was also provided with a stepped bore at the opposite end to the magnets. This bore was spark-eroded on a Wickman Erodomatic machine and then internally ground to a fine finish: the roller circumference and the bore were accurately concentric.

The thermocouples used for roller and cage temperature measurement were made from 1.58mm diameter 'Pyrotenax' stainless steel sheathed, mineral insulated, thermocouple cable, the thermocouple wires being copper/constantan. The thermocouple used to measure roller temperature was fitted with a 5mm diameter rubber 'O' ring on a brass carrier: the 'O' ring helped to locate the thermocouple in the roller and also prevented the air and oil trapped within the roller from escaping too quickly. The open ends of the mineral insulation were sealed with 'Araldite'.

On assembly care was taken to ensure that the roller thermocouple did not restrain the rotation of the instrumented roller. To allow a degree of misalignment between roller and thermocouple, the thermocouple was made as long as possible within the limits

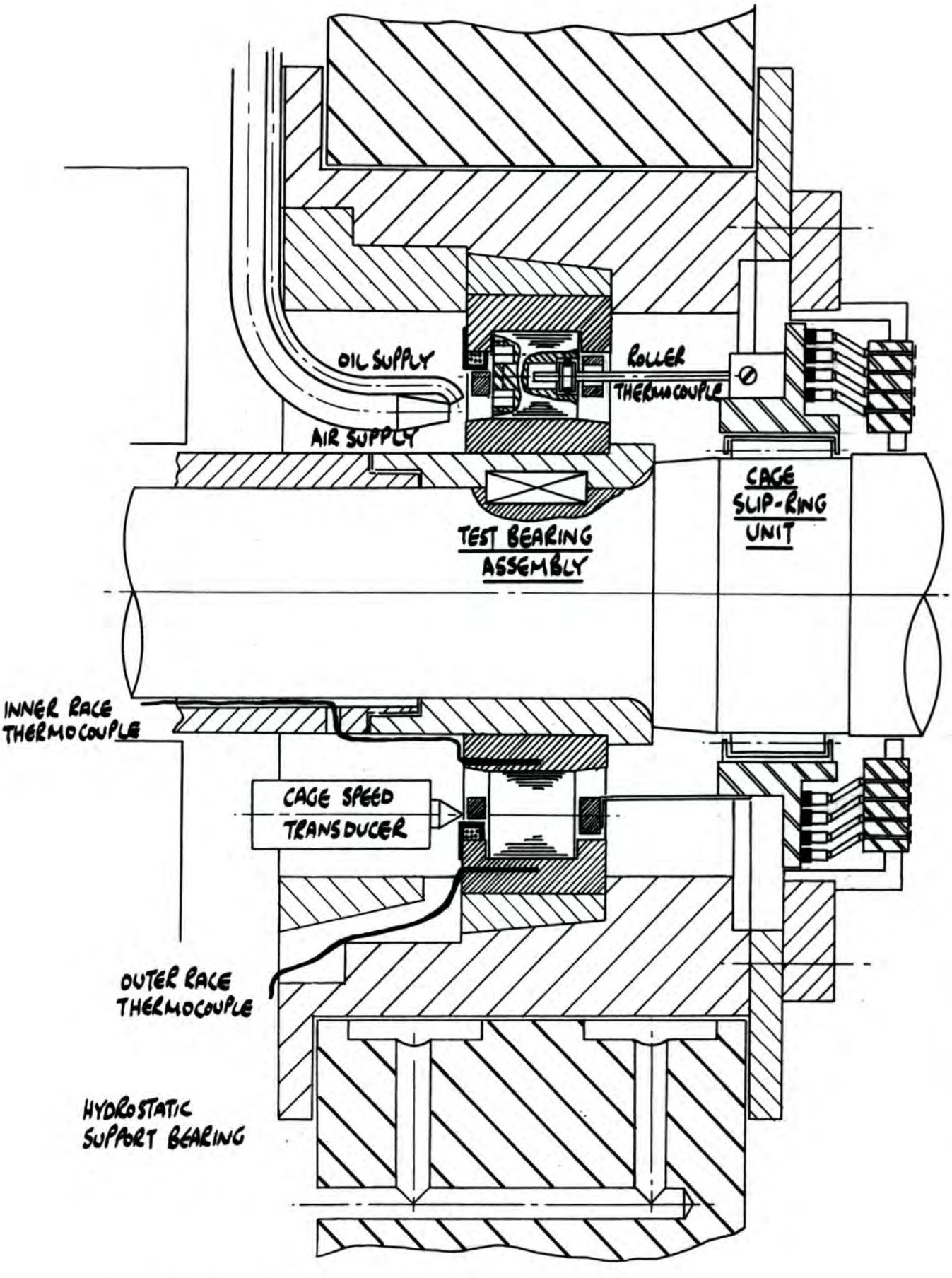

FIGURE L·1 . TEST CELL AND CAGE SLIP RING UNIT

imposed by the design of the slip-ring unit.

The thermocouple used for cage temperature measurement was fitted into a hole drilled close to the face of one of the roller pockets in the cage: the centre-line of the thermocouple was 2mm away from the cage surface, the thermocouple junction being on the cage centre-line.

The slip-ring disc was machined from 'Tufnol' and was mounted on its own needle roller bearing, the bearing running on a track machined on the shaft of the machine. The disc was driven at cage speed by three light springs connecting the disc and the cage of the test bearing.

The roller and cage thermocouples were mounted in a clamping block fastened to the back of the slip-ring disc and each thermocouple wire was connected to one of the 4 brass slip-rings which were embedded in the face of the disc.

The steel cover for the unit contained 'Tufnol' terminal blocks and these were used to mount the slip-ring brushes. Each slip-ring was provided with two brushes connected in parallel, the brushes being made from silver impregnated graphite bonded to berrylium - copper springs by a conducting element.

Compensating leads were used to carry the thermocouple e.m.f. from the slip-ring unit, via a 'Cropico' thermocouple switch, to a Southern Instruments type SM211 digital voltmeter.

The slip-ring tracks were originally silver -

plated, but the amount of silver that could be deposited with the facilities available was very small and was soon worn away. However, the unit worked satisfactorily with brass tracks and so no further attempts to silver-plate the tracks were made.

Figure L.1 shows the close proximity of the slip-ring tracks to the test bearing. Although adequate drainage was provided, the unit was prone to contamination by oil, particularly at higher lubricant flowrates. An attempt to reduce this contamination by fitting an oil thrower to the disc and also be feeding compressed air to the unit was only moderately successful. A more effective way to remove the contaminating oil from the slip-rings themselves was to wipe the disc surface with solvent as the unit was rotating, but it was decided that only by stopping the test machine immediately prior to a reading being taken could a sufficiently reliable temperature reading be obtained. This was the practice during all tests for which roller and cage temperatures have been obtained.

The slip-ring unit has worked satisfactorily with minimal attention for the whole duration of the test programme.

The thermocouples were calibrated by the method described in Appendix (M).

APPENDIX (M)

Calibration of thermocouples for the measurement of race, cage and roller temperatures

As much as possible of the actual circuit wiring used in the build-up of the testing machine was incorporated in the circuits during calibration.

All the copper/constantan thermocouple wires were permanently soldered into the thermocouple switch and the outer race thermocouples were permanently fixed into the test bearing outer race before calibration.

The test bearing outer race (with thermocouples fitted) and the inner race, cage and roller thermocouples were submerged in a Townson and Mercer Type E270 Thermostat Bath filled with Shell Risella 17 oil.

Bath temperature was measured by two I.P calibrated thermometers. During initial calibration tests, the bath temperature was allowed to settle at a number of discrete values within the range 15°C to 100°C and readings of temperature and thermocouple e.m.f. taken, but it became obvious that the temperature/thermocouple e.m.f. curve could be accurately represented by a straight line. For subsequent calibration checks only two discrete temperature values were taken, one at each end of the working range. From the readings obtained, a straight line law was determined and tables of thermocouple e.m.f./temperature values generated for each thermocouple.

As expected, the calibration values for different thermocouples did not vary in total by more than 5% from each other, but the assumption of an overall calibration figure was avoided since accurate temperature readings were considered to be important for the interpretation of test data.

It is thought that outer race temperature measurements taken during the experimental programme are within 1% of the actual temperature in the bearing component.

Measurements of inner race temperature also appeared to be reliable and are expected to be within 5% of the temperature in the bearing component.

Measurements of cage and roller temperatures were less reliable because the cage slip-ring unit was prone to contamination by oil, but reasonable readings could be obtained by stopping the shaft rotation whilst the reading was taken. It is expected that results taken in this way will be well within 10% of component temperatures.

APPENDIX (N)

Erosion technique for thermocouple holes

The inner and outer races of both test bearings contain holes of 0.5mm diameter, 12.7mm deep. Holes of this small diameter and relatively large depth can be difficult to produce accurately in hard steels such as bearing races, but a successful technique was developed. See figure N.1 .

The holes were spark-eroded using a Wickman Erodomatic machine operating at a low level of erosion current. The spark-erosion electrode used was copper hypodermic tube of 0.48mm diameter which was soldered into a suitable terminal block. The bore of the electrode was then connected to a vacuum pump and when the free end of the electrode was below the surface of the electrolyte (paraffin) a flow of electrolyte was established up the bore of the electrode.

The bearing race to be machined was fitted into an insulated former (Tufnol), small guideholes through the former providing an accurate location for the electrode. When eroding, the flow of electrolyte up the bore of the electrode carried away the waste material produced by the machining process and allowed a flow of clean electrolyte to the point of erosion down the side of the electrode in the hole. It should be noted that, if the situation were reversed with the clean electrolyte being supplied down the bore of the

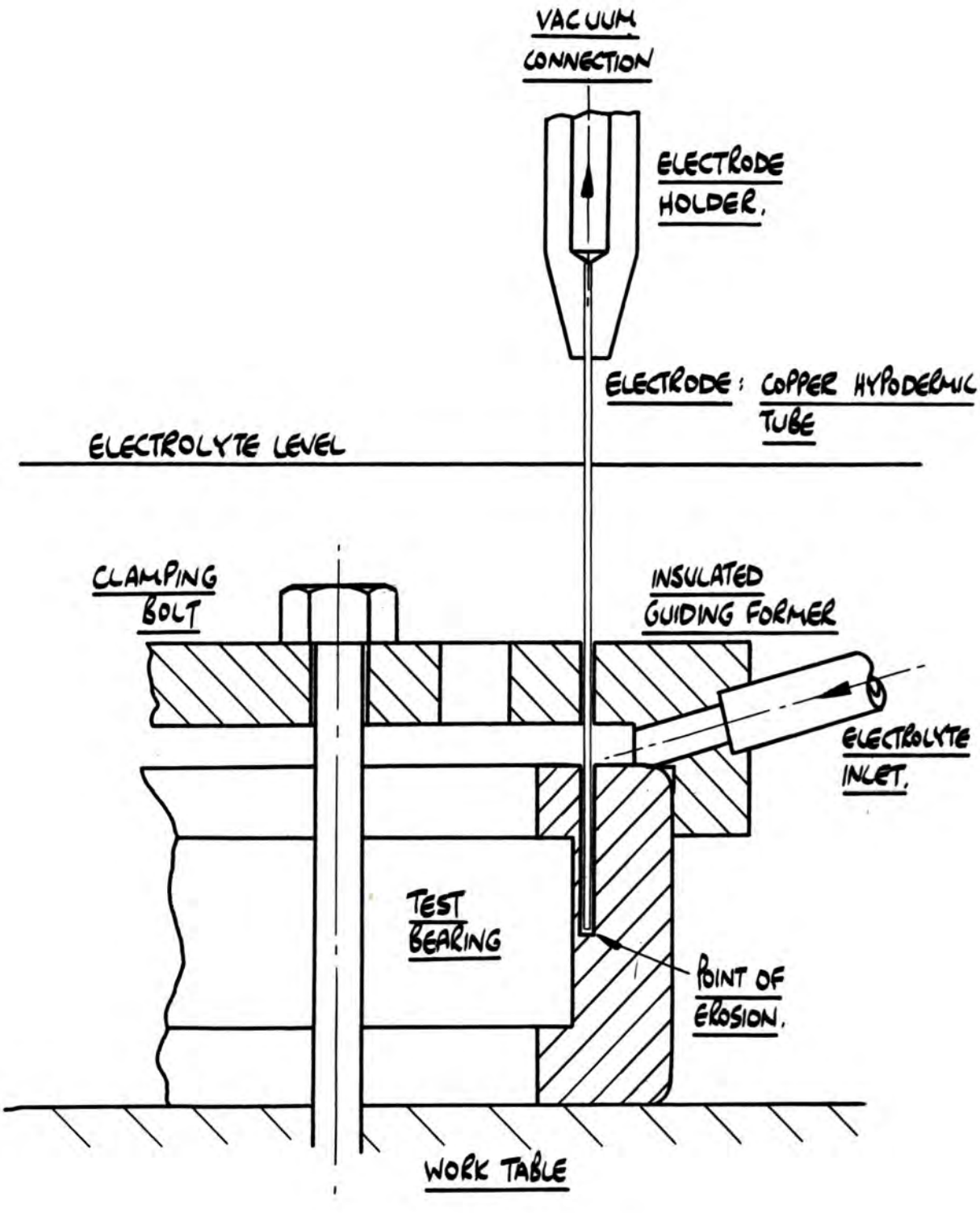

FIGURE N.1 . EROSION TECHNIQUE FOR THERMOCOUPLE HOLES.

electrode, the debris' contained in the electrolyte leaving the point of erosion would allow secondary erosion circuits to be established, resulting in a 'pear shaped' hole.

Using the technique described, the resultant holes were so perfectly eroded that, initially, a 'pip' of material (due to the bore of the electrode) was left in the eroded hole. This problem was overcome by putting a very fine copper wire down the bore of the electrode. This wire, itself acting as an electrode, prevented the development of the central 'pip' of material.

It was found necessary to design the insulated former in such a way that a positive flow of electrolyte was maintained between the former and the material being eroded, <u>across</u> the surface. This flow prevented the build-up of spark erosion debris' at the exit of the eroded hole. This debris' would, if allowed to accumulate, cause an electrical breakdown of the insulated former. If breakdown does occur, the former must be replaced.

APPENDIX (O)

Measurement of test lubricant flowrate

All the lubricants used in the experimental work were supplied to the test bearing in the form of an oil/air mist, the air acting as a coolant for the bearing and also as a transport medium for the oil droplets. The equipment used to provide the oil/air mist is shown in figure O.1 : it will be noted that a 'scent-spray' device was used to generate the mist. The air and lubricant supplies to this device were separately controlled. Details of the calibration of the air flow system are given in Appendix (P).

The test lubricants were contained in graduated burettes and fed from these to the misting device by a Watson-Marlowe peristaltic pump, type MHRE 72L. The flexible tubes used in the peristaltic pump were 'Technicon' Auto-analyser tubes. These are available in a number of sizes and to provide the flowrates required in the experimental programme the following tubes were used.

TUBE REF.	COLOUR REF.	TUBE BORE	FLOWRATES
116-0533-09	White	0.040"	1.6 gm/min.
116-0533-07	Black	0.030"	0.2 gm/min.
116-0533-04	Orange/Green	0.015"	0.06 gm/min.
116-0533-01	Orange/Red	0.0075"	0.004 gm/min.

All the pumping tubes and lubricant transmission tubing used were made from 'Solvaflex' - a Technicon Limited material - since it was found that other flexible plastics and silicone rubber tube tended to

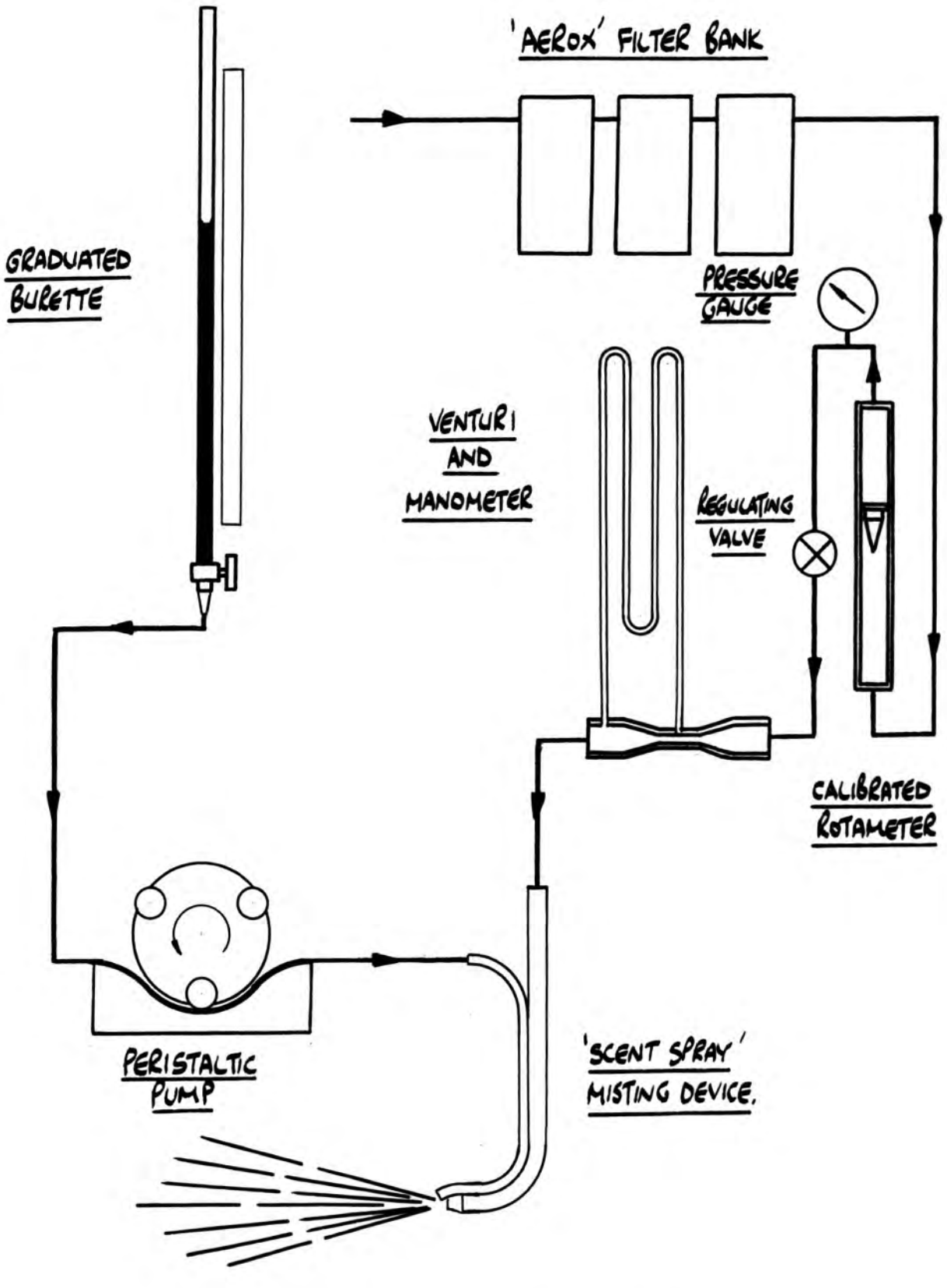

FIGURE .0·1 APPARATUS FOR AIR/OIL MIST LUBRICATION SYSTEM.

degenerate in mineral oil.

It was brought to the attention of the author (Rolls Royce) that an oil/air mist such as that generated by the device used in the present work contains oil droplets of random size. Only the larger droplets are available as lubricant since only these will 'wet-out' on contact with a solid surface. It therefore follows that only a certain proportion of the lubricant supplied to the misting device will be available to lubricate the bearing.

A series of tests were carried out with each of the pumping tubes to allow an estimate of this proportion to be made. The tests consisted of directing the oil/air mist generated by the misting device into a deep glass container of similar size to the test cell of the machine and collecting the oil which wetted out into the vessel over a period of time. A comparison between the amount of oil supplied to the misting device and that collected in the glass container provided an indication of the proportion of the oil supply which would 'wet'out' and would, under ideal conditions, be available to lubricate the bearing. The results of these tests are shown in figure 0·2 .

Such tests, of course, can only provide a very rough guide to the amount of lubricant supplied to a bearing when in operation since a proportion of the lubricant actually wetting out in the test cell will be wasted.

When plotting experimental results concerned with

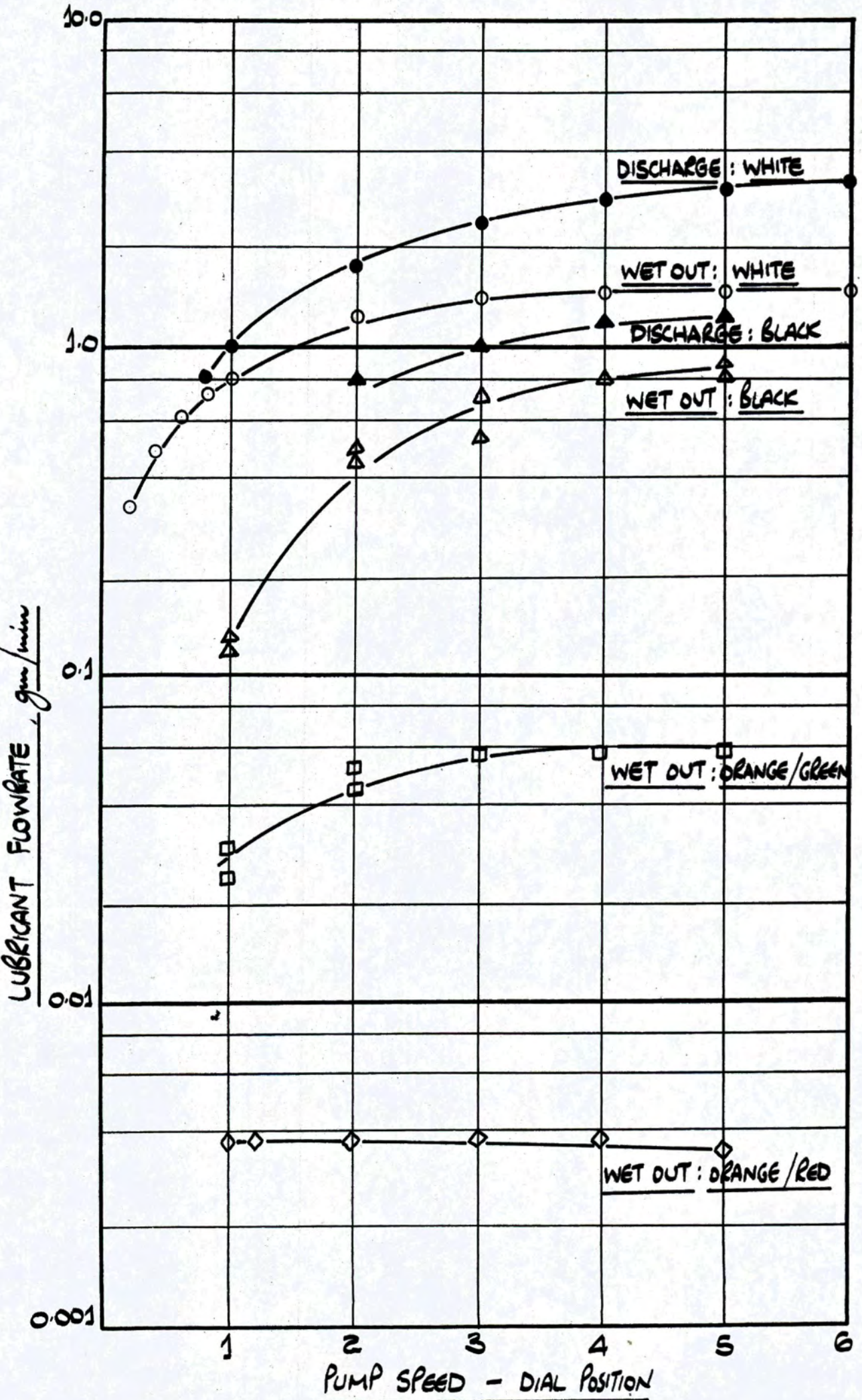

FIGURE 0·2 . PUMPING TUBE CHARACTERISTICS

lubricant flowrate it has been the practice in this present work to use the flowrates of lubricant supplied to the misting device. The results contained in this Appendix would allow some estimate of the lubricant wasteage to be made, if required.

a period of time. During the calibration tests the exit pressure of the 'Rotameter' was maintained at the value used in the experimental work. The air pressure at the misting device was slightly above atmospheric pressure.

During the present work, all the experimental tests were carried out using one value of flowrate only, namely 0.14 kg/min.

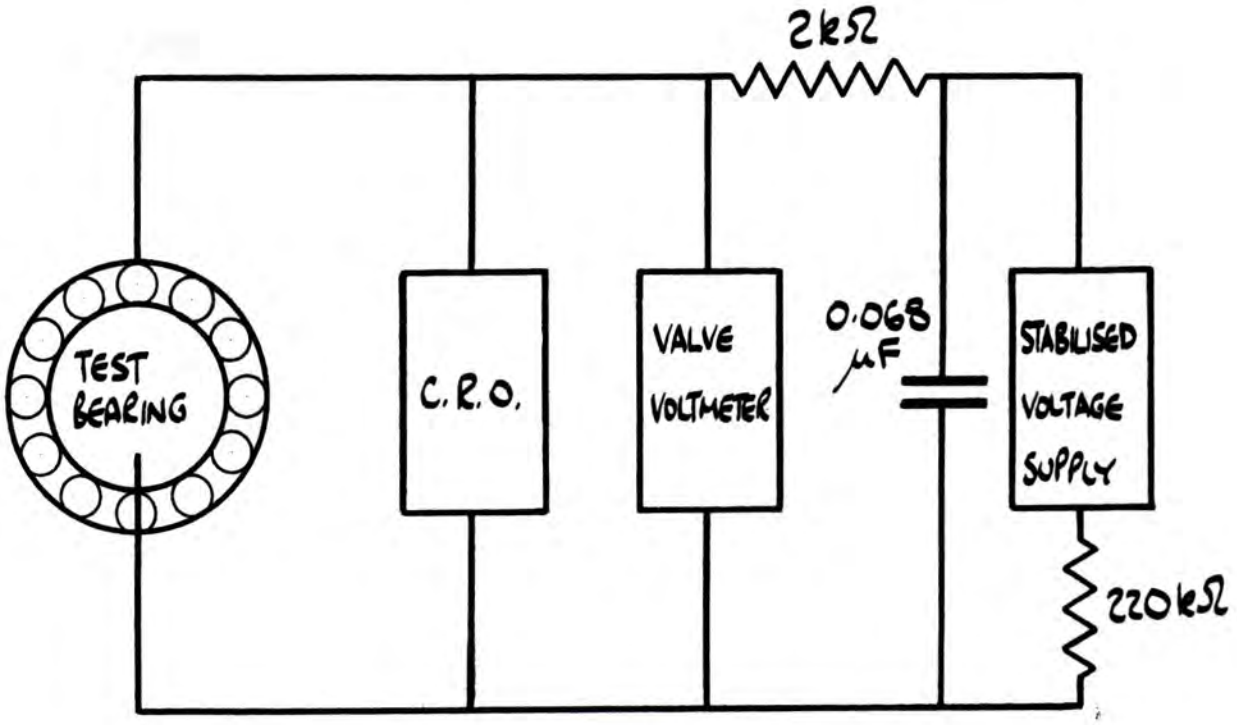

FIGURE Q.1. CIRCUIT FOR THE MEASUREMENT OF OIL FILM ELECTRICAL RESISTANCE

Furey and used by, amongst others, Leaver (25), with the addition of a 0.068 μF. capacitor, included to filter out signal noise. The addition of this component has allowed reasonable oscilloscope traces to be obtained and did not appear to affect the readings obtained from the valve voltmeter. Its effect has not been fully investigated since it was never intended to use readings from this instrumentation in any subsequent calculations.

A fuller analysis of the behaviour of the circuit shown in figure Q.1 and a discussion of its application as a monitoring device as used in this present work, is given by Garnell (19) but it can be briefly summarised as follows.

The combination of the stabilised voltage source and the 220 $k\Omega$. resistor provides a constant current source which is applied to the 2 $k\Omega$. resistor in parallel with the test bearing. The 2 $k\Omega$. resistor limits the current flow through the test bearing to about 7 microamps. Both valve voltmeter and oscilloscope measure the voltage drop across the test bearing, and this is arranged to vary between 0mv and 10mv depending on the resistance of the oil film in the bearing. A reading of 0mv indicates metal-to-metal contact within the bearing and a reading of 10mv indicates infinite resistance, signifying a complete oil film. Intermediate values indicate some metal-to-metal contact although it should be noted that, since lubricating oil has a very high resistivity, even a

lubricating film a few molecules thick will have a very high resistance, giving a corresponding voltmeter reading approaching 10mv.

When the test bearing starts to rotate under load, the oscilloscope trace indicates a 0mv (no film) condition, but as speed increases and lubricant is entrained into the contacts in the bearing, the oscilloscope trace can be seen to 'peak' between the 0mv. and 10mv levels. When the bearing speed is high enough to entrain sufficient lubricant for a full film, the oscilloscope trace settles at a level corresponding to a 10mv signal.

The behaviour of the valve voltmeter during these events is different because of its relatively high damping. At low speed, when only a few 'peaks' are evident on the oscilloscope trace, the valve voltmeter reading will be effectively zero, but as speed is increased and more 'peaks' appear the valve voltmeter reading takes some intermediate value between 0mv and 10mv. For conditions where a full lubricant film is present, the reading settles at 10mv. It can therefore be appreciated that, whereas the oscilloscope trace provides an indication of the instantaneous state of a lubricant film within a bearing, the valve voltmeter provides a longer term, time - average indication.

A typical set of oscilloscope traces showing the development of the lubricant film from 'no - film' to 'full film' conditions are shown in figure Q.2 .

The oscilloscope display and valve voltmeter

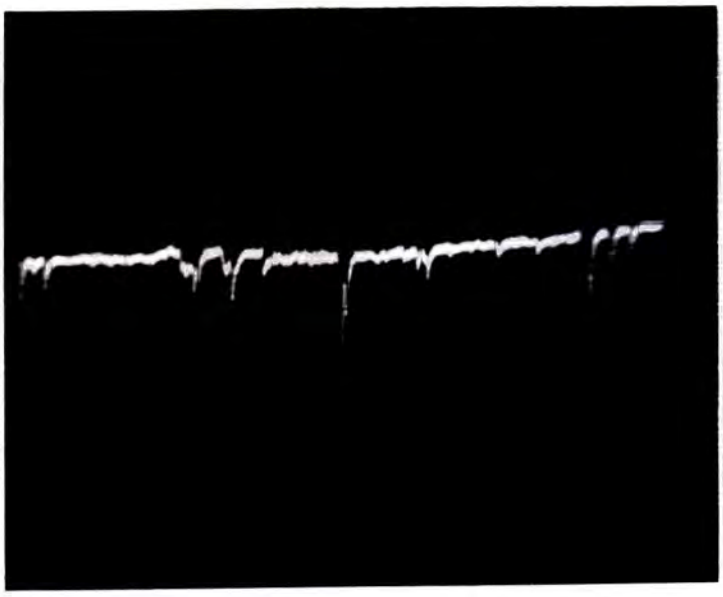

FULL FILM LEVEL

NO FILM LEVEL

APPROACHING FULL FILM

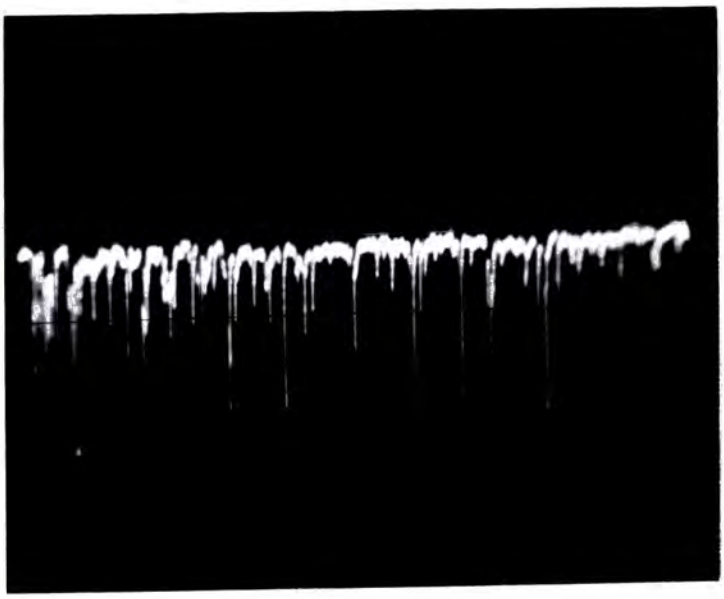

FULL FILM LEVEL

NO FILM LEVEL

INTERMEDIATE FILM

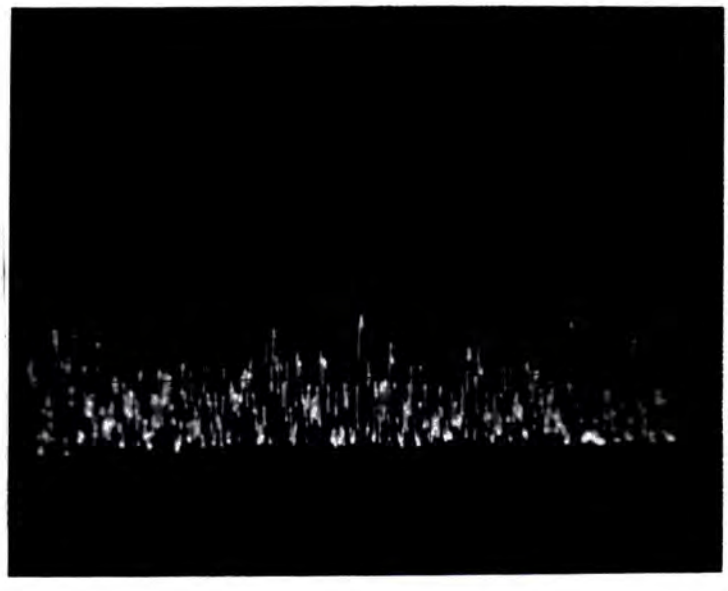

FULL FILM LEVEL

NO FILM LEVEL

ALMOST NO FILM

FIGURE Q·2 STAGES IN THE DEVELOPMENT OF A LUBRICANT FILM AS SHOWN BY THE FILM RESISTANCE MONITOR.

readings were used to monitor the bearing oil films during all tests carried out and it appeared that, for all flowrates, an adequate lubricant film was present in the bearing.

The equipment used in the above monitoring circuit was:

Farnell Stabilised Voltage Supply type L30B

Phillips Valve Voltmeter type PM2440

Telequipment Oscilloscope type D43

fitted with double beam tube, time-base with one shot facility and type G differential amplifier.

The circuit connection to the inner race of the test bearing was achieved by the use of two tracks (in parallel) of an I.D.M. type PL slip-ring unit.

Photographs of the oscilloscope traces were taken using a Shackman Polaroid Land camera model PL1, and by using the one-shot facility on the oscilloscope.

APPENDIX (R)

Load sharing in a roller bearing assembly

For a complete roller bearing assembly as shown in figure R.1 , Dowson and Higginson (13) have analysed the deflection and load sharing between rollers for cases of perfect geometry, initial clearance and initial interference. This appendix uses this work to predict the number of loaded rollers in the bearing assembly at the two experimental loads and for the test bearings used.

Dowson and Higginson have shown that, for a bearing assembly with an initial radial clearance Δ,

$$M = \frac{W}{P_0} = \frac{W'}{P_0'} = 1 + \frac{2}{[\delta_0 - \Delta]} \times \left[\begin{array}{l} \cos\lambda[\delta_0\cos\lambda - \Delta] \\ + \cos 2\lambda[\delta_0\cos 2\lambda - \Delta] \\ + \ldots\ldots \\ \ldots\ldots + \cos n\lambda[\delta_0\cos n\lambda - \Delta] \end{array} \right] \qquad \text{R.1}$$

where

M = load distribution factor

W = total load on bearing

W' = load/unit width on bearing

P_0 = total load on most heavily loaded roller

P_0' = load/unit width on most heavily loaded roller

δ_0 = deflection of most heavily loaded roller

= deflection of the assembly in the direction of the applied load.

Δ = radial clearance

λ = $360^\circ/z$

z = total number of rollers

n = Integral part of $\left(\frac{z-1}{4}\right)$

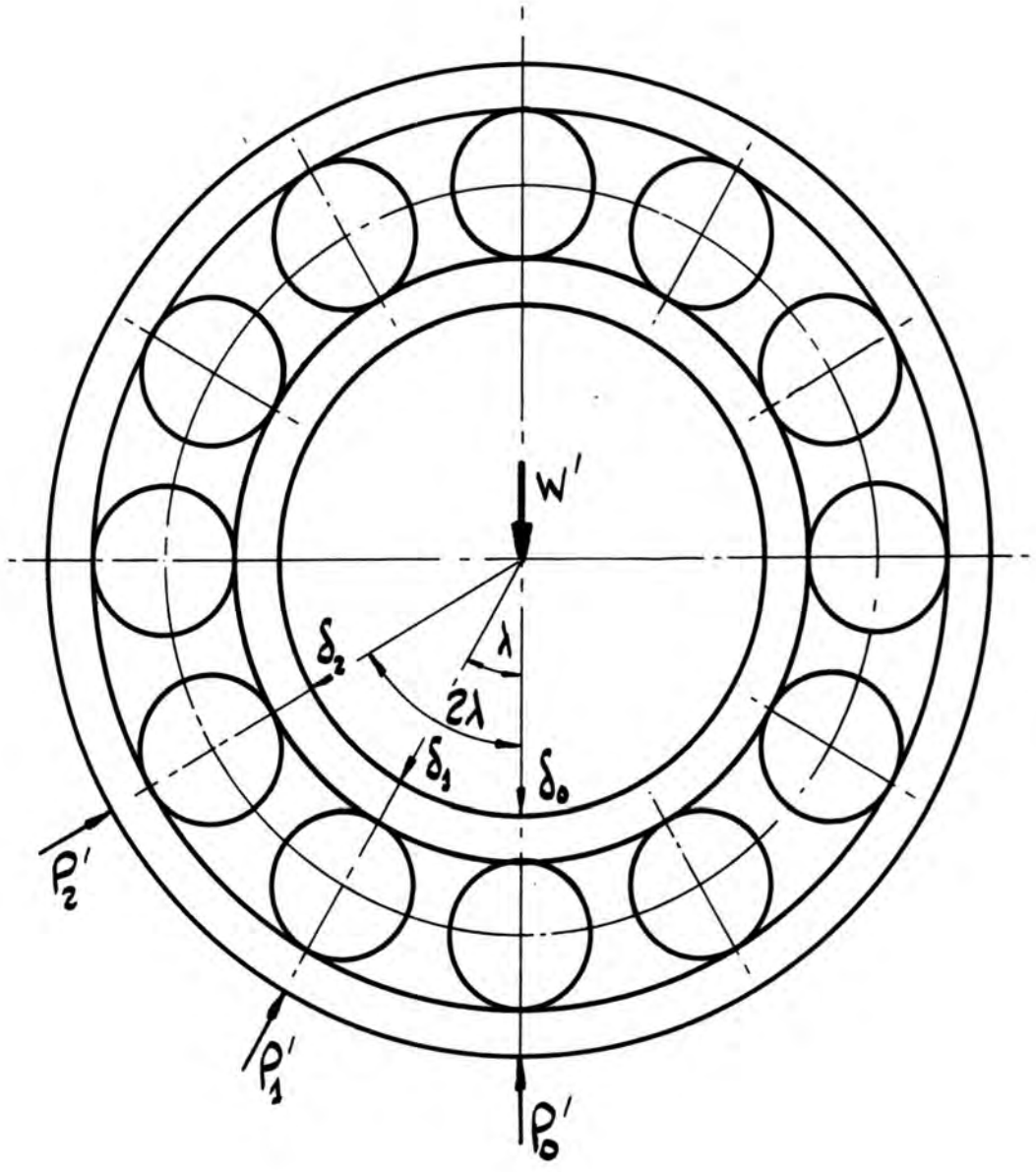

FIGURE R.1. FORCES AND RADIAL COMPONENTS OF DISPLACEMENT IN A ROLLER BEARING ASSEMBLY (REPRODUCED FROM REFERENCE 14)

It should be noted that, in the analysis given by Dowson and Higginson, the expressions in square brackets in equation (8.1) have the Macaulay meaning of

$$[x] = x \quad \text{when } x \geqslant 0$$
$$[x] = 0 \quad \text{when } x < 0 \qquad \text{8.2}$$

Equation (8.1) can be re-expressed as

$$M = \frac{W'}{P_0'} = 1 + \frac{2}{\left[\frac{\delta_0}{\Delta} - 1\right]} \times \begin{bmatrix} \left[\frac{\delta_0}{\Delta}\cos\lambda - 1\right]\cos\lambda \\ + \left[\frac{\delta_0}{\Delta}\cos 2\lambda - 1\right]\cos 2\lambda \\ + \ldots\ldots \\ \ldots + \left[\frac{\delta_0}{\Delta}\cos n\lambda - 1\right]\cos n\lambda \end{bmatrix} \qquad \text{8.3}$$

For values of Δ, n, λ corresponding to those for test bearings NU310 and N310, equation (8.3) provides a means of calculating values of W'/P_0' for incremental values of the ratio δ_0/Δ.

Dowson and Higginson have further shown (14) that, for a single roller/race configuration,

$$\frac{\delta}{r} = 17.5\,\frac{P'K}{r} \qquad \text{8.4}$$

where

δ = deflection; the approach of the two remote points in the races.

r = roller radius

P' = load/unit width, as before

$$K = \frac{2(1-\nu^2)}{\pi E}$$

K is an elastic constant and is also given by

$$K = \frac{2}{\pi E'} \quad \text{where} \quad \frac{1}{E'} = \frac{1}{2}\left[\frac{1-\nu_1^2}{E_1} - \frac{1-\nu_2^2}{E_2}\right] \qquad \text{8.5}$$

Since δ_0 gives the radial displacement in the

direction of the applied load, it follows that equation (R.4) can be written

$$\frac{\delta_o}{r} = 17.5 \frac{\rho_o' K}{r} \qquad R.6$$

For the case of initial clearance Δ, the equation (R.6) becomes

$$\frac{[\delta_o - \Delta]}{r} = 17.5 \frac{\rho_o' K}{r} \qquad R.7$$

giving

$$\frac{K\rho_o'}{r} = \frac{\Delta}{r} \cdot \frac{1}{17.5} \left[\frac{\delta_o}{\Delta} - 1 \right] \qquad R.8$$

and since $\frac{KW'}{r} = \frac{K\rho_o'}{r} \cdot \frac{W'}{\rho_o'}$, $\qquad R.10$

$$\frac{KW'}{r} = \frac{W'}{\rho_o'} \cdot \frac{\Delta}{r} \cdot \frac{1}{17.5} \left[\frac{\delta_o}{\Delta} - 1 \right] \qquad R.11$$

the quantities contained in equation (R.8) must be evaluated for each test bearing considered.

For bearing NU310,

$$z = 12 \ , \ \lambda = 30^\circ \ , \ n = \text{Int}\left[\frac{z-1}{4}\right] = 2 \qquad R.12$$

$$r = 7.5011 \text{ mm} \ , \ \Delta = \frac{0.0312}{2} \text{ mm} \quad \text{(see Appendix B)}$$

giving

$$\frac{K\rho_o'}{r} = 0.119 \times 10^{-3} \left[\frac{\delta_o}{\Delta} - 1 \right] \qquad R.13$$

Similarly for bearing N310,

$$z = 12 \ , \ \lambda = 30^\circ \ , \ n = 2 \qquad R.14$$

$$r = 7.5008 \text{ mm}, \ \Delta = \frac{0.0159}{2} \text{ mm} \quad \text{(see Appendix B)}$$

giving

$$\frac{Kp_0'}{r} = 0.0606 \times 10^{-3}\left[\frac{\delta_0}{\Delta} - 1\right] \qquad (R.15)$$

Equation (R.3) is used to evaluate W'/p_0' at important values of the ratio δ_0/Δ.

For bearing NU310

$\delta_0/\Delta = 1$, first roller touches [for $\frac{\delta_0}{\Delta} < 1$, no rollers in contact]

$$\frac{KW'}{r} = \frac{Kp_0'}{r} \cdot \frac{W'}{p_0'}$$

and equation (R.3) gives $W'/p_0' = 1$

$$\frac{KW'}{r} = 0.119 \times 10^{-3}\left[\frac{\delta_0}{\Delta} - 1\right] \times 1$$

but $\delta_0/\Delta = 1$ so $\frac{KW'}{r} = 0$ as expected

$\delta_0/\Delta = 1.115$ given by $\frac{\delta_0}{\Delta}\cos\lambda = 1$ defines the value at which two more rollers touch. Equation (R.3) again gives that $W'/p_0' = 1$ equation (R.11) giving

$$\frac{KW'}{r} = 0.0137 \times 10^{-3}$$

$\delta_0/\Delta = 2.00$ given by $\frac{\delta_0}{\Delta}\cos 2\lambda = 1$ defines the value at which two more rollers touch. Equation (R.3) gives $W'/p_0' = 2.265$, equation (R.11) giving

$$\frac{KW'}{r} = 0.27 \times 10^{-3}$$

A similar procedure for bearing N310 provides corresponding values for the limits of KW'/r at which various rollers come into contact.

This can be summarised as follows:

δ_o/Δ	KW'/r for NU310	KW'/r for N310	
0	0	0	No Rollers in Contact
1	0	0	1 Roller in Contact
1.115	0.0137×10^{-3}	0.00697×10^{-3}	3 Rollers in Contact
2.00	0.27×10^{-3}	0.137×10^{-3}	5 Rollers in Contact

The applied bearing loads at each of the above limits can be easily evaluated. Assuming that $E = 206\times10^{9}\ N/m^2$ and $\nu = 0.28$ for the bearing material, the elastic constant K have a value of $0.284\times10^{-11}\ m^2/N$. The roller length for the test bearings is equal to the diameter of the roller so

$$W' = W/2r \qquad \text{R.16}$$

and

$$W = \frac{2r^2}{K}\cdot\frac{KW'}{r} \qquad \text{R.17}$$

Equation (R17) allows values of total bearing load to be evaluated for the limiting values of KW'/r given in the previous table.

This can be summarised as follows:

	NU310 $\left(\frac{\Delta}{r} = 2.08 \times 10^{-3}\right)$	N310 $\left(\frac{\Delta}{r} = 1.06 \times 10^{-3}\right)$
1 roller in contact up to total bearing load of:	0.543 kN	0.276 kN
3 rollers in contact up to total bearing load of:	10.7 kN	5.43 kN

5 rollers in contact above these figures.

It will be appreciated that for loads where it is stated that only a single roller is in contact, this will probably not be the case in practice. A second roller, possibly carrying very little load, will also be in contact.

APPENDIX (S)

An alternative analysis to give the variation in test bearing friction torque due to the rolling traction at the outer race/roller contacts

From figure S.1 it will be seen that the variation in roller load has only a moderate effect on the physical geometry at the inlet region to the contact. This alternative analysis assumes that the variation in film inlet point with load can be considered as negligible when compared with variations due to other effects and so assumes that the film inlet points for all rollers in the assembly can simply be described as occuring at a given, and constant, value of x (the distance from the centre-line of the contact), independant of the rollers position in the assembly.

In figure S.2 the roller and race films on the inlet side of the contacts join at the points A and B. Lauder (24), considering this conjunction, suggests that the pressure build-up in the lubricant starts at this point. This is, in this analysis, described in terms of the roller radius and a factor n, as shown in the figure. It follows that the factor n cannot be greater than unity because, of course, Reynolds equation is not applicable for $x > r$. The analysis can therefore be considered as applying to adequate, but not excess, lubrication.

Figure S3 shows the equivalent cylinder system for the contact shown in figure S.2 and it is well

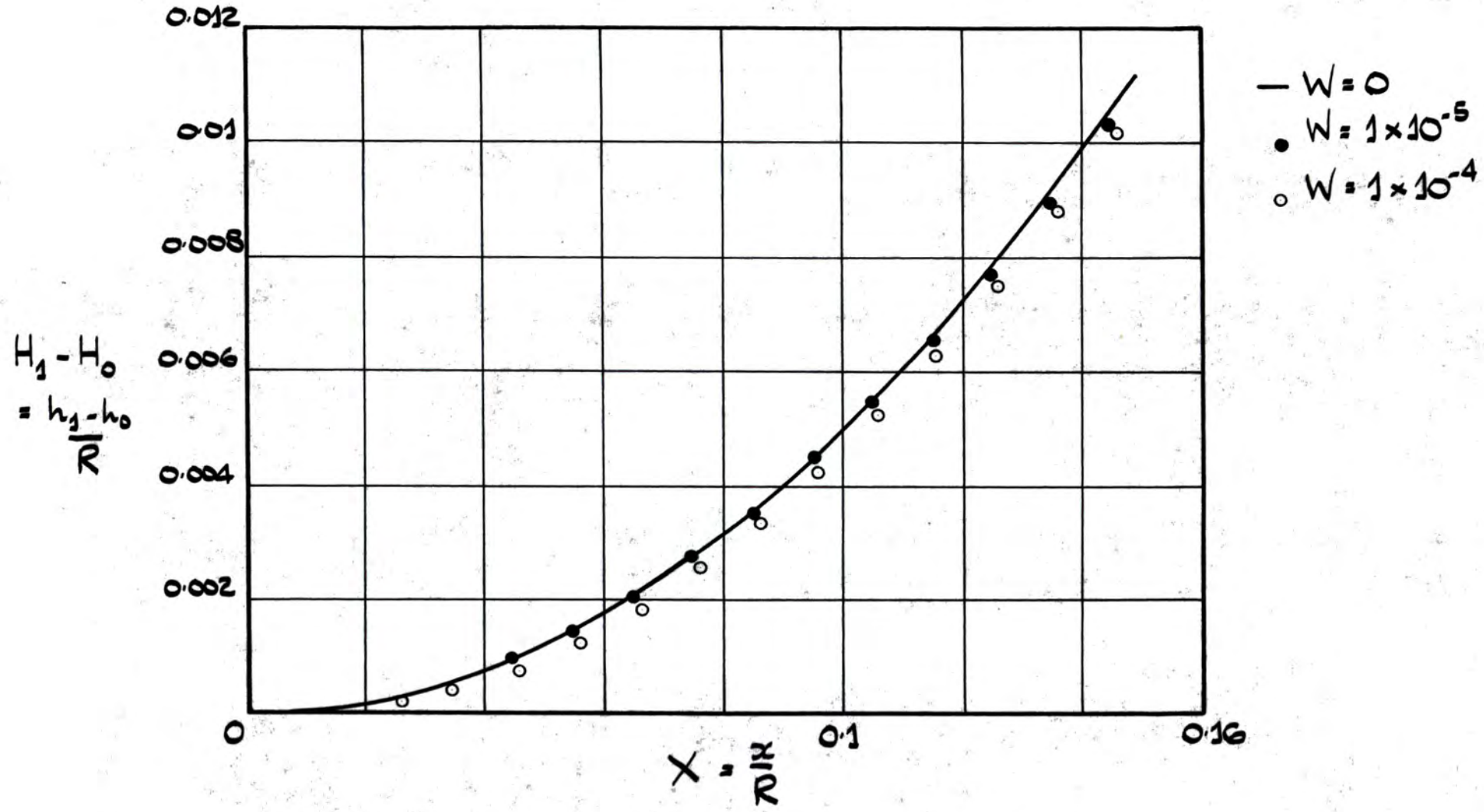

FIGURE 8.1 . VARIATION OF INLET FILM PROFILE WITH LOAD

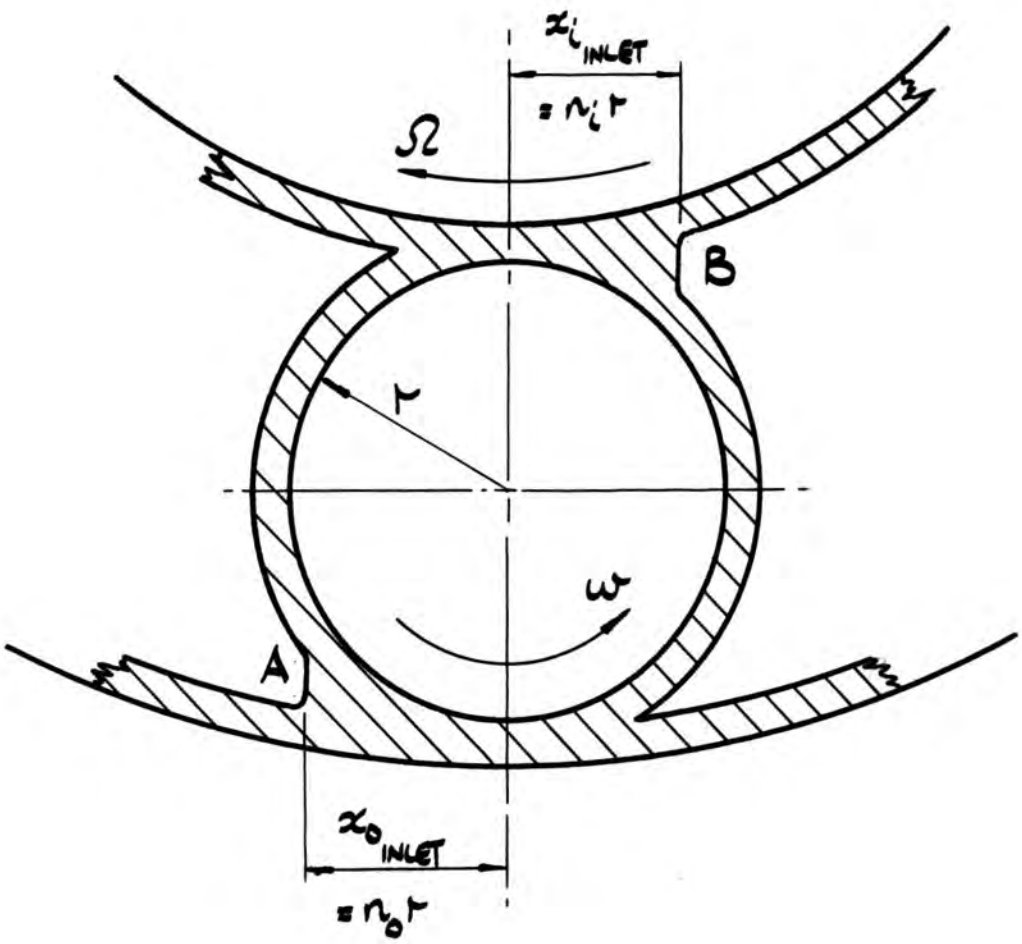

FIGURE 5.2. SINGLE LUBRICATED ROLLER SHOWING THE ASSUMPTION $x_{INLET} = n.r$

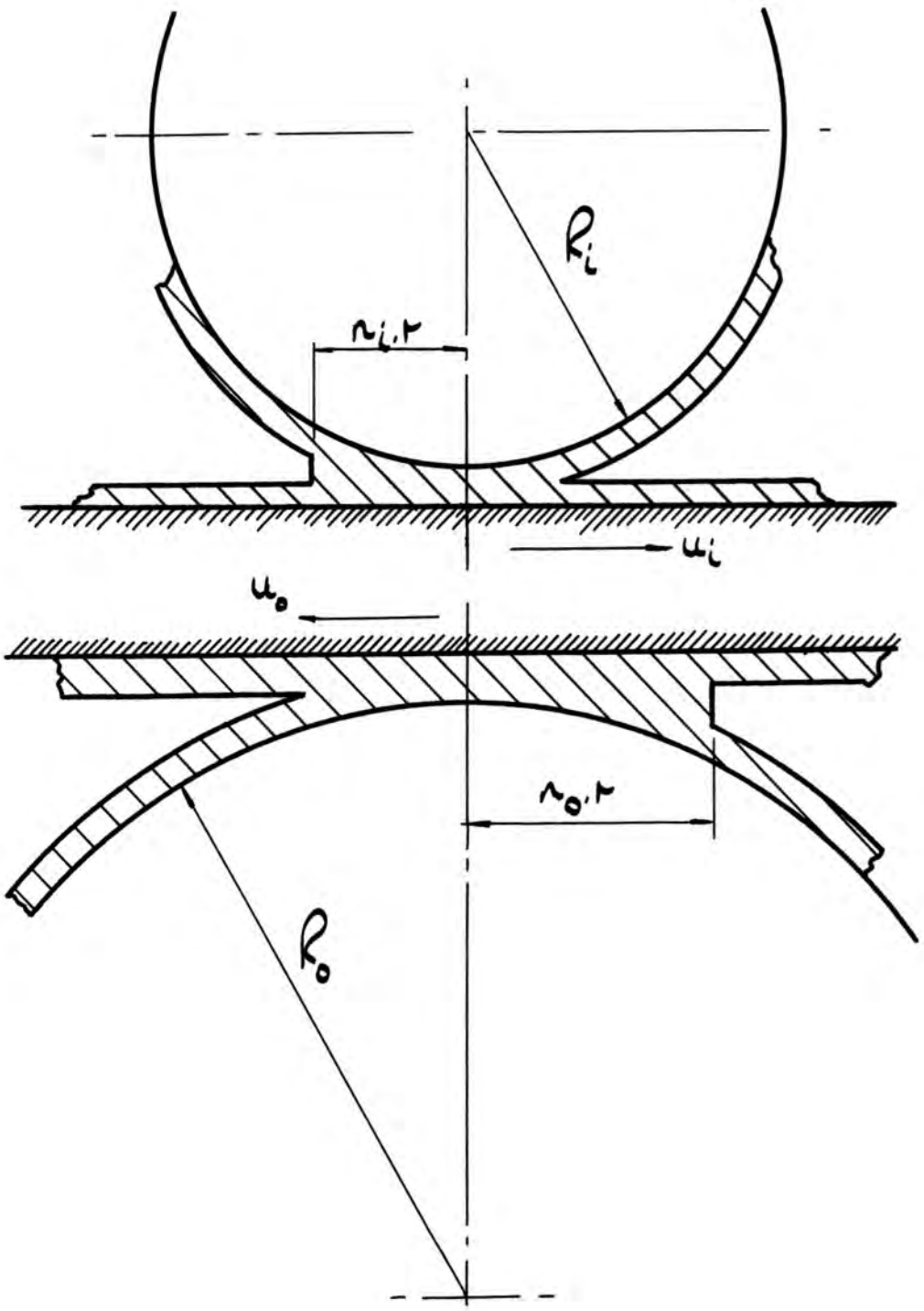

FIGURE 5.3 . EQUIVALENT CYLINDER SYSTEM.

known that

$$R_i = \frac{r}{(1+s)} \; ; \; R_o = r\frac{(1+2s)}{(1+s)} \quad \text{where } s = \frac{r}{R} \tag{5.1}$$

and

$$u = u_i = u_o = \frac{R\Omega(1+2s)}{2(1+s)} \tag{5.2}$$

Considering only the outer contact, the non-dimensional speed U, defined in equation (3.13), is given by

$$U = \frac{u\eta_o(1+s)}{E'r(1+2s)} \tag{5.3}$$

and the non-dimensional film inlet point X_{INLET}

$$X_{INLET} = \frac{n_o(1+s)}{4(1+2s)}\sqrt{\frac{2\pi}{W}} \tag{5.4}$$

, W being defined in equation (3.13). Using the definitions of S and $\bar{S}$ equations (3.17) and (3.19), it follows that

$$\bar{S}_{INLET} = \frac{n_o(1+s)\,W^{1/4}\sqrt{2\pi}}{4(1+2s)(GU)^{1/4}} - \frac{W^{3/4}}{(GU)^{1/2}} \tag{5.5}$$

Writing $\bar{S}_\theta$ as the value of $\bar{S}_{INLET}$ for a roller at angle θ and $\bar{S}_1$ for a roller on the line of action of the load, and noting

$$W_\theta = W_1 \cos\theta \tag{5.6}$$

it can be shown that, to a good approximation,

$$\phi = \frac{\bar{S}_\theta}{\bar{S}_1} = (\cos\theta)^{1/4} \tag{5.7}$$

where ϕ is the inlet parameter ratio. This equation is illustrated in figure 5.4 . Computer analysis of the variation in $\bar{S}$ with angle θ for the inlet condition x_i = constant shows that this equation is closely

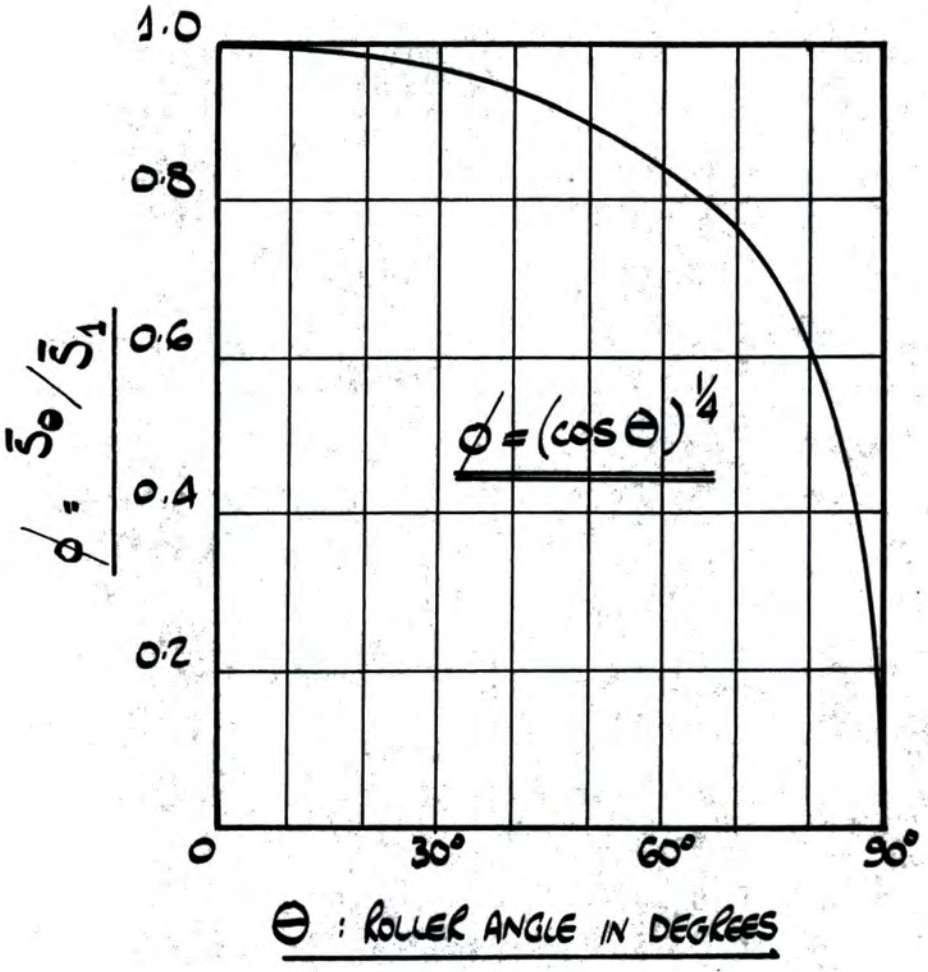

FIGURE 8.4. VARIATION IN INLET PARAMETER RATIO ϕ WITH ROLLER ANGLE θ

followed. Unlike the comparable equation (3.41) for the inlet condition h_i = constant, the inlet parameter ratio in this analysis cannot be considered as unity.

The implications of figure 5.4 are that, as a roller passes from the point of maximum load into the unloaded region, the value of $\bar{S}_{INLET}$ is continuously reduced until at the point of $\theta = 90^{\circ}$, the value is zero. Because of the initial assumption in this analysis, this change takes place without an alteration in the physical inlet point. The analysis therefore suggest- that even a fully lubricated roller (n = 1) at the point of maximum load would be subjected to, effectively, complete lubricant starvation as it passes into the unloaded portion of the bearing assembly.

Further, it follows from figure 15 that a rollers contribution to the total rolling traction will also be continuously reduced from its full value to zero as the roller passes into the unloaded region and also from figure 6 , the effective film thick- ness will also be reduced to zero. The rollers in the unloaded region will therefore be merely floating, and no hydrodynamic lubrication will occur.

The foregoing statements are of course based on the purely theoretical observations contained in this alternative analysis and require some qualification. Further consideration is contained in the general discussion in the body of the work.

Continuing the alternative analysis, figures 6 and 15 show that the variation in film thickness

ratio ρ and rolling traction ratio ψ with inlet parameter $\bar{S}_x$ are of the form:

$$y = \frac{ax^b}{1 + ax^b} \qquad S.8$$

and empirical relationships of this form have been developed to describe each of these curves.

Figure 6 can be adequately represented by

$$\rho = \frac{H_{ox}}{H_{o\infty}} = \frac{(3\bar{S}_x^3)^{1/2}}{1 + (3\bar{S}_x^3)^{1/2}} \qquad S.9$$

for $\bar{S}_x > 1$ this relationship having an error of less than 5% within the valid range. Similarly, figure 15 can be adequately represented by

$$\psi = \frac{Tr_x}{Tr_\infty} = \frac{0.2\,\bar{S}_x^{\pi-2}}{1 + 0.2\,\bar{S}_x^{\pi-2}} \qquad S.10$$

for $\bar{S}_x > 1$ this relationship having an error of less than 3% within the valid range.

Equation (S.7) indicates that the film inlet parameter $\bar{S}_\theta$ for any roller can simply be determined from both the rollers position in the assembly and to $\bar{S}_1$ the film inlet parameter for the most heavily loaded roller. From figure 16 therefore,

$$\begin{aligned} &\text{for roller 1} && \bar{S}_\theta = \bar{S}_1 \\ &\text{for rollers 2} && \bar{S}_\theta = \bar{S}_1 (\cos\lambda)^{1/4} \\ &\text{for rollers 3} && \bar{S}_\theta = \bar{S}_1 (\cos 2\lambda)^{1/4} \\ &\text{for rollers } (n+1) && \bar{S}_\theta = \bar{S}_1 (\cos n\lambda)^{1/4} \end{aligned} \qquad S.11$$

where, after Dowson and Higginson (14),

$$\lambda = \frac{2\pi}{z} \quad ; \quad n = \text{Int}\left[\frac{z-1}{4}\right] \qquad S.12$$

Using equation (S.10), the rolling traction contribution

of each roller can therefore be determined.

Referring again to figure 16 and using equations (S.10) and (S.11) for roller 1

$$T_{R_{x_1}} = T_{R_{\infty_1}} \times \frac{0.2\,(\bar{S}_1)^{\pi-2}}{1 + 0.2\,(\bar{S}_1)^{\pi-2}}$$

for rollers 2

$$T_{R_{x_2}} = 2 \times T_{R_{\infty_2}} \times \frac{0.2\,(\bar{S}_1)^{\pi-2}(\cos\lambda)^{\frac{\pi-2}{4}}}{1 + 0.2\,(\bar{S}_1)^{\pi-2}(\cos\lambda)^{\frac{\pi-2}{4}}} \qquad S.13$$

for roller (n + 1)

$$T_{R_{x_{(n+1)}}} = 2 \times T_{R_{\infty_{(n+1)}}} \times \frac{0.2\,(\bar{S}_1)^{\pi-2}(\cos n\lambda)^{\frac{\pi-2}{4}}}{1 + 0.2\,(\bar{S}_1)^{\pi-2}(\cos n\lambda)^{\frac{\pi-2}{4}}}$$

The total non-dimensional rolling traction is given by the sum of the above equations and so it follows that a total rolling traction ratio, defined as

$$\epsilon = \frac{T_{R_{x\,TOTAL}}}{T_{R_\infty}} \qquad S.14$$

is given by

$$\epsilon = 0.2\,(\bar{S}_1)^{\pi-2}\left[\frac{1}{1 + 0.2\,(\bar{S}_1)^{\pi-2}} + \frac{2\,(\cos\lambda)^{\frac{\pi-2}{4}}}{1 + 0.2\,(\bar{S}_1)^{\pi-2}(\cos\lambda)^{\frac{\pi-2}{4}}} + \cdots + \frac{2\,(\cos n\lambda)^{\frac{\pi-2}{4}}}{1 + 0.2\,(\bar{S}_1)^{\pi-2}(\cos n\lambda)^{\frac{\pi-2}{4}}}\right] \qquad S.15$$

where, as shown in Appendix (T), T_{R_∞} is effectively constant for all the rollers in the assembly.

Equation (S.14) allows the total non-dimensional rolling traction for a starved assembly, $T_{R_{x\,TOTAL}}$, to be evaluated from knowledge of the non-dimensional rolling traction for a single contact under flooded

conditions, Tr_{∞} and the inlet parameter $\bar{S}_1$ for the most heavily loaded roller.

The program shown in figure S.5 determines the value of the total rolling traction ratio ϵ for values of z from 5 to 20 and for values of $\bar{S}_1$ up to 100. Specimen results are shown in graphical form in figure S.6.

Garnell and Higginson (21) have evaluated the non-dimensional rolling traction Tr_{∞} at a fully flooded contact and noted that the rolling traction was virtually independant of load within the range $W = 3 \times 10^{-6}$ to $W = 3 \times 10^{-4}$, values typical of moderately and heavily loaded steel contacts. With this knowledge they evaluated the total rolling traction for the assembly by simply multiplying the rolling traction for a single roller by the number of rollers known to be in contact, the procedure used in the analysis contained in Section 3 of this present work. Figure S.6 , produced by the alternative analysis contained in this Appendix, does suggest that this cannot be considered as valid, since this will over-estimate the friction torque developed. For instance, at $\bar{S}_1 = 20$ when, from figure 6 , the lubricant film for the most heavily loaded roller is at its fully flooded value and, from figure 15 , the rolling traction for this roller is also at its flooded value, the total rolling traction ratio is still less than the number of rollers known to be in contact within the loaded region.

```
    MASTER RAH7
    EVAL,OF ASSEMBLY ROLLING TRACTION RATIO,
    REAL LA,LB,SBAR(50),R1(50),R2(50),R3(50),R4(50),A
    A=((1,14159)/(4,0))
    DO 20, K =5,20,1
    N= (K-1)/4
    LA=((2,0*3,14159)/ (K))
    LB=((360,0)/(K))
    WRITE(1,10) K,LB
10  FORMAT (20X,14HNO,OF ROLLERS=,I8  /,20X,20HROLLER ANGLE LAMBDA=,F1
   13,5,8HDEGREES,///)
    DO 30, L=1,50,1
    SBAR(L) =(L**1,14159)
      R3(L)=0,00000000
    IF(N,GT,1) GOTO 35
       R3(L)=(COS(LA)**A)
      R3(L)=2,0*(R3(L))/(1,0+(0,2*SBAR(L)*(R3(L))))
      R3(L)=R3(L)+((1,0)/(1,0+(0,2*(SBAR(L)))))
    GOTO 45
35  DO 40, J=1,N,1
    R1(J)=(COS(J*LA))**A
      R2(J)=2,0*(R1(J))/(1,0+(0,2*SBAR(L)*(R1(J))))
      R3(L)=R3(L)+R2(J)
40  CONTINUE
      R3(L)=R3(L)+((1,0)/(1,0+(0,2*(SBAR(L)))))
45    R4(L)=R3(L)*(0,2*(SBAR(L)))
30  CONTINUE
    DO50, L=1,50,1
    WRITE(1,70)  L,R4(L)
70  FORMAT(20X,I8,5X,F15,5/)
50  CONTINUE
20  CONTINUE
    STOP
    END
```

FIGURE S·5 PROGRAM FOR THE EVALUATION OF THE ASSEMBLY ROLLING TRACTION RATIO ϵ

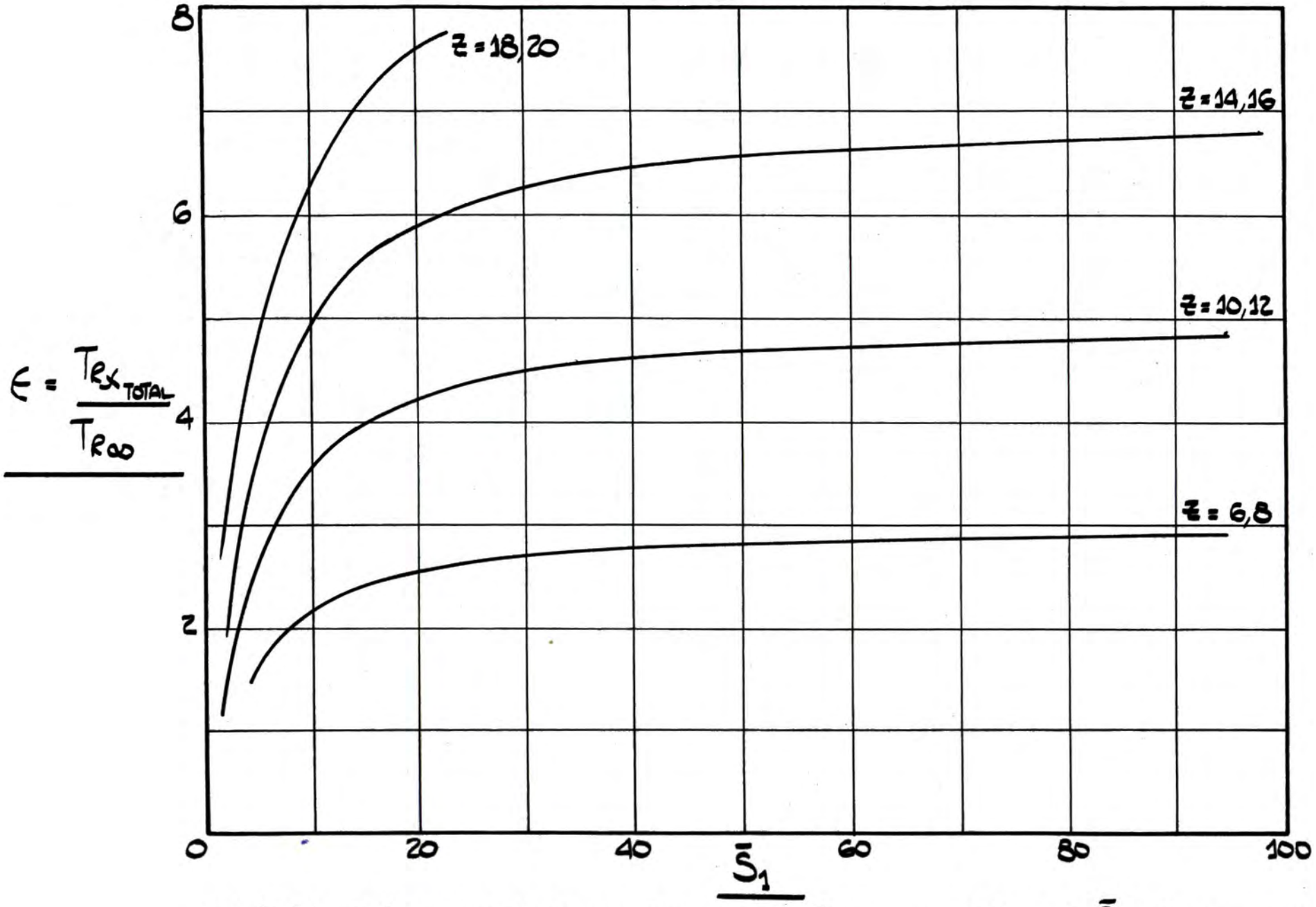

FIGURE 5.6 . VARIATION IN TOTAL ROLLING TRACTION RATIO ϵ WITH INLET PARAMETER $\bar{S}_1$ FOR THE MOST HEAVILY LOADED ROLLER.

The program shown in figure S.7 uses the alternative analysis contained in this Appendix to evaluate the test bearing friction torque due to the rolling traction at the outer race/roller contacts and the variation of this quantity with γ_N is shown in figures S.8, S.9, and S.10 for the test loads and for various values of the starvation factor 'n'.

```
      MASTER RAH9
      EVAL,OF VARIATION IN TOTAL OUTER RACE/ROLLER FRICTION TORQUE WITH
      ETA N FOR TEST BEARINGS NU310 AND N310 USING INLET CONDITION X=X1
      = CONSTANT
      REAL Q(3),W(3),EN(40),HOINF(40),SBAR(40),S(40),Y,S3(500),T13(500),
     1GQ(500),GP(500),P(500),DH(500),PDH(500),TRA,TRB,TRC,TR(40),A,D1,D2
     2,D3,D4,F1,B(10),C(10),H(10),R1,R2,R3(10),R4(10),R5(10),R6(10),R7(1
     30),R8(10),G,U(40)
      INTEGER N,V,K,J,M,F,R
      DIMENSION R8FK(3,10,40),CFK(3,10,40),ESBAR(3,10),EEN(3,10)
      READ(6,1) (Q(V),V=1,3,1)
    1 FORMAT(3G8.1)
      N=100
      G = 5000.
      D1=1.251
      D2=5.848
      A=((1.14159)/(4.0))
      R1=(((3.0**0.5)/2.0)**A)
      R2=(0.5**A)
      DO 5 V = 1,3,1
      W(V)=Q(V)*1.085E-5
      DO 20 K=1,8,1
      EN(K) =500.0*K
      EEN(V,K) = EN(K)
      U(K)=EN(K)*0.985E-15
      SBAR(K) = 100.0
      S(K)=SBAR(K)*(((G*U(K))**0.5)/(1.059*(W(V)**0.75)))
      ESBAR(V,K) = SBAR(K)
      HOINF(K)=2.2049*((G*U(K))**0.75)/(W(V)**0.125)
      Y = S(K)/(N-1)
      S3(1)=S(K)
      S3(N)=1E-10
      DO40 J = 2,(N-1),1
      S3(J)=S(K)-((J-1)*Y)
   40 CONTINUE
      DO 50 M = 1,N,1
      T = S3(M)*(((2.40084*W(V))/HOINF(K))**(2/3.0))
      T2=T**0.5
      T3=T**1.5
      T4=(T*((2*T3)-1))/(9*((1+T3)**2))
      T5=0.5*ALOG(((1+T2)**2)/(1+T-T2))
      T6=(3**0.5)*ATAN((2-T2)/((3**0.5)*T2))
      T7=T5+T6
      T8=T7*2/27.0
      T15=T4-T8
      T13(M)=T15
      GQ(M) = (0.0671777342-T13(M))/0.2687110169
      GP(M)=-(ALOG(1-GQ(M)))
```

FIGURE S-7, SHEET 1. PROGRAM FOR THE EVALUATION OF THE TOTAL TEST BEARING FRICTION TORQUE DUE TO THE ROLLING CONTACTS.

```
      P(M)=((GP(M))/G)
      DH(M)=5.6013*W(V)*(S3(M)**0.5)
      PDH(M)=P(M)*DH(M)
   50 CONTINUE
      TRA=PDH(1)/2.0
      TRB=PDH(N)/2.0
      TRC=0.0000000000
      DO60 R = 2,(N-1),1
      TRC=TRC+PDH(R)
   60 CONTINUE
      TR(K)=(TRA+TRB+TRC)*(Y*0.5)
      D3=(W(V)**0.75)/((G*U(K))**0.5)
      D4=((6.28318/W(V))**0.5)
      DO70 F=5,10,1
      F1=0.01*F
      B(F)=(((F1*D1*D4)/D2)-1.0)
      C(F)=1.059*D5*B(F)
      H(F)=(C(F)**1.14159)
      R3(F)=(2.0*R2)/(1.0+(0.2*H(F)*R2))
      R4(F)=(2.0*R1)/(1.0+(0.2*H(F)*R1))
      R5(F)=1.0/(1.0+(0.2*H(F)))
      IF(V.EQ.1) GOTO 63
      GOTO 64
   63 R6(F) = R4(F) + R5(F)
      GOTO 66
   64 R6(F) = R3(F) +R4(F) +R5(F)
   66 R6(F) = R6(F) * 0.2 * H(F)
      R7(F)=R6(F)*TR(K)
      R8(F)=R7(F)*1.46E6
      R8FK(V,F,K) = R8(F)
      CFK(V,F,K) = C(F)
   70 CONTINUE
   20 CONTINUE
    5 CONTINUE
      DO80 V = 1,5,1
      DO85 F=5,10,1
      F1=0.01*F
      WRITE(1,86)Q(V),G,F1
   86 FORMAT(10X,15HBEARING LOAD=,F5.1,3HKN./,21X,2HG=,F7.1/,9X,14HINLET
     1 POINT N=,F5.3,16HX ROLLER RADIUS,/,4X,65HETA N (POISE*RPM)  SBAR
     2 INF.   SBAR INLET FRICTION TORQUE (N.M.)///)
      DO90 K=1,8,1
      WRITE(1,91) EEN(V,K),ESBAR(V,K),CFK(V,F,K),R8FK(V,F,K)
   91 FORMAT(7X,F7.1,8X,E15.5,1X,E15.5,4X,E13.5//)
   90 CONTINUE
   85 CONTINUE
   80 CONTINUE
      STOP
      END
```

FIGURE S·7, SHEET 2.

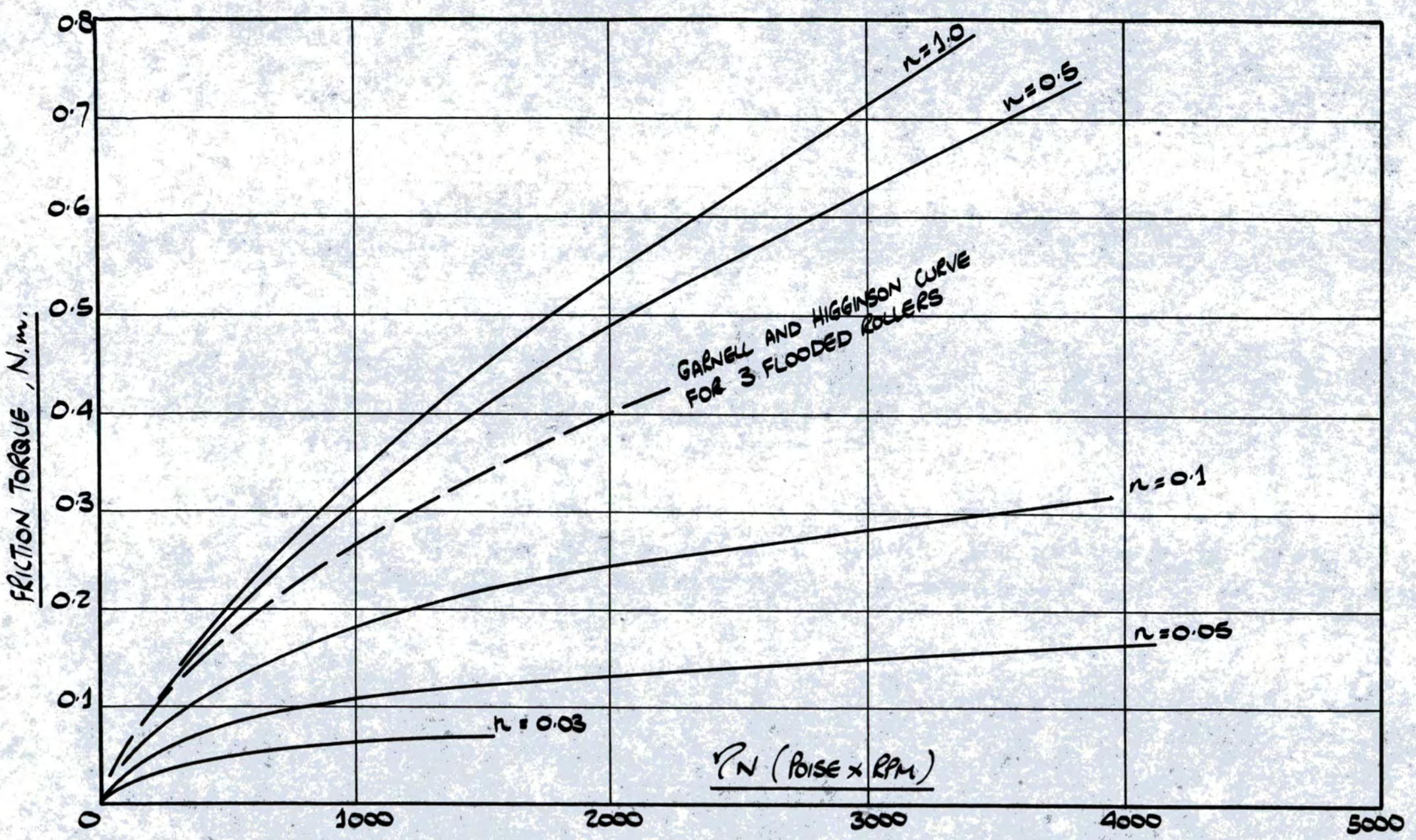

FIGURE 5.8. THEORETICAL TOTAL ROLLING FRICTION CURVES FOR THE TEST BEARINGS, SHOWING THE EFFECT OF LUBRICANT STARVATION. BEARING LOAD 1 kN, 3 ROLLERS IN CONTACT.

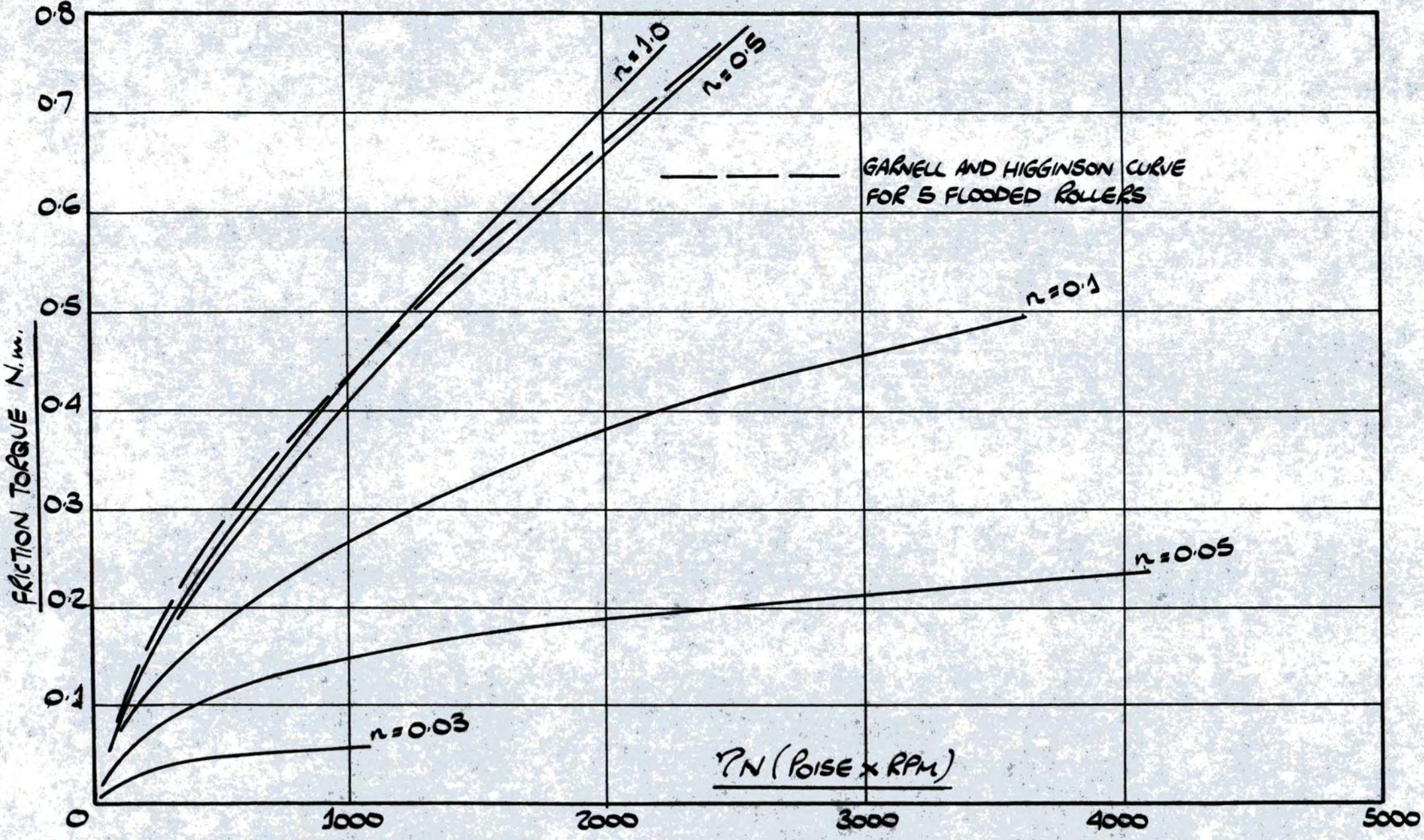

FIGURE 5·9 . THEORETICAL TOTAL ROLLING FRICTION CURVES FOR THE TEST BEARINGS, SHOWING THE EFFECT OF LUBRICANT STARVATION BEARING LOAD 10 kN, 5 ROLLERS IN CONTACT.

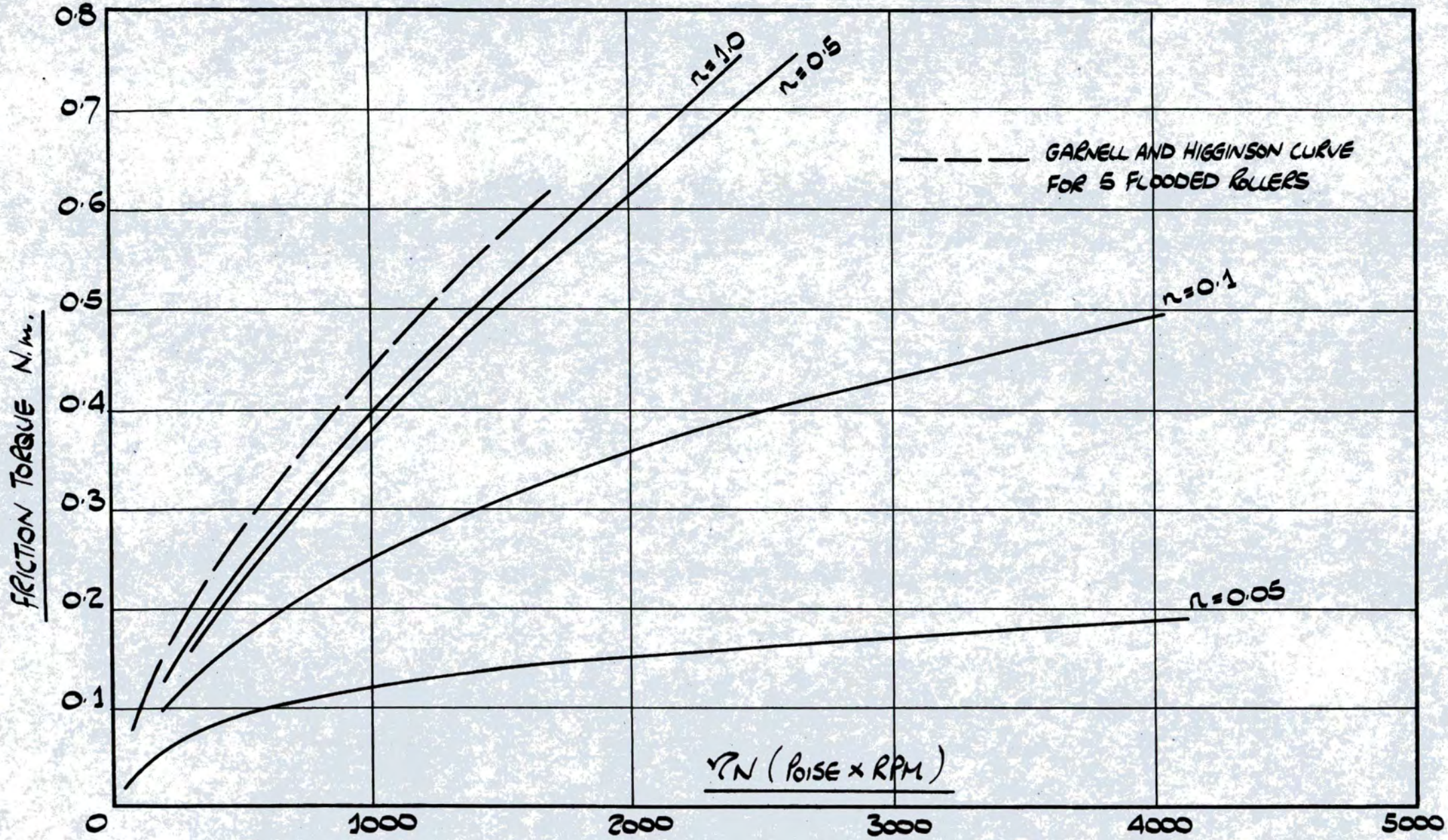

FIGURE 5.10. THEORETICAL TOTAL ROLLING FRICTION CURVES FOR THE TEST BEARINGS, SHOWING THE EFFECT OF LUBRICANT STARVATION BEARING LOAD 20 kN, 5 ROLLERS IN CONTACT

APPENDIX (T)

To determine the relationship between the infinite rolling traction $T_{R\infty}$ for the most heavily loaded roller and the value of $T_{R\infty}$ for the other rollers in the assembly: in short, the variation of $T_{R\infty}$ with angle θ

Equation (S.14) takes

$$T_{R\infty 1} = T_{R\infty 2} = \ldots T_{R\infty (n+1)}$$

and this assumption of $T_{R\infty}$ constant with roller position has been used in the analysis contained in section 3 and also that in Appendix (S).

In any inlet film, the reduced pressure at any point in the film is given by equation (3.2.3) to be

$$GQ_s = \frac{I_{s=s} - I_s}{I_{s=s} - I_0} \qquad T.1$$

and for an inlet point $s = \infty$

$$GQ_s = \frac{I_{s=\infty} - I_s}{I_{s=\infty} - I_0} \qquad T.2$$

$I_{s=\infty}$ and $I_{s=0}$ are constant and therefore GQ_s is a function of $(\bar{\tau})_s$, since $I_s = f^n(\bar{\tau})_s$

Equation (3.1.3) gives

$$P_s = \frac{1}{G}\left(\ln.(1 - GQ_s)\right) \qquad T.3$$

and therefore

$$P_s = \frac{1}{G} f^n(\bar{\tau})_s \qquad T.4$$

From equation (3.113)

$$S = \tau_s \left(\frac{H_{0x}}{2.4W} \right)^{2/3} \qquad T.5$$

and for the particular case of $S = x = \infty$,

$$H_{0x} = H_{0\infty} = \frac{2.2\,(GU)^{3/4}}{W^{1/8}} \qquad T.6$$

giving

$$S = \frac{\tau_s\,(GU)^{1/2}}{1.059\,W^{3/4}} \qquad T.7$$

It will be noted from the definition of $\bar{S}$, (equation (3.139)),

$$\bar{S} = 1.059\,\frac{W^{3/4}}{(GU)^{1/2}} \cdot S \qquad T.8$$

that, for the particular case under consideration,

$$\bar{S} = \tau_s \qquad T.9$$

From equation (T.7) above, it follows that

$$dS = \frac{(GU)^{1/2}}{W^{3/4}} \cdot d\tau_s \qquad T.10$$

neglecting the factor 1.059.

Also, from the equation (3.110),

$$\frac{dH_s}{dS} = 3.6\,W S^{1/2} \qquad T.11$$

giving

$$\frac{dH_s}{dS} = 3.6\,W^{5/8}\,(GU)^{1/4} \cdot (\tau)_s^{1/2} \qquad T.12$$

From the definition of T_e given in equation (3.9)

it follows that

$$T_{R_\infty} = \frac{1}{2} \int_{S=\infty}^{0} P \cdot \frac{dH_s}{dS} \cdot dS \qquad T\cdot13$$

giving

$$T_{R_\infty} = 1.8 \frac{U^{3/4}}{G^{1/4} \cdot W^{1/8}} \cdot f^{\prime\prime}(\tau)_{s=\infty} \qquad T\cdot14$$

Referring to figure 16 ; for the most heavily loaded roller the above equation becomes

$$T_{R_{\infty_1}} = 1.8 \frac{U^{3/4}}{G^{1/4} W_1^{1/8}} f^{\prime\prime}(\tau)_{s_1=\infty} \qquad T\cdot15$$

and for a roller at angle θ,

$$T_{R_{\infty_\theta}} = 1.8 \frac{U^{3/4}}{G^{1/4} W_\theta^{1/8}} \cdot f^{\prime\prime}(\tau)_{s_\theta=\infty} \qquad T\cdot16$$

Equation (5.6) gives

$$W_\theta = \frac{2P \cos\theta}{\pi E' R_{eq}} \qquad T\cdot17$$

where $2P/\pi E' R_{eq} = W_1$, the non-dimensional load on the most heavily loaded roller. So $W_\theta = W_1 \cos\theta$.

An infinite rolling traction ratio μ can be defined as

$$\mu = \frac{T_{R_{\infty_\theta}}}{T_{R_{\infty_1}}} \qquad T\cdot18$$

and using equations (T.14), (T.17) and (T.18) it follows that

$$\mu = \frac{W_1^{1/8}}{(W_1 \cos\theta)^{1/8}} \cdot \frac{f^{\prime\prime}(\tau)_{s_1=\infty}}{f^{\prime\prime}(\tau)_{s_\theta=\infty}} \qquad T\cdot19$$

and of course $$(\tau)_{S_1=\infty} = (\tau)_{S_\theta=\infty} \qquad T\cdot20$$

giving

$$\mu = \frac{1}{(\cos\theta)^{1/8}} \qquad T\cdot21$$

Figure T·1 shows the variation in the infinite rolling traction ratio μ with angle θ.

It will be seen from figure T·1 that the value of the infinite rolling traction ratio μ is essentially unity for values of θ up to about 60°. At higher values of θ the ratio becomes rapidly larger, but it will be appreciated that the equations on which the foregoing analysis is based have been derived for conditions of EHD lubrication. This implies that the equations are not valid for light loads.

It is therefore suggested that equation (T·21) should be restricted to the region of higher load in the assembly and, from figure T·1 that the infinite rolling traction ratio μ can be sensibly taken as unity within this higher load region.

The variation of T_{R_∞} with angle θ shown in figure T·1 raises the interesting deduction that, as the load is reduced, the value of T_{R_∞} increases. This result is however in keeping with the findings of Crook (9) who deduced that

$$T_R \propto \frac{H^*}{\alpha} \qquad T\cdot22$$

where α is the pressure viscosity exponent of the lubricant and H^* is the non-dimensional minimum film

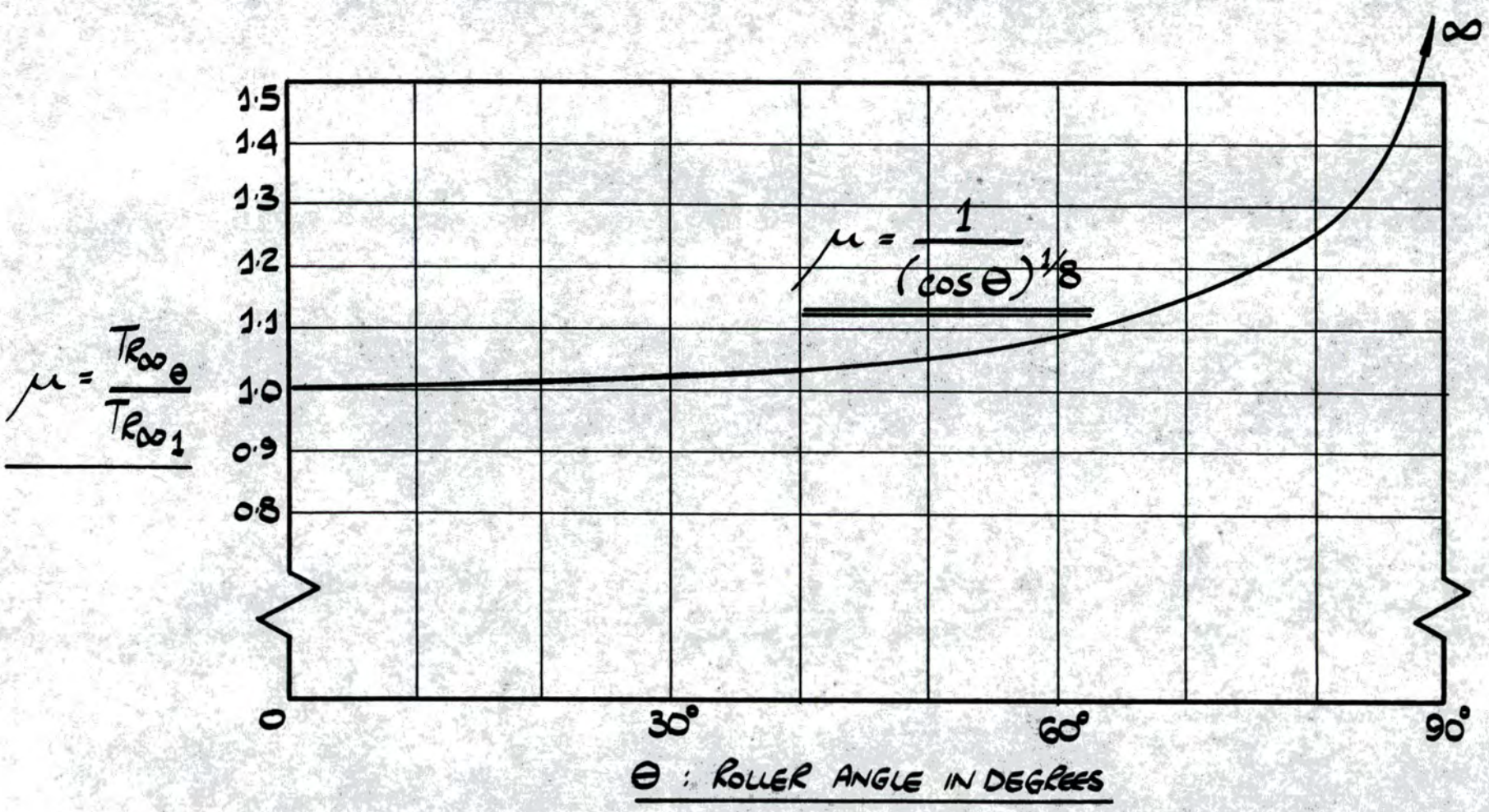

FIGURE T·1 . VARIATION OF THE INFINITE ROLLING TRACTION RATIO μ WITH ROLLER ANGLE θ.

thickness. The value of α is effectively constant for a given lubricant and for the case of a flooded contact

$$H_{0\infty} = 2.2049 \frac{(GU)^{3/4}}{W^{1/8}} \qquad T\cdot23$$

indicating that

$$T_R \propto \frac{1}{W^{1/8}} \qquad T\cdot24$$

Equation (T.23) is therefore in keeping with the findings of Crook but, as stated previously, the infinite rolling traction ratio is effectively unity for EHD conditions.

TRIBOLOGY GROUP

IE STARVED LUBRICATION OF CYLINDERS IN LINE CONTACT

. E. Wolveridge, BSc, PhD* K. P. Baglin† J. F. Archard, BSc, PhD, CEng, FIMechE†

A semi-analytical solution is presented showing the effect of variations in the position of the inlet boundary of the lubricant film upon the load capacity of cylinders in line contact. Firstly, isoviscous conditions and undeformed surfaces are assumed; by the use of appropriate non-dimensional parameters, the results of the theory can be exhibited as a single function applicable to all possible experimental conditions. This can then be transformed to deduce a similar unique expression showing the proportional reduction in the minimum film thickness for variations in the position of the inlet boundary, all other conditions being maintained constant. A similar analytical solution is presented showing the effect of the position of the inlet boundary upon the film thickness under heavy loads. This assumes full elastohydrodynamic conditions and is based upon an analysis similar to the familiar theoretical treatment of Grubin.

Comparisons show that published computer solutions of these problems, for specific sets of conditions, are in good agreement with the more general analytical solutions presented here.

NOTATION

ols used only once are defined at the appropriate in the text.

$\left[\frac{4\sqrt{2}}{3}\right]^{2/3}$.

$b/\sqrt{2Rh^*}$.

Width of Hertzian band of contact.

Film thickness.

Minimum film thickness (classical theory).

Pressure.

Reduced pressure $\left[=\frac{1}{\alpha}(1-e^{-\alpha p})\right]$.

Relative radius of curvature $\left(\frac{1}{R}=\frac{1}{R_1}+\frac{1}{R_2}\right)$.

$_2$ Radii of curvature.

$_2$ Surface velocities.

Rolling speed $[=\frac{1}{2}(U_1+U_2)]$.

Load per unit length of cylinder.

Non-dimensional co-ordinate $[=x/\sqrt{2Rh_0}$, or $=x/\sqrt{2Rh^*}]$.

$x_i/\sqrt{2Rh_0}$ (equation (12a)).

$x_i/\sqrt{2R(h_0)_\infty}$ (equation (11b)).

Co-ordinate.

α Pressure coefficient of viscosity $[=\eta_0 e^{\alpha p}]$.

β Influence of starvation upon h_0 under classical conditions (W constant) $[=h_0/(h_0)_\infty]$.

β^* Influence of starvation upon h^* under elastohydrodynamic lubrication (e.h.l.) conditions (b constant) $[=h^*/h^*_\infty]$.

γ Influence of starvation upon load under classical conditions $[=W/W_\infty]$.

η_0 Controlling viscosity (at atmospheric pressure).

ρ Influence of starvation upon h^* under e.h.l. conditions (B constant) $[=h^*/h^*_\infty$ (equation (19))].

Φ Non-dimensional co-ordinate under e.h.l. conditions $[=B^{1/3}X=b^{1/3}x/(2Rh^*)^{2/3}]$.

Ψ_i Non-dimensional expression for inlet boundary of lubricant film under e.h.l. conditions $[=b^{1/3}x_i/(2Rh^*_\infty)^{2/3}]$.

Subscripts

e Values at the outlet boundary of the lubricant film (classical theory).

i Values at the inlet boundary of the lubricant film.

m Values at the pressure maximum (classical theory).

∞ Values when the inlet boundary is at ∞.

Superscripts

$*$ Values at the pressure maximum (e.h.l. theory).

$—$ Values at the inlet edge of the Hertzian flat (e.h.l. theory).

aper is published for written discussion. The MS. was received 0th November 1970 and accepted for publication on 11th May . 23

ersity of Leicester; now at Shell Research Ltd, Thornton arch Centre, Chester.
artment of Engineering, University of Leicester, LE1 7RH.

INTRODUCTION

Theories of the lubrication of cylinders, or of similar machine elements such as gears and roller bearings, usually make the assumption that the lubricant film in the inlet region extends far away from the position of the minimum film thickness. If a cylindrical shape of radius R is assumed, this means that the boundary of the lubricant film is taken at $x = R$; if the parabolic approximation is adopted for the shape, the boundary is taken at $x = \infty$. The physical justification for this mathematically convenient assumption is that the regions in which the pressure has values of any significance lie close to the position of the minimum film thickness; consequently the boundaries of the hydrodynamic film have little influence upon the load capacity for a particular lubricant, and a given kinematic and geometric configuration.

Under conditions where classical theories are applicable, that is at loads sufficiently small for neither deformation of the surfaces nor increase of viscosity with pressure to be significant, Crook (1)*, Lauder (2) and Boness (3) have provided experimental evidence that the film thickness is less than that forecast by the classical theories, e.g. Martin (4), which make the conventional assumption of an inlet boundary at infinity. This discrepancy has been attributed to the assumed position of the inlet boundary and therefore the influence of the position of this boundary upon the load capacity, for a given set of conditions, becomes of some importance. Dowson and Whitaker (5), Boness (3) and Dowson and Whomes (6) have all made theoretical analyses of the influence of this boundary for the conditions of classical theory. These treatments have been based upon computer solutions of the problem, the load capacity being calculated for various positions of the boundary of the lubricant film in the inlet region; the corresponding boundary of the film in the outlet region has been based upon the familiar condition $p = \mathrm{d}p/\mathrm{d}x = 0$ at outlet. The solutions are presented as a series of curves describing the variation of load capacity with inlet position (expressed in non-dimensional form as x_{inlet}/R) for chosen values of h_0/R. In the first part of the present paper it is shown that, when the appropriate non-dimensional statement of the problem is made, these computer solutions conform to one single semi-analytic solution. However, a more practical statement of the problem is to express the influence of the position of the inlet boundary upon the minimum film thickness for a given load. The film thickness derived from classical theory (4) with inlet boundary at infinity is taken as a guide; the proportional reduction in this minimum film thickness can then be expressed as a single valued function of the inlet boundary position expressed in appropriate non-dimensional form.

The second part of this paper provides a similar solution of the influence of the position of the inlet boundary upon film thickness, for heavily loaded conditions, when the surfaces are elastically deformed and viscosity of the lubricant is increased by the pressures. The analysis uses the same assumptions as Grubin (7) with the exception that the deformed Hertzian shape is replaced b approximation due to Crook (8). As in the treatme the classical theory, it is necessary to transform analytic solution into a form suitable for use in pra Once again, the film thickness derived from the t with the inlet boundary at infinity is taken as a guide proportional reduction in this film thickness can th expressed as a unique function of the inlet bou expressed in suitable non-dimensional form, all variables being held constant.

* *References are given in Appendix 3.*

CLASSICAL THEORY

The parabolic approximation for the shape of the sur as used in earlier theories (4) (9), will be assumed. co-ordinate system used is shown in Fig. 1. The thickness, h, is thus defined by the equation

$$h = h_0 + \frac{x^2}{2R} \quad . \quad . \quad . \quad .$$

where h_0 is the minimum film thickness and R i relative radius of curvature of the surfaces ($1/R = 1$, $1/R_2$). The integrated form of Reynolds equation is

$$\frac{\mathrm{d}p}{\mathrm{d}x} = -12\eta_0 \bar{U}\left(\frac{h-h_m}{h^3}\right) \quad . \quad .$$

where $\bar{U} = \frac{1}{2}(U_1+U_2)$ is the mean velocity o surfaces and h_m is the value of h at the maximum pre

To solve equations (1) and (2) we shall use the stitution

$$X = \frac{x}{(2Rh_0)^{1/2}} \quad . \quad . \quad . \quad .$$

Equation (2) then becomes

$$\frac{\mathrm{d}p}{\mathrm{d}X} = \frac{-12\eta_0 \bar{U}\sqrt{2R}}{h_0^{3/2}} \frac{(X^2 - X_m^2)}{(1+X^2)^3} \quad . \quad .$$

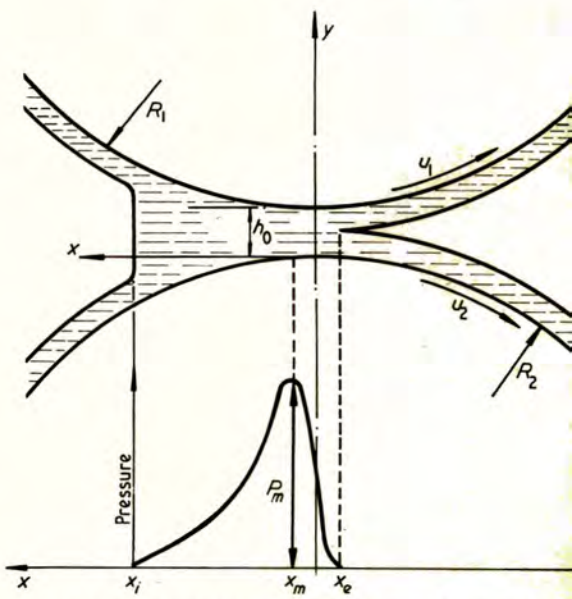

Fig. 1. Classical theory: the shape of the surfaces the co-ordinate system

e $X_m = x_m/(2Rh_0)^{1/2}$ and x_m is the value of x at which ressure maximum occurs.

tegration of equation (4) depends upon the assumed dary conditions:

$$\text{at inlet, } p = 0,\ x = x_i,\ X = X_i \quad . \quad (5a)$$

$$\text{at outlet, } p = 0,\ x = x_e,\ X = X_e \quad . \quad (5b)$$

since $p = dp/dx = 0$ at outlet, inspection of equa-4) gives

$$x_e = -x_m, \quad X_e = -X_m \quad . \quad . \quad (5c)$$

these assumptions Peppler (**9**) has shown that the ration of equation (4) yields:

$$\left(\frac{2h_0^{3/2}}{\bar{U}\sqrt{2R}}\right) = \left[-2(1+\lambda_m^2)\frac{\lambda}{(1+\lambda^2)^2} + 1(1-3\lambda_m^2)\left\{\frac{\lambda}{(1+\lambda^2)} + \tan^{-1}\lambda\right\}\right]_X^{-X_m} \quad (6)$$

e λ is a dummy variable for X.

uation (6) is an expression for the form of the pressure bution in terms of the assumed position of the . Since also $p = 0$ at $X = X_i$ [equation (5a)]:

$$\frac{+X_m^2)}{X_i^2)^2} - X_i\frac{(1-3X_m^2)}{(1+X_i^2)}$$

$$(1-3X_m^2)\{\tan^{-1}X_m + \tan^{-1}X_i\} + X_m\frac{(1+3X_m^2)}{(1+X_m^2)} = 0 \quad . \quad . \quad . \quad (7)$$

is a relation between the position of the inlet dary, X_i, and the position of the maximum pressure, t will be noticed that X_i and X_e are always opposite n. No simple analytic expression between X_i and X_m een found, but equation (7) has been solved numeric-The relationship between the position of the maximum ure X_m, and the inlet boundary X_i, derived from olution of equation (7) is shown in Table 1.

e load capacity W of the system for any given dary conditions may now be calculated. It has been by Blok (**10**) that the load capacity of the system is by

$$W = \frac{\eta_0\bar{U}R}{h_0}\cdot\frac{6}{(1+X_m^2)}\cdot\left(\frac{X_i^2-X_m^2}{1+X_i^2}\right)^2 \quad . \quad (8)$$

, when $X_i = \infty$ becomes the well known Martin on

$$W_\infty = 4{\cdot}89\frac{\eta_0\bar{U}R}{h_0} \quad . \quad . \quad . \quad (9)$$

W_∞ is taken to denote the load capacity with the boundary at infinity. By using equation (8) and 1 it is possible to derive the load capacity of the as a function of the position of the inlet boundary his is best expressed, using equation (9), as

$$\gamma = \frac{W}{W_\infty} \quad . \quad . \quad . \quad (10a)$$

$$W = 4{\cdot}89\gamma\frac{\eta_0\bar{U}R}{h_0} \quad . \quad . \quad . \quad (10b)$$

Table 1. Relationship between non-dimensional parameters of starved classical theory

$(X_i)_\gamma$	X_m	$\gamma = \beta$	$(X_i)_\beta$
0	0	0	0
0·1	0·049 78	0·000 07	0·000 82
0·2	0·098 24	0·001 03	0·006 43
0·3	0·144 23	0·004 84	0·020 87
0·4	0·186 85	0·013 77	0·046 94
0·5	0·225 49	0·029 61	0·086 04
0·6	0·259 91	0·053 09	0·138 25
0·7	0·290 09	0·083 88	0·202 74
0·8	0·316 25	0·120 81	0·278 06
0·9	0·338 71	0·162 25	0·362 53
1·0	0·357 87	0·206 52	0·454 45
1·5	0·417 95	0·425 49	0·978 44
2·0	0·444 70	0·591 80	1·538 57
2·5	0·457 49	0·703 67	2·097 12
3·0	0·464 15	0·778 24	2·646 53
3·5	0·467 88	0·829 10	3·186 92
4·0	0·470 12	0·864 85	3·719 90
4·5	0·471 53	0·890 74	4·247 05
5·0	0·472 47	0·909 99	4·769 68
6·0	0·473 56	0·936 06	5·805 01
7·0	0·474 13	0·952 35	6·831 19
8·0	0·474 45	0·963 17	7·851 28
9·0	0·474 65	0·970 70	8·867 17
10·0	0·474 78	0·976 15	9·880 02
20·0	0·475 09	0·993 93	19·939 21
100·0	0·475 13	0·999 76	99·987 74
∞	0·475 13	1	∞

$(X_i)_\gamma = x_i/\sqrt{2Rh_0}$ is the position of inlet boundary, equation (3).
X_m is the position of the pressure maximum.
γ is W/W_∞, equation (10a).
β is $h_0/h_{0\infty}$, equations (11a), (13).
$(X_i)_\beta = x_i/\sqrt{2R(h_0)_\infty}$, equations (11b), (13).

γ, therefore, represents the proportional reduction in the load capacity of a given system caused by moving the inlet boundary from ∞ to X_i. The relationship between γ and X_i is shown in Table 1.

It will be observed that in Table 1 the proportional reduction in load capacity γ is a single valued function of the inlet boundary, when this is expressed in the appropriate non-dimensional form $(X_i)_\gamma = x_i/(2Rh_0)^{1/2}$. On the

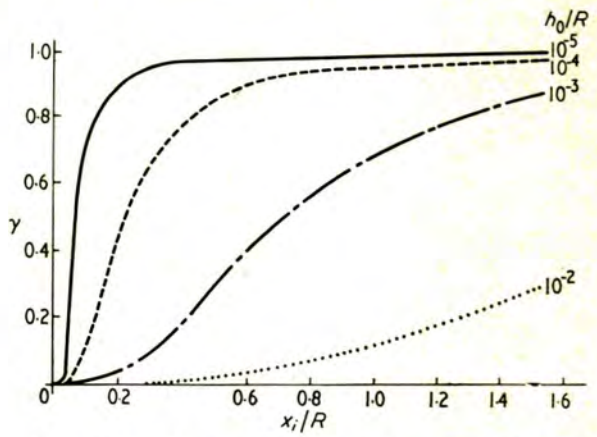

Results as derived by Boness (**11**) from computer solutions for different values of h_0/R.

Fig. 2. Classical theory: the influence of the inlet boundary (x_i/R) upon the load ($\gamma = W/W_\infty$)

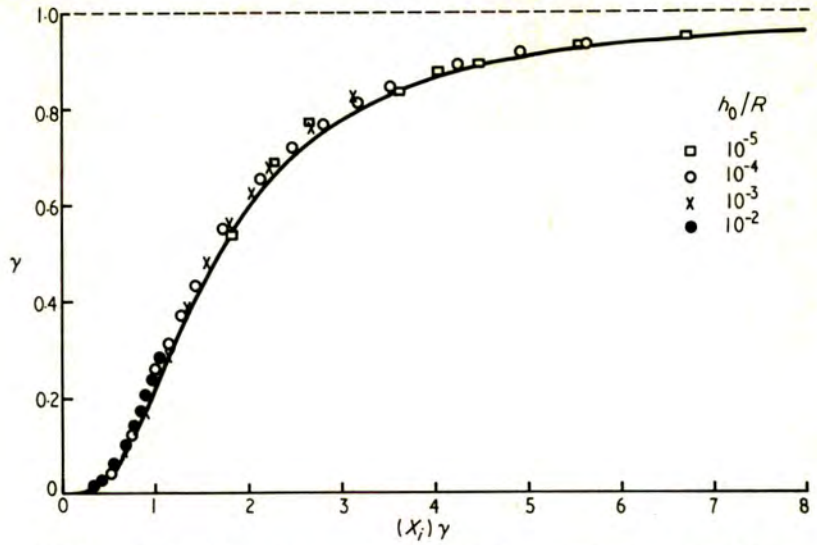

Full line: derived from the general theory of this paper. Points: derived from computer solutions (Fig. 2).

Fig. 3. Classical theory: the influence of the inlet boundary $\{(X_i)_\gamma = x_i/\sqrt{2Rh_0}\}$ upon the load ($\gamma = W/W_\infty$)

other hand the computer solutions of the same problem (3) (5) (6) take a given value of h_0/R and derive the load capacity γ for different positions of the inlet boundary expressed as x_i/R. Fig. 2 shows a set of results derived in this way by Boness (11). In Fig. 3, the full line shows a plot of γ versus $(X_i)_\gamma$ plotted from Table 1 and the points show the values of γ derived by Boness. It will be seen that the computer results of (11) when plotted against $(X_i)_\gamma$ lie very close to the single curve of Fig. 3; it is of interest to note that Boness used a cylindrical shape, whereas the parabolic approximation has been used here.

Transformation of classical theory to a practical form

Neither the presentation of Fig. 2 nor Fig. 3 is of immediate practical use in specifying the effect of the inlet boundary position. The most likely situation is that one is aware of a given set of experimental conditions (η_0, $\bar{U}$, R and W) and the value of the minimum film thickness is then calculated from equation (9), assuming that the inlet boundary is at infinity. By analogy with equation (9), this value of h_0 will be denoted as $(h_0)_\infty$ to indicate that it corresponds to conditions when $x_i = \infty$. We require to know the way in which h_0 varies for these same conditions (in particular for a constant value of the load W) when x_i is varied. By analogy with Fig. 3 and equation (10a) we seek a relationship

$$\beta = \frac{h_0}{(h_0)_\infty} = f_2\{(X_i)_\beta\} \quad . \quad . \quad (11a)$$

where the value of X_i is defined by

$$(X_i)_\beta = \frac{x_i}{(2R(h_0)_\infty)^{1/2}} \quad . \quad . \quad . \quad (11b)$$

β has thus been defined as the proportional reduction in the film thickness of a given system (at constant caused by moving the inlet boundary from ∞ to x_i

From a consideration of given values of η_0, $\bar{U}$, and x_i we have deduced values of the load W. It has shown that all possible values of these variables, co-exist, are connected by the relation

$$\frac{Wh_0}{\eta_0 \bar{U} R} = 4{\cdot}89\gamma = 4{\cdot}89 f_1\{(X_i)_\gamma\} \quad . \quad (1$$

where $(X_i)_\gamma = x_i/(2Rh_0)^{1/2}$.

For the special case of $x_i = \infty$ this becomes

$$\left[\frac{Wh_0}{\eta_0 UR}\right]_\infty = 4{\cdot}89 \quad . \quad . \quad . \quad (1$$

From equations (12a) and (12b) for the case of η_0, and W constant (x_i and h_0 variable) we have

$$\frac{h_0}{(h_0)_\infty} = \gamma = f_1\left[\frac{x_i}{(2Rh_0)^{1/2}}\right] = f_1\{(X_i)_\gamma\} \quad (1$$

where h_0 on the right-hand side is the value of equation (12a).

Thus from equations (11a) and (12c)

$$\beta = \frac{h_0}{(h_0)_\infty} = \gamma = f_1\left\{\frac{x_i}{\sqrt{2R(h_0)_\infty}}\sqrt{\frac{(h_0)_\infty}{h_0}}\right\}$$
$$= f_1\{(X_i)_\beta \beta^{-1/2}\} = f_1\{(X_i)_\gamma\}$$

whence

$$\beta = \gamma, \quad (X_i)_\beta = \gamma^{1/2}(X_i)_\gamma \quad . \quad .$$

From the table of γ versus $(X_i)_\gamma$ (Table 1) it is po using the relationships given in equation (13) to struct a plot of β versus $(X_i)_\beta$. Such a plot is gi Fig. 4. The way in which this graph may be emplo as follows. The experimental conditions (η_0, $\bar{U}$, W) for a given system are known. From equation

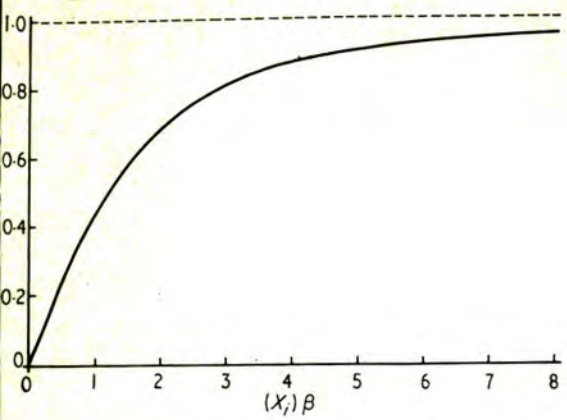

influence of the inlet boundary $(X_i)_\beta = x_i/\sqrt{2R(h_0)_\infty}$ upon ninimum film thickness ($\beta = h_0/(h_0)_\infty$), other experimental itions remaining constant.

ig. 4. Classical theory expressed in practical form (*W* constant)

ossible to calculate a value of h_0 (designated $(h_0)_\infty$) he assumption that the inlet boundary is at infinity. proportional reduction in film thickness (β), for ous values of x_i, can then be obtained from Fig. 4, e $(X_i)_\beta = x_i/\sqrt{2R(h_0)_\infty}$ is calculated using the value $_0)_\infty$ already obtained.

ELASTOHYDRODYNAMIC THEORY

his section we provide an analysis of the effect of the ion of the inlet boundary upon the film thickness h occurs under heavy loads. Under these conditions deformation of the surfaces and increase of lubricant sity are significant. The methods adopted below are lar to those used in the pioneer study of Grubin (7); xplanation of this approach, and evidence that it ides a value of the film thickness close to that obtained more detailed theoretical treatments can be found in son (12) and Dowson and Higginson (13).

accordance with the technique adopted by Grubin, ll be assumed that the shape of the surfaces is Hertz- therefore in the main load bearing region (Fig. 5), surfaces are separated by a parallel film of thickness This parallel region is a band of width $2b$, which esponds exactly to the band of contact obtained under c conditions for the same load, in the absence of a icant. The film thickness h^* in the parallel regions en determined by the criterion that at the entry to conjunction ($x = 0$ in Fig. 5) the pressure is suf- ntly large to maintain an effectively parallel film. It been shown (7) that this is met by the condition

$$\bar{q} = \frac{1}{\alpha} \quad . \quad . \quad . \quad . \quad . \quad (14)$$

e q is the 'reduced pressure', i.e. the pressure cal- ed for the given geometry on the assumption that the icant has a constant viscosity η_0; $\bar{q}$ is the value of q

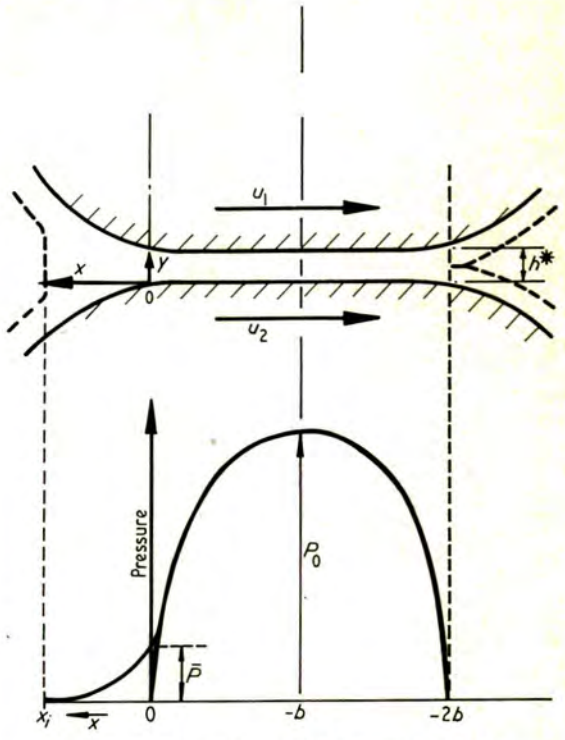

$\bar{p}$ corresponds to the reduced pressure $\bar{q} \to 1/\alpha$.

Fig. 5. Elastohydrodynamic theory: the shape of the surfaces and the co-ordinate system

at $x = 0$, and α is the pressure coefficient of viscosity in the relationship between viscosity and pressure

$$\eta = \eta_0 \exp(\alpha p) \quad . \quad . \quad . \quad . \quad (15)$$

Note also that $q = 0$ at $x = x_i$, where x_i is the boundary of the lubricant film in the entry region.

As shown in Fig. 5, the origin of the system of axes is chosen at the entry to the parallel region. Then, according to Crook (8), the shape of the film in the converging entry region is, to a good approximation, given by

$$h = h^*\left[1+\frac{4\sqrt{2}}{3}\Phi^{3/2}\right] \quad . \quad . \quad . \quad (16)$$

where $\Phi = B^{1/3}X$. $X = x/(2Rh^*)^{1/2}$ is a non-dimensional co-ordinate analogous to that used previously in the discussion of classical theory, and $B = b/(2Rh^*)^{1/2}$ is a similar non-dimensional presentation of the half-width of the Hertzian flat b. As before, R is the relative radius of curvature of the surfaces in their undeformed state.

The integrated form of Reynolds equation for this problem is equation (2) with q replacing p. Using equation (16) and the associated definition of Φ, one obtains

$$\frac{dq}{d\Phi} = \frac{-12\eta_0\bar{U}}{h^{*3/2}}\frac{R^{1/2}\sqrt{2}}{B^{1/3}}\left[\frac{4\sqrt{2}}{3}\frac{\Phi^{3/2}}{\left[1+\frac{4\sqrt{2}}{3}\Phi^{3/2}\right]^3}\right] \quad (17)$$

To obtain $\bar{q}$, the reduced pressure at $x = 0$, equation (17)

can be integrated by straightforward techniques (see Appendix 2) to give the following expression:

$$\bar{q} = \frac{12\eta_0 \bar{U} R^{1/2}\sqrt{2}}{h^{*3/2} B^{1/3} a} [I]_0^{(a\Phi_i)} \quad . \quad . \quad (18a)$$

where $a = [(4\sqrt{2})/3]^{2/3}$ and I is given by

$$I = \frac{(2\tau^{3/2}-1)\tau}{9(1+\tau^{3/2})^2} - \frac{2}{27}\left[\frac{1}{2}\ln\left\{\frac{(1+\tau^{1/2})^2}{(\tau-\tau^{1/2}+1)}\right\} + \sqrt{3}\tan^{-1}\left\{\frac{(2-\tau^{1/2})}{\sqrt{3}\tau^{1/2}}\right\}\right] \quad (18b)$$

τ is a dummy variable for $(a\Phi)$, $\Phi_i = B^{1/3}X_i$ and $X_i = x_i/(2Rh^*)^{1/2}$.

Values of $[I]_0^{a\Phi_i}$ for values of Φ_i between 0 and 500 are listed in Table 2. It will be observed that $[I]_0^{\infty} = 0{\cdot}268\,71$.

Using now the criterion of equation (14) it is possible to derive from equation (18a) a value for h^* for any position of the inlet boundary expressed in terms of the non-dimensional parameter Φ_i. One obtains for $x_i = \Phi_i = \infty$ the result

$$h^*_{\infty} = 2{\cdot}0742(\alpha\eta_0\bar{U})^{2/3}R^{1/3}B^{-2/9} \quad . \quad (19a)$$

and for the more general case with the inlet boundary of the lubricant film at x_i

$$h^* = 4{\cdot}9812(\alpha\eta_0\bar{U})^{2/3}R^{1/3}B^{-2/9}\{[I]_0^{(a\Phi_i)}\}^{2/3} \quad (19b)$$

which, using equation (19a) may be rewritten as

$$h^* = 2{\cdot}0742\rho(\alpha\eta_0\bar{U})^{2/3}R^{1/3}B^{-2/9} \quad . \quad . \quad (19c)$$

where, if B is held constant,

$$\rho = \frac{h^*}{h^*_{\infty}} = \left[\frac{1}{0{\cdot}2687}[I]_0^{(a\Phi_i)}\right]^{2/3} \quad B \text{ constant} \quad (19d)$$

A plot of ρ as a function of Φ_i is shown in Fig. 6. It may be noted in passing that equation (19a) can be cast in the form

$$h^*_{\infty} = K(\alpha\eta_0\bar{U})^{3/4}R^{1/2}b^{-1/4} \quad . \quad . \quad (20)$$

where K is a numerical constant which is found, by the integration given in Appendix 2 to be 2·4776, w compares favourably with the value of 2·4 found by C (8) using numerical integration*.

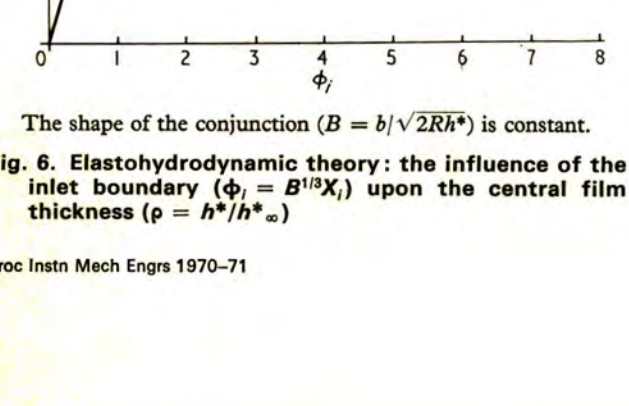

The shape of the conjunction ($B = b/\sqrt{2Rh^*}$) is constant.

Fig. 6. Elastohydrodynamic theory: the influence of the inlet boundary ($\Phi_i = B^{1/3}X_i$) upon the central film thickness ($\rho = h^*/h^*_{\infty}$)

Table 2. Relationship between the inlet parameter and the integral $[I]_0^{a\Phi_i}$

Φ_i	$[I]_0^{a\Phi_i}$	Φ_i	$[I]_0^{a\Phi_i}$
0·0	0·000 00	6·0	0·263 1
0·1	0·003 27	7·0	0·264 5
0·2	0·015 39	8·0	0·265 4
0·3	0·034 29	9·0	0·266 1
0·4	0·056 34	10·0	0·266 6
0·5	0·078 76	15·0	0·267 7
0·6	0·099 93	20·0	0·268 1
0·7	0·119 11	25·0	0·268 3
0·8	0·136 09	30·0	0·268 4
0·9	0·150 93	35·0	0·268 5
1·0	0·163 81	40·0	0·268 5
2·0	0·228 66	45·0	0·268 6
3·0	0·248 51	50·0	0·268 6
4·0	0·256 67	100·0	0·268 6
5·0	0·260 78	500·0	0·268 7

We return now to a consideration of the phy significance of equations (19a, b, c, d). Equation gives an expression, of the Grubin type, for the thickness in the main load bearing region when inlet boundary is far removed from the edge of the pa region. In this equation the load dependence of thickness is contained within the parameter B. As has explained elsewhere (15), in theories of the Grubin this is essentially a parameter which expresses the ov shape of the deformed configuration and the interp lubricant film; B is the appropriate non-dimens statement of this shape and can be regarded as the of the local depression of the surfaces to the film thick in the parallel region. Similarly in equation (19c expresses the proportional reduction in the film thick h^*, arising from a movement of the inlet boundary ∞ to x_i whilst, at the same time, the general shape o geometric configuration (expressed by B) is mainta constant. It will be observed that ρ is a function only, where

$$\Phi_i = B^{1/3}X_i = \left(\frac{b}{\sqrt{2Rh^*}}\right)^{1/3}\frac{x_i}{\sqrt{2Rh^*}} \quad . \quad (2$$

Φ is therefore a non-dimensional co-ordinate for the region. It contains, as the dominant element, the meter $X_i = x_i/(2Rh^*)^{1/2}$ which appeared in the treat of classical theory given previously. The fact tha depends strongly upon X (or x) and is relatively we dependent upon B (or b) is the reason why the load small influence upon film thickness, and the limiting thickness derived from an undeformed shape is a approximation to the film thickness derived from the of the Grubin type; see Archard and Cowking Greenwood (16).

* *This result was confirmed independently by Dyson* (14) *who, gamma function theory to evaluate Crook's integral for the s case of the inlet boundary placed at infinity, obtained a va 2·478 for K.*

sformation of e.h.l. theory to a practical form

y we return to equation (19c) and its practical . As in the classical case, considered above, the priate non-dimensional presentation of the theory in a form which can be used directly in common ce. Once again it can be assumed that the operating ions are known; i.e. $\bar{U}$, α, η_0, R and b (b is known elastic theory). A value of $h^*(h^*_\infty)$ may then be ated from equation (20) (or from Grubin's theory) ing that the inlet boundary, x_i, is at infinity. We equire to know the way in which h^* will vary, for same experimental conditions (specifically for the value of b), as x_i varies. By analogy with equation e define a proportional reduction in the film thick- β^*, occurring as the inlet boundary is moved in ∞ to x_i, all other experimental conditions remaining nt.

have shown (equation (19c)) that for any chosen set ditions, i.e. values of α, η_0, $\bar{U}$, R, $B = b/\sqrt{2Rh^*}$ and deduced value of h^* for all possible conditions is by the relation

$$\frac{h^* B^{2/9}}{(\alpha\eta\bar{U})^{2/3}R^{1/3}} = 2{\cdot}074\rho = 2{\cdot}074 f_1[\Phi_i] \qquad (22)$$

$$\Phi_i = B^{1/3}X_i = b^{1/3}x_i/(2Rh^*)^{2/3}$$

pecifically, in this expression for Φ_i, h^* has the for these given conditions).

the special case $x_i = \infty$

$$\left[\frac{h^* B^{2/9}}{(\alpha\eta\bar{U})^{2/3}R^{1/3}}\right]_\infty = 2{\cdot}074 \quad . \quad . \quad (23)$$

quire a relationship of the form

$$\frac{h^*}{h^*_\infty} = \beta^* = f_2(\Psi_i) \quad . \quad . \quad . \quad (24)$$

$$\Psi_i = b^{1/3}x_i/(2Rh^*_\infty)^{2/3}$$

' and h^*_∞ correspond to the same values of α, η_0, nd b.

ations (22) and (23) may be re-written in terms of b than B as follows

$$\frac{h^{*8/9}b^{2/9}}{2^{1/9}(\alpha\eta_0\bar{U})^{2/3}R^{4/9}} = 2{\cdot}074\rho = 2{\cdot}074 f_1(\Phi_i) \qquad (22a)$$

$$\left[\frac{h^{*8/9}b^{2/9}}{2^{1/9}(\alpha\eta_0\bar{U})^{2/3}R^{4/9}}\right]_\infty = 2{\cdot}074 \quad . \quad (23a)$$

ning (22a) and (23a) and (24) gives (for α, η_0, $\bar{U}$, b nt)

$$\left.\right]^{8/9} = \rho = f_1(\Phi_i) = (\beta^*)^{8/9} = [f_2(\Psi_i)]^{8/9} \qquad (25a)$$

$$\Phi_i = \frac{b^{1/3}x_i}{(2Rh^*)^{2/3}} = \frac{b^{1/3}x_i}{(2Rh^*_\infty)^{2/3}}\left(\frac{h^*_\infty}{h^*}\right)^{2/3}$$
$$= \Psi_i(\beta^*)^{-2/3} = \Psi_i\rho^{-3/4} \quad . \quad . \quad . \quad (25b)$$

Thus (from equations (25a), (25b)) to obtain values of β^* and Ψ_i from given values of ρ and Φ_i we write

$$\left.\begin{aligned}\beta^* &= \rho^{9/8}\\ \Psi_i &= \rho^{3/4}\Phi_i\end{aligned}\right\} \quad . \quad . \quad . \quad (25c)$$

An alternative derivation of these relationships, based upon physical reasoning, is given in Appendix 1.

From a plot of ρ as a function of Φ_i (Fig. 6) it is possible, using equations (25c), to construct a plot of β^* as a function of Ψ_i. Such a graph, constructed in this way, is shown by the full line in Fig. 7.

The way in which this graph may be used is as follows. Once again the experimental conditions (η_0, $\bar{U}$, α, R and W) for a given system are known. From the equations governing elastic deformation, it is possible to derive the Hertzian half-width b whence, from equation (20), a value of h^* (designated h^*_∞) may be calculated on the assumption that the inlet boundary is at infinity. The proportional reduction in film thickness (β^*) at a fixed load, for various values of x, can then be obtained from Fig. 7 where $\Psi_i = b^{1/3}x_i/(2Rh^*_\infty)^{2/3}$ is calculated using the values of h^*_∞ and b already obtained.

It is not possible to present so complete a comparison with published computer solutions as with the classical theory, because few computer solutions of the starved lubrication problem exist. However, Orcutt and Cheng (17) have shown a specific example of a starvation curve for one set of experimental conditions. Orcutt and Cheng's results have been re-calculated in a form appropriate for comparison with the theory of the present paper. They present values of $h_{\min}$, the minimum film thickness, which occurs at outlet; the present paper is concerned with h^*, the film thickness in the parallel region. It is assumed that

$$\frac{h^*}{h^*_\infty} = \frac{h_{\min}}{h_{\min,\,\infty}} \quad \text{and} \quad h_{\min} = 0{\cdot}85h^*$$

Results derived from Orcutt and Cheng's computer solution are compared with the more general theory of this paper in Fig. 7. It will be seen that there is excellent agreement.

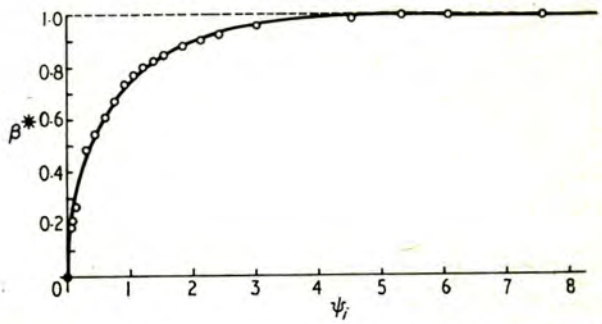

The influence of the position of the inlet boundary (ψ_i) upon the central film thickness ($\beta^* = h^*/h^*_\infty$) other experimental conditions remaining constant. The inlet boundary is expressed as $\psi_i = b^{1/3}X_i/2Rh^*_\infty)^{2/3}$; equation (24). The points are derived from the computer solution of Orcutt and Cheng (17).

Fig. 7. Elastohydrodynamic theory expressed in practical form

DISCUSSION AND CONCLUSIONS

Early theories of the lubrication of cylinders, and most subsequent discussion, have assumed that the inlet boundary of the lubricant film is so far removed from the position of minimum film thickness that a theoretical assumption of an inlet boundary at infinity is a completely acceptable description of the operational conditions. However, sufficient evidence now exists to suggest that the influence of the position of the inlet boundary upon film generation requires serious and detailed consideration. This paper has therefore presented semi-analytical solutions of the problem both for the undeformed isoviscous case and for full e.h.l. conditions. In both examples the theory has first been presented as a single function of the inlet boundary, the position of this boundary being presented in the appropriate non-dimensional form. It has then been shown how these solutions can be transformed into a form more readily applicable to practice.

The main alternative procedure to that presented here is to present solutions to the problem for a wide range of assumed conditions, these solutions being derived from computer solutions. Several workers have presented numerical solutions to the undeformed isoviscous case and it has been shown (Fig. 3) that all such solutions lie on a single curve when the appropriate non-dimensional groups are used. This semi-analytical solution has the advantage over numerical solutions that dependence on experimental parameters is immediately obvious. The only previous known attempt to produce a single semi-analytical solution, such as that given above, is contained in an unpublished report by Walther and Sassenfeld*. However, no earlier work tackles the problem of transforming the solution into a form more readily applicable in practice, namely the variation of film thickness with inlet boundary for constant load.

There is far less published work upon the effects of the position of the inlet boundary under e.h.l. conditions, perhaps because of difficulties experienced with numerical techniques†. The solution provided here avoids these difficulties by using an analytical approach similar to that of Grubin (7), the only difference being the use of the Crook approximation for the Hertzian shape. The use of this approximation seems perfectly justified if it forecasts reasonably accurate values of $(h-h^*)/h^3$ in those regions where values of dq/dx of significant magnitude occur, e.g. for $h/h^* < 10$ (see Fig. 8). It has been found that this is true if $B^2 > 50$. However, if $B^2 < 50$, the starvation curve of Fig. 6 is still an acceptable statement of the reduction of film thickness arising from starvation, but care must be

* *An account of this work is to be found in a book by Cameron* (**18**) *which also contains some details of computer solutions of the classical problem by Floberg.*

† *After the completion of the work described in this paper and its submission for publication our attention was drawn to computer solutions, as yet unpublished, of starved lubrication at point contacts by L. D. Wedeven and starved lubrication at line contacts by P. Castle and D. Dowson. The publication of this work and its comparison with our analytic solution are awaited with interest.*

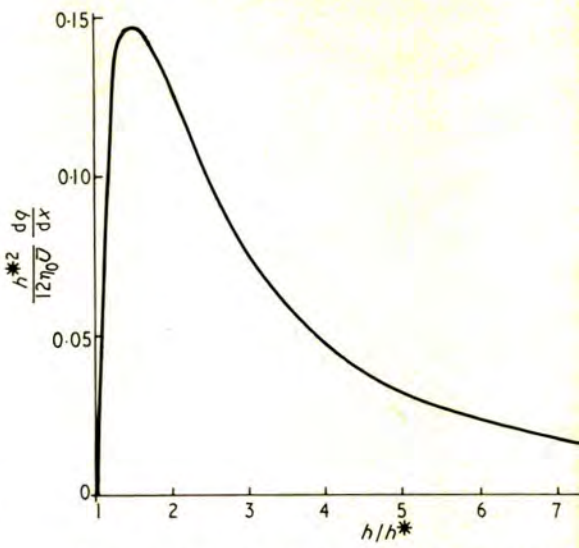

Fig. 8. The variation of the non-dimensional redu pressure gradient ($h^{*2}/12\eta_0 U$) dq/dx with h/h

exercised in choosing the correct value of h^*_∞; t values of h^*_∞ must be derived using the true Hertz rather than the Crook approximation. The nec numerical integrations have been performed by C (7) and by Greenwood (**16**). In the context of the p paper it is appropriate to express their results in similar to equation (19a). Thus

$$h^*_\infty = C(\alpha\eta_0\bar{U})^{2/3}R^{1/3}B^{-2/9} \quad . \quad .$$

where C is a numerical constant weakly dependen B as shown in Table 3. It will be observed that eq (26) tends to equation (19a) for large values of B.

One merit of the approach used in this paper i because a single solution of the problem is sough can only be achieved when the theory is presented appropriate non-dimensional form. This, in turn, re physical explanation and in this way the fact significance in the lubrication of cylinders becom strongly apparent. Thus it is seen that the effect

Table 3. Relationship between C and B^2 in $h^*_\infty = C(\alpha\eta_0\bar{U})^{2/3}R^{1/3}B^{-2/9}$; see equation (26)

B^2	C
∞	2·0742
200	2·0664
100	2·0593
40	2·0478
20	2·0325
10	2·0138
4	1·9755
2	1·9349
1	1·8831
0·4	1·7964
0·2	1·7183
0·1	1·6317
0·04	1·5089
0·02	1·4140
0·01	1·3197

lubrication under e.h.l. conditions is effected, arily, through its influence upon the geometric shape e system expressed by the parameter B. With the boundary at infinity, the convergent inlet region nes less efficient as a generator of hydrodynamic ures as W, b and B increase. A rather more surprising is concerned with the influence of load upon the h of the inlet region (in the x direction) which is icant in film generation. An increase in W, b, or B s the length of this region to decrease; moreover it d be emphasized that this decrease is in the physical nsions of the region and not merely in its size as a on of b, which is the form in which the results of uter solutions are often presented.

has been claimed that the way in which the theories been developed in this paper, and in particular their opment in non-dimensional form, has the advantage physical insight is improved. However, the theories a major disadvantage; they are presented in a way h is not applicable to normal practice. Indeed, this vantage applies to most alternative methods of nting results, including the earlier presentation of uter solutions. This problem arises because con-onal treatments of hydrodynamic theories start with sumed geometrical configuration, including an as-d value of the minimum film thickness, and end with ormal load as the integration of the normal pressures. actice we start with known values of the operational tions, including the normal load, and need to deduce ie of the minimum film thickness. When the position e inlet boundary is introduced as a new variable the likely situation is that this will not be known with certainty. Values of film thickness deduced from iments may be at variance with those deduced from ieories which assume an inlet boundary far removed the position of minimum film thickness. One then res to know what change in the position of the inlet dary will bring agreement between theory and experi-, and this information can be derived directly from 4 or Fig. 7.

an example of the use of these theories we consider y the divergencies between theory and experiment istohydrodynamic lubrication. For cylinders in line ct, the most extensive set of experimental results, of Dyson, Naylor and Wilson (**19**), are in good ment with theory. Although other experimental urements show significant departures from the theory for example, a review by Archard (**20**)) they are all omprehensive and cover a smaller range of condi-than the measurements of Dyson, Naylor and n. Therefore, on balance, it seems reasonable to st that there is an acceptable agreement between y and experiment for line contacts.

point contacts the situation is less satisfactory. The comprehensive set of experimental measurements are of Archard and Kirk (**21**) which cover a range of s from approximately 1 to 500 cm/s. In presenting results it was pointed out that agreement between the experiments and the theory requires that the measured values of film thickness, if correct at the lowest speed, be too low by a factor of about 2 at the highest speed. In these experiments it was observed that, as the speed was increased, the extent of oil filling in the region of closest approach was reduced. We will therefore consider whether the factors considered in the present paper could contribute to the observed divergence between theory and experiment. The not unreasonable assumption will be made that the arguments developed here for line contact apply also to point contacts, since the theory used by Archard and Kirk is essentially similar to that of Grubin with the additional assumption of a constant side leakage factor in the entry region.

The theory of Archard and Cowking (**15**) (Part 1) used for comparison with the experimental measurements is

$$h^* = 1{\cdot}30(\alpha\eta_0\bar{U})^{2/3}R^{1/3}(a^2/2Rh^*)^{-1/10} \qquad (27)$$

where a is the radius of the Hertzian circular area. Apart from this replacement of b by a, equation (27) is equivalent to equation (19a), $(a/\sqrt{2Rh^*})$ replacing B. The stated divergence between theory and experiment is based upon the assumption that $h^* \propto \bar{U}^{2/3}$; this therefore assumes that the experiments were carried out at constant values of (a^2/Rh^*). In the experiments, as the speed was increased, both the mean load employed increased (increased values of a) and also the values of h^* became larger. On balance, over a speed range of 500 to 1, the values of $(a^2/2Rh^*)$ fell by a factor of between 2 and 3. This factor could account for a discrepancy of about 12 per cent, whereas the divergence between theory and experiment is by a factor of 2.

We are therefore left with the assumption that, at the highest speeds, incomplete filling of the entry region was such as to reduce the values of film thickness by a factor of 0·56. Thus, using Fig. 7, $\beta^* = 0{\cdot}56$, $\Psi = 0{\cdot}52$. From the experimental results, $b\,(=a) = 3{\cdot}5\times10^{-2}$ cm, $h^*_\infty = 2\times10^{-4}$ cm, $R = 1{\cdot}97$ cm; these figures give a value of x_i of approximately $1{\cdot}2\times10^{-2}$ cm. Thus, use of the theory given above suggests that the divergence between theory and experiment found in (**21**) could be explained if it be assumed that, at the highest speeds, the inlet boundary of the lubricant film was $1{\cdot}2\times10^{-2}$ cm from the edge of the Hertzian circle of contact, whose radius was $3{\cdot}5\times10^{-2}$ cm.

It is of interest to observe that at the lowest speeds used by Archard and Kirk this same position of the inlet boundary ($x_i = 1{\cdot}2\times10^{-2}$ cm) would have practically no influence upon the film thickness ($\beta^* > 0{\cdot}97$). In fact, as noted above, it was observed during the experiments that a much greater degree of inlet filling occurred at low speeds. There are other features in these experiments, associated with the experimental techniques, which could contribute to the divergence between theory and experiment; these will be discussed elsewhere (**22**). Nevertheless, it seems clear that in these experiments, and also, perhaps, in others such as those of Crook, the effects of starvation and its variation with speed could well have had an influence upon the results.

ACKNOWLEDGEMENTS

We are indebted to Dr R. J. Boness for the use of results derived from his thesis and displayed in Fig. 2. We also thank Professor H. S. Cheng for additional information required to present his results in Fig. 7. P. E. Wolveridge is indebted to the Shell International Petroleum Company Ltd for a research studentship.

APPENDIX 1

Alternative derivation of equation (25c)

Values of β^* may be derived from values of ρ by a physical argument concerned with changes in a system operating throughout with constant values of η_0, $\bar{U}$, α and R. The changes considered are summarized in Table 4 and will be presented in detail below.

The initial conditions (Stage 1) are

$$h^* = h^*_\infty = h_1, \quad b = b_1,$$
$$B = B_\infty = B_1 = b_1/(2Rh_1)^{1/2}, \quad x_i = X_i = \infty \quad (28)$$

(Change 1→2) x_i is changed from ∞ to x_1, keeping b constant at b_1. h^* changes to h_2. Then from equation (24),

$$h_2 = \beta^* h_1 \quad . \quad . \quad . \quad . \quad (29)$$

where β^* corresponds to a value of Ψ given by

$$\Psi = \left(\frac{b_1}{\sqrt{2Rh_1}}\right)^{1/3} \frac{x_1}{\sqrt{2Rh_1}} = \frac{{b_1}^{1/3} x_1}{(2Rh_1)^{2/3}} \quad (30)$$

The operating conditions (Stage 2) are now

$$h^* = h_2, \quad b = b_1, \quad B = B_2 = b_1/(2Rh_2)^{1/2},$$
$$x_i = x_1, \quad X_1 = x_1/(2Rh_2)^{1/2} \quad (31)$$

(Change 2→3) x_i is now changed from x_1 to ∞ keeping B constant at B_2. h^* changes from h_2 to h_3 so that, by equations (19a), (19c) and (19d)

$$h_2 = \rho h_3 \quad . \quad . \quad . \quad . \quad . \quad (32)$$

where ρ corresponds to a value of Φ_i given by

$$\Phi = {B_2}^{1/3} X_1 = \left(\frac{b_1}{\sqrt{2Rh_2}}\right)^{1/3} \frac{x_1}{\sqrt{2Rh_2}} = \frac{{b_1}^{1/3} x_1}{(2Rh_2)^{2/3}} \quad . \quad . \quad . \quad (33)$$

To maintain B constant and equal to B_2, b changes b_1 to b_2.

The operating conditions (Stage 3) are now

$$h^* = h^*_\infty = h_3, \quad b = b_2, \quad B = B_\infty = B_2, \quad x_i = X_i$$

and using equation (31)

$$B_2 = \frac{b_2}{\sqrt{2Rh_3}} = \frac{b_1}{\sqrt{2Rh_2}} \quad . \quad . \quad (\text{illegible})$$

If we now compare the initial and final cond given above, using equations (19a) (29) and also equ (28) (31), we obtain

$$\frac{h_1}{h_3} = \left(\frac{B_2}{B_1}\right)^{2/9} = \left(\frac{h_1}{h_2}\right)^{1/9} = \left(\frac{1}{B^*}\right)^{1/9} \quad . \quad (\text{illegible})$$

Using equations (29) and (32)

$$\frac{h_1}{h_3} = \frac{\rho}{\beta^*} \quad . \quad . \quad . \quad . \quad . \quad (\text{illegible})$$

From equations (30), (33) and (29)

$$\frac{\Psi}{\Phi_i} = \left(\frac{h_2}{h_1}\right)^{2/3} = \beta^{*2/3} \quad . \quad . \quad . \quad (\text{illegible})$$

We now obtain the necessary relation between β^* a Using equations (35) and (36)

$$\beta^* = \rho^{9/8} \quad . \quad . \quad . \quad . \quad (\text{illegible})$$

From equations (37) and (38) we obtain the plementary relation between Ψ and Φ_i:

$$\Psi = \rho^{3/4} \Phi_i \quad . \quad . \quad . \quad . \quad (\text{illegible})$$

It will be noted that equations (38) and (39) corre to equation (25c).

Equation (13) for the classical theory may be deri a similar way.

APPENDIX 2

We require to integrate

$$\frac{dq}{d\Phi} = \frac{12\eta_0 \bar{U}}{h^{*3/2}} \frac{R^{1/2}}{B^{1/3}} \sqrt{2} \left[\frac{4\sqrt{2}}{3} \frac{\Phi^{3/2}}{\left(1 + \frac{4\sqrt{2}}{3}\Phi^{3/2}\right)^3}\right] \quad . \quad . \quad . \quad (\text{illegible})$$

Table 4. Deduction of values of β* and Ψ from values of ρ and Φ_i

STAGE	h^*	b	B	x_i	X_i	
STAGE 1	h_1	b_1	B_1	∞	∞	
CHANGE 1→2	$\frac{h_2}{h_1} = \beta^*$	—	$\frac{B_1}{B_2} = \sqrt{\beta^*}$	—	—	β^* correspond $\Psi = \frac{{b_1}^{1/3} x}{(2Rh_2)}$
STAGE 2	h_2	b_1	B_2	x_1	X_1	
CHANGE 2→3	$\frac{h_2}{h_3} = \rho$	$\frac{b_1}{b_2} = \sqrt{\rho}$	—	—	—	ρ corresponds $\Phi_i = \frac{{b_1}^{1/3} x}{(2Rh_2)}$
STAGE 3	h_3	b_2	B_2	∞	∞	

$= a\Phi$, where $a = (4\sqrt{2}/3)^{2/3}$. This becomes

$$\bar{q} = \frac{12\eta_0 \bar{U}}{h^{*3/2}} \frac{R^{1/2}}{B^{1/3}} \frac{\sqrt{2}}{a} [I]_0^{a\Phi_i} \quad . \quad . \quad (18a)$$

$$I = \int \frac{\tau^{3/2}}{(1+\tau^{3/2})^3} \, d\tau \quad . \quad . \quad . \quad (40)$$

rating by parts twice

$$= -\frac{\tau}{3(1+\tau^{3/2})^2} - \frac{2}{9} \frac{1}{\tau^{1/2}(1+\tau^{3/2})} - \frac{1}{9} \int \frac{d\tau}{\tau^{3/2}(1+\tau^{3/2})} \quad . \quad . \quad . \quad (41)$$

ntegral may be separated by partial fractions into

$$\int \frac{d\tau}{\tau^{3/2}(1+\tau^{3/2})} = -\frac{2}{\tau^{1/2}} - \int \frac{d\tau}{(1+\tau^{3/2})} \, . \quad (42)$$

ce

$$I = \frac{(2\tau^{3/2}-1)\tau}{9(1+\tau^{3/2})^2} + \frac{1}{9} \int \frac{d\tau}{(1+\tau^{3/2})} \quad . \quad . \quad (43)$$

lve the last integral let $\tau^{1/2} = 1/Z$, whence

$$\int \frac{d\tau}{(1+\tau^{3/2})} = -2 \int \frac{dz}{(1+z^3)}$$

in a standard form

$$= -2\left\{\frac{1}{3}\left[\frac{1}{2} \ln \frac{(1+z)^2}{(1-z+z^2)} + \sqrt{3} \tan^{-1}\left\{\frac{2z-1}{\sqrt{3}}\right\}\right]\right\}$$

APPENDIX 3

REFERENCES

ROOK, A. W. 'The lubrication of rollers—I' *Phil. Trans. R. Soc.* 1958 **A250**, 387.

AUDER, W. 'Hydrodynamic lubrication of proximate cylindrical surfaces of large relative curvature', *Proc. Instn mech. Engrs* 1965 **180** (Pt 3B), 101.

ONESS, R. J. 'Isoviscous lubrication of rigid cylinders—a modification to classical theory', *J. mech. Engng Sci.* 1966 **8** (No. 3), 276.

ARTIN, H. M. 'Lubrication of gear teeth', *Engineering, Lond.* 1916 **102**, 199.

OWSON, D. and WHITAKER, A. V. 'A numerical procedure for the solution of the elastohydrodynamic problem of rolling and sliding contacts lubricated by a Newtonian fluid', *Proc. Instn mech. Engrs* 1965 **180** (Pt 3B), 57.

(6) DOWSON, D. and WHOMES, T. L. 'Side-leakage factors for a rigid cylinder lubricated by an isoviscous fluid', *Proc. Instn mech. Engrs* 1967 **181** (Pt 3B), 165.

(7) GRUBIN, A. N. and VINOGRADOVA, I. E. *Central Scientific Research Institute for Technology and Mechanical Engineering Book 30* (Moscow); (1949) D.S.I.R. Trans. No. 337.

(8) CROOK, A. W. 'The lubrication of rollers—II. Film thickness with relation to viscosity and speed', *Phil. Trans. R. Soc.* 1961 **A250**, 387.

(9) PEPPLER, W. 'Druckübertragung und geschmierten zylindrischen Gleit und Wälzflachen', V.D.I. Forschung 1938, 391.

(10) BLOK, H. Discussion, *Proc. Instn mech. Engrs* 1965 **180** (Pt 3B), 107.

(11) BONESS, R. J. 'The lubrication of cylinders with particular reference to roller bearings', Ph.D. thesis, Royal Military College of Science, 1969.

(12) DOWSON, D. 'Elastohydrodynamic lubrication: An introduction and review of theoretical studies', *Proc. Instn mech. Engrs* 1965 **180** (Pt 3B), 7.

(13) DOWSON, D. and HIGGINSON, G. R. *Elastohydrodynamic lubrication* 1966 (Pergamon Press, Oxford).

(14) DYSON, A. and WILSON, A. R. 'Film thickness in elastohydrodynamic lubrication at high slide/roll ratios', *Proc. Instn mech. Engrs* 1968–69 **183** (Pt 3P), 81.

(15) ARCHARD, J. F. and COWKING, E. W. 'A simplified treatment of elastohydrodynamic lubrication theory for a point contact', *Proc. Instn mech. Engrs* 1965 **180** (Pt 3B), 47.

(16) GREENWOOD, J. A. 'Presentation of elastohydrodynamic film thickness results', *J. mech. Engng Sci.* 1969 **11** (No. 2), 128.

(17) ORCUTT, F. K. and CHENG, H. S. 'Lubrication of rolling contact instrument bearings, gyro spin-axis', *Hydrodynamic Bearing Symposium*, Vol. 2, Dec. 1966 (M.I.T. Instrument Lab., Cambridge, Mass.).

(18) CAMERON, A. *Principles of lubrication* 1966, 175–179 (Longmans, London).

(19) DYSON, A., NAYLOR, H. and WILSON, A. R. 'The measurement of oil film thickness in elastohydrodynamic contacts', *Proc. Instn mech. Engrs* 1965 **180** (Pt 3B), 119.

(20) ARCHARD, J. F. 'Experimental studies of elastohydrodynamic lubrication', *Proc. Instn mech. Engrs* 1965 **180** (Pt 3B), 17.

(21) ARCHARD, J. F. and KIRK, M. T. 'Lubrication at point contacts', *Proc. R. Soc.* 1961 **A261**, 532.

(22) SNIDLE, R. W. and ARCHARD, J. F. 'Experimental investigation of elastohydrodynamic lubrication at point contacts', *Elastohydrodynamic Lubrication: 1972 Symposium* (I.Mech.E., London) (in the press).

Discussion

Allen Chico, California

uthors have shown the influence of the forward ary on the minimum film thickness for line con- hey have also extended their conclusions to cover e of point contact. The authors have not, however, ered the formation of the conjunction forming the oundary. This would seem to be the next step in oing a complete elastohydrodynamic theory under ion conditions.

simple approach to the problem, we could con- he confluence of the surface films occurring at the where the separation of the two surfaces is equal to mbined film thickness of the surface films on the linders. We make a further simplification that the ss of the surface film on each rolling element is ne.

lying the foregoing simplifications to the authors' s, and assuming, as did the authors, that their can be applied to point contact, we can obtain an imation for the necessary thickness of the lubricant

a typical set of operating conditions with a 0·281 in er ball and a synthetic paraffinic lubricant, our ter programme, based on an infinite boundary, central film thickness of 21 μin. The semi-minor the Hertzian ellipse is 0·003 in.

n Fig. 7 of the paper, a value of $\psi = 1$ gives a film thickness which is 70 per cent of the nominal Using our bearing conditions, the necessary sur- n thickness is 42 μin on each surface, and the con- occurs 0·002 in in front of the entry to the Hertzian For values of $\psi = 5$ or greater, the central film ss is the same as that obtained with the boundary ity. At $\psi = 5$, the boundary is 0·011 in ahead of rtzian entry, and requires a surface film thickness μin. Reverse flow and surface tension effects in et region would tend to move the boundary out- o that the values calculated would appear to be a ound for the central film thickness.

Anderson Cleveland, Ohio

own that ball and roller bearings require very little , even at considerable speeds and temperatures. the minimum required oil flow rates for 30 and bore bearings were investigated over a range of speeds, loads and temperatures. The minimum required oil flow is defined as the lowest steady state flow rate at which thermal equilibrium can be maintained. When the oil flow rate does not equal or exceed the minimum required oil flow, thermal equilibrium is upset and bearing seizure follows. As shown in Fig. 9, the minimum required oil flow varies as the 6th power of speed, the 8th power of temperature, the square of the load, and the cube of bearing size.

These results suggest that surfaces in rolling and sliding contact must be wetted, if thermal failures are to be avoided. At high speeds, centrifugal effects become important to oil retention on the surfaces requiring lubrication. At elevated temperatures, oil evaporation becomes important. The question that remains to be answered is this: When operating speeds and temperatures become significant, is the oil flow required to avoid thermal failures great enough to prevent e.h.l. starvation? Alternatively, is it possible for e.h.l. starvation to occur in a high speed bearing, or will thermal failure occur first under conditions of sparse lubrication?

Surface distress is known to occur in bearings which operate with marginal e.h.l. films. These usually result when the ratio of film thickness to surface roughness is such that frequent asperity contacts occur, despite the presence of copious quantities of oil. It seems reasonably safe to presume that similar surface distress will appear under conditions of e.h.l. starvation. Unfortunately the experiments of (23) were not run for long enough periods of time to determine whether surface distress would occur.

A lubrication system which employs minimum flow into the contacts requiring lubrication, and auxiliary cooling for heat removal, has advantages over high flow systems. The lubrication system size and weight can be reduced, especially if a throw away system is feasible, and power losses from lubricant churning are reduced.

Perhaps some enterprising researcher will attempt to answer the questions I have posed.

REFERENCE

(23) NEMETH, Z. N. and ANDERSON, W. J. 'Effect of speed, load, and temperature on minimum oil flow requirements of 30 and 75 millimetre bore ball bearings', *NASA TN D-2908*, July 1965.

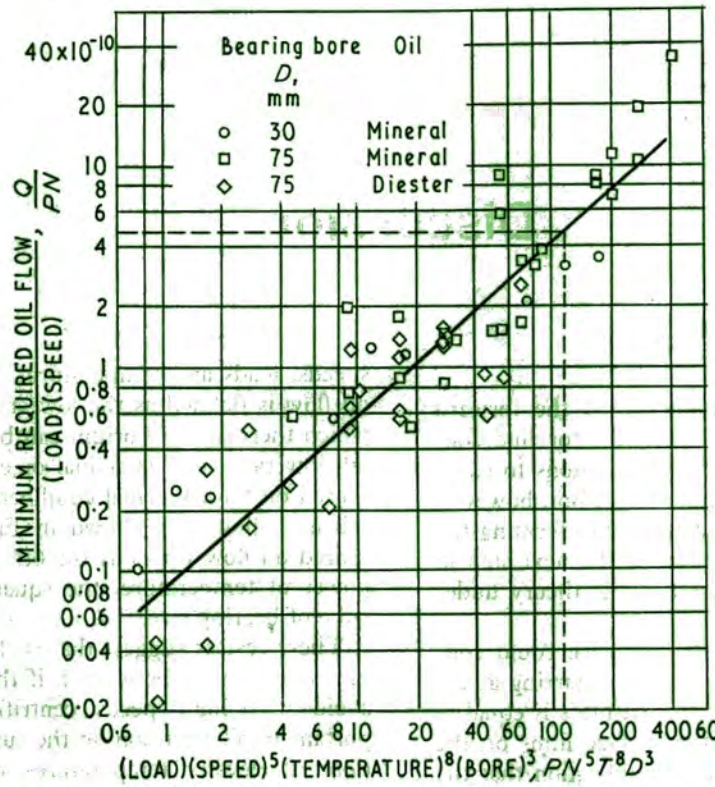

DN range $0{\cdot}6\times10^6$ to $0{\cdot}975\times10^6$; thrust load range, 265 to 3000 lb; bearing temperature range, 225° to 500°F. Example (dashed line): load, *P*, 265 lb; speed, *N*, 30 000 rev/min; bearing temperature, *T*, 400°F; bearing bore, *D*, 30 mm; $PN^5T^8D^3 = 114\times10^{48}$; $Q/PN = 4{\cdot}65\times10^{-10}$; minimum required oil flow, *Q*, $3{\cdot}7\times10^{-3}$ lb/min.

Fig. 9. Generalized correlation of minimum-required-oil-flow data for two bearing sizes and two lubricants

H. Blok Delft, Holland

In their treatment of the effects of the variation of viscosity with pressure, the authors have confined themselves to an exponential variation, such as expressed by their relationship (15). However, along the lines followed in reference (**24**), the results thus obtained may readily be generalized for arbitrary, non-exponential variations. This may be done simply by replacing their pressure coefficient, α, of viscosity by the more general 'representative' one, α^*, as defined by

$$\alpha^* = \left[\int_0^\infty \frac{\eta_0}{\eta(p)}\,\mathrm{d}p\right]^{-1} \quad . \quad . \quad (44)$$

where $\eta(p)$ denotes the viscosity as a known function of pressure and at the same representative film temperature as that of the authors; cf. definition (44) of α^* and the treatment in (**24**).

In case the function $\eta(p)$ is known only experimentally, the integration can still be worked out numerically. It is admitted that physically speaking there is properly no sense in extending this integration to an infinite pressure. But this objection is inherent in the nature of the treatment that the authors have attributed to A. N. Grubin (**7**). Fortunately, with any ordinary oil and within the usual range of temperatures, the integral in definition (4 therefore α^*, is primarily determined by the pressur extending from zero to about 2000 atmospheres bars $= 2\times10^8$ N/m², or about $2{\cdot}8\times10^4$ lb/in²). I the contribution that, on the basis of an extrapolat analytical expressions fitted to the experimental tr $\eta(p)$, may be expected of the pressure range rem up to infinity, will in general amount to no more few per cent of the total sought.

In passing, the discusser wishes to bring out tha carefully weighing some unpublished evidence av to him, he is convinced that the above-mentioned ment is attributable not to Grubin but to A. M. Only by stretching compromise to the utmost is h ing to call this the Ertel–Grubin treatment. In an it would appear that I. E. Vinogradova, who, basis of reference (**7**), might be considered a co- to Grubin, was not involved at all in the p treatment.

As a final comment, it is pointed out that the re ships depicted in Figs 4, 6, 7 and 8 might still be ca somewhat more refined forms that are even more ticable to designers, and that moreover are more with the general usage of dimensionless groups. I

o-ordinates used in these figures are somewhat un-
kinds of dimensionless groups, in that in addition
e essential influential variables, they contain also
rical factors. Such factors, however, are not only
vant, but also complicate the evaluation of these
s, albeit merely to a minor extent. For instance,
e case of Fig. 4, the co-ordinate β still contains the
rical factor 1/4·89, which originates from expres-
(12b). The removal of such numerical factors is,
urse, a trivial affair. In the present case one may
luce $4{\cdot}89\beta = (h_0/R)(W/\eta_0 U)$, and replace the ver-
cale in Fig. 4 by one corresponding with the present
nsionless group. Several other dimensionless co-ordi-
and scales might be replaced accordingly in the
s concerned.

REFERENCE

LOK, H. 'Inverse problems in hydrodynamic lubrication and design directives for lubricated flexible surfaces', *Proc. Instern. Symp. Lubric. Wear*, Univ. of Houston, Texas, June 1963, 1–151 (McCutchan Corp., Berkeley, Calif., U.S.A.).

Chiu King of Prussia, Pennsylvania

ilar but more complex analysis with experimental
rt has been published by Wedeven *et al.* (25) for
se of a circular meniscus line.

ce the first paper on starvation published by Flo-
26), there has been increased interest in finding the
cal parameters that control the degree of starvation
denced by the meniscus location.

e authors point out in this paper that point contacts
rone to starvation at high speed. J. F. Archard's
us experiments have shown that at a rolling velocity
0 cm/s, measured values of film thickness are too
y a factor of 2. A recent paper by Westlake *et al.* (27)
, on log–log plots of measured film thickness against
the speed–viscosity parameter ($\bar{U}$) the curves have a tendency of bending off at high values of $\bar{U}$. The writer believes that these film reductions may be caused by starvation in the inlet. Optical experiments with ball–flat contact using several lubricants, in the discusser's laboratory, reveal that at high speed the plateau film thickness becomes thinner than theory predicts. Knowing the measured meniscus distance and operating conditions, it was possible to compute the film thickness reduction ratio by using Wedeven's theory. We found that the computed film thickness reduction based on measured meniscus location agrees with the measured film thickness reduction.

Furthermore, the following general trends have been observed in our experiments:

(*a*) The meniscus distance decreases rapidly with increasing viscosity at high speed. At low rolling speed, the meniscus distance decreases with viscosity at a lower rate.

(*b*) The meniscus distance also decreases with increasing rolling velocity. The rate of decrease is higher for high viscosity oils than for low viscosity oils.

(*c*) There is no significant dependence of meniscus distance on oil supply rate above a minimum limit.

(*d*) There is strong correlation between the meniscus distance and the product of rolling velocity $\bar{U}$ and viscosity η.

(*e*) The film thickness increases at a progressively slower rate as the rolling speed increases. At high values of $\eta\bar{U}$, the film thickness shows a tendency to reach a maximum and then drop.

The measured plateau film thickness data in our experiments, for an ester based lubricant and a synthetic paraffinic hydrocarbon (ambient viscosity 49 cS and

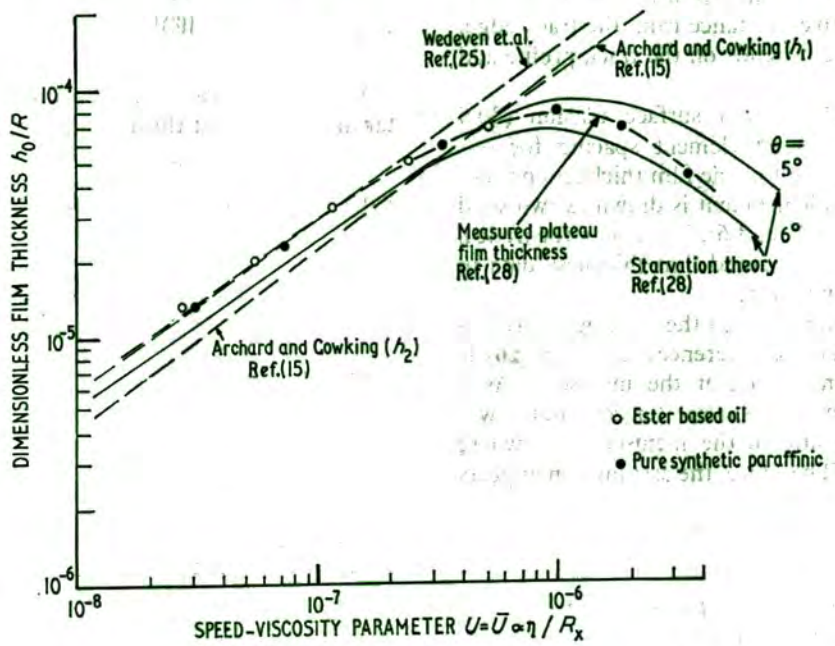

Fig. 10

900 cS respectively) under 5 lb load and mean rolling speed up to 200 in/s, are plotted against a non-dimensional speed–viscosity parameter U in Fig. 10.

Theoretical film thickness relations by Wedeven (25) and Archard and Cowking (15) are plotted as straight lines for comparison. The data show that, at 200 in/s, the film thickness reduction for the low viscosity ester oil is about 30 per cent, and for the high viscosity synthetic hydrocarbon, there is about sevenfold reduction in plateau film thickness from theoretical value.

It is of importance to be able to predict such phenomena by means of lubrication theory. The theory should not rely on meniscus location as an input parameter, since that is not a known quantity in service.

The discusser has conceived a model capable of explaining the phenomenon of starvation on the basis of known fluid and operating parameters. Its principles are as follows.

A film replenishment mechanism in the rolling track controls the height of half films approaching the inlet of a following contact. The rate of replenishment is slowed by oil viscosity and increases with oil–air surface tension and the time elapsed between two contacts.

The elastohydrodynamic (plateau) film thickness as well as the meniscus location depends on the height of the half films far upstream of the inlet.

The details of our experiments and analysis are given in (28). The film replenishment model used by the discusser considers the surface tension in the depression as the driving force for film recovery. The particular two-dimensional configuration used in the model is that of an indented surface with a flat film thickness h_0 at the central portion and two straight ramped sides of slope angle θ. It is based on the recognition that in the centre plane of the passing contact, the curvature of the two contacting bodies forms a wedge-shaped gap which limits the oil layer thickness at any given distance from the track edge. The shape of the wedge depends on the track profile and on conformity.

Using typical values of fluid surface tension (30·5 dyne/cm) and known rolling element spacing for our experiments ($\frac{3}{4}$ in), the result of the film thickness prediction considering film replenishment is drawn as two solid curves in Fig. 10 for $\theta = 5°$ and 6°. These two theoretical curves appear to fit the measured film thickness data in the high speed–viscosity region.

One of the basic assumptions in the existing starvation analysis by the authors and references (25) and (26) is that the pressure begins to rise at the meniscus. As a matter of fact, a non-zero surface-tension fluid will cause a pressure differential at the meniscus line where the two half films join. Therefore, the assumption appears to require further scrutiny.

REFERENCES

(25) WEDEVEN, L. D., EVANS, D. and CAMERON, A. 'Optical analysis of ball bearing starvation', *J. Lubric. Technol., Trans. Am. Soc. mech. Engrs* 1971 **93** (No. 3), 349–363.

(26) FLOBERG, L. 'Lubrication of two cylindrical surfaces sidering cavitation', *Trans. Chalmers Univ. Techn.* No. 234 (Gothenburg).

(27) WESTLAKE, D. J. and CAMERON, A. 'Optical elastoh dynamic fluid testing', A.S.L.E. Preprint 71LC-12.

(28) CHIU, Y. P., HAHN, D. and ROSENBERG, N. 'Explo analysis of elastohydrodynamic properties of lubri (SKF Industries Report No. AL72P001) U.S. Navy tract No. N00019-71-C-0425 Quarterly Progress R No. 2, January 1972.

A. Dyson Fellow

Tables 1 and 2 are especially valuable, and with their it is possible to solve directly a problem of some pra interest. The problem concerns a slider bearing, e.g. ton ring, with the geometry shown in Fig. 11. The is loaded with a force W per unit transverse length ag a plane surface which is moving with a velocity U re to the slider. A copious supply of lubricant with viscos and pressure coefficient of viscosity α is provided, an width of the slider in the direction of motion is fix $2x_i$.

The problem is to determine the radius of re curvature R which will give the thickest film of lubr between the slider and the opposing surface. If the city U may be directed in either sense, the curvature be symmetrical, i.e. the centre C of curvature o slider is located in the central section.

For the solution of this problem, the results giv Tables 1 and 2 of the paper may be recalculated so the variables h and R are separated. The relations for this purpose in the classical case are

$$(\eta_0 \bar{U}/W)^{1/2}(R/x_i) = (9{\cdot}78\gamma)^{-1/2}[(X_i)_\gamma]^{-1}$$

$$(W/\eta_0 \bar{U})^{1/2}(h_0/x_i) = (2{\cdot}445\gamma)^{1/2}/(X_i)_\gamma$$

and in the elastohydrodynamic case

$$h^*(\eta_0 \bar{U}\alpha x_i)^{-1/2} = 3(2/3)^{1/6}\{[I]_0^{q\phi_i}/\phi_i\}^{1/2}$$

$$R(\eta_0 \bar{U}\alpha/x_i^2)^{2/3}(E'/W)^{1/3} = 2^{-5/9}3^{-10/9}\pi^{-1/3}\phi_i^{-4/3}\{[I]_0^{q\phi}$$

In this latter case, the dependence of b on R has taken into account through the usual Hertzian relati

$$b = 2(2WR/\pi E')^{1/2}$$

where $$2/E' = (1-\nu_1^2)/E_1 + (1-\nu_2^2)/E_2$$

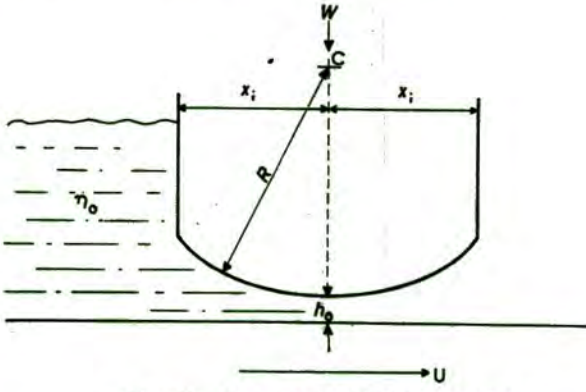

Fig. 11. Geometry of slider bearing

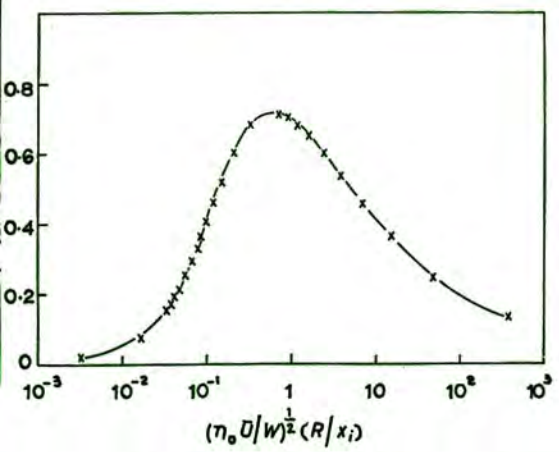

12. Results of calculations for the case of classical hydrodynamic lubrication

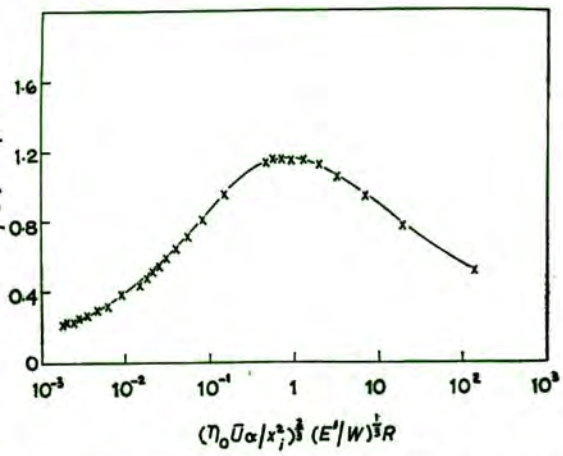

13. Results of calculations for the case of elastohydrodynamic lubrication

E_1, E_2 and ν_1, ν_2 are the Young's moduli and Poisson's of the materials of the slider and of the plane.

e relations between the quantities are shown in 12 and 13. In the classical case, the maximum value

$$(h_0)_{\max} = 0{\cdot}71 x_i (\eta_0 \bar{U}/W)^{1/2}$$

tained at a value of the radius of relative curvature

$$R \simeq 0{\cdot}70 x_i (W/\eta_0 \bar{U})^{1/2}$$

the elastohydrodynamic case, the maximum value

$$h^*_{\max} = 1{\cdot}16 (\eta_0 \bar{U} \alpha x_i)^{1/2}$$

tained for a radius of relative curvature

$$R \simeq 0{\cdot}9 (x_i^2/\eta_0 \bar{U}\alpha)^{2/3} (W/E')^{1/3}$$

e curve in the neighbourhood of the maximum is in the elastohydrodynamic case than in the classical

the optimum condition, the ratio of the film thickness at the point of entry to the minimum film thickness is approximately 2·0 for classical hydrodynamics and 2·1 for elastohydrodynamics. These values are very close to the optimum of 2·2 found in the classical solution for inclined-plane infinite-slider bearings.

Application of the above relations will often give optimum values of R which are considerably greater than those which it is practicable or convenient to employ. The graphs may then be used to show the consequent reduction in the film thickness from the highest value which it is theoretically possible to attain.

L. Floberg Lund, Sweden

The first part of this report, treating lightly loaded rotating cylinders with variable lubricant supply was published in reference (**26**). The authors criticize Martin's solution on the basis of experiments by other authors. Martin's solution is difficult to reach. The authors imply that this depends on difficulties in oil supply. As the lubricant consumption in a rolling contact is extremely low, the lubricant supply is not a problem. In reference (**29**), tests are made at the load values $P_0 = Ph_{\min}/\eta(U_1+U_2)r = 2{\cdot}24$ and 2·23, which should be compared to Martin's value $P_0 = 2{\cdot}45$; this is close to the Martin solution. Recent tests gave the maximum load value $P_0 = 2{\cdot}36$. The basic assumption in the present solution is that the tensile strength of the lubricant is zero. At light loads this is very difficult to reach in practice. The oil can withstand negative pressures, which will give completely different results as shown in (**29**); see Figs 14, 15 and 16, which show theoretical and experimental pressure distributions, where n is the number of oil streams in the cavitation region per non-dimensional unit width. The negative pressures will give considerable decrease in load capacity. The tensile strength of liquids is treated in reference (**30**). The authors show, in their Fig. 2, data from an unpublished Ph.D. thesis by Boness, treating lubrication of a rotating cylinder on a plane surface. This case was published in (**31**).

The second part of the report treats heavily loaded lubricated contacts. The deformations of the surfaces are taken into account, but even here the authors do not consider the behaviour of the oil. At higher pressures the oil will solidify and a completely new theory is needed. This was shown in reference (**32**). B. Jacobson's solidification theory is very close to the experimental evidence. It explains why the very high pressure peaks derived by Dowson and Higginson are of a considerably smaller size.

REFERENCES

(**29**) FLOBERG, L. 'On hydrodynamic lubrication with special reference to sub-cavity pressures and number of streamers in cavitation regions', *Acta polytechnica scandinavica, Mech. Eng. Series* (*e*), *No. 19, 1965 Stockholm.*

(**30**) FLOBERG, L. 'Sub-cavity pressures and number of oil streamers in cavitation regions with special reference to the infinite journal bearing', *Acta polytechnica scandinavica, Mech. Eng. Series* (*e*), *No. 37, 1968 Stockholm.*

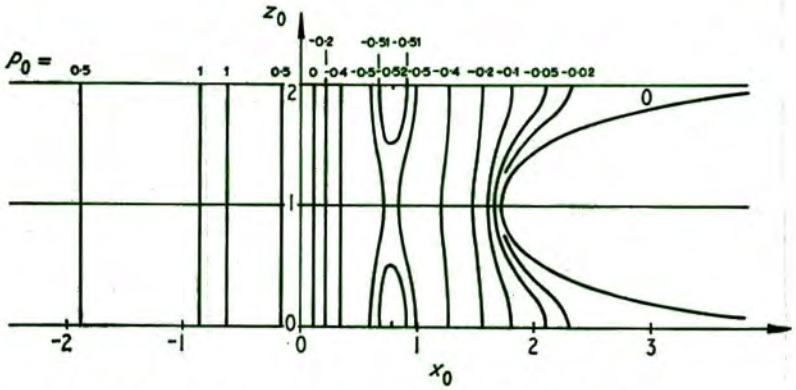

Fig. 14. Theoretical pressure field at $n = 1/2$

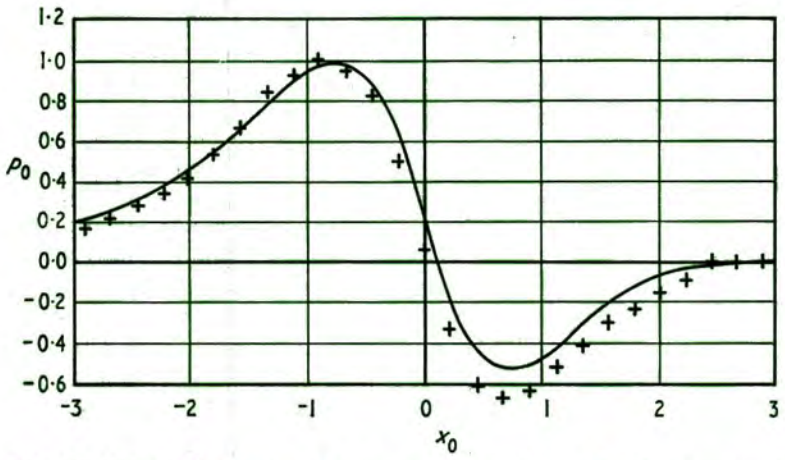

Fig. 15. Theoretical pressure curve and experimental points at $n = 1/2$ and $z_0 = 0$

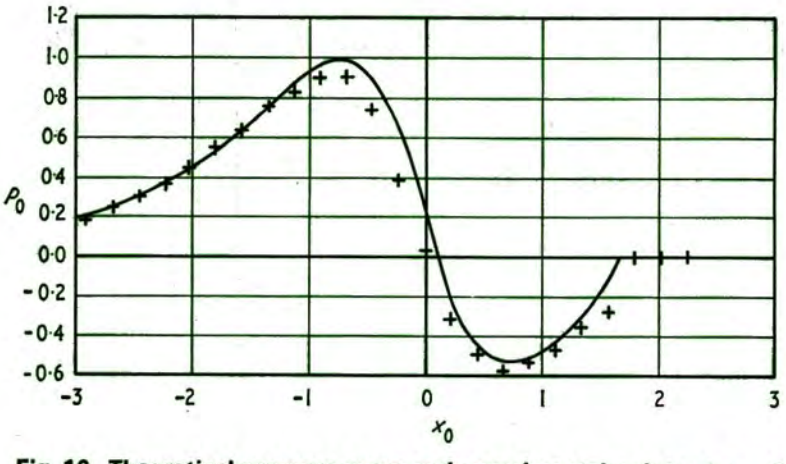

Fig. 16. Theoretical pressure curve and experimental points at $n = 1/2$ and $z_0 = 1$

(31) FLOBERG, L. 'Lubrication of a rotating cylinder on a plane surface, considering cavitation', *Trans. Chalmers Univ. Techn.* 1959 No. 216 (Gothenburg).

(32) JACOBSON, B. 'On the lubrication of heavily loaded spherical surfaces considering surface deformations and solidification of the lubricant', *Acta polytechnica scandinavica, Mech. Eng. Series (e), No. 54, 1970 Stockholm.*

J. A. Greenwood Cambridge

When the suggestion that the development of fluid
sure did not begin at infinity was first put forwa
Lauder (2) at the Leeds e.h.l. Symposium, it m
undeservedly hostile reception. Lauder did not me

rook (1) in his disc experiments had obtained film esses much lower than the Martin value under low onditions; and the experimental evidence has since e stronger when Dyson, Naylor and Wilson (19) oberts and Swales (33) obtained the same result. with its adoption by J. F. Archard, the suggestion e deemed to have become respectable; but only on ion that it is attributable to 'oil starvation'. This efinitely *not* Lauder's idea: his experiments clearly d that the oil boundary took up a particular posi- nder starved conditions, and that *the pressure dis- on remained the same when the oil supply was in- l.* A similar observation was made by Roberts and s: 'The point at which the pressure started to rise ccurs well inside the flooded region'. The bearing ell be starved, but the process appears to be a kind ger strike!

s agrees with Crook's observation, that the changes thickness when the oil supply was turned off could mpletely explained as thermal effects. Presumably the only oil supply is that carried round on the the discs are starved; the film thickness remains at arved' value even when there is an abundant sup-

epting that the pressure build-up does not occur at y, the question is, where does it begin? The authors that a pressure boundary at a fixed distance of 10^{-2} cm would explain the observed film thickness. hey offer any suggestion as to a physical basis for istance? Is it in any way associated with the film ess at this point? Is it worth considering using r's rule, that the pressure build-up starts at the of incipient reversed flow (the 'separation' exit ion applied to the inlet)? It appears that when ap- to a sphere in pure sliding conditions, Lauder's ion gives:

$$\frac{h_i}{h_m} = 2{\cdot}25$$

ared to $h_i/h_m = 1{\cdot}5$ for a roller in pure sliding. ing this to equation (18a), the film thickness reduc- s found to be 0·57. No doubt the agreement with perimental value of 0·56 is purely coincidental.

REFERENCE

OBERTS, A. D. and SWALES, P. D. 'The elastohydrodynamic lubrication of a highly elastic cylindrical surface', *Brit. J. Appl. Phys.* 1969 **2**, 1317–1326.

Hargreaves Graduate and **G. R. Higginson** ber

contribution is to the second part of the paper, hydrodynamic theory; we suggest a further, al- h more speculative, extension to calculate the rol- riction at such a contact.

r interest in this topic is primarily in roller bearings ng with minimal oil supply. Although the rolling n is small, it is known to be a major contributor to the friction torque of roller bearings when they are running in their usual mode, which is very close to pure rolling motion.

The tractions per unit face width on the surfaces in an elastohydrodynamic contact are given by (see reference (34) for instance)

$$t_{1,2} = t_R \mp t_S$$

where t_R is the rolling friction and t_S is the friction due to sliding. Considering here the rolling friction in particular,

$$t_R = -\frac{1}{2}\int_e^i h\frac{\mathrm{d}p}{\mathrm{d}x}\,\mathrm{d}x$$

using the authors' notation. This can be recast as follows:

$$\int_e^i h\frac{\mathrm{d}p}{\mathrm{d}x}\,\mathrm{d}x = [hp]_e^i - \int_e^i p\frac{\mathrm{d}h}{\mathrm{d}x}\,\mathrm{d}x$$

$p = 0$ at the points e and i, so $[hp]_e^i = 0$. Furthermore, a region of constant h, or one which is symmetrical in p and h, makes no contribution to the other term in the expression; so we would expect the Hertzian region to make no substantial contribution to t_R. There will be a small contribution from the outlet constriction, but that is neglected in this simple treatment. So

$$t_R \approx \frac{1}{2}\int_0^i p\frac{\mathrm{d}h}{\mathrm{d}x}\,\mathrm{d}x$$

This integral has been evaluated numerically, using expressions for p and $\mathrm{d}h/\mathrm{d}x$ derived from the paper. Now it cannot reasonably be expected that the value of t_R will be accurate, without some supporting evidence at any rate, because neither p nor $\mathrm{d}h/\mathrm{d}x$ is accurately represented in the paper. So plainly some test of the accuracy must be applied. There are very few cases of full computer solutions with rolling traction available, but those given by Dowson and Higginson on p. 92 of (13) compare reasonably well with the corresponding (fully flooded) values calculated by the method of this note. Furthermore, the Grubin model, which is the foundation of the calculation, would be expected to become a more accurate representation of the real situation as the contact becomes more and more starved of lubricant. So, speculative as the analysis is, there are grounds for hoping that the result will be reasonably accurate.

If we use the symbol $t_{R\infty}$ to denote the value of t_R in the fully flooded condition, it can be shown that the ratio $t_R/t_{R\infty}$ is a function of ψ_i only; its variation is shown in Fig. 17, along with the variation of β^*, the film thickness ratio.

As would be expected, the rolling traction is affected by starvation much more than is the film thickness. As the inlet point moves in towards the Hertzian zone, the rolling traction falls steadily. When the film thickness has 95 per cent of its flooded value, the traction has fallen by 45 per cent, and when the film thickness has 80 per cent of its flooded value the traction is down by more than 70 per cent.

Although the critical distance of the inlet boundary from the Hertzian zone varies with load, speed, etc., the

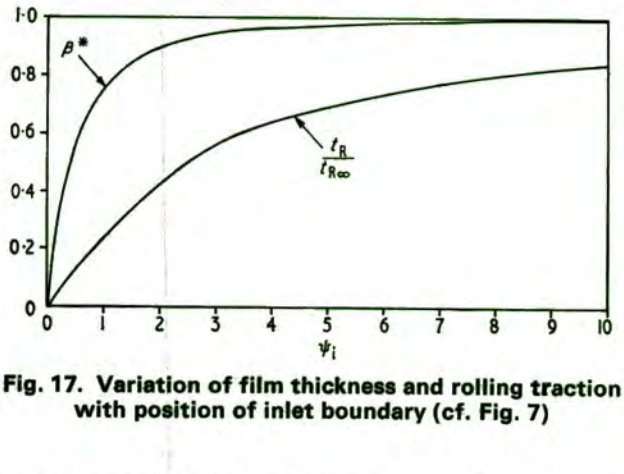

Fig. 17. Variation of film thickness and rolling traction with position of inlet boundary (cf. Fig. 7)

results can be described in a simple, general way in terms of the film thickness, or size of the gap, at the point where the pressure curve starts. Expressing that gap in terms of the calculated flooded film thickness ($h_{0\infty}$), we find the following.

The traction has 80 per cent of its flooded value when the gap at inlet is about 45 times $h_{0\infty}$; the film thickness has 80 per cent of its flooded value when the gap is about 3 times $h_{0\infty}$.

The film thickness has 95 per cent of its flooded value when the gap is 11 times $h_{0\infty}$. Wedeven, Evans and Cameron (25) give a corresponding figure of 9 times $h_{0\infty}$ for a starved point contact.

REFERENCE

(34) Crook, A. W. 'The lubrication of rollers—IV', *Phil. Trans. R. Soc.* 1963 **A255**, 281.

R. A. Hobbs Member

Although the paper refers specifically to cylinders, it should also be applicable to balls running in deep, close conformity grooves where the ellipticity factor approaches unity. In such a bearing operating under typical conditions, $R = 0{\cdot}2$, $b = 0{\cdot}008$ in and $h^*_\infty = 10\times10^{-6}$ in, we find that $x_i = 0{\cdot}005$ in for $\psi_i = 4$. Thus, if an oil film thickness of this order adheres to the rolling elements and raceways, it would seem that the e.h.d. lubrication film thickness would not be affected. In high speed ball and roller bearings, however, the centrifugal force may be sufficient to prevent the adherence of such a film, and lubrication could be seriously impaired.

An interesting further development from this theory would be an estimation of the effect of the inlet boundary condition on the rolling friction. Crook (35) has shown that rolling friction depends on the inlet conditions and is developed primarily in the inlet zone.

$$F \propto \int p \frac{\partial h}{\partial x} \mathrm{d}x$$

so that when h is constant, there is no contribution to rolling friction. The inlet boundary condition will influence the value of this integral, and it would be interesting to know if the degree of this influence wou physically significant.

B. Jacobson Lund, Sweden

In the first part of the paper the classical case of loaded cylinders is treated. This case was publish reference (26). The only difference is that Floberg diagram has the load as a function of the position cavitation boundary, i.e. the oil flow, instead of th of the pressure build-up.

In the second part of the paper, the elastohydrody case is treated. In equation (14), $\bar{q} = 1/\alpha$, the value reduced pressure at the point $x = 0$ is given to be to $1/\alpha$. This means that the pressure at this po infinite, as

$$q = \frac{1}{\alpha}(1-\mathrm{e}^{-\alpha p}) = \frac{1}{\alpha}$$

This is obviously not true.

Equation (14) is given by the exponential pre viscosity relationship. This relationship is only va relatively low pressures if the fluid is a mineral high pressures, the oil converts from a liquid to a so the pressure build-up is determined by the strength of the solidified oil, the compressibility solidified oil and of the elastic properties of the surfaces (32).

As the pressure distributions are approximate same, a heavily loaded starved contact has approxi the same form of the metal surfaces as the uns contact. This means that the relation between the mum oil film thickness and the film thickness parallel region is not a constant as in Fig. 7.

J. F. O'Callaghan Graduate

The authors approximate the thin film zone to on Hertzian shape separated by a parallel film of thi h^* and the converging region according to Croo Since our recent work on e.h.l. (35), C. Taylor and used the true Hertzian shape as a first approximat our thin film zone, which we have found to redu number of iterations required for convergence of a tion to a specific problem.

A great deal of ambiguity has arisen over whe inlet boundary should be located to be equated infinite distance from the contact zone. Hargreave Higginson (36) have shown that as long as the st point is at least more than two Hertzian contact away from the inlet edge of the Hertzian zone, th no drastic effect on the film thickness. In our recent (35) we have stated that the inlet boundary (regard at infinity) is located two Hertzian contact widths from the inlet edge of the Hertzian zone.

It appears we are justified in doing so, since our sentative curve (Fig. 18) of the authors' Fig. 6 show for the finite element solutions ϕ_i varies between 0·9 6·55 respectively. It is seen from the authors' curve

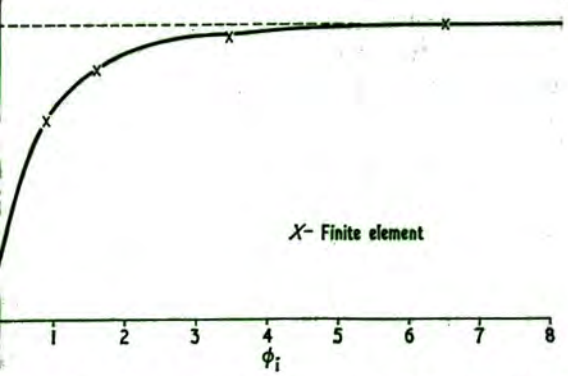

. Elastohydrodynamic theory: the influence of the et boundary ($\phi_i = B^{1/3}X_i$) upon the central film ckness ($\rho = h^*/h^*_\infty$), showing finite element solu- ns

imates very closely to 1·0 for heavily loaded con- nd thin films, whereas our lowest value of ϕ_i corre- to a very lightly loaded contact ($W = w/E'R = \times 10^{-6}$). It would appear that, for this case, the oundary position should have been further away he Hertzian inlet zone. However, from calculations pressure distributions, the effect of increasing this e has negligible effect on the load carrying capa- the oil film, since pressures at the inlet region were to be very small.

REFERENCES

AYLOR, C. and O'CALLAGHAN, J. F. 'A numerical solu- tion of the elastohydrodynamic lubrication problem using finite elements', *J. mech. Engng Sci*, 1972 **14** (No. 4), 229–237.

ARGREAVES, R. A. and HIGGINSON, G. R. Private com- munication, October 1970.

Thompson Schenectady, New York

aking use of certain physically significant non- sional parameters, the authors have developed a predict the effect of starvation on minimum film ess. The theory takes account of both lightly and (Hertzian) loaded cylindrical contacts, and it is ted so as to be readily applicable to engineering ms. More specifically, parameters such as lubricant ties and bearing geometry are inputs from which um film thickness can be calculated, in terms of the n of the lubricant inlet boundary. Therefore, the should be a useful aid in establishing bearing tion requirements and in designing adequate tion systems.

authors' results are directed toward the easy tion of h_0, the minimum film thickness, in terms extent to which the contacts are starved. This is ppropriate, because film thickness is important to and to avoid wear it is advantageous to maximize wever, on the other side of the coin we see from that it is more difficult to starve a thin film than a ne. Therefore, could it not be argued that in cases where starvation is a potential problem, bearings should be designed to run with a thin film? Is this a paradox?

As the authors have pointed out, Boness' computer solution for a cylindrical shape is nearly identical to their own analytical solution for a parabolic assumption. This can be observed in Fig. 3 where the authors' solutions, indicated by the solid line, are only slightly below Boness' solutions, represented by the points. This is strong justification for using the mathematically simpler parabolic approximation, but could the authors comment on the reason for the slight difference in results? Could it be that because Boness' analysis is based on a cylinder, his values of W_∞ are less than those calculated from a parabolic assumption? Thus for a given value of $(X_i)_r$, the load supported by Boness' contact is a slightly greater percentage of the total (W_∞) than its counterpart for the parabolic model.

Next, if one compares Figs 4 and 7, it becomes immediately clear that starvation is more critical in the classical than in the elastohydrodynamic case. Thus, it would appear that the maintenance of proper lubrication is more critical in journal type bearings than in highly loaded contacts such as gears. Is this a physically reasonable result? It would seem that it is, because when machines such as automobile engines fail from lack of lubrication, the damage is generally most severe in the journal bearings.

Finally, equations (19d) and (25a) are somewhat misleading. Equation (19d) is given as

$$\rho = h^*/h^*_\infty \qquad B \text{ constant}$$

while equation (25a) is written as

$$[h^*/h^*_\infty]^{8/9} = \rho$$

Could the authors clarify why ρ is defined differently in the two different cases?

L. D. Wedeven Cleveland, Ohio

The e.h.l. point contact starvation problem has been investigated both experimentally and theoretically by Wedeven, Evans and Cameron (**25**). Therefore, I would like to address my comments to the e.h.l. starvation problem only, noting particularly the lack of experimental results available for the line contact condition.

In (**25**) a semi-transparent race was used in the experiments. This allowed the location of the inlet boundary x_i to be determined along with the measurement of film thickness h^* using interferometry. The starvation problem was solved theoretically, using a Grubin type solution with the true Hertzian shape rather than an approximate shape. Two significant points emerge. First, the starvation problem can be represented by a single parameter; and second, the starvation solutions for line and point contact are very similar.

In (**25**), an approximate inlet shape for point contact was used to derive the following starvation parameter:

$$\frac{S}{S_f} = \frac{Sa^{1/3}}{3{\cdot}52[R(h_0)_f]^{2/3}}$$

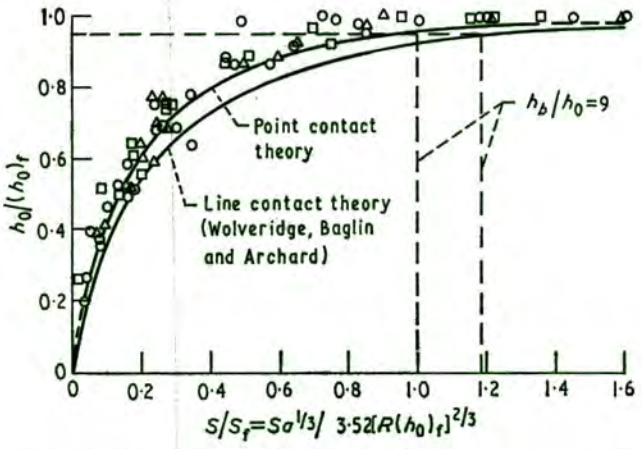

Fig. 19. Comparison of point and line contact results. Data points from point contact experiments

Here, a is the Hertzian radius of contact, S is equivalent to x_i, and $(h_0)_f$ is equivalent to h^*_∞. The constant 3·52 is a result of choosing the condition for the onset of starvation at $h_b/h^* = 9$ where h_b is the gap thickness at the inlet boundary x_i. The importance of this ratio can be seen in Fig. 8, which indicates that the generation of hydrodynamic film building pressure does not become significant until approximately $h/h^* < 9$. If, for comparison purposes, the line and point contacts are assumed to have similar geometries, i.e. $a = b$, and the relative radii of curvature R are equal, then it can be shown that $\psi = 2{\cdot}21S/S_f$.

The line and point contact results can now be compared. This is shown in Fig. 19. Since the line and point contact solutions are similar, the point contact experimental results shown in the figure can therefore be used to complement the line as well as the point contact starvation solutions.

P. E. Wolveridge Chester, **K. P. Baglin** Leicester and **J. F. Archard** Fellow **(Authors)**

The number and the diversity of the contributions to the discussion, together with a number of private communications, clearly suggests considerable interest in the subject of the paper and its possible practical significance. However, this makes it more difficult for us, in this reply, to cover adequately all aspects of the subject.

Our discussion of the classical theory included a reference to the earlier paper of L. Floberg (**26**). In retrospect, it appears that insufficient emphasis was given to this work, and therefore we offer our sincere apologies. We also failed to note the earlier work of M. V. Korovchinskii (**37**) and we are indebted to R. M. Matveevskii for drawing this paper to our attention. However, as a number of discussers have recognized, we tried to incorporate into our statement of the theory the important features of generality and ready applicability to practical conditions. In our view, these characteristics are less strongly a feature of most of the earlier treatments.

In his contribution, H. Blok, like A. Cameron (**18**), decides to attribute credit for the Grubin approach, at least in part, to A. M. Ertel. We have preferred to the traditional attitude of judging these questions evidence of the open literature. However, Korovc also gives Ertel equal credit; therefore our final v this controversy must await a closer examination references cited in (**37**) which are not yet available

On the role and significance of negative pressu the diverging outlet region, we can only express o agreement with L. Floberg. We do not think th deviation of the outlet boundary condition fro usually accepted criterion $p = dp/dx = 0$ is suffi large to affect markedly the load capacity under tions of engineering significance; see, for examp evidence of D. Dowson (**38**). Both L. Floberg Jacobsen, in effect, question the validity of the approach which we have used. We can justify this a using H. Blok's discussion, and writing for the con at $x = 0$

$$\bar{q} = \int_0^{\bar{p}} \frac{\eta_0}{\eta}\,dp = \int_0^{\infty} \frac{\eta_0}{\eta}\,dp = \frac{1}{\alpha^*}$$

where the right-hand side of the equation is seen close approximation, because of the increase of vi with pressure. In comparison with full compute tions, and with experimental results, the Grubin ap has been shown to be an adequate approximation wide range of conditions. Our application of thi approach to the problem of starvation also seems justified on similar grounds; see Fig. 7 of our a forthcoming paper by P. Castle and D. Dowso and the experimental results shown in the contribu L. D. Wedeven, which we consider below. Moreo cannot see how B. Jacobsen's work (**32**), even thou an important and significant paper, has any releva the questions discussed here. It is generally recogniz the film thickness is determined by conditions in th vergent entry region, so that whether or not solidi of the lubricant occurs in the Hertzian zone is question which markedly influences the magnitude film thickness.

H. Blok raises the question of the best form o dimensional presentation. We still prefer our app which implies that the user will first wish to ca calculations assuming fully flooded conditions, a then require a starvation factor in, say, the form o tion (24), $\beta^* = h^*/h^*_\infty$. As far as the rest of the pr tion is concerned, we wonder whether there yet wide acceptance of a 'general usage of dimens groups'. There is certainly no generally accepted for dimensionless presentation of the x dimensio it was the aim of one part of our paper to emphas physical significance of the dimensionless groups $x/\sqrt{2Rh^*}$, $B = b/\sqrt{2Rh^*}$, $\phi = XB^{1/3}$.

We think that the problems of the non-dime presentation of the x direction are well illustra J. F. O'Callaghan's contribution. It was on the b our paper in its preliminary form (**40**), and of preliminary reports of a computer solution (**39**), tha

aves and G. R. Higginson (36) drew the conclusion
conditions typical of rolling contact bearings the
point of the pressure could be taken as two Hertz-
tact widths from the inlet edge. However, there
gers in the uncritical application of such a criterion
der range of conditions. If such a simplified guide
ht, it is perhaps preferable to use the magnitude
ilm thickness at the starting point of the pressure.
the discussion of Hargreaves and Higginson (36),
by Greenwood (41) and the contribution of L. D.
en all indicate the way in which such a criterion
formulated.

. Thompson has raised a number of interesting
rtinent questions about the interpretation of the
The apparent anomaly of equations (19d) and
an best be resolved by re-writing the essential
nt. Thus, we define

$$\rho = h^*/h^*_\infty \qquad (B, \text{constant}) \quad . \quad (19d)$$

ilarly we define

$$\beta^* = h^*/h^*_\infty \qquad (b, \text{constant}) \quad . \quad (24)$$

then shown that for a system in which b is main-
constant

$$[h^*/h^*_\infty]^{8/9} = \rho \quad . \quad . \quad . \quad (25a)$$

ore the interrelationship between ρ and β^* is

$$\beta^* = \rho^{9/8} \quad . \quad . \quad . \quad . \quad (25c)$$

ncerned with a system whose geometric shape B
constant. β^* is concerned with a system whose
ng parameters (including b) are kept constant.

. Thompson also raises an interesting question
ing the use of the parabolic approximation for the
cal shape. In integrating the pressure distribution
∞ for a parabola, or to $x = R$ for a cylinder, we
rget that we are extending the analysis to a region
he basic assumptions of Reynolds' equation (e.g.
are no longer valid. Thus J. A. Greenwood (41)
out that the formal adoption of a cylindrical shape
ot necessarily result in a more 'exact' solution; in
provides evidence to suggest that, if a realistic
for the flow is sought, one finds that a conventional
using a parabolic shape, e.g. (4), gives a better
e of the load capacity than similar solutions, e.g.
), using a cylindrical shape.

. A. Thompson points out, it is easier to starve
classical than under e.h.l. conditions. By this we
hat for equal values of X_i (and for rational values
β (Fig. 4) is smaller than β^* (Fig. 7). This is in
with the discussion on p. 1167, which pointed out
increase in W, b or B causes a reduction in the
of region which is significant in pressure genera-
ut it is far more difficult to make definitive state-
about the practical consequences of this fact,
one needs further information about the causes
effects of starvation. Similarly, there is no general
to R. A. Thompson's question about optimal
design for starvation conditions. One cannot be categorical about whether it is better to design for a thick or a thin film under fully flooded conditions, unless some additional statements are made about the way in which the total supply of lubricant is disposed upon the surfaces. The contributions of C. W. Allen, W. J. Anderson, Y. P. Chiu, R. A. Hobbs and J. A. Greenwood are all relevant in this connection.

R. A. Hobbs stresses the importance of extending our analysis to the problem of rolling balls, and L. D. Wedeven has made a valuable contribution by comparing our theory with his own theoretical and experimental study of the starved lubrication of point contacts (25). However, L. D. Wedeven's comparison of the theories, and also our own extension of line contact theory to point contacts which was given in the paper, both miss the most important point. As was shown in (25), the approximate film thickness formulae for point and line contacts differ in the constant of proportionality in the equations

$$\left[\frac{h-h^*}{h^*}\right]_{\text{point}} = \left[\frac{16\sqrt{2}}{3\pi}\right] B^{1/2}X^{3/2} = (a\phi)^{3/2} \quad (45)$$

$B^2 = b^2/2Rh^*$, where, in this context, b = radius of circular area of contact, whilst

$$\left[\frac{h-h^*}{h^*}\right]_{\text{line}} = \left[\frac{4\sqrt{2}}{3}\right] B^{1/2}X^{3/2} = (a\phi)^{3/2} \quad (46)$$

where b is now the half-width of the Hertzian band of contact. In the body of the paper we have defined $a = (4\sqrt{2}/3)^{2/3}$ and have derived an expression for $I_0^{a\phi}$, powers of which have been plotted against Φ_i on the assumption that for a line contact $a = (4\sqrt{2}/3)^{2/3}$. However, using equations (45) and (46) we note that to compare starvation theories for point and line contacts we need to use

for line contacts, $a = (4\sqrt{2}/3)^{2/3}$

for point contacts, $a = (16\sqrt{2}/3\pi)^{2/3}$

Despite the slightly different definition of starvation parameters, L. D. Wedeven *et al.* (25) have plotted their results on the assumption that for both point and line contacts $a = (16\sqrt{2}/3\pi)^{2/3}$. Similarly, in the discussion of the paper we failed to note the need for different values of a. If both theories are plotted against $a\Phi_i$ (or $a\psi_i$) *using the value of the constant of proportionality appropriate to the geometry*, then the two theoretical curves are brought, as far as we can judge from replotting L. D. Wedeven's graph, into coincidence. This is a highly satisfactory result. It suggests [see equations (45), (46)] that similar effects of starvation occur, for both point and line contacts, when the ratio h_b/h^* has the same value (h_b is the film thickness at the inlet boundary as defined by L. D. Wedeven).

In this paper we have briefly summarized some of the evidence for the assumption that the development of fluid pressure does not start at infinity, and have then set out some of the consequences which arise from this assumption. We have not tackled, in any depth, the more

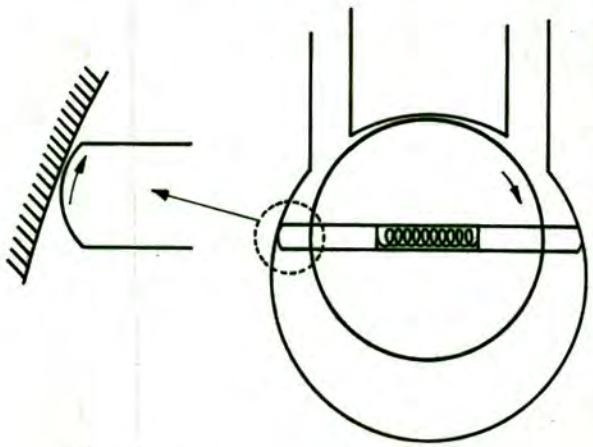

Fig. 20. Gaede type rotary vacuum pump

difficult and complex question of what factors may influence the effective boundary of the film. However, there are certain situations of practical significance where the inlet boundary is determined simply by the geometric shape of the surfaces. In his valuable discussion, A. Dyson has outlined one such application of starvation theory. In a private communication, R. S. Fein has pointed out that the same consideration also applies to his theory of micro-elastohydrodynamic lubrication (**43**); if asperities are to be lubricated by mechanisms of elastohydrodynamic lubrication, their geometry must be such that, in their deformed state, they present an entry region capable of generating the necessary pressures. In our own laboratory we have also investigated the lubrication conditions between the tips of the blades and the bore of a Gaede-type vacuum pump (Fig. 20). Making certain simplifying assumptions, it can be shown that the classical theory of the first half of the paper is applicable, and with sufficient conformity between blade tips and the bore, starvation can be significant in the most disadvantageous configuration shown in the diagram. Perhaps this is an example of optimal design, as suggested by R. A. Thompson.

In the paper we considered starvation as a possible factor contributing to a less rapid rise in film thickness with speed than that forecast by isothermal e.h.l. theories, and a number of contributors have also discussed this theme. However, it is worth emphasizing that two other factors can have a similar influence. First, in capacitance measurements at point contacts, the change in film shape with speed can have this same effect upon deduced values of the film thickness (**22**). Second, theoretical studies of inlet region shear heating (**44**) (**45**) require serious consideration. However, it now seems almost certain that starvation can be an important factor in the divergence between theory and experiment, particularly at high speeds. J. A. Greenwood was right to draw attention to the important role which W. Lauder (**2**) has played in the development of these concepts, but it is entirely a different question as to whether we accept that the specific mechanism of starvation proposed by Lauder is the important one. Indeed, is there one mechanism of starvation or many? To these questions our discussors have buted a number of ideas and, at the risk of being by J. A. Greenwood of cowardice in not accordi the doubtful accolade of respectability, we can o gest that this is an area which requires further in tion.

R. A. Hobbs suggests an extension of our ana include rolling friction under starved conditions has been provided by the excellent discussion o Hargreaves and G. R. Higginson. It may be of to point out that our own extension of the th evaluate rolling traction, follows slightly different

Thus, following the notation of Hargreaves and son, we write

$$-2t_R = \int_e^i h\frac{\mathrm{d}p}{\mathrm{d}x}\mathrm{d}x = \int_0^i h\frac{\mathrm{d}p}{\mathrm{d}x}\mathrm{d}x + h^* \int_e^o \frac{\mathrm{d}p}{\mathrm{d}x}$$

Using the condition $p = -1/\alpha \ln(1-\alpha q)$, and su ing for h, we obtain

$$2t_R = \frac{12\eta \bar{U}(2Rh^*)^{1/2}}{h^{*2}(4\sqrt{2}/3)^{2/3}B^{1/3}} \times h^* \int_0^i \frac{\tau^{3/2}\,\mathrm{d}\tau}{(1-\alpha q)(1+\tau^{3/2})^2} + \frac{h^*}{\alpha}[\ln(1-$$

where, as in equation (18b), τ is a dummy vari $(a\phi)$. For numerical integration, it is necessary $\bar{q} = c/\alpha$ where $c \to 1$. It was found that, provid $(1-10^{-3})$, the result was virtually independent o

Thus using equation (18a) and the notation of ou

$$2t_R = \frac{h^*}{\alpha}\cdot c \int_0^{a\phi_i} \frac{\tau^{3/2}\,\mathrm{d}\tau}{[I]_0^{a\phi_i}(1-\alpha q)(1+\tau^{3/2})^2} + \frac{h^*}{\alpha}\ln($$

or

$$2t_R = \frac{h^*}{\alpha}[F]_0^{a\phi_i}$$

Following a procedure similar to that used in ou it may be shown that

$$\frac{t_R}{t_{R\infty}} = \beta^*.\lambda \quad . \quad . \quad . \quad .$$

where $\lambda = [F]_0^{a\phi_i}/[F]_0^{\infty}$. There are difficulties in upon a suitable value for infinity; therefore we ha the same value as Hargreaves and Higginson; calculated in this way is in excellent agreeme Fig. 20.

The form of expression given in equation (47 specifically that the influence of starvation upon traction can be separated into two factors. First, tion reduces t_R through its influence upon film th (β^*), since t_R is proportional to h^*/α (**34**). Second, tion affects t_R through the extent of the filling of th region *per se* (λ). The dominance of the latter factor i mining t_R is clearly seen in Fig. 20.

Finally, W. J. Anderson's contribution sugges in engineering practice, the interaction of a nun different mechanisms must be considered. Sta may reduce bearing life because it reduces film thi

Fig. 20 shows, a moderate degree of starvation
ve advantages, because it markedly reduces losses
ly a minor influence upon film thickness. Clearly
need to consider the role of lubricant supply in
ing the heat balance of the system.

e paper it was possible only to provide a broad
of the theory and to suggest some ways of applying
ctice. The contributions have extended the range
aper and, we hope, have enhanced its value.

REFERENCES

OVCHINSKII, M. V. 'Certain problems of elastorheology having an application in the theory of friction', *rict. Wear Mach.* 1964 **18**, 89.

WSON, D. 'Investigation of cavitation in lubricating ims supporting small loads', *Proc. Conf. on Lubrication nd Wear* 1957, 93 (I.Mech.E., London).

TLE, P. and DOWSON, D. 'A theoretical analysis of the starved lubrication problem for cylinders on line contact', *Elastohydrodynamic Lubrication, 1972 Symposium* C35/72, 131 (I.Mech.E., London).

(40) WOLVERIDGE, P. E., BAGLIN, K. P. and ARCHARD, J. F. University of Leicester Department of Engineering Report 69-31 (Dec. 1969).

(41) GREENWOOD, J. A. 'Lubrication of highly elastic surfaces', *J. Phys. D. (Appl. Phys.)* 1970 **3**, 1977.

(42) GREENWOOD, J. A. Private communication, University of Salford Department of Mechanical Engineering Report USME/T/14/70.

(43) FEIN, R. S. and KREUTZ, K. L. *Interdisciplinary approach to friction and wear, NASA SP-181* 1968, 358.

(44) CHENG, H. S. 'Calculation of elastohydrodynamic film thickness in high speed rolling and sliding contacts', Mechanical Technology Inc. Latham, N.Y., Report MTI-67 TR24 (1967).

(45) GREENWOOD, J. A. and KAUZLARICH, J. J. 'Inlet shear heating in elastohydrodynamic lubrication.' Paper submitted for publication in *Trans. A.S.L.E.*

Corrigenda

P. 1165, Fig. 7 sub-caption, second sentence should read: 'The inlet boundary is expressed as $\psi_i = b^{1/3}x_i/(2R\bar{h}^*_\infty)^{2/3}$; . . .'.

P. 1169, Ref. (22) For '(in the press)' read 'Paper C2/72, 5'.

W. C. & S. Ltd, England

7. Boness, R. J.

Ph. D. Thesis

Royal Military College of Science, 1969

8. Castle, P. and Dowson, D.

"A theoretical analysis of the starved elastohydrodynamic lubrication problem for cylinders in line contact."

Proc. Inst. Mech. Engnrs. EHD Lub. Symposium, 1972, Paper C35/72.

9. Crook, A.W.

"The lubrication of rollers I"

Phil. Trans. R. Soc. 1958, A250, 387.

10. Crook, A. W.

"The lubrication of rollers II - Film thickness with relation to viscosity and speed."

Phil. Trans. R. Soc. 1961, A254, 223.

11. Crook, A. W.

"The lubrication of rollers III - A theoretical discussion of friction and temperatures in the oil film."

Phil. Trans. R. Soc. 1961, A254,237

12. Crook, A. W.

"The lubrication of rollers IV - Measurement of friction and effective viscosity."

Phil. Trans. R. Soc. 1963, A255, 281.

13. Dowson, D. and Higginson, G. R.

"Theory of roller bearing lubrication and deformation."

Inst. Mech. Engnrs. Lubrication and Wear Convention, 1963.

14. Dowson, D. and Higginson, G. R.

"Elasto-hydrodynamic lubrication - The fundamentals of roller and gear lubrication."

Pergamon Press, 1966.

15. Dowson, D., Higginson, G. R. and Whitaker, A.

"Elasto-hydrodynamic lubrication - a survey of isothermal solutions."

Jln. Mech. Engng. Sci., 4, 2, 121

16. Facer, J. E.

"Lubrication of roller bearings."

Final year Honours, project, Dept. of Eng. Sci., Univ. Durham, 1972.

17. Floberg, L.

"Lubrication of two cylindrical surfaces, considering cavitation."

Trans. Chalmers Univ. Tech. Gothenberg. Nr. 234, 1961

18. Fogg, A. and Webber, J. S.

"The lubrication of ball and roller bearings at high speed."

Proc. Inst. Mech. Engnrs. 1953, Vol. 39, No. 359.

19. Garnell, P.

"Further investigations of the mechanics of roller bearings."

Proc. Inst. Mech. Engnrs. 1966-67, Vol. 181, Pt. 1

20. Garnell, P.

M. Sc. Thesis

Dept. Mech. Eng. Royal Military College of Science.

21. Garnell, P. and Higginson, G. R.

"The mechanics of roller bearings."

Proc. Inst. Mech. Engnrs.
1965-66, 180 (Pt. 3B), 197.

22. Grubin, A. N. and Vinogradova, I. E.

Central Scientific Research Institute for Technology and Mechanical Engineering, Book No. 30, Moscow.
(D.S.I.R. Translation No. 337).

23. Greenwood, J. A.

Discussion to paper by Wolveridge, Baglin and Archard, contained in Appendix (U).

24. Lauder, W.

"Hydrodynamic lubrication of proximate cylindrical surfaces of large relative curvature."

Proc. Inst. Mech. Engnrs.
1965-66. Vol 180, Pt. 3B.

25. Leaver, R.H.

M.Sc. Thesis, "An investigation of the mechanics of tapered roller bearings".

Univ. Durham, 1969.

26. Münnich, H.

"Einflüsse auf den Schmierzustand von Wälzlagern"

S.K.F. Kugellagerfabriken
GMBH., Schweinfurt, WTS 69 04 20

27. Münnich, H.

"Einfluss der Schmierung auf lebensdauer, Reibung und Verschleiss von Wälzlagern".

S.K.F. Kugellagerfabriken
GMBH., Schweinfurt, WTS 98.

28. Münnich, H., Erhard, M. and Niemeyer, P.

"The effect of elastic deformation on load distribution in rolling bearings".

The Ball Bearing Journal,
SKF. 155, 1968.

29. Norlander, G. and Stackling, H.

"Anew way to measure temperature".

Ball Bearing Journal,
SKF., 172, 1972.

30. Skurka, J. C.

"Elastohydrodynamic lubrication of roller bearings".

Jln. Lub. Tech. 1970.
69 - LUB- 18

31. Smith, C.F.

"Some aspects of the performance of high speed, lightly loaded cylindrical roller bearings".

Proc. Inst. Mech. Engnrs.
1962, Vol. 176, No.22

32. Timoshenko, S. and Goodier, J. N.

"Theory of Elasticity".

Engineering Societies
Monographs,
McGraw-Hill Co. 1951

33. Townsend, D. P. and Zaretsky, E. V.
Kannel, J.
Danner, C. H.

Discussion to reference 30.

34. Vaessen, G. H. G. and DeGee, A. W. H.

"Rolling contact fatigue of maraging steels of different production history: influence of film thickness/roughness ratio."

Proc. Inst. Mech. Engnrs.
EHD. Lub. Synposium
1972, Paper C7/72.

35. Wedeven, L. D., Evans, D. and Cameron, A.

"Optical analysis of ball bearing starvation."

Jnl. Lub. Tech. 1970
70 - LUB - 19

36. Wolveridge, P. E., Baglin, K. P. and Archard, J. F.

"The starved lubrication of cylinders in line contact."

Proc. Inst. Mech. Engnrs.
1970-71, Vol.185, 81/71

See Appendix (U).